# SYNTHESIS AND OPERABILITY STRATEGIES FOR COMPUTER-AIDED PROCESS INTENSIFICATION

A Dissertation

by

YUHE TIAN

Submitted to the Graduate and Professional School of
Texas A&M University
in partial fulfillment of the requirements for the degree of

DOCTOR OF PHILOSOPHY

| | |
|---|---|
| Chair of Committee, | Efstratios N. Pistikopoulos |
| Committee Members, | Mahmoud El-Halwagi |
| | M. M. Faruque Hasan |
| | Hongcai Zhou |
| Head of Department, | Arul Jayaraman |

August 2021

Major Subject: Chemical Engineering

# ABSTRACT

Today's chemical process industry is faced with pressing challenges to sustain the increasingly competitive global market with rising concerns on energy, water, food, and environment. Process intensification (PI) offers the potential to address these challenges by realizing step changes in process economics, energy efficiency, and environmental impacts through the development of novel process schemes and equipment. However, early PI breakthroughs mostly relied on Edisonian efforts while lack of theoretic development driving for systematic innovation. Meanwhile, PI technologies bring new challenges such as task-integrated design, new operating conditions, vulnerability to disturbance, etc. Thus, advanced computational and systems-based methods are essential means to support the analysis and optimization of PI systems at the early design stage.

In this thesis, we aim to address two key open questions for computer-aided PI: (i) how to systematically generate innovative and intensified process systems? and (ii) how to ensure that the derived intensified designs are operable under varying operating conditions? To answer the first question, we propose a PI synthesis strategy based on the Generalized Modular Representation Framework. A superstructure representation is developed to model chemical processes leveraging modular phenomenological building blocks (i.e., pure heat exchange module, mass/heat exchange module). Novel process structures can be systematically identified to enhance process performance without pre-postulation of equipment design. The proposed approach is further integrated with model-based operability strategies towards a holistic framework for the synthesis of operable process intensification systems. The following operability aspects are investigated with design optimization: (i) multiperiod process synthesis with flexibility considerations to generate design solution with guaranteed feasibility under uncertainty, (ii) inherently safer design by integrating risk analysis metrics as process constraints, and (iii) simultaneous design and control to deliver optimal design with optimal control actions. The applicability and versatility of the framework are demonstrated with a number of real-world applications to deliver intensified operable process systems, e.g. reactive separation, extractive separation with novel materials, dividing wall columns.

# ACKNOWLEDGMENTS

Above all, I would like to express my sincere gratitude to my supervisor, Professor Efstratios N. Pistikopoulos. I want to thank him for giving me the opportunity to work in his research group for my Ph.D. program. His vision, acumen, and passion in pursuit of engineering innovation with theoretical breakthrough have always been the driving force to inspire my scientific, professional, and cerebral developments. His continuous guidance, insightful feedback, and generous support on my research project have led to the production of this thesis.

I am also very grateful to the support and mentoring from my thesis committee members – Professor Mahmoud El-Halwagi, Professor M. M. Faruque Hasan, and Professor Hongcai Zhou. The valuable insights, enthusiastic encouragement, and strong expertise of Professor El-Halwagi, as a pioneer of the mass exchange network concepts, have stimulated many new ideas to enhance this project. I am very fortunate to be collaborating with Professor Hasan and his research group through the years. His strong work ethic, meticulosity, and creative thinking have a profound impact on my training to become a professional researcher. The multidisciplinary vision of Professor Zhou on materials design have strongly motivated the exploration of multi-scale PI in this work.

I would like to take the opportunity to thank Professor Rafiqul Gani for his constructive inputs, patient guidance, and fruitful discussions on my research project. His short courses and pioneering work on computer-aided PI have been constantly guiding me to explore this exciting research area.

Moreover, I really appreciate the collaboration with Dr. Rahul Bindlish from The Dow Chemical Company on PI operability and DWC design. His strong support and engagement in the project provides a great opportunity to synergize our methodologies with real industrial applications.

I would like to acknowledge my late advisor Professor Christodoulos A. Floudas for my undergraduate research internship. It was the first time I learned about Process Systems Engineering, but deeply impressed with the multi-scale nature and systems-based thinking. His gentleness, perpetual passion for research excellence, and insistence on high standards will always be motivating my academic developments. I can still remember how excited I was through my entire undergraduate

senior year, looking forward to pursuing my Ph.D. at Texas A&M University.

I would like to acknowledge late Professor M. Sam Mannan as my Ph.D. co-supervisor, for his kindness and generosity. The support from late Professor M. Nazmul Karim was indispensable to smooth the transition to start my studies here.

I want to express my special thanks to Ms. Vickie Garcia as our administrative coordinator. Her warmth and being considerate for everyone make the feeling of home and belonging. I am beyond grateful to my graduate mentors, Dr. Alexander M. Niziolek and Dr. Onur Onel, who are always there to help. I also want to thank Dr. Salih Emre Demirel, my closest collaborator on research publications and project reports. Moreover, it has been such a pleasure and honor for working with the process intensification team in Pistikopoulos group, with Dr. Konstantinos Pappas as our most reliable, responsive, and supportive project manager, and the technical team including Shivam Vedant, Vaishnav Meduri, Cristian Arnoldo García López, Moustafa Ali, Mary Rivera Atencio, Xiaoqing Cai, Dustin Kenefake, and Iosif Pappas. I cannot find anything more inspiring than generating new ideas and pushing the research boundaries through the collaborations with the team. It has been indeed a great privilege for me to work with all my awesome labmates – Dr. Melis Onel, Dr. Yaling Nie, Dr. Nikolaos Diangelakis, Dr. Styliani Avaraamidou, Dr. Gerald Ogumerem, Dr. William Tso, Dr. Doga Demirhan, Dr. Baris Burnak, Dr. Justin Katz, Dr. Burcu Beykal, Dr. Christopher Gordon, Denis Su-Feher, Stefanos Baratsas, Cory Allen, Sean Niknezhad, Rahul Kakodkar, Marcello Di Martino, Zhihao Chen, Julie Cook, and Ioannis Koumentis.

Last but not least, my deepest gratitude and love to my parents, my brother, and my kitty cat for always being there with me and supporting me.

# CONTRIBUTORS AND FUNDING SOURCES

## Contributors

This work was supported by a dissertation committee consisting of Professor Efstratios N. Pistikopoulos, Professors Mahmoud El-Halwagi, and Professor M. M. Faruque Hasan of the Department of Chemical Engineering and Professor Hongcai Zhou of the Department of Chemistry.

The industrial patent analyzed for Chapter 4 was provided by Dr. Rahul Bindlish from The Dow Chemical Company. The simulation analyses presented in Chapter 4.3 were jointly conducted with Vaishnav Meduri of the Department of Chemical Engineering. The control analyses presented in Chapter 7.3.2 were jointly conducted with Iosif Pappas, Dr. Baris Burnak, and Dr. Justin Katz of the Department of Chemical Engineering. All other work conducted for the dissertation was completed by the student independently.

## Funding Sources

Financial support from the Texas A&M Energy Institute, Shell, NSF PAROC Project (Grant NO. 1705423), and DOE RAPID SYNOPSIS Project (DE-EE0007888-09-03, Partner Organizations: Texas A&M University, Georgia Institute of Technology, Auburn University, Shell, The Dow Chemical Company, Process Systems Enterprise Limited) is gratefully acknowledged. Teaching assistantship from Texas A&M University Department of Chemical Engineering is also gratefully acknowledged.

TABLE OF CONTENTS

Page

LIST OF FIGURES

FIGURE Page

# LIST OF TABLES

TABLE Page

# 1. INTRODUCTION[†]

In this chapter, we provide an overview on state-of-the-art advances and challenges of Process Systems Engineering (PSE) approaches for process intensification (PI), with particular focus towards the synthesis of operable process intensification systems. We also highlight major research challenges and thereby identify the objectives of this thesis.

## 1.1 Process intensification: an overview

Facing a highly competitive global market with increasing awareness on environmental and safety issues, chemical production is making its way towards a paradigm shift to more efficient, more environmentally friendly, and more versatile [1, 2]. Process intensification (PI) is regarded as a promising solution to pursue this structural transformation, by utilizing the synergy between multi-functional phenomena at different time and spatial scales, and by enhancing process driving forces such as the mass, heat, and/or, momentum transfer rates, through the use of novel process schemes and equipment [3, 4, 5]. Intensified processes have also been well-recognized to synergize the advances in energy systems [6], smart manufacturing [7], and circular economy [8].

The concept of PI was first introduced into Chemical Engineering discipline in 1983 marked by the paper published by Colin Ramshaw from the ICI New Science Group, who described their studies on centrifugal fields (so-called "HiGee") in distillation processes [9]. Since then, several definitions of PI have been proposed, the differences of which mainly stem from the targeted diversity in PI outcomes and proposed strategies to achieve these outcomes. An indicative list of PI definitions is presented in Table 1.1 [10]. Interestingly, this also shows the evolution of PI principles and targets from initially emphasizing equipment size reduction and cost savings to recognizing PI with a broader impact towards more efficient, more sustainable, and safer processes.

[†]Reproduced in part with permission from Tian, Y., Demirel, S. E., Hasan, M. F., & Pistikopoulos, E. N. (2018). An overview of process systems engineering approaches for process intensification: State of the art. Chemical Engineering and Processing – Process Intensification, 133, 160-210. Copyright 2018 Elsevier Ltd. Reproduced in part with permission from Tian, Y., & Pistikopoulos, E. N. (2019). Synthesis of operable process intensification systems: Advances and challenges. Current Opinion in Chemical Engineering, 25, 101-107. Copyright 2019 Elsevier Ltd.

Table 1.1: Evolution of process intensification definitions and principles (Reprinted from [10]).

| **Reference** | **Definition** | **Year** |
|---|---|---|
| Ramshaw [9] | Devising exceedingly compact plant which reduces both the main plant item and the installation costs | 1983 |
| Stankiewicz & Moulijn [3] | Substantially decreasing equipment volume, energy consumption, or waste formation; Leading to cheaper, safer, sustainable technologies | 2000 |
| Arizmendi-Sanchez & Sharratt [11] | Synergistic integration of process tasks and coupling of phenomena; Targeted intensification of transport processes | 2008 |
| Becht et al. [12] | To sustain profitability even in the presence of increasing uncertainties | 2009 |
| Van Gerven & Stankiewicz [13] | Maximize the effectiveness of intra- and intermolecular events; Give each molecule the same processing experience; Optimize the driving forces at every scale; Maximize the synergistic effects for multitasking | 2009 |
| Lutze et al. [14] | Add/enhance phenomena in a process through the integration of operations, functions, phenomena; Or through the targeted enhancement of phenomena | 2010 |
| Ponce-Ortega et al. [15] | Smaller equipment size; Higher throughput; Higher performance; Less usage of utility materials and feedstock | 2012 |

Based on these principles, we have summarized at least seven activities which can result in an intensified process system [10]: (i) combining multiple process tasks or equipment into a single unit (e.g., reactive distillation, membrane reactor), (ii) tight process integration (i.e., material or energy integration), (iii) use of novel multifunctional materials (e.g., ionic liquid, zeolite), (iv) miniaturization of process equipment (e.g., micro-reactor), (v) changing of operation modes (e.g., pressure swing adsorption), (vi) application of enhanced driving forces (e.g., rotating packed bed), and (vii) advanced operational strategies (e.g., dynamic operation via model-based control).

Many excellent reviews have been offered to elucidate the state-of-the-art development of PI technologies and applications. In Table 1.2, we provide a summary of the latest review/perspective papers to highlight the major scientific and industrial interests in this field since 2018. An extensive review on the advances up to 2018 can be found in Tian et al. [10]. As can be noted, a diversity of PI technologies are being investigated to address the dual challenge of energy productivity/efficiency

and environmental sustainability [16], e.g. reactive distillation [17], intensified reactors [18], alternative energy sources [19], advanced materials [20], etc. Another rapidly emerging research theme is computer-aided process intensification [10, 21]. From modeling and simulation point of view, Fig. 1.1 illustrates the growth profile based on the number of publications on the modeling and simulation of seven representative process intensification technologies, namely membrane reactor, simulated moving bed, dividing wall column, rotating packed bed, membrane distillation, microreactor, and reactive distillation. The statistics were collected from a search of the citation database Web of Science™ Core Collection (updated on April 27, 2021). From Fig. 1.1, it is clear that the number of articles has been steadily increasing during the past two decades, with a particularly notable surge during the last four years. Moreover, the advanced system-based methods and tools developed from the Process Systems Engineering (PSE) community has attracted more and more attention, which can support quantitative decision making by providing techno-economic analysis capability as well as predictive proficiency on the design [22, 23], optimization [24, 25, 17], and operation [26, 27, 28] of PI and modular systems. In the subsequent sections, we briefly review recent work on process intensification through PSE approaches, thereby to identify the major gaps and challenges – some of which will be tackled in this thesis.

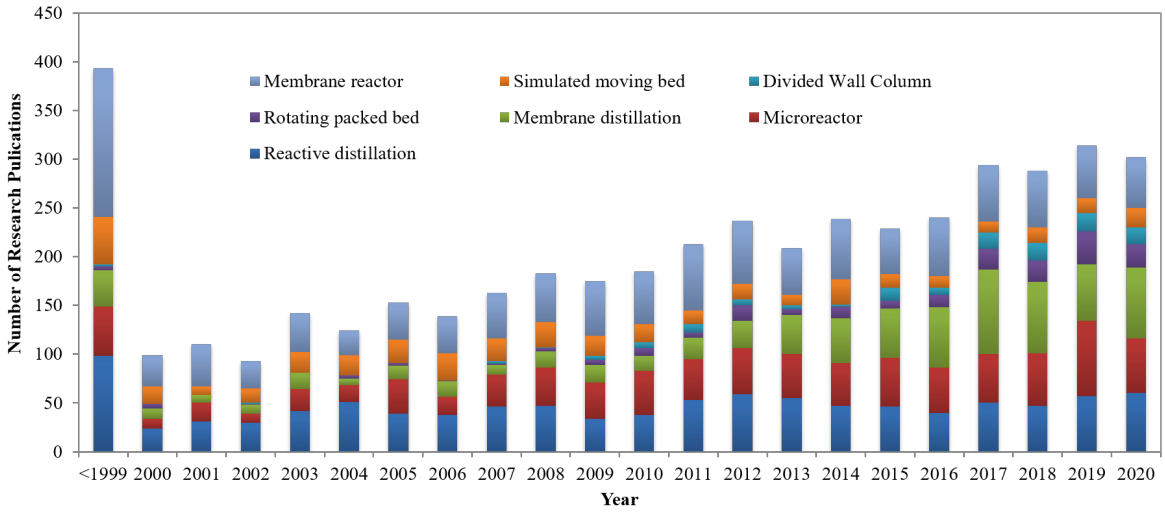


Figure 1.1: Statistics of research articles on PI modeling and simulation.

Table 1.2: Latest review/perspective articles on process intensification (Reprinted from [29])

| Reference | Highlight | Year |
|---|---|---|
| Weinfeld et al. [30] | Experimentation, modeling, and dynamic control of reactive dividing wall columns | 2018 |
| Gude and Martinez-Guerra [19] | Microwave- and ultrasound-enhanced biodiesel production and roles of catalysts/solvents | 2018 |
| Stephen and Periyasamy [18] | Biofuel production from organic wastes with PI technologies | 2018 |
| Coward et al. [31] | PI technologies and application opportunities in water industry | 2018 |
| Keil [5] | PI definitions and state-of-the-art technology development | 2018 |
| Baldea et al. [32] | Status, challenges, and opportunities for modular manufacturing processes | 2018 |
| Suryawanshi et al. [33] | Microreactor fabrication, design, and applications | 2018 |
| Tian et al. [10] | PSE approaches for PI design, synthesis, and operability analysis | 2018 |
| Skiborowski [24] | PSE approaches for design and synthesis of intensified reaction and/or separation systems | 2018 |
| Kiss et al. [34] | Reactive distillation and its novel technology variants | 2018 |
| Daoutidis et al. [27] | Distributed optimization, control, and monitoring of large-scale PI systems | 2019 |
| Dias and Ierapetritou [28] | Optimal operation, control, and scheduling of PI processes | 2019 |
| Sitter et al. [25] | Process synthesis and optimization approaches for PI design and retrofit | 2019 |
| Masuku and Biegler [17] | Optimization-based tools for PI in gas-to-liquids processes | 2019 |
| Tian and Pistikopoulos [22] | Challenges and opportunities for synthesis of operable PI systems | 2019 |
| Demirel et al. [23] | Systematic approaches and procedures to generate, assess, and analyze PI solutions | 2019 |
| Bielenberg and Palou-Rivera [35] | Activities under the RAPID Institute to accelerate modular chemical process intensification | 2019 |
| Aglave et al. [36] | Role of simulation and digitalization tools to assist modular process intensification | 2019 |
| Jiang and Agrawal [37] | Thermally coupled distillation processes for multi-component separation | 2019 |
| Stankiewicz and Yan [38] | Role of (advanced) materials in PI | 2019 |
| Pereira and Patel [16] | PI activities at ExxonMobil to address the dual challenge of energy and environment | 2019 |
| Gazzaneo et al. [39] | Model-based operability theory, applications, and software tools for modular PI systems | 2019 |
| Tula et al. [21] | Perspectives on computer-aided process intensification | 2020 |
| Adamu et al. [20] | Equipment, material, and process innovation for carbon capture and conversion | 2020 |

## 1.2 Process Systems Engineering approaches for process intensification: state of the art

Process Systems Engineering (PSE) can provide a wide range of systematic methodologies and tools for PI design and operation as summarized in Table 1.2. Despite these efforts, key open questions in this area remain on: (i) how to systematically represent, generate, and evaluate intensified process configurations and explore the combinatorial design space in a computationally efficient way? (ii) how to ensure the actual operational performances of intensified systems by developing control, operability, and safety metrics? and (iii) how to integrate operability assessment during the conceptual design of PI systems?

In what follows, we first give an overview on process intensification synthesis methods which aim to systematically deliver novel out-of-the-box process solutions. Then we focus on advanced operability and control approaches which are developed to address the unique operational challenges in intensified process systems.

### 1.2.1 Conceptual synthesis of intensified processes

Given desired products and available raw materials, process synthesis strives for determining the optimal equipment and interconnections in a process network among plethora of alternatives, with respect to the goal of optimizing economic, environmental, and/or social objectives [40, 41]. To enrich the design space with novel process solutions advocated by process intensification, a promising solution is to develop synthesis representation methods from a lower aggregated level (e.g., phenomena or tasks) than conventional unit operations to identify the most promising design configurations without a pre-postulation of plausible equipment or flowsheet [22, 23, 25]. This leads to a bottom-up representation hierarchy to enable flexible combination of phenomena for creation of innovative process solutions, as depicted in Fig. 1.2. The comparison of superstructure network formulation of phenomena-based synthesis and unit operation-based synthesis, in terms of the structural building blocks and representation accuracy, is illustrated in Fig. 1.3.

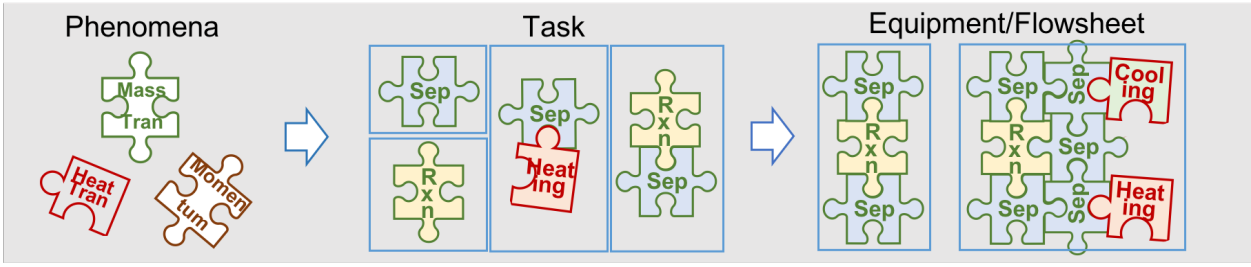


Figure 1.2: Phenomena-based representation of chemical process.

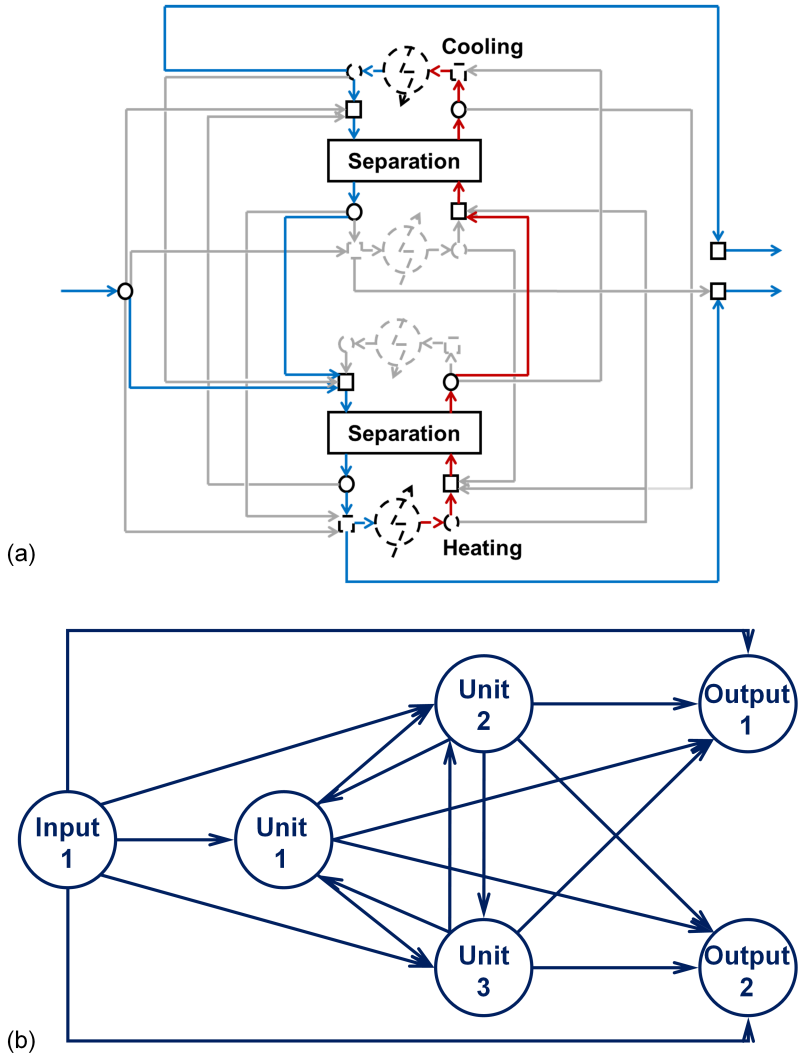


Figure 1.3: Superstructure network formulation –
(a) Phenomena-based synthesis for a binary distillation column,
(b) Unit operation-based synthesis for reaction-separation.

In this way, phenomena-based synthesis brings in the opportunity to *re-invent unit operations, or even flowsheets, without any pre-postulation of unit operation or flowsheet alternatives* for systematic innovation rather than merely based on engineering heuristics or trial-and-error. By using basic chemical phenomena as structural building blocks (e.g., mass transfer, heat transfer), it also allows to exploit the synergy between multi-functional phenomena (e.g., combined reactive/separation) and to de-bottleneck process performance by directly intensifying process fundamentals (e.g., shift chemical/physical equilibrium).

Several phenomena-based process intensification synthesis methods have been developed and demonstrated for the synthesis of various intensified systems, an indicative list of which is presented in Table 1.3. The first four methodologies in Table 1.3 aim to define chemical processes as an aggregation of physicochemical phenomena-based building blocks (e.g., reaction, mixing, phase transition). Through the "smart combination of tasks" [42], they particularly exploit PI opportunities via synergistic integration of multiple tasks into a single process step. However, as these building blocks are still defined implicitly based on unit operations (conventional units or emerging ones), a sufficiently large set of plausible tasks needs to be pre-defined, together with all possible interconnections, to fully capture the PI design space, which may lead to a combinatorial explosion in the resulting model formulation. Moreover, after obtaining the optimal flowsheet configuration based on phenomenological representation, a further step needs to be taken for the identification of corresponding (intensified) equipment-based flowsheet. Skiborowski and co-workers presented a step-wise procedure for the translation and validation between phenomena-based building blocks and rigorous steady-state equipment-based simulation for (reactive) distillation systems [43, 44]. Nevertheless, the development of systematic identification approaches, which can verify the feasibility and optimality of phenomena-based configurations to arrive at practical unit-operation-based flowsheets without discarding the potential for discovering brand new equipment, is still a subject of ongoing research.

In addition to the combination of tasks, several methods take advantage of the "ultimate" thermodynamic space to determine the maximum potential of a process. Introduced by Pistikopoulos and co-workers, the Generalized Modular Representation Framework aims to discover novel intensified pathways by improving mass/heat transfer and/or shifting reaction equilibrium via the use of multi-functional mass/heat transfer modules [45]. The underlying phenomena (e.g., reaction and/or separation) in each module are characterized by the "driving force constraints" derived from Gibbs free energy change. For the design of intensified reaction systems, Sundmacher and co-workers proposed the elementary process functions to identify the optimal mass and energy flux profile in the state space [46, 47].

Table 1.3: Phenomena-based process intensification synthesis frameworks (Reprinted from [48]).

| **Author** | **Synthesis approach** | **Building block** | **Notes** |
|---|---|---|---|
| Gani & co-workers [49, 50] | Sustainable process synthesis-intensification framework | Phenomena building block (PBB) | Hierarchical approach |
| Manousiouthakis & co-workers [51, 52] | Infinite-DimEnsionAl state-space framework | Process operators & distribution network | State-space representation, Infinite Linear Programming |
| Skiborowski & co-workers [43, 44] | Optimization-based approach to process synthesis | Reactor-Network--PBB | State-space representation |
| Hasan & co-workers [53, 54] | Superstructure-based building block | Phenomenological building block | 2-D superstructure representation |
| Pistikopoulos & co-workers [45] | Generalized Modular Representation Framework | Multifunctional mass/heat exchange module | Superstructure-based optimization |
| Sundmacher & co-workers [46, 47] | Elementary process functions | Mass & Energy flux | Dynamic trajectory profile |

Functional materials (e.g., ionic liquids, zeolites) play a key role to drive innovation in chemical processes. Hence, material selection has also been incorporated in conceptual PI synthesis approaches. The choice of mass separating agents or reaction catalysts can be integrated with the existence of a set of phenomena building blocks. For example, in Tula et al. [50], the following combination of phenomena building blocks – PT(VV), i.e. phase transition (vapor-vapor) – suggested the adoption of membrane for vapor permeation PT(VV). In the 2-D superstructure representation approach presented in Demirel et al. [53], the existence (or not) of a functional material can be placed either in the interior of a building block (e.g., catalysis to make a reactive building block) or at the boundaries (e.g., barrier material between adjacent blocks to represent membrane separation). The candidate materials can be generally considered in two ways: (i) a set of enabling materials are pre-defined and their characteristic property data are directly supplied to the process model [53], (ii) property constraints are determined first based on optimization results or process feasibility checks, and the availability of desired material is then checked with available database [50] or synthesized via molecular design [55]. For the efficient screening through a large material

database, a multi-scale approach was developed for combined material selection at atomistic scale among 200 candidate zeolites and process optimization at macroscopic scale with the objective to reduce the overall cost of PSA-based separation systems [56].

The synthesis of periodically operated processes (e.g., temperature/pressure swing adsorption (TSA/PSA), simulated moving bed, which comprises an important category of PI applications for advanced reaction and/or separation, is implemented mostly at unit level described by differential-algebraic equation models. There are also ongoing attempts to derive such intrinsically dynamic process within a unified PI framework. Arora et al. [57] presented the GRAMS (Generalized Reaction-Adsorption Modeling and Simulation) platform for the simulation and optimization of periodic adsorption-reaction systems (e.g., PSA/TSA, sorption-enhanced reaction process) utilizing simulation-based grey-box method [58]. The pseudo-transient optimization framework, in which the original steady-state models are reformulated to statically equivalent DAE systems, was applied for the design of periodic processes (i.e., PSA, TSA) [59].

### 1.2.2 Operability, safety, and control analysis of PI systems

Practical implementation of any process cannot be possible if it is not operable and safe. Compared with conventional unit operations, intensified systems typically feature higher degree of task integration, less degrees of freedom, narrower operating windows, and faster process dynamics [60, 29]. In this context, the consideration of control, operability, and safety aspects at conceptual design stage becomes even more critical for intensified process systems.

*Process control in process intensification*

Baldea [61] has theoretically justified that the inputs from internal process streams (i.e., non-inlet and outlet streams to the process) were no longer available for control in intensified systems, thus causing the loss of degrees of freedom. Control studies of PI systems are performed mostly in a process-specific manner, closely related to the development of: (i) "high-fidelity" models to accurately describe process dynamics, (ii) model reduction techniques to reduce computational complexity while sufficiently capture process dynamics, and (iii) advanced model-based control

strategies [62, 63, 64]. It is worth noting that major research efforts in this area are oriented towards advanced model- and optimization-based control (particularly model predictive control, MPC), while conventional proportional–integral–derivative (PID) control is still the most widely applied in industrial practice [60]. MPC has been proved to provide superior control performance than PID control in a number of intensified and/or modular systems by accurately capturing their highly nonlinear behavior, complex dynamic characteristics, and strong variable interactions. Several case studies on MPC vs. PID control in intensified systems can be found in: PSA design and control optimization [65], control of semi-continuous multicolumn counter-current solvent gradient purification process [66], and methyl tert-butyl ether reactive distillation [67]. Extensive discussions on recent work in this area can be found in [10, 29].

*Process Operability and Flexibility in Process Intensification*

Operable processes can be synthesized by linear or nonlinear mapping among input and output sets [68]. Towards this direction, an operability-based analysis approach has recently been applied to the design of process intensification systems by Carrasco and Lima [69, 70]. They proposed a bilevel/parallel programming-based approach to simultaneously address process design constraints and process intensification targets using high-dimensional nonlinear process models. Motivated by the advent of the shale gas revolution, their proposed strategy was demonstrated on the design of a catalytic membrane reactor for direct methane aromatization as well as a natural gas combined cycle system for power generation, indicating potential footprint reduction and efficiency maximization via modular plant design.

Steady-state performance under varying conditions of process intensified and/or conventional systems can be effectively addressed by flexibility analysis [71, 72, 73]. Recently, Sudhoof et al. [74] suggested the use of a graphical "flexibility map" for the analysis of complex systems such as rotating packed beds for distillation, which illustrated the trade-off between cost objective, design parameters, and flexibility indicator in a spider web diagram.

*Process Safety in Process Intensification*

Classical safety evaluation methods (e.g., hazard and operability study) are often based on semi-heuristics and are employed as posterior evaluation tool after the implementation of detailed plant design. However, during the conceptual design stage, only very limited equipment (or plant) design and operating information is available for safety analysis. Current efforts include the application of Quantitative Risk Assessment for the inherently safer design of extractive distillation systems with simultaneous solvent selection [75]. Inherent safety indices provide another evaluation strategy using chemical properties and operating conditions [76]. An integrated methodology was introduced by Ortiz-Espinoza et al. [77] to select technology alternatives based on economics, environmental factors, and safety index assessment (i.e., Process Stream Index, Process Route Index). However, such safety analysis strategies typically focus on identifying the safety "hot spot" within a given unit operation-based flowsheet, while leaving synthesis decision at a "a posterior" stage. As an attempt to systematically address risk analysis within an optimization formulation, Nemet et al. [78] proposed a risk analysis approach which could be incorporated as a constraint in the synthesis model and demonstrated it with heat exchanger network synthesis. From a dynamic perspective, Albalawi et al. [79, 80] defined a safe operation region via a Safeness Index function integrated with economic model predictive control.

## 1.3 Research gaps and key challenges

Although the phenomena-based process synthesis representation methods clearly offer the potential to derive novel intensified systems, major research challenges remain open. One of the key challenges lies in the resulting combinatorial design space with possibly excessive computational load. For example, given a flowsheet consists of one PFR reactor and two succeeding distillation columns. Assume that the PFR can be represented with five reaction building blocks for consideration of axial distribution, and every distillation column consists of fifteen column trays each of which corresponds to a separation building block. The superstructure formulation expands from the originally three unit blocks (1 reactor + 2 distillation columns) to thirty-five building blocks

(5 reaction + 15×2 separation), which results in the explosion of binary variables for structural combinations and the nonlinearities for repetitively describing the same phenomena. If more detailed phenomena definition is used, such as phase separation and selective separation, the scale of the resulting synthesis problem grows even larger. To alleviate this disadvantage, the definition and mathematical description of phenomenological building blocks need to be physically and computationally compact. This observation also necessitates the effective incorporation of (multi-scale) driving force concepts [81, 82] or bounding strategies to tighten the search space (such as the attainable region-based method for reactor network synthesis [83, 84]).

Most synthesis frameworks for PI applications have typically focused on steady-state reaction/separation process systems. To the best of our knowledge, the systems investigated in open literature using phenomena-based synthesis are mostly conventional scale reactors, distillation systems (e.g., divided wall columns, reactive distillation columns), and membrane systems. Expanding the scope to other important classes of PI designs, especially those characterized by the significant enhancement of mass/heat transfer phenomena is essential (such as micro-reactors, rotating packed bed reactors, etc.) – especially if the degree of modularization is desired. Another open question lies on how to formally incorporate the temporal domain within the main building blocks/tasks of PI representation methods. Periodically operated systems often offer advantages from a PI view point compared to their conventional counterparts. Hence, the analogy of discretization of partial differential algebraic equations to both spatial and temporal domain [85] may offer a feasible and promising direction if computational issues can be equally addressed.

Operability concerns result from the violation of inequality process constraints during actual operation (under uncertainty and disturbances). Theoretical developments are necessitated to fully understand the unique operability characteristics in PI systems due to task-integration, equipment size reduction, alternative energy sources, etc. For example, the effects on degrees of freedom (DOF), process dynamics, operating window. Key open questions include but not limited to: (i) How does the loss of DOFs affect the operation of an intensified task-integrated process compared to its conventional process counterpart? (ii) For the role of process constraints, what is the differ-

ence between intensified vs. conventional processes? (iii) What is the trade-off between PI design numbering up vs. scaling up considering the gain or loss in cost efficiency vs. design/operation agileness? (v) Inspired by the periodic processes, is it possible to operate the process in a dynamic manner following an optimal trajectory (such as to minimize energy consumption)? etc.

In tandem with the theory development, model-based analysis approaches discussed in Chapter 1.2.2 should be tailored to address these operational challenges. Taking the seminal flexibility analysis [86] as an example, it requires a rigorous and sophisticated mathematical reformulation of the process model incorporating Karush-Kuhn-Tucker optimality conditions with detailed derivative information under the assumption of convexity. The application of such approaches to large-scale, nonconvex, and nonlinear process systems is challenging, which is mostly the case for PI systems. Moreover, operability metrics which can simultaneously assess multiple operational aspects of such systems are very limited (e.g., flexibility, operability, safety, controllability, availability, etc.).

The integration of operability and control metrics at an early PI design stage still poses a formidable challenge. The match of information between design approaches and operational analysis methods is important to integrate these decisions as early as possible and to provide a consistent estimation of operational performance throughout the multi-scale design procedure. In this context, operability analysis for the phenomena-based synthesis intensification is kind of challenging since the synthesis is done using abstract phenomena building blocks (e.g., reaction, separation) with no available equipment information (e.g., reactor, membrane). More suitable criteria for operability at this stage may include elements of flexibility [71] and structural controllability [87]. On the other hand, most existing process safety analysis approaches [75, 76, 77] typically require very detailed equipment or flowsheet information – which may not be readily available at the PI synthesis level. Therefore, a hierarchical step-wise framework to decompose the problem can be beneficial to integrate operability, safety, and dynamic control at different design stages.

From software tools point of view, to the best of our knowledge, currently there is no available commercial software which can: (i) generate novel conceptual process designs without prepostulation of equipment or flowsheet and account for process intensification opportunities, (ii)

provide tailored operability and control analysis approaches or metrics to PI systems operation, (iii) integrate operability analysis with design and synthesis tasks to deliver optimal process solutions with guaranteed operability performance, and (iv) supply readily developed PI model library consisting of process models and physical property models on a consistent basis.

However, attempts have been initiated from academia to develop software toolkits for computer-aided PI. ProCAFD [50], developed by Gani and co-workers as part of the ICAS tool set [88], supports flowsheet synthesis and design using process-groups to represent unit operations and following a hierarchical procedure to generate optimal process alternatives. More recently, the authors have published another toolkit, ProCACD [89], which enables controller design and integrated design-control. MIPSYN [90] and Pyosyn [91] are two notable software prototypes for process synthesis. MIPSYN is one of the pioneers to introduce synthesis capabilities into an algebraic modeling environment with custom modeling – note that so far there is no available commercial software supporting process synthesis activities. As part of the Department of Energy IDAES project [92], Pyosyn presents a newer synthesis framework using Generalized Disjunctive Programming model based in Python/Pyomo algebraic modeling platform.

To summarize the major gaps identified for computer-aided PI design and operation:

- Lack of PI synthesis approaches with compact physicochemical building block representation, which can efficiently screen the large design space and systematically generate a wide range of intensified designs

- Lack of operability, safety, and control analysis metrics which can accurately capture and quantitatively reflect PI operational characteristics

- Lack of a generally accepted methodology and/or 'protocol' which can integrate PI synthesis, operability, safety, and control to ensure the feasibility and optimality of the derived intensified structures during actual operation

- Lack of commercial software [or even a software prototype] – to fully support systematic PI with operability, safety, and control

## 1.4 Thesis objectives and outline

To address some of the above challenges, we propose a holistic framework to fully integrate process intensification synthesis, operability analysis, and control optimization. The following research objectives are defined (Fig. 1.4):

**Objective 1: To develop a phenomena-based modular representation approach for process intensification synthesis**

The Generalized Modular Representation Framework (GMF) is applied in this work towards a unified strategy for the synthesis of PI systems. In addition to extend GMF for representation of diverse PI systems (reactive separation, dividing wall column, etc.), we aim to explore the following research questions: (i) how to systematically synergize multi-functional phenomena – taking reaction and separation as an example – without pre-postulation of tasks? (ii) how to benchmark intensified designs with the ultimate thermodynamic or kinetics bounds? (iii) how to encapsulate intensified designs and their conventional counterparts in a unified synthesis representation and to identify when intensified designs will outperform in terms of economics, energy savings, etc.? and (iv) What is the role of materials in process intensification?

**Objective 2: To integrate model-based flexibility and safety analysis into process intensification synthesis to systematically generate steady-state optimal and operable designs**

We aim to address two research questions: (i) what are the unique operational challenges and needs resulted by PI (e.g., task-integration, periodic operation)? and (ii) how to integrate operability analysis at early design stage? To explore the first question, we perform rigorous model-based analyses to compare the degrees of freedom, role of process constraints, numbering up vs. scaling up for a reactive distillation system vs. a sequential reactor-distillation system. To highlight the importance of considering operability criteria in the design of intensified systems, we propose an integrated GMF-flexibility-safety synthesis approach that enables the automated generation of safely operable PI systems from phenomena level. The results have shown that operability considerations may result in significant structural and operating changes of the process optimal solutions.

**Objective 3: To develop a systematic framework for the synthesis of operable process intensification systems accounting for both steady-state design and dynamic operation**

We propose a step-wise framework which synergizes: (i) phenomena-based process synthesis with GMF to derive novel intensified design configurations, (ii) flexibility analysis to accommodate process uncertainty, (iii) risk analysis to evaluate inherent safety for both steady-state and dynamic design, (iv) explicit/multi-parametric model predictive control following the PAROC (PARametric Optimisation and Control) framework to ensure dynamic operation under uncertainty, and (v) simultaneous design and control via dynamic optimization to close the loop for the design of verifiable, operable, and optimal intensified systems. Multiple process solutions can be generated to showcase the trade-offs between economic and operational performances.

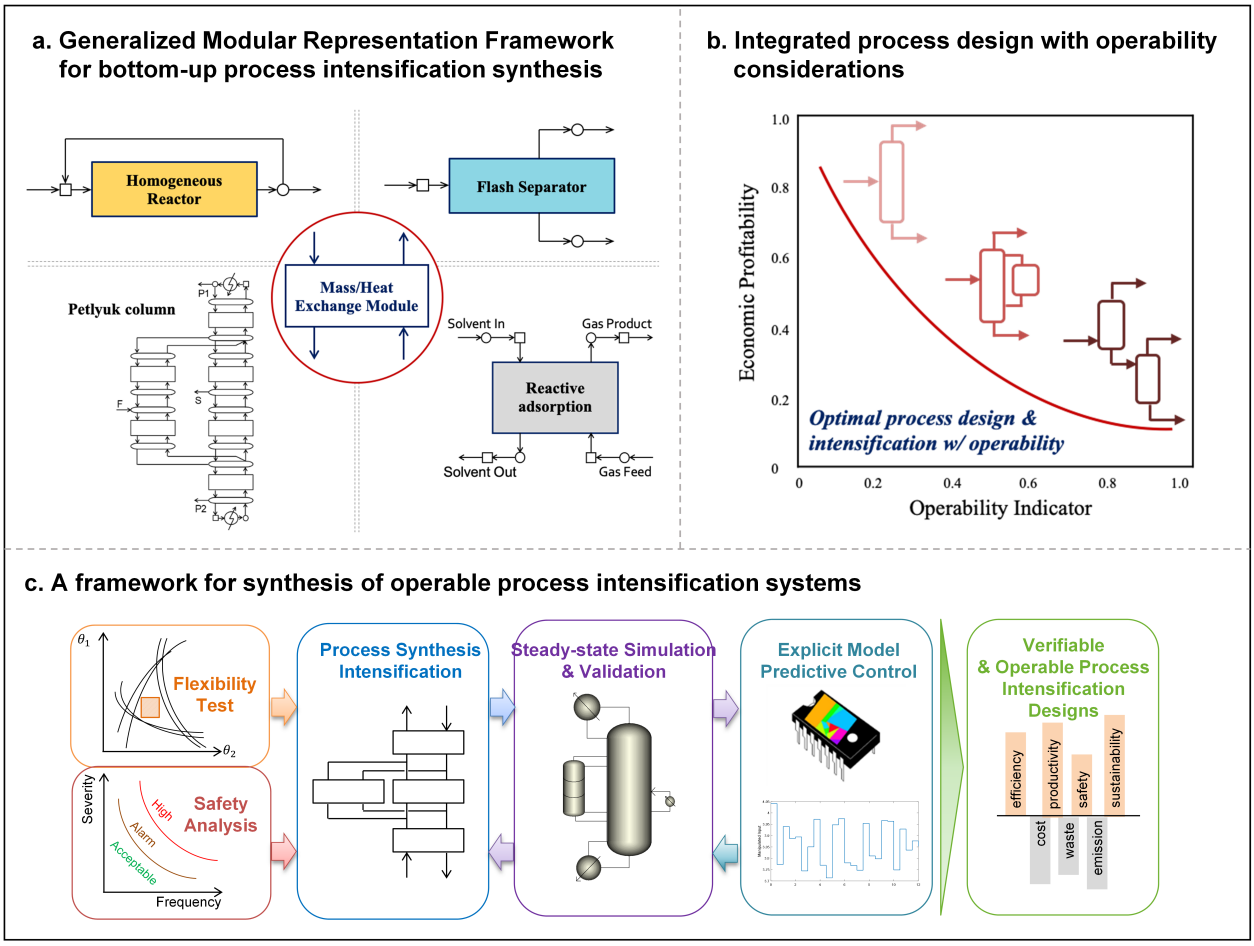


Figure 1.4: An overview of the proposed thesis work.

The thesis is organized as follows: Chapter 2 introduces the Generalized Modular Representation Framework for process intensification synthesis, which lays the foundation for this thesis to drive innovation. We discuss in detail the mass/heat exchange modular representation concepts, the key GMF synthesis features, and the driving force constraints based on total Gibbs free energy change. We then present the full mathematical model formulation for GMF synthesis as a mixed-integer nonlinear programming problem and the tailored solution strategy. Extension of GMF with orthogonal collocation is also detailed.

Chapter 3 integrates GMF with attainable region-based theory to develop an envelope of design solutions for reaction/separation systems. The Continuous Flow Stirred Tank Reactor Equivalence Principle, based on reaction attainable region theory, is applied to characterize design boundaries for a given chemistry independent of process design. GMF is then employed to generate candidate process alternatives along the design boundaries. The proposed approach is showcased via a case study on olefin metathesis. We also highlight the need to incorporate the attainable region-based constraints into synthesis strategies to assist effective bounding of the PI design space.

Chapter 4 extends GMF to synthesize heterogeneous multi-component separation systems, with particular interest in exploring the use of dividing wall columns. Leveraging the GMF superstructure-based representation, conventional or novel process structures, such as two-column sequences and dividing wall columns, can be systematically generated without pre-postulation of equipment design. The applicability and versatility of the proposed approach is showcased via an industrial case study on methyl methacrylate purification by Dow Global Technologies. Two new dividing wall column designs are obtained, both of which can achieve equipment size reduction and substantial energy savings compared to the original patent design.

Chapter 5 presents a systematic approach for solvent selection and process intensification synthesis based on GMF. Material selection is achieved by incorporating physical property models (e.g., NRTL) in GMF model formulation to describe the nonideal liquid mixture behaviors and to assess solvent performance in facilitating separation. In this context, solvent selection and process synthesis intensification are simultaneously addressed within a superstructure-based optimization

formulation. The proposed approach is demonstrated on two case studies for ethanol-water extractive separation, with two sets of solvents evaluated: (i) ethylene glycol vs. methanol to obtain 99 mol% ethanol, and (ii) ethylene glycol vs. 1-ethyl-3-methyl-imidazolium acetate ([EMIM][OAc]) to obtain 99.8 mol% ethanol and 99 mol% water.

Chapter 6 proposes an integrated approach to synthesize PI systems with guaranteed flexibility and safety performances. To ensure that the designs can be operated under a specified range of uncertain parameters, a multiperiod GMF representation is developed based on the critical operating conditions identified by flexibility test. Risk analysis, accounting for equipment failure frequency and consequence severity, is incorporated as constraints into this synthesis model to derive inherently safer designs. We demonstrate the proposed approach through a case study for the production of methyl tert-butyl ether. The solutions indicate that operability considerations may result in significant structure changes of the process optimal solution, which emphasizes the need of operability analysis during the early design stage rather than posterior evaluation.

Chapter 7 performs rigorous model-based analyses towards a fundamental understanding of operability, safety, and control challenges in process intensification and modular designs. We first investigate the impact of key design and operation factors including: (i) degrees of freedom, (ii) process constraints, and (iii) numbering up vs. scaling up. Comparative examples are presented to showcase the pros and cons in intensified and modular systems versus their conventional counterparts from operability and control aspects. A comparative study on inherent safety metrics in reactive distillation process is then presented to stress the need for new safety metrics at early design stage. Based on the observations, we highlight the need to develop a holistic strategy towards the full integration of process intensification, operation, and control.

Chapter 8 extends the above synthesis and operability developments to a systematic framework accounting for both steady-state design and dynamic operational optimization. A step-wise procedure is outlined which synergizes: (i) phenomena-based process synthesis with GMF to derive novel intensified design configurations, (ii) flexibility and risk analysis for evaluation of operability and inherent safety performances at conceptual design stage, (iii) simultaneous design and

explicit/multi-parametric model predictive control optimization following the PAROC (PARametric Optimisation and Control) framework to close the loop for the design of verifiable, operable, and optimal intensified systems. The proposed framework is showcased through: (i) a heat exchange network synthesis case study, and (ii) a methyl tert-butyl ether production case study. It has been demonstrated that the proposed approach can systematically integrate design and operability considerations at different stages and lead to the design of operable PI systems.

Chapter 9 concludes this thesis by highlighting the original contributions of this work and proposing future research directions.

# 2. GENERALIZED MODULAR REPRESENTATION FRAMEWORK FOR PROCESS INTENSIFICATION SYNTHESIS[†]

As discussed in Chapter 1.2.1, process synthesis can provide systematic approaches for the discovery of novel intensified designs by synergizing multifunctional phenomena to boost process improvements. However, key research questions remain on: (i) how to define the driving forces to intensify process schemes? (ii) how to systematically derive process solutions which fully exploit intensification opportunities? and (iii) how to explore the combinatorial PI design space in a computationally efficient way?

In this chapter, we introduce a systematic approach for process intensification synthesis based on the Generalized Modular Representation Framework (GMF). Herein, the chemical processes are represented as aggregated pure heat exchange modules and multi-functional mass/heat exchange modules, with which conventional or novel process solutions can be generated without a pre-postulation of equipment or flowsheet configurations. Driving force constraints, derived from total Gibbs free energy change, are employed to characterize mass/heat transfer feasibility from thermodynamic perspective, thus resulting in a more compact modular representation of the chemical systems. Mass and/or heat integration are simultaneously addressed in the superstructure representation of the modular network, without pre-postulation of steam properties. The resulting synthesis problem is formulated as a mixed-integer nonlinear optimization problem.

## 2.1 Mass/Heat exchange modular representation

Originally proposed by Papalexandri and Pistikopoulos [81], GMF is built on the idea that most process operations can be characterized by a set of mass- and heat- transfer phenomena, concerning mainly the mass transfer of one component from one phase to another (e.g., separation) or from one substance to another (e.g., reaction) due to the difference in their chemical potential. In this

[†]Reproduced in part with permission from Tian, Y., & Pistikopoulos, E. N. (2018). Synthesis of operable process intensification systems – Steady-state design with safety and operability considerations. Industrial & Engineering Chemistry Research, 58(15), 6049-6068. Copyright 2018 American Chemical Society.

context, two types of building blocks are utilized in GMF to represent chemical processes as shown in Fig. 2.1, namely:

- *Pure heat exchange module (HE)* – where the participating streams do not come into mass active contact but only perform heat exchange driven by temperature gradient;
- *Mass/Heat exchange module (M/H)* – where mass and heat transfer take place between two contacting streams. The mass transfer feasibility within this type of module is ensured by imposing the driving force constraints derived based on the change of total Gibbs free energy.

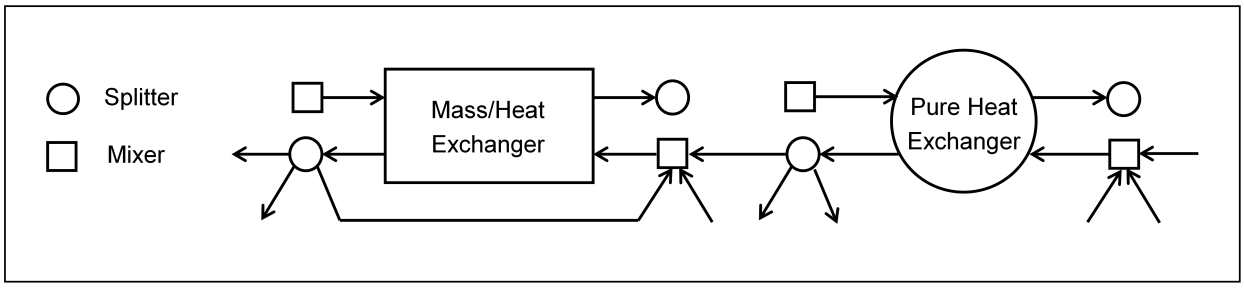


Figure 2.1: Mass/Heat exchange module and pure heat exchange module (Reprinted from [48]).

Using these modular building blocks with higher level of abstraction, GMF provides a generic strategy to overcome process bottlenecks by directly improving mass/heat transfer and/or shifting reaction equilibrium, thus readily to discover novel intensified pathways without pre-postulation of plausible units/flowsheets. Meanwhile, GMF generates optimization model with compact size from lower-aggregated phenomena level while avoiding the use of potentially limiting simplifying assumptions (e.g., physical/chemical equilibrium). A detailed comparison can be found in Proios and Pistikopoulos [93] on the model statistics between GMF model and rigorous stage-wise model for binary distillation optimization. As illustrated in Fig. 2.2, so far GMF has been mostly applied to chemical systems where conventional mass/heat transfer is taking place (e.g., distillation, absorption, etc.), simultaneously with nonideal mixture properties (e.g., azeotropes), hybrid reaction/separation scheme, heat integration, etc. A number of intensified systems have been synthesized using GMF including reactive distillation [94], reactive absorption [95], homogeneous azeotropic separation [96], and heat-integrated distillation [97].

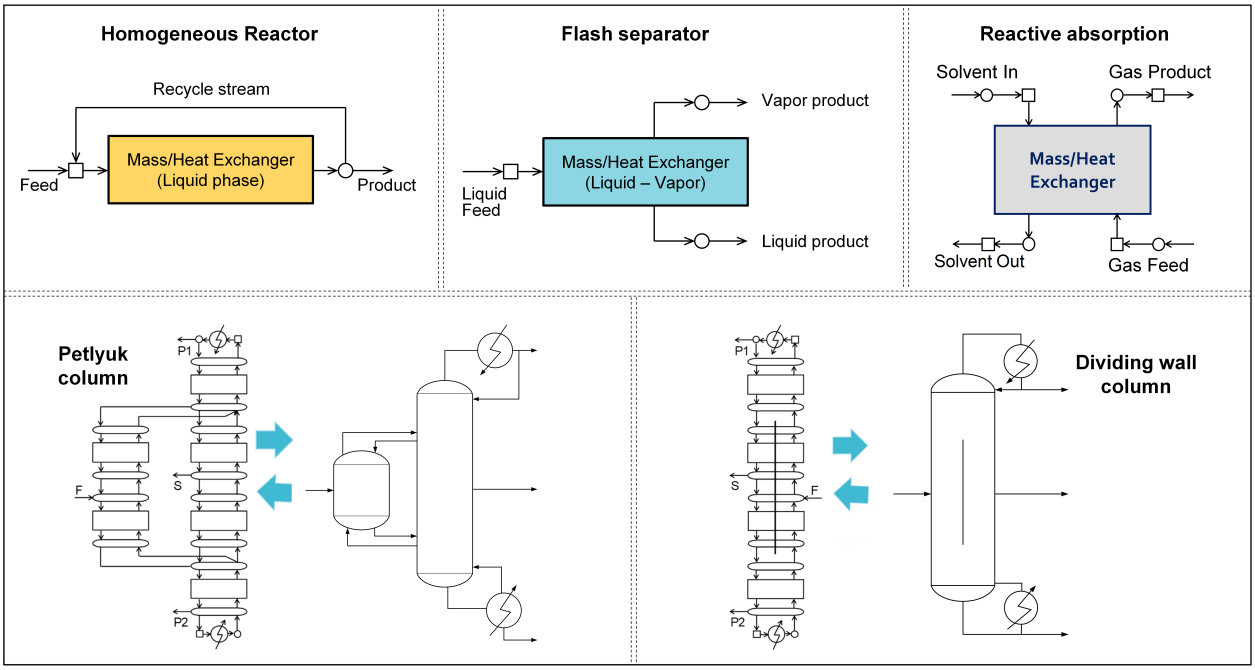


Figure 2.2: GMF modular representation examples.

## 2.2 Driving force constraints

The root of GMF representation lies in how to appropriately define the driving force constraints to characterize the mass transfer feasibility in a M/H module. As developed in Ismail et al. [94], the driving force constraints are derived from the change of total Gibbs free energy. However, different forms of driving force constraints are used for separation, reaction, and combined separation/reaction modules. Thus in the synthesis model, a set of separation modules, a set of separation/reaction modules, and a set of reaction modules are defined separately. In this work, we revisit the development of driving force constraints from thermodynamic point of view [94] and show that a unified form of driving force constraints can be obtained to systematically identify necessary reaction or separation tasks without any pre-postulation.

Considering a most generic M/H module containing multicomponent liquid-vapor mixture, if constant temperature and pressure are assumed, mass transfer between inlet streams can occur

when the total Gibbs free energy $(nG)^{tot}$ is decreasing, namely:

$$d(nG)^{tot}_{T,P} \leq 0 \tag{2.1}$$

To assist the expression of this decreasing trend, $dn_i^L$ is introduced to describe the mole amount changes of component $i$ in the liquid inlet and outlet streams as a result of reaction and/or separation taking place in the module:

$$dn_i^L = f^{LO}x_i^{LO} - f^{LI}x_i^{LI} \tag{2.2}$$

Thus Eq. 2.1 is consistent with the following "driving force constraints":

$$G1_i \times G2_i \leq 0, \qquad \forall i = 1, ..., NC \tag{2.3}$$

where

$$G1_i = dn_i^L = f^{LO}x_i^{LO} - f^{LI}x_i^{LI} \tag{2.4}$$

$$G2_i = \Big[\frac{\partial(nG)^{tot}}{\partial(n_i^L)}\Big]_{T,P} \tag{2.5}$$

Before proceeding with the expansion of $G2_i$ term, several notes can be made here: (i) the driving force constraints characterize the mass transfer feasibility by a decreasing total Gibbs free energy rather than the minimization of Gibbs free energy, thus it does not enforce kinetic and/or physical equilibrium to be reached; (ii) $G2_i$ can be used to indicate how far the component is from its kinetic and/or physical equilibrium state. The illustration of these features will be addressed in the following chapters through the case studies.

To describe the numerator in $G2_i$: the general form of total Gibbs free energy for systems with T, P as the independent variable is given by

$$d(nG)^{tot} = -(nS)dT + (nV)dP + \sum_i \mu_i dn_i \tag{2.6}$$

With an assumption of constant $T$ and $P$,

$$d(nG)^{tot}_{T,P} = \sum_i \mu_i dn_i = \sum_i (\mu_i^L dn_i^L + \mu_i^V dn_i^V) \tag{2.7}$$

Consider the mass conservation for each component in this module containing multicomponent liquid-vapor mixture with $k$ reactions taking place:

$$n_i^L + n_i^V = n_i^0 + \sum_k \nu_{ik}\epsilon_k \tag{2.8}$$

where $n_i^0$ denotes the initial number of moles for each component, $\nu_{ik}$ is the stoichiometric coefficient for each component $i$ in reaction $k$, and $\epsilon$ is the extent of reaction $k$ in this module determined by reaction rate, catalyst mass, etc. Differentiation of Eq. 2.8 gives:

$$\begin{aligned} dn_i^L + dn_i^V &= \sum_k \nu_{ik} d\epsilon_k \\ dn_i^V &= -dn_i^L + \sum_k \nu_{ik} d\epsilon_k \end{aligned} \tag{2.9}$$

Eq. 2.7 can be reformulated as:

$$\begin{aligned} d(nG)^{tot}_{T,P} &= \sum_i \mu_i^L dn_i^L + \sum_i \mu_i^V (-dn_i^L + \sum_k \nu_{ik} d\epsilon_k) \\ &= \sum_i (\mu_i^L - \mu_i^V) dn_i^L + \sum_i \sum_k \nu_{ik} \mu_i^V d\epsilon_k \end{aligned} \tag{2.10}$$

Thus, if approximating $\partial \mu_i / \partial n_i^L$ to be 0,

$$G2_i = \Big[\frac{\partial (nG)^{tot}}{\partial (n_i^L)}\Big]_{T,P} = \mu_i^L - \mu_i^V + \sum_i \sum_k \nu_{ik} \mu_i^V \frac{\partial \epsilon_k}{\partial n_i^L} \tag{2.11}$$

Note that $\frac{\partial \epsilon_k}{\partial n_i^L}$ needs to be analytically derived for each reaction (see Ismail et al. [94] for illustration

examples). Substituting with the following expression for chemical potential:

$$\begin{aligned} \mu_i^L &= \Delta G_i^f + RT\ln(\gamma_i^L x_i^L P_i^{sat,L}) \\ \mu_i^V &= \Delta G_i^f + RT\ln(\phi_i^V x_i^V P_{tot}) \end{aligned} \tag{2.12}$$

where $\Delta G_i^f$ is the standard Gibbs function of formation of $i$ from its elements at $T$ and 1 atm. $G2_i$ is then expanded as:

$$G2_i = RT[\ln(\gamma_i^L x_i^L P_i^{sat,L}) - \ln(\phi_i^V x_i^V P_{tot})] + \sum_i \sum_k \nu_{ik} \Big[\Delta G_i^f + RT\ln(\phi_i^V x_i^V P_{tot})\Big] \frac{\partial \epsilon_k}{\partial n_i^L} \tag{2.13}$$

Divided by $RT$ which will not affect the sign of this term, the expression used for Eq. 2.3, i.e. the driving force constraints, can be obtained:

$$G2_i = \ln\Big[\frac{\gamma_i^L x_i^L P_i^{sat,L}}{\phi_i^V x_i^V P_{tot}}\Big] + \sum_i \sum_k \Big[\frac{\nu_{ik}\Delta G_i^f}{RT} + \nu_{ik}\ln(\phi_i^V x_i^V P_{tot})\Big] \frac{\partial \epsilon_k}{\partial n_i^L} \tag{2.14}$$

### 2.3 Key features of GMF synthesis

We would like to highlight the following key points on the GMF driving force constraints and modeling capability, which enable GMF to leverage phenomena-based PI synthesis but to overcome potential computational disadvantages:

- **Systematic identification of reaction and/or separation tasks from heat and/or mass transfer phenomena**

  As can be noted, $G2_i$ comprises two components:

  i separation component: $\ln\Big[\frac{\gamma_i^L x_i^L P_i^{sat,L}}{\phi_i^V x_i^V P_{tot}}\Big]$

  ii reaction component: $\sum_i \sum_k \Big[\frac{\nu_{ik}\Delta G_i^f}{RT} + \nu_{ik}\ln(\phi_i^V x_i^V P_{tot})\Big] \frac{\partial \epsilon_k}{\partial n_i^L}$

  If a pure separation or pure reaction process is of interest (as in Sections 4 and 5), the corresponding $G2_i$ separation or reaction formulations can be used without losing generality.

However, for a hybrid reaction/separation system (as in Sections 3 and 6), a key question is how to dictate the identity of a M/H module to perform pure separation task, pure reaction task, or reactive separation task. To this purpose, we introduce two sets of binary variables to denote the existence of separation and reaction phenomena in each M/H module, i.e. $y_{sep}$ and $y_{rxn}$. If $y_{sep} = 1$ then separation takes place; similarly $y_{rxn} = 1$ indicates the existence of reaction (otherwise the binary variables take the value of 0). If both $y_{sep} = 1$ and $y_{rxn} = 1$, the M/H module undertakes combined reaction and separation task.

Through the following big M constraints, reaction and/or separation phenomena can be systematically activated or deactivated in each M/H module without pre-postulation of reaction, separation, reactive separation tasks:

$$\begin{aligned} &- My_{sep} \leq \ln\Big[\frac{\gamma_i^L x_i^L P_i^{sat,L}}{\phi_i^V x_i^V P_{tot}}\Big] \leq My_{sep} \\ &- My_{rxn} \leq \sum_i \sum_k \Big[\frac{\nu_{ik}\Delta G_i^f}{RT} + \nu_{ik}\ln(\phi_i^V x_i^V P_{tot})\Big]\frac{\partial \epsilon_k}{\partial n_i^L} \leq My_{rxn} \end{aligned} \tag{2.15}$$

This formulation of $G2_i$ with assistance of binary variables gives consistent driving force constraints as presented in Ismail et al. [94]. However, in earlier works [94], feasible mass transfer in a pure separation module is ensured by constraining its adjacent streams on both sides of the module, while mass transfer feasibility is only checked at the liquid outlet side for a reaction (and separation) module. With Eq. 2.15, feasible mass transfer can only be ensured at the liquid outlet side of a M/H module, regardless that the module is for separation, reaction, or hybrid. We will show later through the case studies that the "reduced" driving force constraints are still able to correctly characterize the mass transfer behaviors in a M/H module, and a steady-state validation step will be used to verify the overall feasibility of a GMF-based flowsheet.

- **Automated characterization of equilibrium or non-equilibrium tasks**

Note that the driving force constraints are derived based on $d(nG)^{tot}_{T,P} \leq 0$ for feasible mass

transfer, rather than $d(nG)^{tot}_{T,P} = 0$ to reach the equilibrium state. In other words, no physical or chemical equilibrium is enforced in GMF synthesis representation. Thus equilibrium-limited tasks ($G1_i \times G2_i = 0$) or non-equilibrium tasks ($G1_i \times G2_i < 0$) will be identified as per process inherent characteristics or as per optimization results.

- **Enabling selection of functional materials within process tasks**

  Material selection is achieved in GMF by utilizing rigorous thermodynamic models (e.g., NRTL, Redlich-Kwong-Soave equation) for calculation of phase equilibrium parameters (e.g., liquid activity coefficient $\gamma_i$, vapor fugacity coefficient $\phi_i$) to describe the nonideal mixture properties, as well as by using rigorous reaction kinetics expression (e.g., reaction rate $r_k$) to capture the impact of catalysts.

- **Compact/Aggregated representation to avoid combinatorial explosion**

  Another key question is what dictates the number of M/H exchange modules necessitated for each system representation. Actually, each M/H module is characterized by a certain mass transfer pattern (e.g., component A transfers from liquid phase to vapor phase, while components B & C from vapor to liquid). If component A transfers from liquid phase to vapor phase, or is consumed by liquid phase reaction, the number of moles of component A in the liquid streams of the M/H module is decreasing, i.e.

$$G1_A = f^{LO}x_A^{LO} - f^{LI}x_A^{LI} \leq 0 \tag{2.16}$$

The driving force constraints require $G1_A \times G2_A \leq 0$. Therefore, as a function of module temperature, pressure, and compositions – which are optimization variables to be determined – $G2_A$ should satisfy:

$$G2_A = \ln\Big[\frac{\gamma_A^L x_A^L P_A^{\text{sat},L}}{\phi_A^V x_A^V P_{tot}}\Big] + \sum_A \sum_k \Big[\frac{\nu_{Ak}\Delta G_A^f}{RT} + \nu_{Ak}\ln(\phi_A^V x_A^V P_{tot})\Big]\frac{\partial \epsilon_k}{\partial n_A^L} \geq 0 \tag{2.17}$$

Similarly, if A is transferred from vapor to liquid, or is produced by liquid phase reaction:

$$G1_A = f^{LO}x_A^{LO} - f^{LI}x_A^{LI} \geq 0 \tag{2.18}$$

$$G2_A = \ln\Big[\frac{\gamma_A^L x_A^L P_A^{\text{sat},L}}{\phi_A^V x_A^V P_{tot}}\Big] + \sum_A \sum_k \Big[\frac{\nu_{Ak}\Delta G_A^f}{RT} + \nu_{Ak}\ln(\phi_A^V x_A^V P_{tot})\Big]\frac{\partial \epsilon_k}{\partial n_A^L} \leq 0 \tag{2.19}$$

In this context, taking distillation column representation as an example, each M/H module identifies an aggregation of column trays, or in other words a column section (i.e. portion of a column not interrupted by entering or exiting streams or heat flows). In another reactive absorption example by Algusane et al. [95], GMF is applied, coupled with orthogonal collocation techniques, to synthesize a 70-stage absorption column with two M/H modules. Thus, due to this aggregated representation capability benefited from Gibbs free energy based driving force constraints, the GMF synthesis optimization problem is in a more compact size avoiding combinatorial explosion.

## 2.4 GMF mathematical model formulation

### 2.4.1 Problem statement

The generalized synthesis problem addressed in this section is defined in what follows:

*Given:*

- A set of process streams to be used as raw materials with given composition (their flowrates and supply temperatures can be either given or incorporated as optimization variables);
- A set of desired products and specifications on their flowrates, temperatures, and/or purities;
- A set of available heating/cooling utilities such as steam and cooling water with their availability, supply temperatures, and compositions;
- A set of available mass utilities such as mass separating agents (e.g., solvent, adsorbent) and reaction catalysts;

- All reaction schemes and kinetics data;
- All physical property models;
- Cost data of feeds, mass and heat utilities, and equipment.

The *objective* is to synthesize an optimal process solution, consisting of conventional or intensified unit operations, which is able to satisfy the afore-defined product specifications. The optimality of the solution can be evaluated with respect to economic performances (e.g., operating cost or total annualized cost). Other process performance criterion can also be readily incorporated into this problem formulation, taking the minimization of energy usage or carbon footprint as examples.

### 2.4.2 Synthesis model

In this representation approach, each stream is defined by its phase (i.e., liquid, vapor), while no lean or rich stream properties are pre-postulated for mass change and no hot or cold steam properties for heat exchange. The GMF superstructure utilizes mass/heat exchange modules and pure heat exchange modules as basic building blocks (Fig. 2.1). For simplification purposes in this work, no stream heat integration is considered, and each mass/heat exchange module is explicitly connected to two utility heat exchange modules [96], as shown in Fig. 2.3. However, heat integration can be systematically addressed within GMF, as demonstrated in Proios et al. [97]. To allow for all possible interconnections within the superstructure, auxiliary mixers and splitters are assigned to these modules at their inlet and outlet streams, respectively. An assumption is made that no phase change is allowed at mixers or splitters. An example of GMF full superstructure network and one of its structural variants is given in Fig. 2.4.

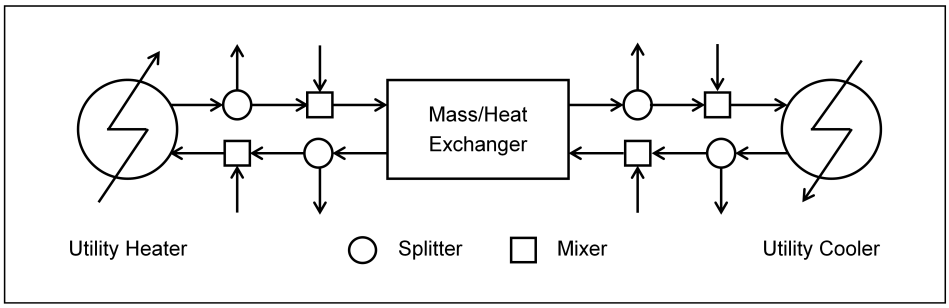


Figure 2.3: GMF modular building blocks (Reprinted from [48]).

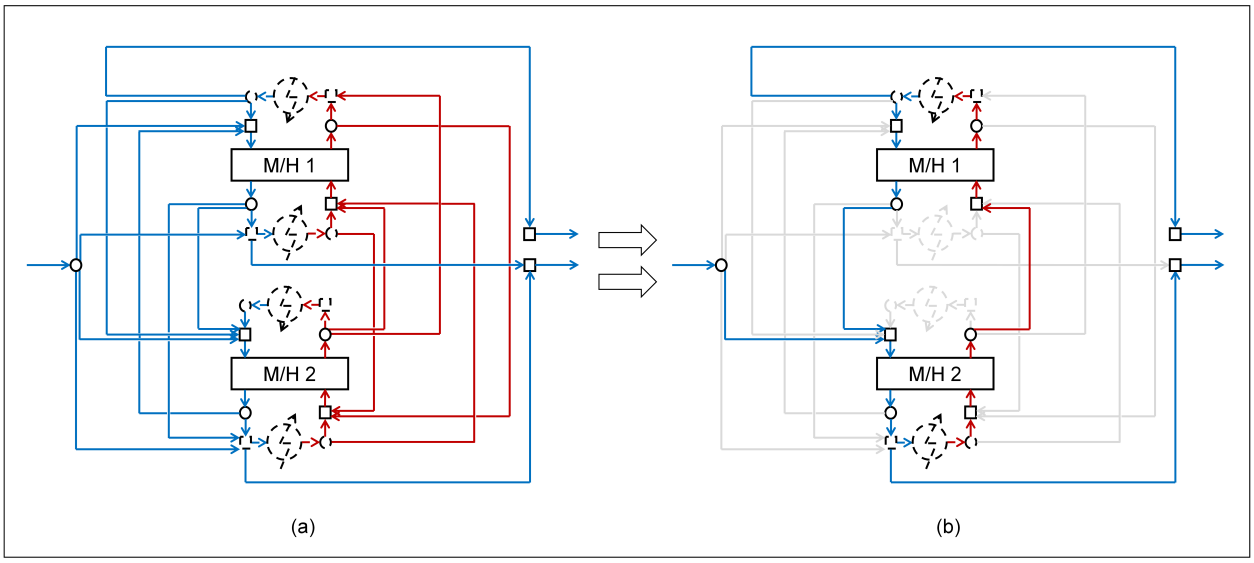


Figure 2.4: GMF superstructure network – (a) Full superstructure network, (b) Structural connections activated or deactivated by binary variables.

The following sets are defined for the GMF superstructure:

$C$ $= \{c \mid \text{components}\}$

$I$ $= \{n \mid \text{available feeds}\}$

$P$ $= \{p \mid \text{product streams}\}$

$E$ $= \{e \mid \text{available M/H modules}\}$

$LI_e$ $= \{s \mid \text{liquid inlet stream in module } e\}$

$LO_e$ $= \{s \mid \text{liquid outlet stream in module } e\}$

$VI_e$ $= \{s \mid$ vapor inlet stream in module $e\}$

$VO_e$ $= \{s \mid$ vapor outlet stream in module $e\}$

$HI_e$ $= \{s \mid$ inlet stream in utility heater of module $e\}$

$HO_e$ $= \{s \mid$ outlet stream in utility heater of module $e\}$

$CI_e$ $= \{s \mid$ inlet stream in utility cooler of module $e\}$

$CO_e$ $= \{s \mid$ outlet stream in utility cooler of module $e\}$

$LL_{e,e'}$ $= \{s \mid$ interconnecting stream from liquid outlet splitter of $e$ to liquid inlet mixer of $e'\}$

$LH_{e,e'}$ $= \{s \mid$ interconnecting stream from liquid outlet splitter of $e$ to utility heater of $e'\}$

$LC_{e,e'}$ $= \{s \mid$ interconnecting stream from liquid outlet splitter of $e$ to utility cooler of $e'\}$

$LP_{e,p}$ $= \{s \mid$ interconnecting stream from liquid outlet splitter of $e$ to final mixer of product $p\}$

$VV_{e,e'}$ $= \{s \mid$ interconnecting stream from vapor outlet splitter of $e$ to vapor inlet mixer of $e'\}$

$VC_{e,e'}$ $= \{s \mid$ interconnecting stream from vapor outlet splitter of $e$ to utility cooler of $e'\}$

$VP_{e,p}$ $= \{s \mid$ interconnecting stream from vapor outlet splitter of $e$ to final mixer of product $p\}$

$IL_{n,e}$ $= \{s \mid$ interconnecting stream from initial stream $n$ to liquid inlet mixer of $e\}$

$IV_{n,e}$ $= \{s \mid$ interconnecting stream from initial stream $n$ to vapor inlet mixer of $e\}$

$IH_{n,e}$ $= \{s \mid$ interconnecting stream from initial stream $n$ to utility heater of $e\}$

$IC_{n,e}$ $= \{s \mid$ interconnecting stream from initial stream $n$ to utility cooler of $e\}$

$IP_{n,p}$ $= \{s \mid$ interconnecting stream from initial stream $n$ to final mixer of product $p\}$

$HL_{e,e'}$ $= \{s \mid$ interconnecting stream from utility heater of $e$ to liquid inlet mixer of $e'\}$

$HV_{e,e'}$ $= \{s \mid$ interconnecting stream from utility heater of $e$ to vapor inlet mixer of $e'\}$

$HP_{e,p}$ $= \{s \mid$ interconnecting stream from utility heater of $e$ to final mixer of product $p\}$

$CL_{e,e'}$ $= \{s \mid$ interconnecting stream from utility cooler of $e$ to liquid inlet mixer of $e'\}$

$CP_{e,p}$ $= \{s \mid$ interconnecting stream from utility cooler of $e$ to final mixer of product $p\}$

Available feed streams and product streams can be further classified as per their phase states:

$$I = N^{\text{liq}} \cup N^{\text{vap}}$$

$$P = P^{\text{liq}} \cup P^{\text{vap}}$$

Binary variables are introduced to denote the existence (or not) of each module ($y_e$), the existence (or not) of reaction or separation task in each module($y_{rxn}, y_{sep}$), as well as the existence (or not) of process streams (Table 2.1). However, the binary variables for process streams are not necessary, but will facilitate the formulation of structural model and simplify the solution of this mixed-integer nonlinear programming (MINLP) problem.

The resulting mathematical model comprises: (i) a physical model to represent the physical phenomena taking place in each module (with mass and energy balances, mass transfer driving force constraints, phase defining constraints, etc.), (ii) a structural model to generate structural alternatives (with logical constraints), and (iii) an objective function to evaluate optimality [94].

1. **Physical model**

   (A) Mass balances for total stream flows at

   - initial stream splitters

$$f_n^I - \sum_e f_{ne}^{IL} - \sum_e f_{ne}^{IH} - \sum_e f_{ne}^{IC} - \sum_{p \in P^{liq}} f_{np}^{IP} = 0 \qquad \forall n \in N^{liq} \tag{2.20}$$

$$f_n^I - \sum_e f_{ne}^{IV} - \sum_e f_{ne}^{IC} - \sum_{p \in P^{vap}} f_{np}^{IP} = 0 \qquad \forall n \in N^{vap} \tag{2.21}$$

   - splitters at the outlets of each side of module $e$

$$f_e^{LO} - \sum_{e'} (f_{ee'}^{LL} + f_{ee'}^{LH} + f_{ee'}^{LC}) - \sum_{p \in P^{liq}} f_{ep}^{LP} = 0 \tag{2.22}$$

$$f_e^{VO} - \sum_{e'} (f_{ee'}^{VV} + f_{ee'}^{VC}) - \sum_{p \in P^{vap}} f_{ep}^{VP} = 0 \tag{2.23}$$

Table 2.1: GMF binary variables for process streams (Reprinted from [48]).

| **Variable** | **To define the existence of** |
|---|---|
| $yh_e$ | utility heater of module $e$ |
| $yc_e$ | utility cooler of module $e$ |
| $yll_{ee'}$ | interconnecting stream from liquid outlet splitter of $e$ to liquid inlet mixer of $e'$ |
| $ylh_{ee'}$ | interconnecting stream from liquid outlet splitter of $e$ to utility heater of $e'$ |
| $ylc_{ee'}$ | interconnecting stream from liquid outlet splitter of $e$ to utility cooler of $e'$ |
| $ylp_{ep}$ | interconnecting stream from liquid outlet splitter of $e$ to final mixer of product $p$ |
| $yvv_{ee'}$ | interconnecting stream from vapor outlet splitter of $e$ to vapor inlet mixer of $e'$ |
| $yvc_{ee'}$ | interconnecting stream from vapor outlet splitter of $e$ to utility cooler of $e'$ |
| $yvp_{ep}$ | interconnecting stream from vapor outlet splitter of $e$ to final mixer of product $p$ |
| $yIl_{ne}$ | interconnecting stream from initial stream $n$ to liquid inlet mixer of $e$ |
| $yIv_{ne}$ | interconnecting stream from initial stream $n$ to vapor inlet mixer of $e$ |
| $yIh_{ne}$ | interconnecting stream from initial stream $n$ to utility heater of $e$ |
| $yIc_{ne}$ | interconnecting stream from initial stream $n$ to utility cooler of $e$ |
| $yIp_{np}$ | interconnecting stream from initial stream $n$ to final mixer of product $p$ |
| $yhl_{ee'}$ | interconnecting stream from utility heater of $e$ to liquid inlet mixer of $e'$ |
| $yhv_{ee'}$ | interconnecting stream from utility heater of $e$ to vapor inlet mixer of $e'$ |
| $yhp_{ep}$ | interconnecting stream from utility heater of $e$ to final mixer of product $p$ |
| $ycl_{ee'}$ | interconnecting stream from utility cooler of $e$ to liquid inlet mixer of $e'$ |
| $ycp_{ep}$ | interconnecting stream from utility cooler of $e$ to final mixer of product $p$ |

$$f_e^H - \sum_{e'}(f_{ee'}^{HV} + f_{ee'}^{HL}) - \sum_p f_{ep}^{HP} = 0 \tag{2.24}$$

$$f_e^C - \sum_{e'} f_{ee'}^{CL} - \sum_{p \in P^{liq}} f_{ep}^{CP} = 0 \tag{2.25}$$

- mixers at the inlets of each side of module $e$

$$f_e^{LI} - \sum_{n \in N^{liq}} f_{ne}^{IL} - \sum_{e'}(f_{e'e}^{LL} + f_{e'e}^{CL}) - \sum_{e'} f_{e'e}^{HL} = 0 \tag{2.26}$$

$$f_e^{VI} - \sum_{n \in N^{vap}} f_{ne}^{IV} - \sum_{e'}(f_{e'e}^{VV} + f_{e'e}^{HV}) = 0 \tag{2.27}$$

$$f_e^C - \sum_n f_{ne}^{IC} - \sum_{e'}(f_{e'e}^{VC} + f_{e'e}^{LC}) = 0 \tag{2.28}$$

$$f_e^H - \sum_{n \in N^{liq}} f_{ne}^{IH} - \sum_{e'} f_{e'e}^{LH} = 0 \tag{2.29}$$

- final product mixers

$$f_p^P - \sum_{n \in N^{liq}} f_{np}^{IP} - \sum_e (f_{ep}^{LP} + f_{ep}^{CP} + f_{ep}^{HP}) = 0 \qquad \forall p \in P^{liq} \tag{2.30}$$

$$f_p^P - \sum_{n \in N^{vap}} f_{np}^{IP} - \sum_e (f_{ep}^{VP} + f_{ep}^{HP}) = 0 \qquad \forall p \in P^{vap} \tag{2.31}$$

(B) Mass balances for each component at

- mixers prior to liquid and vapor sides and utility exchangers of module $e$

$$f_e^{LI} x_{ei}^{LI} - \sum_{n \in N^{liq}} f_{ne}^{IL} x_{ni}^{I} - \sum_{e'}(f_{e'e}^{LL} x_{e'i}^{LO} + f_{e'e}^{CL} x_{e'i}^{C}) - \sum_{e'} f_{e'e}^{HL} x_{e'i}^{H} = 0 \tag{2.32}$$

$$f_e^{VI} x_{ei}^{VI} - \sum_{n \in N^{vap}} f_{ne}^{IV} x_{ni}^{I} - \sum_{e'}(f_{e'e}^{VV} x_{e'i}^{VO} + f_{e'e}^{HV} x_{e'i}^{H}) = 0 \tag{2.33}$$

$$f_e^C x_{ei}^C - \sum_n f_{ne}^{IC} x_{ni}^I - \sum_{e'}(f_{e'e}^{VC} x_{e'i}^{VO} + f_{e'e}^{LC} x_{e'i}^{LO}) = 0 \tag{2.34}$$

$$f_e^H x_{ei}^H - \sum_{n \in N^{liq}} f_{ne}^{IH} x_{ni}^I - \sum_{e'} f_{e'e}^{LH} x_{e'i}^{LO} = 0 \tag{2.35}$$

- final mixer of each product stream

$$f_p^P - \sum_{n \in N^{liq}} f_{np}^{IP} x_{ni}^I - \sum_e (f_{ep}^{LP} x_{ei}^{LO} + f_{ep}^{CP} x_{ei}^C + f_{ep}^{HP} x_{ei}^H) = 0 \qquad \forall p \in P^{liq} \tag{2.36}$$

$$f_p^P x_i^P - \sum_{n \in N^{vap}} f_{np}^{IP} x_{ni}^I - \sum_e (f_{ep}^{VP} x_{ei}^{VO} + f_{ep}^{HP} x_{ei}^H) = 0 \qquad \forall p \in P^{vap} \tag{2.37}$$

- around each mass/heat exchange module

$$f_e^{LI} x_{ei}^{LI} + f_e^{VI} x_{ei}^{VI} - f_e^{LO} x_{ei}^{LO} - f_e^{VO} x_{ei}^{VO} + \sum_k \nu_{ik} r_{ek} Mcat = 0 \tag{2.38}$$

(C) Energy balances at

- mixers prior to liquid and vapor sides and utility exchangers of module $e$

$$f_e^{LI} h_e^{LI} - \sum_{n \in N^{liq}} f_{ne}^{IL} h_n^I - \sum_{e'} (f_{e'e}^{LL} h_{e'}^{LO} + f_{e'e}^{CL} h_{e'}^{CO}) - \sum_{e'} f_{e'e}^{HL} h_{e'}^{HO} = 0 \tag{2.39}$$

$$f_e^{VI} h_e^{VI} - \sum_{n \in N^{vap}} f_{ne}^{IV} h_n^I - \sum_{e'} (f_{e'e}^{VV} h_{e'}^{VO} + f_{e'e}^{HV} h_{e'}^{HO}) = 0 \tag{2.40}$$

$$f_e^C h_e^{CI} - \sum_n f_{ne}^{IC} h_n^I - \sum_{e'} (f_{e'e}^{VC} h_{e'}^{VO} + f_{e'e}^{LC} h_{e'}^{LO}) = 0 \tag{2.41}$$

$$f_e^H h_e^{HI} - \sum_{n \in N^{liq}} f_{ne}^{IH} h_n^I - \sum_{e'} f_{e'e}^{LH} h_{e'}^{LO} = 0 \tag{2.42}$$

- final mixer of each product stream

$$f_p^P h^P - \sum_{n \in N^{liq}} f_{np}^{IP} h_n^I - \sum_e (f_{ep}^{LP} h_e^{LO} + f_{ep}^{CP} h_e^{CO} + f_{ep}^{HP} h_e^{HO}) = 0 \qquad \forall p \in P^{liq} \tag{2.43}$$

$$f_p^P h^P - \sum_{n \in N^{vap}} f_{np}^{IP} h_n^I - \sum_e (f_{ep}^{VP} h_e^{VO} + f_{ep}^{HP} h_e^{HO}) = 0 \qquad \forall p \in P^{vap} \tag{2.44}$$

- around each mass/heat exchange module

$$f_e^{LI}h_e^{LI} + f_e^{VI}h_e^{VI} - f_e^{LO}h_e^{LO} - f_e^{VO}h_e^{VO} - \sum_k r_{ek}Mcat\Delta H_{\text{reac},k} = 0 \quad (2.45)$$

where $\Delta H_{\text{reac},k}$ is the heat of reaction $k$

- around utility exchangers of each module $e$

$$Qh_e - f_e^H(h_e^{HO} - h_e^{HI}) = 0 \quad (2.46)$$

$$Qc_e - f_e^C(h_e^{CI} - h_e^{CO}) = 0 \quad (2.47)$$

(D) Summation of molar fractions

- for streams $s = LI, LO, VI, VO, C, H, P$

$$\sum_i x_{ei}^s - 1 = 0 \quad (2.48)$$

(E) Phase defining constraints

- for liquid streams

$$\sum_i (\gamma_{ei}^s P_{ei}^{sat,s} x_{ei}^s)/(\phi_{ei}^s P_{tot}) \leq 1 \quad (2.49)$$

- for vapor streams

$$\sum_i (x_{ei}^s \phi_{ei}^s P_{tot})/(\gamma_{ei}^s P_{ei}^{sat,s}) \leq 1 \quad (2.50)$$

(F) Mass transfer driving force constraints for each component

$$G1_{ei} \times G2_{ei} \geq 0 \quad (2.51)$$

$$G1_{ei} = f^{LI}x_{ei}^{LI} - f^{LO}x_{ei}^{LO} \quad (2.52)$$

$$G2_{ei} = \ln\Big[\frac{\gamma_{ei}^{LO}x_{ei}^{LO}P_{ei}^{sat,LO}}{\phi_{ei}^{VI}x_{ei}^{VI}P_{tot}}\Big] + \sum_i \sum_k \Big[\frac{\nu_{ik}\Delta G_i^f}{RT_e^{LO}} + \nu_{ik}\ln(\phi_{ei}^{VI}x_{ei}^{VI}P_{tot})\Big]\frac{\partial \epsilon_k}{\partial n_{ei}^L} \quad (2.53)$$

(G) Thermodynamic property calculation

- Reaction rate

$$r_{ek} = f(x_{ei}^{LO}, T_e^{LO}) \tag{2.54}$$

- Density

$$\rho_e^{LO} = f(x_{ei}^{LO}, T_e^{LO}) \tag{2.55}$$

- Saturated vapor pressure, enthalpy, activity coefficient, and fugacity coefficient for $s = LI, LO, VI, VO, HI, HO, CI, CO, P$

$$p_{ei}^{sat,s} = f(T_e^s) \tag{2.56}$$

$$h^s = f(x_{ei}^s, T_e^s) \tag{2.57}$$

$$\gamma_{ei}^s = f(x_{ei}^s, T_e^s, P_{tot}) \tag{2.58}$$

$$\phi_{ei}^s = f(x_{ei}^s, T_e^s, P_{tot}) \tag{2.59}$$

2. **Structural model**

(A) To define the existence of process streams – i.e. no stream flows exist if the module does not exist

$$[f_e^{LI} + f_e^{LO} + f_e^{VI} + f_e^{VO}] - y_e F^{max} \leq 0 \tag{2.60}$$

where $F^{max}$ is the upper bound for stream flowrates.

(B) To define the existence of interconnecting streams

$$f_{ee}^s - y_{ee}^s F^{max} \leq 0 \tag{2.61}$$

(C) To define the existence of utility exchangers

$$yh_e - y_e \leq 0 \tag{2.62}$$

$$yc_e - y_e \leq 0 \tag{2.63}$$

$$f_e^C - yc_e F^{max} \leq 0 \tag{2.64}$$

$$f_e^H - yh_e F^{max} \leq 0 \tag{2.65}$$

$$Qh_e - yh_e Q^{max} \leq 0 \tag{2.66}$$

$$Qc_e - yc_e Q^{max} \leq 0 \tag{2.67}$$

where $Q^{max}$ is the upper bound for heat transfer loads.

(D) To define that if a module exists, there will be an inlet flow

$$y_e - [\sum_{n \in N^{liq}} yIl_{ne} + \sum_{e'} yll_{e'e} + \sum_{e'} ycl_{e'e} + \sum_{e'} yhl_{e'e}] \leq 0 \tag{2.68}$$

$$y_e - [\sum_{n \in N^{vap}} yIv_{ne} + \sum_{e'} yvv_{e'e} + \sum_{e'} yhv_{e'e}] \leq 0 \tag{2.69}$$

$$yh_e - [\sum_{n \in N^{liq}} yIh_{ne} + \sum_{e'} ylh_{e'e}] \leq 0 \tag{2.70}$$

$$yc_e - [\sum_{n} yIc_{ne} + \sum_{e'} yvc_{e'e} + \sum_{e'} ylc_{e'e}] \leq 0 \tag{2.71}$$

(E) To define that if a module exists, there will be an outlet flow

$$y_e - [\sum_{e'} yll_{ee'} + \sum_{e'} ylh_{ee'} + \sum_{e'} ylc_{ee'} + \sum_{p \in P^{liq}} ylp_{ep}] \leq 0 \tag{2.72}$$

$$y_e - [\sum_{e'} yvv_{ee'} + \sum_{e'} yvc_{ee'} + \sum_{p \in P^{vap}} yvp_{ep}] \leq 0 \tag{2.73}$$

$$yh_e - [\sum_{e'} yhv_{ee'} + \sum_{e'} yhl_{ee'} + \sum_{p} yhp_{ep}] \leq 0 \tag{2.74}$$

$$yc_e - [\sum_{e'} ycl_{ee'} + \sum_{p} ycp_{ep}] \leq 0 \tag{2.75}$$

(F) To ensure that at least one feed point per initial stream

$$1 - [\sum_{e} yIl_{ne} + \sum_{e} yIh_{ne} + \sum_{e} yIc_{ne} + \sum_{p \in P^{liq}} yIp_{np}] \leq 0 \qquad n \in N^{liq} \tag{2.76}$$

$$1 - [\sum_{e} yIv_{ne} + \sum_{e} yIc_{ne} + \sum_{p \in P^{vap}} yIp_{np}] \leq 0 \qquad n \in N^{vap} \tag{2.77}$$

(G) To ensure that at least one source per product

$$1 - [\sum_{n \in N^{liq}} yIp_{np} + \sum_{e} ylp_{ep} + \sum_{e} ycp_{ep} + \sum_{e} yhp_{ep}] \leq 0 \qquad p \in P^{liq} \tag{2.78}$$

$$1 - [\sum_{n \in N^{vap}} yIp_{np} + \sum_{e} yvp_{ep} + \sum_{e} yhp_{ep}] \leq 0 \qquad p \in P^{vap} \tag{2.79}$$

(H) To constrain the number of streams allowed at existing mixers

$$[\sum_{n \in N^{liq}} yIl_{ne} + \sum_{e'} yll_{e'e} + \sum_{e'} ycl_{e'e} + \sum_{e'} yhl_{e'e}] - y_e Nmix^{max} \leq 0 \tag{2.80}$$

$$[\sum_{n \in N^{vap}} yIv_{ne} + \sum_{e'} yvv_{e'e} + \sum_{e'} yhv_{e'e}] - y_e Nmix^{max} \leq 0 \tag{2.81}$$

$$[\sum_{n \in N^{liq}} yIh_{ne} + \sum_{e'} ylh_{e'e}] - yh_e Nmix^{max} \leq 0 \tag{2.82}$$

$$[\sum_{n} yIc_{ne} + \sum_{e'} yvc_{e'e} + \sum_{e'} ylc_{e'e} - yc_e Nmix^{max} \leq 0 \tag{2.83}$$

(I) To constrain the number of splits allowed at existing splitters

$$[\sum_{e'} yll_{ee'} + \sum_{e'} ylh_{ee'} + \sum_{e'} ylc_{ee'} + \sum_{p \in P^{liq}} ylp_{ep}] - y_e Nsplit^{max} \leq 0 \tag{2.84}$$

$$[\sum_{e'} yvv_{ee'} + \sum_{e'} yvc_{ee'} + \sum_{p \in P^{vap}} yvp_{ep}] - y_e Nsplit^{max} \leq 0 \tag{2.85}$$

$$[\sum_{e'} yhl_{ee'} + \sum_{p} yhp_{ep}] - yh_e Nsplit^{max} \leq 0 \tag{2.86}$$

$$[\sum_{e'} ycl_{ee'} + \sum_{p} ycp_{ep}] - yc_e Nsplit^{max} \leq 0 \tag{2.87}$$

(J) To constrain the number of splits allowed at initial splitters

$$[\sum_{e} yIl_{ne} + \sum_{e} yIh_{ne} + \sum_{e} yIc_{ne} + \sum_{p \in P^{liq}} yIp_{np}] - Nsplit^{max} \leq 0 \qquad n \in N^{liq} \tag{2.88}$$

$$[\sum_{e} yIv_{ne} + \sum_{e} yIc_{ne} + \sum_{p \in P^{vap}} yIp_{np}] - Nsplit^{max} \leq 0 \qquad n \in N^{vap} \tag{2.89}$$

(K) To constrain the number of product sources

$$[\sum_{n \in N^{liq}} yIp_{np} + \sum_{e} ylp_{ep} + \sum_{e} ycp_{ep} + \sum_{e} yhp_{ep}] - Nmix^{max} \leq 0 \qquad p \in P^{liq} \tag{2.90}$$

$$[\sum_{n \in N^{vap}} yIp_{np} + \sum_{e} yvp_{ep} + \sum_{e} yhp_{ep}] - Nmix^{max} \leq 0 \qquad p \in P^{vap} \tag{2.91}$$

where $Nmix^{max}$ and $Nsplit^{max}$ give the maximum number of streams allowed to be mixed or split at mixers or splitters. Initially, $Nmix^{max} = Nsplit^{max} = 3$ is used and is relaxed if the constraint is active. These bounds are introduced to aid the solution of the resulting optimization problem.

(L) Non-redundancy constraints

$$y_{e+1} - y_e \leq 0 \tag{2.92}$$

3. **Objective function**

The objective function (Eq. 2.93) can be formulated to optimize cost performances, considering: (i) cost of raw materials, (ii) cost of heating and cooling utilities, and (iii) cost of modules.

$$Obj = \sum_{n} C_n f_I^n + \sum_{e} C_{cw} Qc_e + \sum_{e} C_{st} Qh_e + \sum_{e} Cost_e y_e \tag{2.93}$$

While operating costs can be calculated via the heat transfer loads in utility heat exchange modules, capital costing correlations cannot be applied as no equipment information is avail-

able at this stage. A pseudo-capital module cost function, Eq. 2.94 [94] was developed which estimated the module cost as a function of operating conditions (e.g., stream flows, module holdup). Despite that a truly economically optimal process option cannot be obtained, this approximation can provide an initial idea on equipment sizing, with the assumption that more GMF modules correspond to larger equipment units. The detailed derivation of the pseudo-capital module cost for reaction and/or separation systems can be found in Ismail et al. [94].

$$Cost_e(\$) = \begin{cases} 99.507(\frac{MW_e^{VI}}{\rho_e^{VI}})^{0.25}\sqrt{f_e^{VI}}H^{0.802}(2.18+F_c) & \text{if (reactive) separation module} \\ 583.295V_e^{0.623}(2.18+F_c) & \text{if reaction module} \end{cases} \tag{2.94}$$

### 2.4.3 Synthesis model with orthogonal collocation

To further enhance the intra-module representation and to estimate module design parameters of a highly compact and abstract mass/heat exchange module, Proios and Pistikopoulos [93] proposed to couple the Orthogonal Collocation (OC) method [98] with GMF. Each mass/heat exchange module is discretized with a number of "collocation points" to define a minimum essential set of "intra-segments" as depicted in Fig. 2.5 (reproduced from [93]). Since only continuous variables are introduced to describe the physical phenomena at the collocation points, the combinatorial size of the resulting GMF/OC synthesis problem remains compact in terms of binary variables. The detailed application of GMF/OC for process intensification synthesis is to be illustrated in Chapter 5 for extractive separation with material selection.

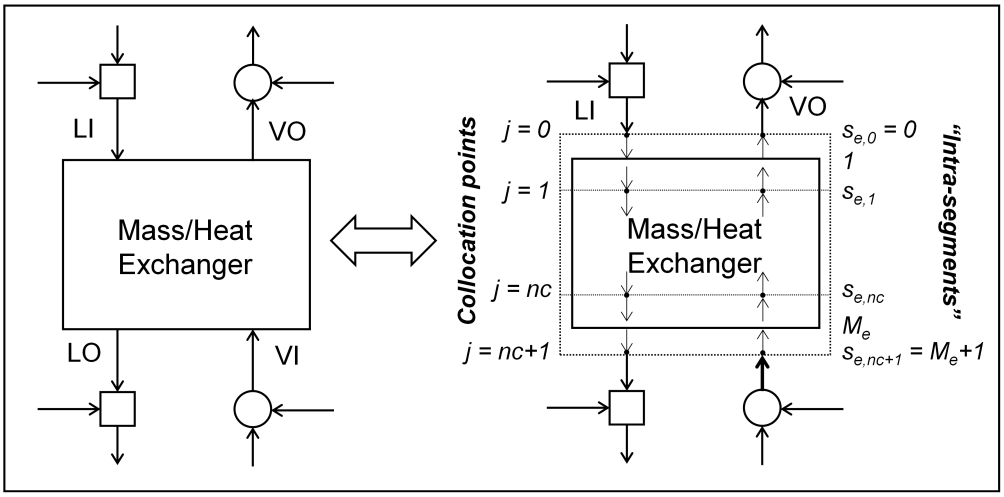


Figure 2.5: GMF and GMF/OC representations.

In analogy to the OC method for multistage separation systems [99], $nc$ interior collocation points are used to discretize each module in addition to 2 exterior collocation points. These collocation points correspond to a total of $M_e$ "intra-segments" related by the roots of Hahn polynomials following orthogonality conditions (Fig. 2.5). If we denote the location of each interior collocation point as $s_{e,j}$, then $s_{e,j} = s_j(M_e)$. Liquid and vapor flow rates, enthalpies and other stream property variables also need to be approximated at these collocation points by introducing intra-module physical constraints, such as mass and energy balances, etc. Additional physical constraints are imposed to link the intra-module GMF/OC representation with the inlet and outlet streams from the GMF module as presented in Chapter 2.4.2. Thus, the GMF/OC model consists of the following modeling constraints [93]:

- Collocation point location calculation

$$s_{e,0} = 1 \tag{2.95}$$

$$s_{e,j} = s_j(M_e) \tag{2.96}$$

$$s_{e,nc_e+1} = (M_e + 1) \tag{2.97}$$

where $j$ is the set for collocation points, $j = 1, ..., nc_e$. For example, if 1 interior collocation point is selected (i.e., $nc_e = 1$), then:

$$s_{e,0} = 1 \tag{2.98}$$

$$s_{e,1} = s_1(M_e) = \frac{M_e + 1}{2} \tag{2.99}$$

$$s_{e,2} = (M_e + 1) \tag{2.100}$$

- Lagrange polynomial weighting functions

$$W_{j'}^V(s_e) - \prod_{z=1, z\neq j'}^{nc_{e+1}} \frac{s - s_{e,j}}{s_{e,j'} - s_{e,z}} = 0 \tag{2.101}$$

$$W_{j'}^L(s_e) - \prod_{z=1, z\neq j'}^{nc_e} \frac{s - s_{e,j}}{s_{e,j'} - s_{e,z}} = 0 \tag{2.102}$$

where $W_j^V(s_e)$ and $W_j^L(s_e)$ are the Lagrange polynomial weighting functions to the number of "intra-segments" per module respectively on the vapor and liquid side.

- Component mass and energy balances

$$\sum_{j'=1}^{nc_e+1} W_{j'}^V(s_{e,j} + 1) fc_i^V(s_{e,j'}) - fc_i^V(s_{e,j}) + \sum_{j'=0}^{nc_e} W_{j'}^L(s_{e,j} - 1) fc_i^L(s_{e,j'}) - fc_i^L(s_{e,j'}) = 0 \tag{2.103}$$

$$\begin{aligned} &\sum_{j'=1}^{nc_e+1} W_{j'}^V(s_{e,j} + 1) f^V(s_{e,j'} h^V(s_{e,j'}) - f^V(s_{e,j}) h^V(s_{e,j}) \\ &+ \sum_{j'=0}^{nc_e} W_{j'}^L(s_{e,j} - 1) f^L(s_{e,j'}) h^L(s_{e,j'}) - f^L(s_{e,j'}) h^L(s_{e,j'}) = 0 \end{aligned} \tag{2.104}$$

where $fc_c^V(s_{e,j})$ and $fc_c^L(s_{e,j})$ are respectively the vapor and liquid flow rates for component $i$ at collocation point $s_{e,j}$, $f^V(s_{e,j})$ and $f^L(s_{e,j})$ are respectively the total vapor and liquid flow rates at collocation point $s_{e,j}$.

- Molar fraction summations

$$\sum_i \frac{fc_c^V(s_{e,j})}{f^V(s_{e,j})} - 1 = 0 \tag{2.105}$$

$$\sum_i \frac{fc_c^L(s_{e,j})}{f^L(s_{e,j})} - 1 = 0 \tag{2.106}$$

- Driving force constraints

$$G1_i(s_{e,j}) \times G2_i(s_{e,j}) \leq 0 \tag{2.107}$$

$$G1_i(s_{e,j}) = fc_c^L(s_{e,j}) - fc_c^L(s_{e,j} - 1) \tag{2.108}$$

$$G2_i(s_{e,j}) = \ln \frac{\gamma_i(s_{e,j}) P_i^{sat}(s_{e,j}) \frac{fc_c^L(s_{e,j})}{f^L(s_{e,j})}}{\phi_i(s_{e,j}) P(s_{e,j}) \frac{fc_c^V(s_{e,j})}{f^V(s_{e,j})}} \tag{2.109}$$

- Equations to link the interior collocation points with the inlet/outlet streams of the module

$$f_e^{VO} - \sum_i (\sum_{j=1}^{nc_e+1} W_j^V(1) fc_i^V(s_{e,j})) = 0 \tag{2.110}$$

$$f_e^{VO} x_{e,i}^{VO} - \sum_{j=1}^{nc_e+1} W_j^V(1) fc_i^V(s_{e,j}) = 0 \tag{2.111}$$

$$f_e^{VO} h_e^{VO} - \sum_{j=1}^{nc_{e+1}} W_j^V(1) f^V(s_{e,j}) h^V(s_{e,j}) = 0 \tag{2.112}$$

$$f_e^{LI} - f^L(s_{e,0}) = 0 \tag{2.113}$$

$$f_e^{LI} x_{e,i}^{LI} - fc_i^L(s_{e,0}) = 0 \tag{2.114}$$

$$f_e^{LI} h_e^{LI} - f^L(s_{e,0}) h^L(s_{e,0}) = 0 \tag{2.115}$$

## 2.5 Solution strategy

For the solution of the mixed-integer nonlinear programming problem resulted from GMF synthesis, several methods can be used [100], such as the Branch and Bound [101], the Generalized Benders Decomposition (GBD) [102], the Outer Approximation [103], etc. In this work, the GBD method is adapted because of the control it provides during the solution procedure, which is essential for this type of highly nonconvex MINLP problems to avoid the large infeasible portion of the design space. Due to the highly nonconvex and nonlinear nature of the model, GBD cannot guarantee that the problem is solved to global optimality. However, arguably even intermediate solutions can provide significant insights to the process designs. Several notes regarding GBD for solution of GMF problems:

- The structure of GMF model formulation (i.e., a synthesis model with continuous variables and a structural model with mixed-integer variables) fits very well with the GBD decomposition strategy. This will help to decompose the computational complexities resulted respectively by model nonlinearities and by binary variables during the solution procedure. The infeasible space – which can be quite large for these phenomena-based synthesis approaches – can also be efficiently ruled out with the infeasibility cut constraints, after which previous feasible solutions can be recovered to re-initialize the iteration.

- The iterative characteristic of GBD enables the record of any intermediate feasible solutions generated throughout the solution procedure, which can be used as design intermediate solutions. The integer cut constraint can also be used to rule out the optimal GBD solution, and to generate the second or third best solutions with different design structures determined by the different sets of binary variables [104].

- GBD also allows for flexible manipulation of binary variable combinations – in the case of retrofit design, certain binary variables can be fixed to maintain the original structure while optimizing other ones for minor design changes.

## 2.6 Motivating examples

In this section, we apply GMF for the representation and simulation-based analysis of simple reaction and/or separation systems, as a prelude to showcasing GMF synthesis intensification capabilities in the following chapters. Via the two motivating examples, we aim to demonstrate: (i) how GMF can identify more promising process improvements than equipment-based modeling, and (ii) the conjunctive thermodynamic basis of GMF with other physical/chemical equilibrium-based equipment models.

### 2.6.1 Four-tray simulation in distillation column

Given a single GMF mass/heat exchange module, the design space predicted by the Gibbs free energy-based driving force constraints is a superset of that for a single distillation tray based on phase equilibrium calculations. This is due to the facts that: (i) GMF allows more degrees of freedom for stream variables – e.g., each module inlet/outlet stream can have different temperatures while satisfying the overall energy balance, (ii) mass transfer feasibility is characterized between liquid inlet stream and vapor outlet stream, as well as between liquid outlet stream and vapor inlet stream. Both the two factors can result in a more "powerful" separation performance in a GMF mass/heat exchange module compared to a single distillation tray. However, if the driving force constraints are set between the liquid and vapor outlet streams while enforcing physical equilibrium to be reached, a mass/heat exchange module models exactly a distillation tray with 100% separation efficiency.

In what follows, we consider a set of four distillation trays/modules from a pentene (PEN), butene (BUT), and hexene (HEX) separation process (Fig. 2.6). The liquid and vapor inlet stream conditions are given at the two ends of the column section in a counter-current manner. We apply GMF for: (i) equilibrium-based simulation which is identical to tray-by-tray simulation (i.e., no degrees of freedom for optimization), and (ii) modular optimization to maximize pentene molar fraction in the liquid outlet stream using the driving force constraints. The resulting liquid molar fraction profiles from the above two types of GMF modeling setups are summarized in Table 2.6.

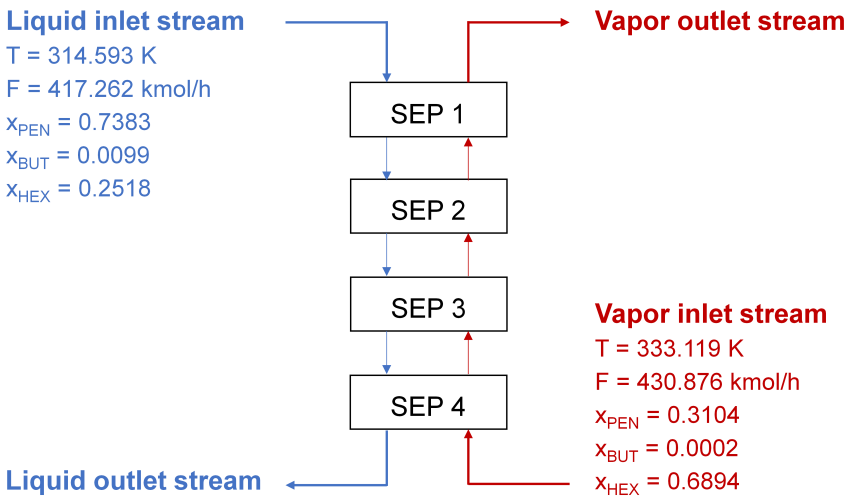


Figure 2.6: Four-tray simulation in a ternary distillation column.

Table 2.2: GMF results for equilibrium-based simulation and modular optimization.

| Module number | $x_{PEN}$ , mol/mol | | $x_{BUT}$ , mol/mol | | $x_{HEX}$ , mol/mol | |
|---|---|---|---|---|---|---|
| | Equilibrium | Modular | Equilibrium | Modular | Equilibrium | Modular |
| 1 | 0.6038 | 0.7383 | 0.0027 | 0.0069 | 0.3935 | 0.2548 |
| 2 | 0.4219 | 0.4226 | 0.0006 | 0.0014 | 0.5775 | 0.5760 |
| 3 | 0.2457 | 0.4217 | 0.0001 | 0.0002 | 0.7542 | 0.5781 |
| 4 | 0.1278 | 0.0946 | 2.27E-05 | 1.0E-5 | 0.8722 | 0.9054 |

As can be noted from the equilibrium-based simulation results, from the first separation module to the last separation module (numbered in a descending order), pentene and butene consistently transfer from the liquid phase to the vapor phase, while hexene from vapor to liquid. This monotonic trend is also correctly captured by the GMF modular optimization. Moreover, the modular optimization is able to identify a higher (or optimal) hexene composition in the liquid outlet stream compared to the equilibrium-based simulation. This provides the opportunity to evaluate the maximum possible performance improvements from an enriched design space within the thermodynamic limits, with both known and unknown process solutions. The promising process

solutions identified by GMF can be further validated with equipment-based simulation. It can also be observed that, the composition profile obtained from modular optimization is not as smooth as that from the equilibrium-based simulation. This indicates that the GMF modules are not always optimized at their equilibrium conditions, which is also approved by the non-zero $G2_i$ values in these modules.

### 2.6.2 Reactor-separator simulation

Now we consider the reaction-separation process for pentene metathesis to produce butene and hexene. Two simple reaction-separation process configurations are of interest, i.e. an integrated CSTR and flash column process and a reactive flash column process (Fig. 2.7). The raw material is a saturated liquid stream of 100 kmol/h pure pentene, and the design objective is to maximize butene production rate.

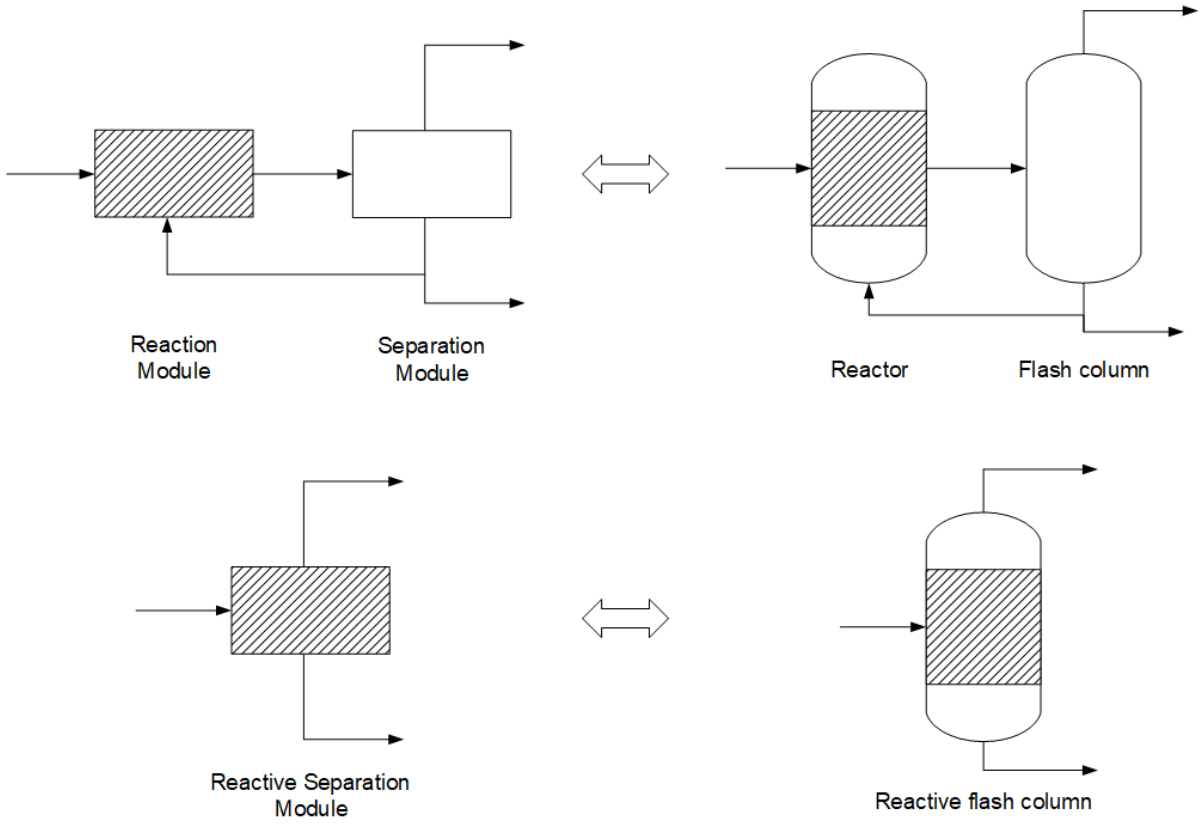


Figure 2.7: Reactor-separator systems representation.
(Left: GMF representation, Right: equipment-based modeling)

The following models are utilized in the analysis:

(i) Rigorous equipment-based models – A CSTR reactor model with reaction equilibrium expressions and a flash column with liquid-vapor phase equilibrium calculations are used to describe the integrated reactor and flash column process. A reactive flash column model is used which assumes chemical and physical equilibrium.

(ii) GMF representation – With the driving force constraints formulation introduced in Chapter 2.2, a reaction module, a separation module, and a reactive separation module can be obtained to describe reactor, separator, and reactive separator, respectively. Since only 1-stage reaction or separation is considered in the systems, the driving force constraints are set between the liquid and vapor outlet streams of the mass/heat exchange module, instead of constraining the mass transfer feasibility at the two ends of the module.

(iii) Attainable region calculation – The kinetic attainable region-based approach is applied to identify the maximum butene production potential and to benchmark the solutions obtained from equipment-based modeling and GMF representation.

The maximum butene production rates, pertaining to different reaction volumes, are summarized in Fig. 2.8a. As can be noted, the maximum butene production rates from the sequential reaction and separation process are the same for equipment-based modeling and GMF representation. In other words, the GMF reaction module and separation module in this case are respectively at chemical and physical equilibrium. This is because that the maximum production rate in a single liquid-phase reactor is reached at the reaction equilibrium. The same is with the 1-stage separator to achieve the best butene separation performance at vapor-liquid equilibrium conditions.

If reaction and separation are integrated into a single unit, the production rates can be shifted to higher than the pure reactor equilibrium condition. The equipment-based reactive flash column offers a slightly better butene production rate by vaporizing the butene instantaneously to the vapor phase. By allowing for additional design degrees of freedom to intensify the module mass transfer capability (e.g., different vapor and liquid temperatures), GMF identifies a higher butene

production rate than the reactive flash column, but well within the attainable region. As shown in Fig. 2.8b, only the desired product component, i.e. butene, is pushed to reach a driving force ($G1_i \times G2_i$) near 0 in the reactive separation module. The pentene and butene components are at non-equilibrium conditions. As will be observed from other chapters, for a GMF reactive separation module, the optimal process design may not always be obtained at $G1_i \times G2_i = 0$. A detailed derivation of the relationship between GMF zero driving forces with chemical/physical equilibrium conditions is presented in Appendix A.

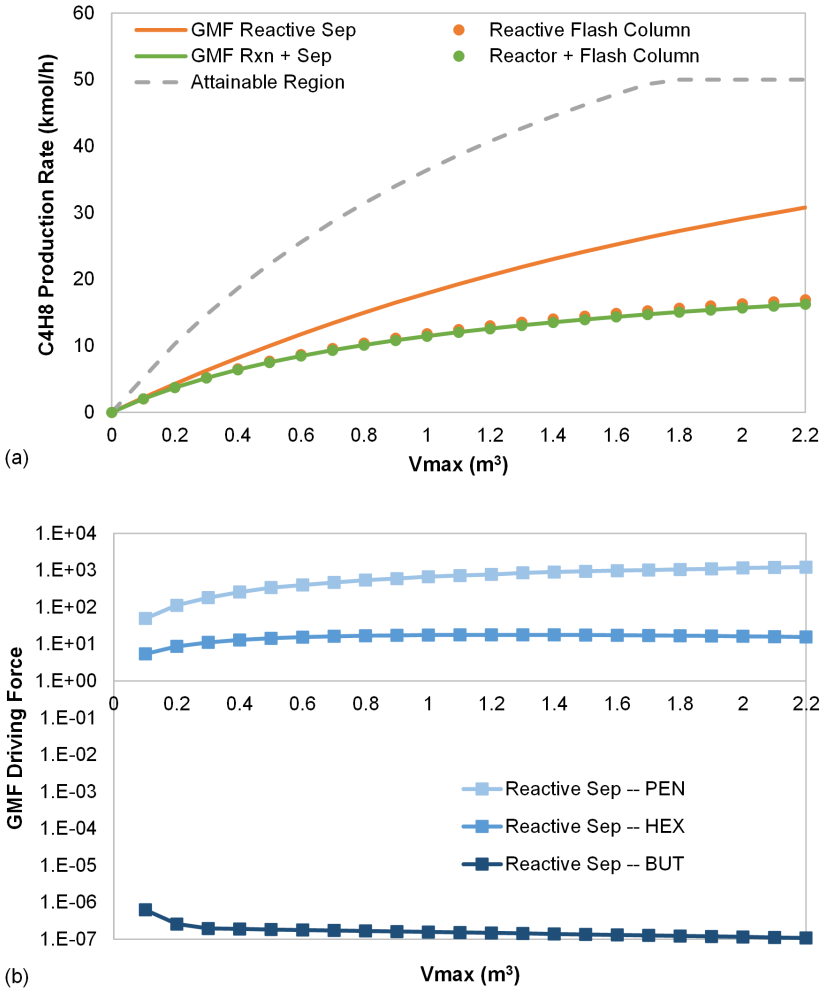


Figure 2.8: Reactor-separator systems comparison –
(a) Butene (C4H8) production rates, (b) GMF driving forces in reactive separation module.

## 2.7 Nomenclature

***Variables***

| | |
|---|---|
| $a$ | Activity |
| $D$ | Module diameter |
| $f$ | Molar flowrate |
| $F^{max}$ | Upper bound of molar flowrate |
| $Fc$ | Factor accounting for pressure vessel material |
| $G$ | Gibbs free energy |
| $H$ | Module height |
| $h$ | Enthalpy |
| $k$ | Rate constant |
| $Ka$ | Reaction equilibrium constant |
| $Level$ | Liquid level |
| $M$ | Big M constraint |
| $Mcat$ | Catalyst mass |
| $MW$ | Molecular weight |
| $P^{\text{sat}}$ | Saturated vapor pressure |
| $P_{tot}$ | Pressure |
| $Q$ | Heat load |

| | |
|---|---|
| $Q^{max}$ | Upper bound of heat load |
| $r$ | Reaction rate |
| $T$ | Temperature |
| $V$ | Volume |
| $x$ | Molar fraction |
| $y$ | Binary variable |

***Subscripts***

| | |
|---|---|
| $c$ | Component |
| $e, e'$ | Module |
| $n$ | Feed stream |
| $p$ | Product stream |

***Greek letters***

| | |
|---|---|
| $\epsilon$ | Reaction extent |
| $\gamma$ | Activity coefficient |
| $\mu$ | Chemical potential |
| $\nu$ | Reaction stoichiometric coefficient |
| $\phi$ | Fugacity coefficient |
| $\rho$ | Density |

# 3. ENVELOPE OF DESIGN SOLUTIONS FOR REACTION/SEPARATION SYSTEMS[†]

## 3.1 Introduction

Given the enriched design space including both conventional and innovative process options, a key open question remains on how to derive an envelope of possible design solutions prior to establishing any process alternatives, hereby to identify the ultimate bounds of process improvements that can be achieved as well as to rapidly screen the design space with respect to productivity, economics, and/or safety objectives.

A classic development to identify process boundaries is the attainable region (AR) theory for reactor network synthesis [105, 106], where the entire physically realizable outlet conditions can be characterized for a given set of feed conditions and reactions with prescribed kinetics independent of actual reactor design. The AR theory has also been extended to systems involving reaction, mixing, and separation. Feinberg and Ellison [83] introduced an optimization-based approach, namely the continuous flow stirred tank reactor (CFSTR) equivalence principle, to explore the molar productivity limits of a given chemistry in any steady-state reactor-mixer-separator (RMS) systems. Hereafter, we refer to this approach as "Feinberg Decomposition (FD)". Frumkin and Doherty [84, 107, 108] further extended the FD approach to characterize selectivity bounds in RMS systems. Despite the indispensable boundary information given by the CFSTR principle, this approach cannot generate candidate process alternatives at, or within, the derived bounds. On the other hand, process synthesis approaches have also been applied to identify the performance limits of a reactive separator network as presented in da Cruz and Manousiouthakis [52]. However, there is no guarantee that the obtained performance limits can serve as the absolute "upper bound" of process improvements as those derived from AR approaches. Thus it remains an open question **– how close can actual intensified designs, e.g. derived by the PI synthesis methods, approach these ultimate attainable region bounds.**

[†]Reproduced in part with permission from Tian, Y., & Pistikopoulos, E. N. (2020). Toward an Envelope of Design Solutions for Combined/Intensified Reaction/Separation Systems. Industrial & Engineering Chemistry Research, 59(24), 11350-11354. Copyright 2020 American Chemical Society.

In this chapter, we investigate how an envelope of design solutions based on the FD theory can be effectively incorporated within a phenomenological synthesis/intensification strategy using thermodynamic driving force constraints, using the Generalized Modular Representation Framework (GMF) as an example.

## 3.2 The Feinberg Decomposition

We first provide a brief overview on the Feinberg Decomposition approach before applying it to identify design boundaries in the subsequent sections.

The Continuous Flow Stirred Tank Reactor (CFSTR) Equivalence Principle, proposed by [83], allows one to decompose any arbitrary steady-state reactor-mixer-separator (RMS) system with total reaction volume $V > 0$ into a new system (Fig. 3.1) which has the same effluent molar flow rates as the original system. The new system comprises only CFSTRs as reactors with no more than $\mathcal{R} + 1$ in number (where $\mathcal{R}$ is the number of linearly independent reaction), each of which coupled to a perfect separator system as shown in Fig. 3.1. Thus, the CFSTR principle, i.e. the Feinberg Decomposition (FD), provides a unified CFSTR-based representation which can capture any and every steady-state combined reaction/separation system with equivalent production rates under given kinetics and capacity resource, regardless known process designs or "out-of-the-box" innovative ones.

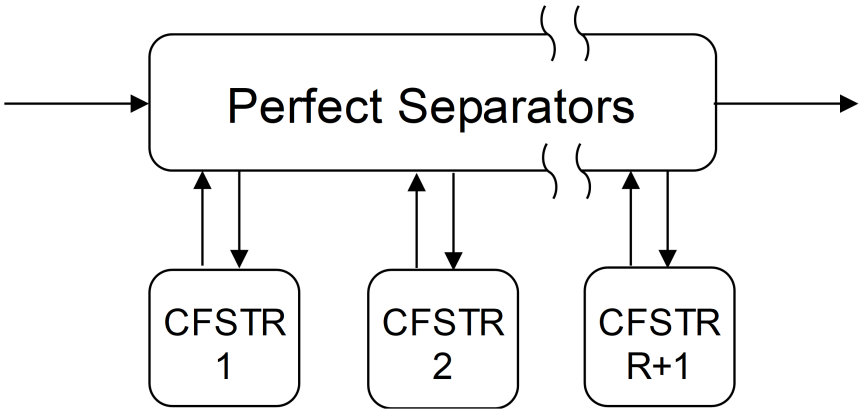


Figure 3.1: The Feinberg Decomposition approach with Continuous Flow Stirred Tank Reactors. (Reprinted from [109])

The new CFSTR-based system retains key design and operating characters from the original RMS system [83]: (i) the total reaction volume of CFSTRs is no greater than the reactive volume $V$ in the original RMS system, and (ii) the mixture states within these CFSTRs, such as temperatures, pressures, and compositions, are no more extreme than those within the original system. Moreover, an optimization-based formulation [110] is utilized in FD approach to assess bounds with respect to a specific process performance (e.g., productivity, selectivity) without having to first mapping out the AR or its boundary as that in conventional geometrically-based AR approaches. Frumkin and Doherty [108] further extended the FD optimization formulation as a nonlinear programming problem (NLP) for RMS systems with relatively larger number of components. The full NLP formulation, which can be found in Appendix B, is adapted in this work to explore the olefin metathesis design boundaries as detailed later in Chapter 3.3.2.

## 3.3 Case study: Olefin metathesis

### 3.3.1 Process description

The metathesis of 2-pentene ($C_5H_{10}$) to form 2-butene ($C_4H_8$) and 3-hexene ($C_6H_{12}$) (Eq. 3.1) is an equilibrium-limited reaction. The reaction takes place in liquid phase at atmospheric pressure and can be described with ideal vapor-liquid equilibrium [111]. The reaction kinetics are given in Eq. 3.2 adapted from Okasinskin and Doherty [112].

$$2C_5H_{10} \rightleftharpoons C_4H_8 + C_6H_{12} \tag{3.1}$$

$$\begin{aligned} r &= k_f(x_{C_5H_{10}}^2 - \frac{x_{C_4H_8}x_{C_6H_{12}}}{K_{eq}}) \quad (h^{-1}) \\ k_f &= 1.0661 \times 10^5 e^{(-3321.2/T(K))} \quad (h^{-1}) \\ K_{eq} &= 0.25 \end{aligned} \tag{3.2}$$

This process has been widely investigated in literature especially featuring the use of reactive distillation as a promising design solution to enhance the conversion of pentene by removing the low boiling component butene from liquid reactive mixture [112, 113, 114]. However, these

design studies were mostly driven by cost minimization. In a more recent work, da Cruz and Manousiouthakis [52] applied the Infinite Dimensional Steady State (IDEAS) framework to identify the performance limits by minimizing reactive holdup.

Herein, we revisit this example with FD and GMF to investigate its design envelope. The synthesis task is to produce 50 kmol/h of 98% butene and 50 kmol/h of 98% hexene at 1 atm, given as raw material a saturated liquid stream of 100 kmol/h pure pentene.

### 3.3.2 Design boundaries via Feinberg Decomposition

We characterize the design space under a certain production task in accordance to the FD theory [83, 107]. Since the pentene metathesis reaction takes place in liquid phase at fixed atmospheric pressure, the available design parameters are reaction temperature (T) and reactive volume (V). Reaction kinetics for this chemistry are valid between 277.15 K and 340.15 K, which provide the largest feasible temperature range. To identify the design boundaries in the space of Temperature-Volume (T-V), the following parametric studies are performed with the NLP model provided in Supporting Information with specific focus on equations S1k and S1l:

- Step 1: The total reactive volume is increased from 0 $m^3$ at a step size of 0.1 $m^3$ to maximize butene production, while CFSTR temperatures are constrained between 277.15 K and 340.15 K. The results showed that at least 1.68 $m^3$ reactive volume is required to produce butene at a rate of 49 kmol/h. Moreover, it is worth noting that the two CFSTRs are both operated at 340.15 K for each reactor volume, which illustrates that the reaction is favored by higher temperature operation. This gives the upper design/operation limit shown in Fig. 3.2.

- Step 2: The maximum allowable reaction temperature ($T^{max}$) is varied from 277.15 K to 340.15 K at a step size of 2 K and butene production is constrained to be greater than 49 kmol/h. Then the optimization problem is set to minimize reactive volume to identify the minimum V required at different operation temperatures, which results in the lower design/operation limit shown in Fig. 3.2.

The resulting T-V design space is depicted in Fig. 3.2, and more information can be found in Supporting Information on characterizing this design space via Feinberg Decomposition. Fig. 3.2 provides boundary information on:

- the ultimate minimum reactive volume required for the desired production task (i.e., the leftmost vertex at 1.68 $m^3$)
- for a given reactive volume, the range of operation temperatures
- for a given reaction temperature, the candidate reactive volumes.

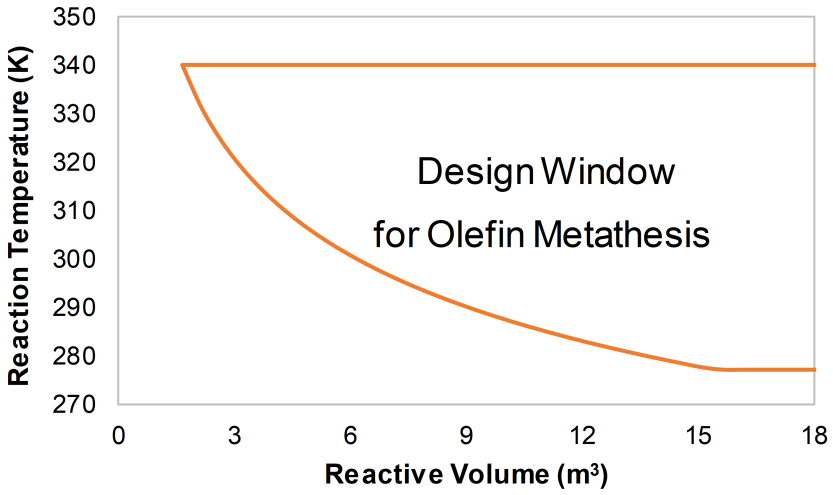


Figure 3.2: Temperature-Volume design boundaries for olefin metathesis (Reprinted from [109]).

### 3.3.3 Design boundaries via Generalized Modular Representation Framework

In this section, we present the application of the Generalized Modular Representation Framework (GMF) to the olefin metathesis process. A number of design configurations are generated and discussed in what follows, while detailed flowsheet and stream conditions can be found in Supporting Information.

#### *3.3.3.1 Design 1*

Design 1 is shown in Fig. 3.3. Note that the blue-colored streams denote liquid flows, red streams are vapor flows, the shaded M/H module denotes a reactive module, and blank M/H module

is for pure separation. It corresponds to a GMF solution with an objective function to minimize reactive volume, which provides a valid underestimation of equipment size determined by reaction kinetics while independent of separation schemes. It features 3.77 $m^3$ reactive volume, which is 20.6% less than the minimal reactive volume given in Ref. [52]. This configuration comprises two GMF mass/heat (M/H) exchange modules: a reactive separation module (i.e., M/H 1) and a pure separation module (i.e., M/H 2). The pure pentene feed stream is partially vaporized before entering M/H 1 to provide the energy for reaction and separation taking place later in M/H 1. In M/H 1, the metathesis reaction takes place to form bentene and hexene from pentene, coupled with separation which vaporizes the produced butene to give the desired product P1 (50 kmol/h, $C_4H_8$ 98 mol%). However, the heavier components pentene and hexene are kept in liquid phase (200 kmol/h, $C_5H_{10}$ 70.8 mol%, $C_6H_{12}$ 29.0%, $C_5H_{10}$ 0.2 mol%) and then sent to M/H 2. M/H 2 separates the above liquid mixture to a stream of desired Product 2 (50 kmol/h, $C_6H_{12}$ 98 mol%), and also recycle the excessive pentene reactant back to M/H 1 for reaction.

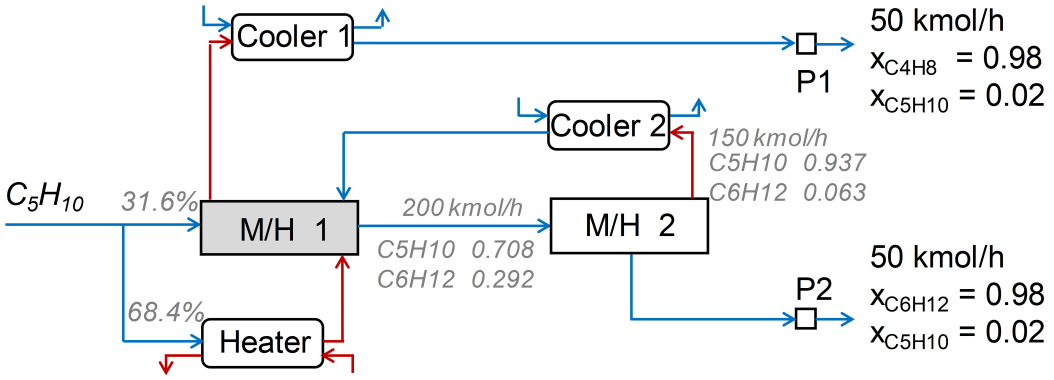


Figure 3.3: GMF Design 1 – Optimal solution for reactive volume minimization. (Reprinted from [109])

The detailed stream temperature, flowrate, and molar composition data for GMF Design 1 is summarized in Table 3.1. The pressures in each design are fixed to 1 atm. For brevity, we only include outlet stream information in the tables below, while the inlet stream conditions can be readily obtained via the combinatorial structure in the GMF design solution.

Table 3.1: Design 1 – Flowsheet data (Reprinted from [109]).

| Module ID | Liquid Outlet Stream | | | | | Vapor Outlet Stream | | | | |
|---|---|---|---|---|---|---|---|---|---|---|
| | T (K) | F (kmol/h) | $x_{C_5H_{10}}$ | $x_{C_4H_8}$ | $x_{C_6H_{12}}$ | T (K) | F (kmol/h) | $x_{C_5H_{10}}$ | $x_{C_4H_8}$ | $x_{C_6H_{12}}$ |
| M/H 1 | 316.0 | 200.0 | 0.708 | 0 | 0.292 | 278.2 | 50.0 | 0.020 | 0.980 | 0 |
| M/H 2 | 310.0 | 50.0 | 0.020 | 0 | 0.980 | 339.5 | 150.0 | 0.937 | 0 | 0.063 |
| Heater | | | | | | 340.1 | 68.4 | 1 | 0 | 0 |
| Cooler 1 | 277.2 | 50.0 | 0.020 | 0.980 | 0 | | | | | |
| Cooler 2 | 277.2 | 150.0 | 0.937 | 0 | 0.063 | | | | | |

### *3.3.3.2 Design 2*

The results of Design 2 are presented in Fig. 3.4 and Table 3.2, as an intermediate design solution alternative for reactive volume minimization. It has a reactive volume of 4.41 $m^3$, 17.6% better than the optimal result in Ref. [52]. It features a reactive distillation type of design as have been reported in our previous GMF works. The "column section" includes two pure separation modules in rectification section, one reactive separation modules in reaction zone, and another pure separation module in stripping section. The pentene feed stream is fed to the reactive module.

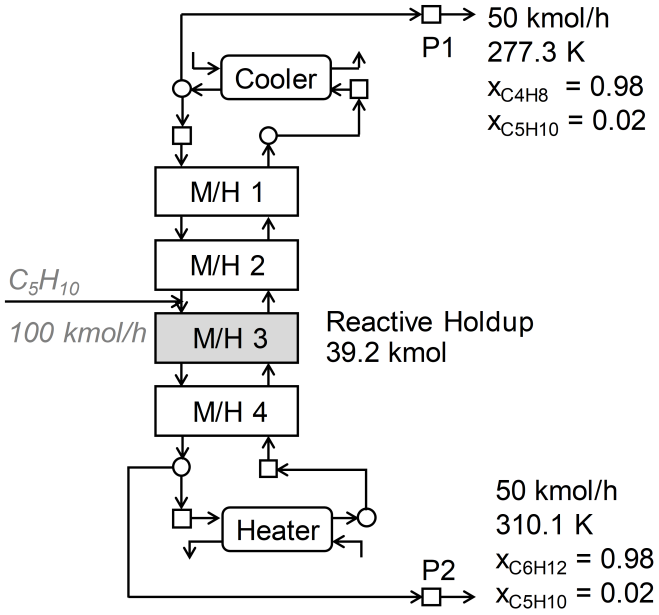


Figure 3.4: GMF Design 2 – Intermediate solution for reactive volume minimization. (Reprinted from [109])

Table 3.2: Design 2 – Flowsheet data (Reprinted from [109]).

| Module ID | Liquid Outlet Stream | | | | | Vapor Outlet Stream | | | | |
|---|---|---|---|---|---|---|---|---|---|---|
| | T (K) | F (kmol/h) | $x_{C_5H_{10}}$ | $x_{C_4H_8}$ | $x_{C_6H_{12}}$ | T (K) | F (kmol/h) | $x_{C_5H_{10}}$ | $x_{C_4H_8}$ | $x_{C_6H_{12}}$ |
| M/H 1 | 292.1 | 51.0 | 0.996 | 0.004 | 0 | 310.6 | 50.2 | 0.020 | 0.980 | 0 |
| M/H 2 | 321.1 | 100.0 | 0.508 | 0.002 | 0.490 | 298.7 | 101.0 | 0.513 | 0.487 | 0 |
| M/H 3 | 309.8 | 200.0 | 0.754 | 0.001 | 0.245 | 326.6 | 150.0 | 0.345 | 0.328 | 0.327 |
| M/H 4 | 310.1 | 200.0 | 0.020 | 0 | 0.980 | 340.1 | 150.0 | 0.999 | 0.001 | 0 |
| Heater | | | | | | 340.1 | 150.0 | 0.020 | 0 | 0.980 |
| Cooler | 277.2 | 50.2 | 0.02 | 0.98 | 0 | | | | | |

#### *3.3.3.3 Design 3*

Design 3 is depicted in Fig. 3.5 and results summarized in Table 3.3, which is the GMF optimal solution to minimize operating cost accounting for separation energy consumption. The design configuration comprises three mass/heat exchange modules, as well as two pure heat exchange modules. All the three modules perform both reaction and separation tasks, adding up to a total of 20 $m^3$ reactive volume. Moreover, the pentene feed stream is split before fed to M/H 2 and M/H 3.

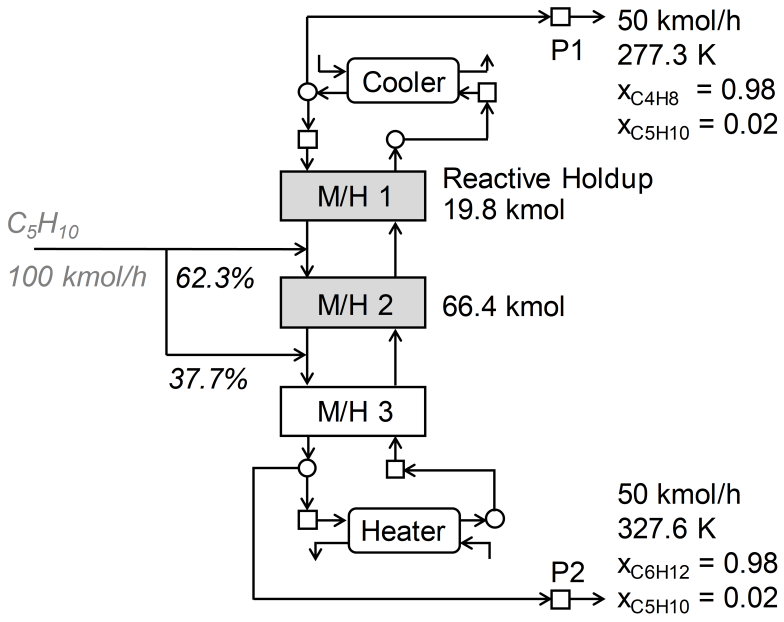


Figure 3.5: GMF Design 3 – Operating cost minimization (Reprinted from [109]).

Table 3.3: Design 3 – Flowsheet data (Reprinted from [109]).

| Module ID | Liquid Outlet Stream | | | | | Vapor Outlet Stream | | | | |
|---|---|---|---|---|---|---|---|---|---|---|
| | T (K) | F (kmol/h) | $x_{C_5H_{10}}$ | $x_{C_4H_8}$ | $x_{C_6H_{12}}$ | T (K) | F (kmol/h) | $x_{C_5H_{10}}$ | $x_{C_4H_8}$ | $x_{C_6H_{12}}$ |
| M/H 1 | 326.2 | 95.0 | 0.136 | 0 | 0.864 | 278.0 | 70.0 | 0.016 | 0.984 | 0 |
| M/H 2 | 304.7 | 124.6 | 0.604 | 0 | 0.396 | 326.3 | 145.0 | 0.115 | 0.329 | 0.556 |
| M/H 3 | 286.6 | 70.0 | 0.016 | 0 | 0.984 | 321.8 | 112.3 | 0.998 | 0 | 0.002 |
| Heater | | | | | | 339.3 | 20.0 | 0.016 | 0 | 0.984 |
| Cooler | 277.2 | 70.0 | 0.016 | 0.984 | 0 | | | | | |

#### *3.3.3.4 Remarks*

The identification of the three GMF design solutions (i.e., Design 1, 2, 3) in the FD design boundaries is illustrated in Fig. 3.6. Design 1 and 2 have provided two candidate process solutions on the FD lower boundary. Moreover, the trade-off between separation energy consumption and reactive equipment volume can be clearly seen from the design envelope. However, further investigations are needed to identify if there exists a feasible process configuration corresponding to the FD leftmost vertex at the ultimate minimal reactive volume.

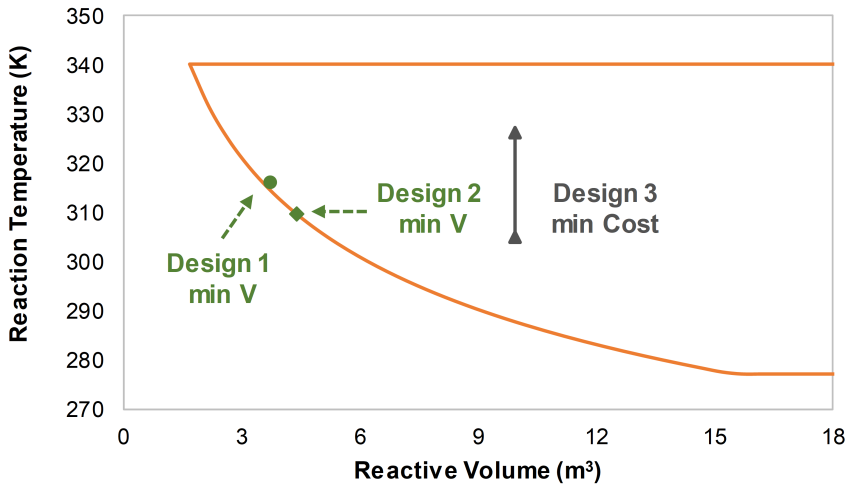


Figure 3.6: GMF design solutions in comparison with FD boundaries (Reprinted from [109]).

Another GMF design obtained during optimization is shown in Fig. 3.7 with a reactive volume of 2.20 $m^3$. Two mass/heat (M/H) exchange modules are selected as well as two pure heat exchange modules. Reaction only takes place in Module M/H 1. However, the liquid inlet and outlet streams of M/H 1 turns out to be exactly the same in flowrates, compositions, and temperature. This deactivates the driving force constraints (Driving force $= G1_i \times G2_i \geq 0$) [48] in M/H 1 by having $G1_i = f^{LO}x_i^{LO} - f^{LI}x_i^{LI}$ always equals to 0. Thus, M/H 1 has a most "intensified" and "de-bottlenecked" reactive holdup where the reaction mixture only contains pentene (i.e., pure reactant), with no limitation of reaction equilibrium since the products butene and pentene are all taken away by the vapor streams.

However, this design requires in situ, instantaneous, and perfect separation of products from the reactants to totally shift reaction equilibrium – which is doubtful if possible to find or create such separators in reality to meet this ideal separation scheme. More important is that it is *not a thermodynamically feasible design* due to the deactivation of driving force constraints. If comparing with the FD boundaries (Fig. 3.8), this design also *lies outside the FD boundaries* which cross-validates the consistency and accuracy of FD and GMF from the other way around.

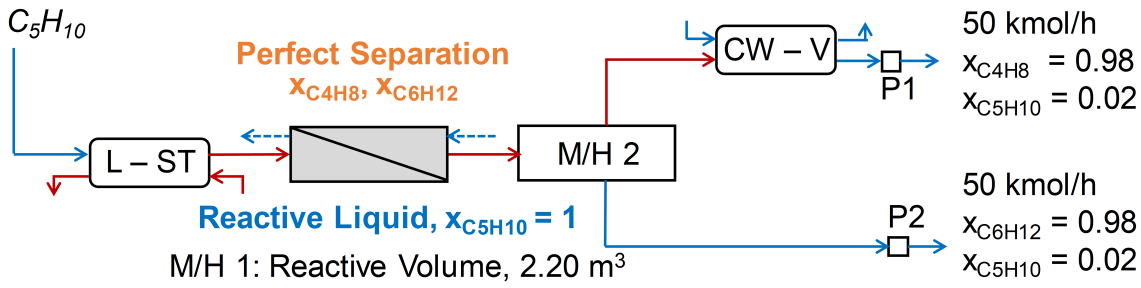


Figure 3.7: A thermodynamically infeasible design for reactive volume minimization. (Reprinted from [109])

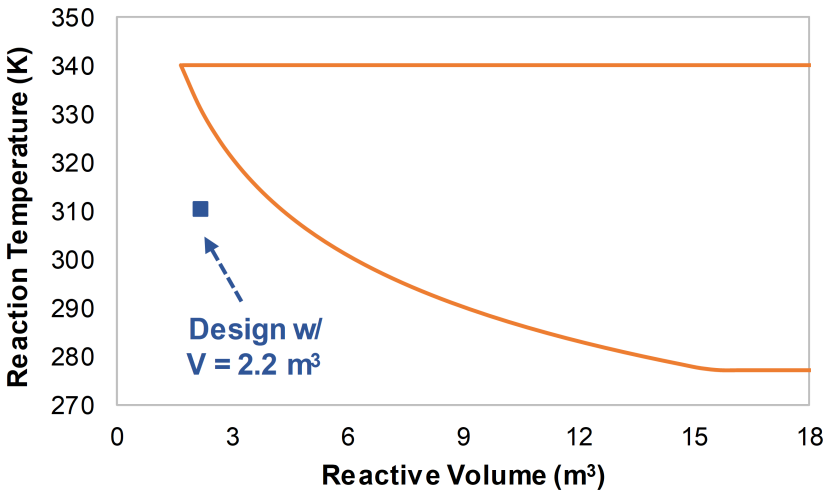


Figure 3.8: A thermodynamically infeasible design in comparison with FD boundaries. (Reprinted from [109])

## 3.4 Summary

In this work, we have developed the design envelope of a combined reaction/separation process for olefin metathesis. The attainable region-based Feinberg Decomposition theory provides the potential to characterize the ultimate design boundaries under given kinetics regardless process design configurations. The incorporation of FD approach into process intensification synthesis methods, such as the Generalized Modular Representation Framework, can: (i) provide thermodynamic/kinetic verification to the abstract phenomena-based representation, (ii) assist rapid screening of the combinatorial PI design space. Based on the discussions in this chapter, it will be worthy to further explore the following two open questions: (i) For the ultimate minimum reactive volume identified in Fig. 3.2, will there be a practical design to realize the miniaturization potential? How can this serve as a driving force pushing for innovative design? and (ii) How to formulate the FD design boundaries into the GMF driving force constraints to systematically intensify the process performance towards the ultimate bounds? This may provide a promising way to identify the "global" optimal process solution using GMF from mechanistic perspective compared to seeking global optimization techniques from numerical point of view.

# 4. PROCESS DESIGN AND INTENSIFICATION OF DIVIDING WALL COLUMNS[†]

## 4.1 Introduction

In this chapter, we investigate the process design and intensification of multi-component separation systems, with particular interest in the use of dividing wall columns (DWCs). DWC features a fully thermally coupled and single-shell distillation column [115, 116, 117]. The task-integrated design scheme, with improved thermodynamic efficiency, can lead to approximately 30% savings in capital expenditure, space, and energy [118, 119]. An indicative list of the process design approaches for DWC (or thermally coupled columns) is presented in Table 4.1. The pioneering process synthesis strategies by [120, 121, 122, 123] used "column sections" as the elementary components to construct a superstructure representation, which enabled the systematic generation of conventional distillation sequences, thermally coupled columns, and dividing wall columns by activating or deactivating the stream connections. However, the columns were generally modeled using short-cut methods (e.g., Underwood [124]) assuming sharp splits, constant volatility, etc. The pre-postulated superstructure of the column section interconnections also significantly affected the solution space as indicated by Agrawal [125]. With the recent advancements in deterministic and data-driven optimization algorithms, high-fidelity tray-by-tray models started to be applied for DWC design optimization [126, 127, 128]. While the column representation accuracy can be improved in this way, the resulting numerical complexity and computational load normally did not allow for simultaneous considerations of other structural variants beyond DWC systems.

GMF has also been applied to complex separation systems by Proios and Pistikopoulos [129]. GMF was able to systematically navigate the design space and to generate distillation sequences, heat-integrated distillation, and dividing wall column (Fig. 4.1), while providing a more efficient approach to balance representation accuracy and computational load. However, a simplified superstructure network was adapted which restricted the discovery of non-intuitive structural variants.

[†]This work is based on the article under review: Tian, Y., Meduri, V., Bindlish, R., & Pistikopoulos, E.N. A Process Intensification Synthesis Framework for Dividing Wall Column Systems. Computers & Chemical Engineering.

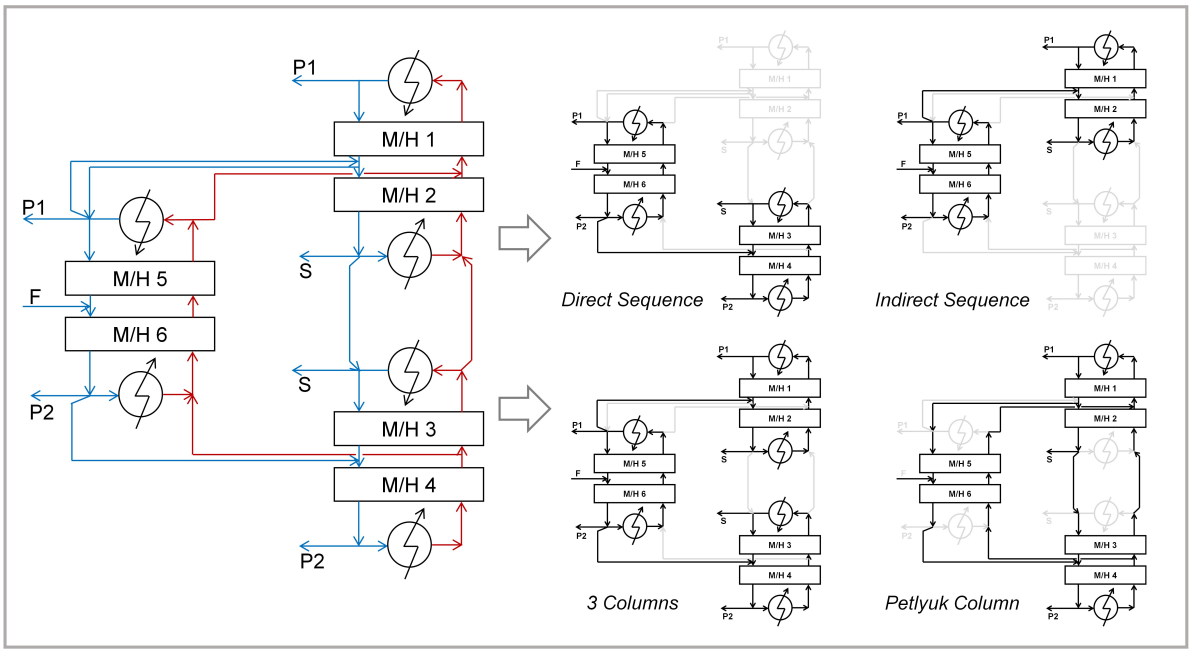


Figure 4.1: GMF structural variants for complex separation systems.

Herein, we extend the GMF synthesis approach with full superstructure representation capability to design and intensify a heterogeneous separation system for methyl methacrylate (MMA) purification. MMA is the foundational monomer for large-scale poly-methyl methacrylate production and the co-monomer widely used in plastics, paints, and coatings industry [130, 131]. Such applications also set a very high purity specification for the commercial MMA monomers (typically at 99.8%). A number of process alternatives have been proposed to purify the MMA reactor product at industrial scale, including the use of two distillation columns with water decanter [132, 133], two distillation columns with extraction [134], membrane-assisted separation [135], etc. In a patent by Jewell et al. [136] from Dow Global Technologies, a dividing wall column design, integrated with a water decanter, was proposed to improve MMA separation efficiency. It has been reported that, with the same number of column trays and the same energy consumption, the recovery of MMA product from the invented DWC design can be 12.2 kmol/h (or 7.6%) higher than a two-column design. This patented MMA purification process will be revisited hereafter as the case study to explore more energy- and cost-efficient process solutions using GMF.

Table 4.1: Process design for complex distillation column sequences – An indicative list.

| Authors | Design formulation | Process systems | Case studies | Key features |
|---|---|---|---|---|
| Sargent and Gaminibandara [120] | NLP | Complex distillation sequences | Multi-component separation | Superstructure representation with $n(n-1)$ column sections |
| Agrawal [125] | Superstructure generation | Complex distillation sequences | Near-ideal multi-component separation | Superstructure representation with $4n-6$ column sections or $n-2$ satellite columns with a central distillation column |
| Dünnebier and Pantelide [123] | MINLP | DWCs & Thermally coupled columns | Separation of close boiling C4's<br>Separation of alkane mixtures | Superstructure representation for systematic capture of conventional & thermally coupled columns |
| Caballero and Grossmann [121, 122] | MI(N)LP | DWCs & Thermally coupled columns | Separation of alcohols mixture<br>Separation of a hydrocarbons mixture | Two-stage superstructure representation to determine sequences of separation tasks & thermal states |
| Proios and Pistikopoulos [129, 93] | MINLP | DWCs & Thermally coupled columns | Benzene-toluene-o-xylene separation | Superstructure representation for systematic capture of conventional, heat-integrated & thermally coupled columns |
| Bravo-Bravo et al. [137] | Constrained stochastic multi-objective optimization | Extractive DWC | n-heptane/toluene/aniline<br>tetrahydrofuran/water/1,2-propanediol<br>isopropyl alcohol/water/dimethyl sulfoxide<br>acetone/water/octanoic acid | Optimal Extractive DWC design wrt. energy consumption & total annualized cost |
| Ramirez-Corona et al. [138] | NLP using shortcut models | Kaibel columns & Petlyuk columns | n-pentane/n-hexane/n-heptane<br>n-butane/i-pentane/n-pentane<br>i-pentane/n-pentane/n-hexane | Minimize total annualized cost |
| Okoli and Adams [126] | Rigorous simulation with particle swarm optimization | DWC | Lignocellulosic biomass to butanol process | Minimize total annualized cost |
| Gutiérrez-Antonio and Briones-Ramírez [139] | Surrogate-based optimization using neural networks | DWC | n-pentane/n-hexane/n-heptane<br>methanol/n-butanol/methyl formate | Reduced computational time to obtain the Pareto-optimal solutions |
| Rawlings et al. [127] | NLP<br>MINLP<br>GDP | Kaibel columns | methanol-ethanol-propanol-butanol | Rigorous tray-by-tray model for Kaibel column design |
| Waltermann et al. [128] | A series of relaxed MINLP models | DWC | n-butane/n-pentane/n-heptane<br>acetone/methanol/water<br>n-butane/n-pentane/n-heptane/n-octane, etc. | Equilibrium-stage based superstructure model<br>Multiple dividing walls<br>Three- and four-product separations |
| Yan et al. [140] | Static & dynamic analysis | DWC design based on conventional distillation sequences | monoethylene glycol, water, and other heavier glycols (di-, tri-, and tetraethylene glycol) | Static & dynamic process intensification |

Note: NLP – Nonlinear programming, MINLP – Mixed-integer nonlinear programming, GDP – General disjunctive programming

## 4.2 Case study: Methyl methacrylate purification

### 4.2.1 Process description

For the MMA purification case study defined in Jewell et al. [136], the raw material is considered as a reaction product mixture from MMA preparation consisting of MMA, Water (H2O), Methanol (MeOH), and MMA oligomers (MMAOLG). The oligomers of MMA include the dimer of MMA and smaller amounts of higher oligomers. The component feed flowrates are summarized in Table 4.2.

The quaternary mixture can exhibit liquid-vapor and liquid-liquid phase behaviors. Multiple methanol-MMA and water-MMA azeotropes can be formed in the system under different pressures and temperatures [141]. To accurately capture the complex phase behaviors, the UNIQUAC model and the associated parameters are adapted from Wu et al. [132] as given in Table 4.3, which have been compared and validated with experimental data and other activity coefficient models. The extended Antoine equation is applied for vapor pressure calculation, the coefficients of which are summarized in Table 4.4. Note that the MMA oligomers are treated as a pseudo component, with the major physical properties identical with MMA. The extended Antoine equation coefficients for MMA oligomers are estimated based on a C7 compound (i.e., C7H14O3), which can best approximate its volatility compared to the patent result data.

Table 4.2: MMA purification – Summary of component flowrates in feed mixture.

| Component | MMA | H2O | MeOH | MMAOLG |
|---|---|---|---|---|
| Flowrate (kmol/h) | 175.259 | 15.7643 | 0.332871 | 9.60129 |

UNIQUAC model:

$$\ln\gamma_i = \ln\frac{\Phi_i}{x_i} + \frac{z}{2}q_i\ln\frac{\theta_i}{\Phi_i} - q_i^{'}\sum_j \frac{\theta_j^{'}\tau_{ij}}{t_j^{'}} + l_i + q_i^{'} - \frac{\Phi_i}{x_i}\sum_j x_j l_j$$

$$\theta_i = \frac{q_i x_i}{q_T}, \quad q_T = \sum_k q_k x_k, \quad \theta_i^{'} = \frac{q_i^{'} x_i}{q_T^{'}}, \quad q_T^{'} = \sum_k q_k^{'} x_k,$$

$$\Phi_i = \frac{r_i x_i}{r_T}, \quad r_T = \sum_k r_k x_k, \quad l_i = \frac{z}{2}(r_i - q_i) + 1 - r_i^{'}$$

$$t_i^{'} = \sum_k \theta_k^{'}\tau_{ki}, \quad \tau_{ij} = exp(a_{ij} + \frac{b_{ij}}{T}), \quad z = 10$$

Table 4.3: MMA purification – UNIQUAC model parameters.

| Binary interaction parameters | | | | | |
|---|---|---|---|---|---|
| component i | component j | $a_{ij}$ | $a_{ji}$ | $b_{ij}$ | $b_{ji}$ |
| MMA | MMA | 0 | 0 | 0 | 0 |
| MMA | H2O | 0 | 0 | -474.33 | -194 |
| MMA | MeOH | 0 | 0 | -411.619 | 44.6284 |
| MMA | MMAOLG | 0 | 0 | 0 | 0 |
| H2O | H2O | 0 | 0 | 0 | 0 |
| H2O | MeOH | 0.6437 | -1.0662 | -322.131 | 432.879 |
| H2O | MMAOLG | 0 | 0 | -194 | -474.33 |
| MeOH | MeOH | 0 | 0 | 0 | 0 |
| MeOH | MMAOLG | 0 | 0 | 44.6284 | -411.619 |
| MMAOLG | MMAOLG | 0 | 0 | 0 | 0 |

| Relative molecular volume and surface area | | | | |
|---|---|---|---|---|
| Parameters | MMA | H2O | MeOH | MMAOLG |
| $r_i$ | 3.92156 | 0.92 | 1.43111 | 3.923 |
| $q_i$ | 3.564 | 1.4 | 1.432 | 3.68 |

Extended Antoine equation:

$$\ln P_i = C_{1i} + \frac{C_{2i}}{T + C_{3i}} + C_{4i}T + C_{5i}lnT + C_{6i}T^{C_{7i}} \quad (bar, K)$$

Table 4.4: MMA purification – Antoine equation coefficients for vapor pressure calculation.

| Component | $C_{1i}$ | $C_{2i}$ | $C_{3i}$ | $C_{4i}$ | $C_{5i}$ | $C_{6i}$ | $C_{7i}$ |
|---|---|---|---|---|---|---|---|
| MMA | 95.8471 | -8085.3 | 0 | 0 | -12.72 | 8.3307e-6 | 2 |
| H2O | 62.1361 | -7258.2 | 0 | 0 | -7.3037 | 4.1653e-6 | 2 |
| MeOH | 71.2051 | -6904.5 | 0 | 0 | -8.8622 | 7.4664e-6 | 2 |
| MMAOLG | 65.8111 | -8481.4 | 0 | 0 | -7.6565 | 6.4118e-18 | 6 |

The product specifications are set to obtain:

- MMA product with a MMA purity of at least 99.80 wt% and a maximum of 0.05 wt% water as per The Dow Chemical Company Sales Specification [142]. To ensure the product purity particularly to restrict the existence of low molecular weight components, the MMA product purity is also required to reach at least 99.80 mol%
- MMA product with a flowrate of at least 172 kmol/h, which is the best product recovery rate reported in the patent [136] with the integrated DWC and water decanter process
- Water recovery with a purity of at least 99.0 mol%

### 4.2.2 Synthesis objective

The *objective* is to synthesize the optimal process solution(s) for the above MMA purification process by minimizing total annualized cost. The DWC-decanter design invented in the patent [136] is used as a base case and new process solutions are to be developed with improved energy efficiency and cost efficiency. The use of dividing wall columns is of particular interest, while the applied GMF synthesis strategy, as detailed in Chapter 2, can systematically generate process options without equipment pre-postulation, thus not restricting the design solutions.

The solution of this problem will identify: (i) the unit operation selection and integrated process scheme (for multiple promising process design alternatives), (ii) the optimal process design and operating parameters, and (iii) the estimated total annualized cost.

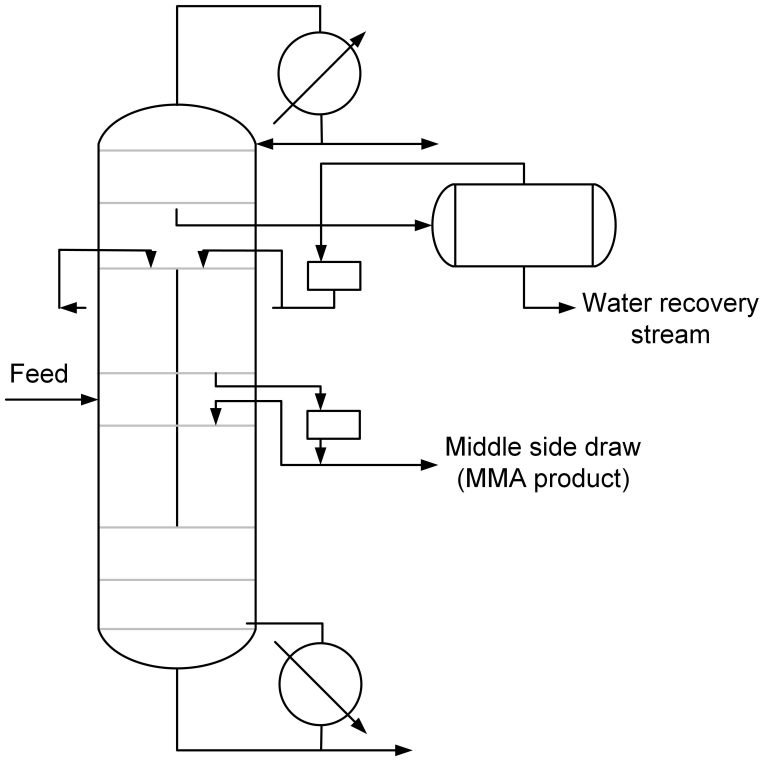


Figure 4.2: MMA purification using dividing wall column integrated with water decanter.

### 4.3 Base case design and simulation analysis

Fig. 4.2 (reproduced from U.S. Patent 10,392,337 [136]) depicts the integrated DWC-decanter design for MMA purification proposed by [136]. The key design characteristics are summarized as follow:

- The dividing wall column consists of 20 column stages (note that theoretical stages are assumed with 100% efficiency)
- The dividing wall extends vertically within the column
- The section of the column above the dividing wall can have 2 to 6 stages, the section below the dividing wall can have 2 to 6 stages, and the divided section can have 6 to 15 stages
- The column is operated at reduced pressure from 1 to 50 mmHg (note that the process temperature is preferably below 373.5 K to prevent MMA polymerization [143])

- Feed tray is located from the column bottom at a distance of 35% to 65% of the height of the dividing wall
- In addition to the distillate stream and the bottom stream, two side draws are removed from the column, namely:
  - Upper side draw: removed from one stage above the divided section and sent to the water decanter at a flowrate of 376 kmol/h
  - Middle side draw: i.e. the MMA product stream, removed from 35% to 65% height of the dividing wall at a flowrate of 172 kmol/h
- The water decanter separates the upper side draw to a dewatered organic stream and an aqueous stream
- The aqueous stream gives the water recovery stream
- The dewatered organic stream is returned to the column one stage below the stage from which the upper side draw is removed
- The dewatered stream is split between the divided sections preferably no more than 52% to each section

The integrated dividing wall column and water decanter flowsheet simulation is set up in Aspen Plus as shown in Fig. 4.3. The Aspen PETLYUK module is used to model the dividing wall column as a Petlyuk column, assuming no heat transfer across the dividing wall. The water decanter is modeled via the DECANTER module in which the liquid-liquid equilibrium calculations are employed for phase separation. Based on the patent design parameters, sensitivity analysis-based optimization is performed to minimize reboiler duty, condenser duty, and number of trays. The degrees of freedom for optimization include: (i) number of trays, (ii) feed tray location, (iii) distillate rate, (iv) reflux ratio, (v) vapor connect stream flowrates, and (vi) liquid connect stream flowrates. The resulting Petlyuk column design results are summarized in Table 4.5. The water decanter is

designed at 1 atm and 323.15 K, which requires a heating duty of 596.8 kW. This design configuration, after preliminary optimization in Aspen Plus, will be used as the base case and benchmark the energy and cost improvements resulted by the new design alternatives.

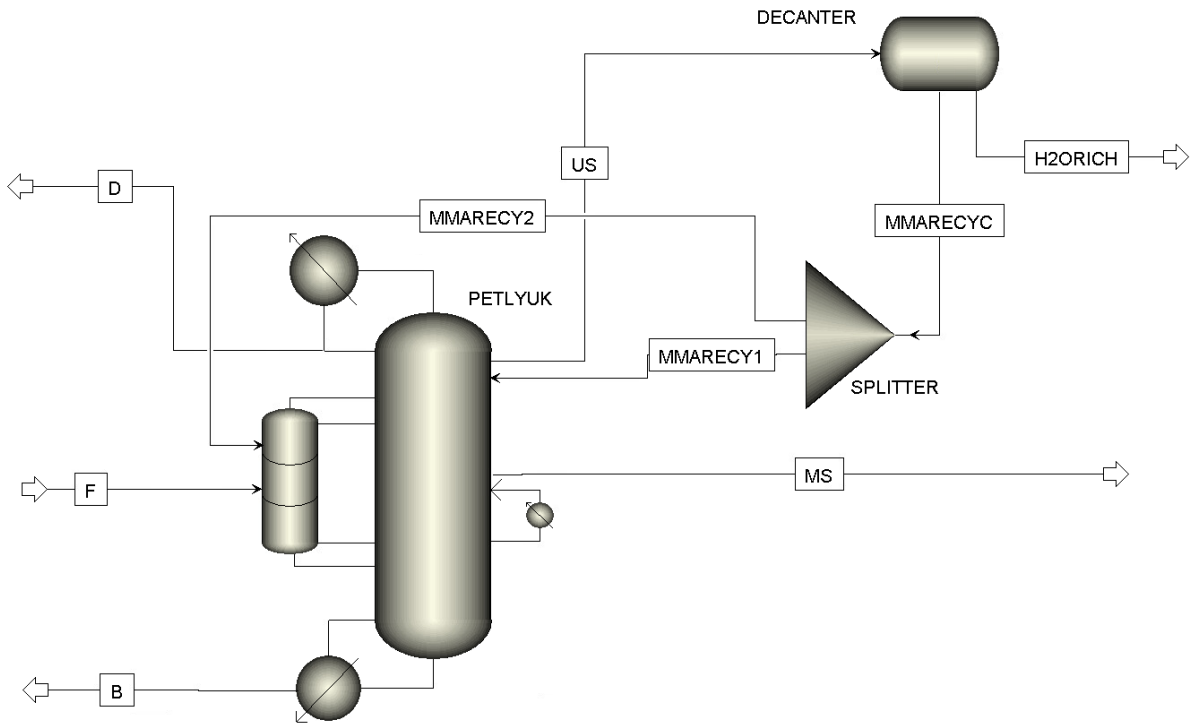


Figure 4.3: Base case design and simulation in Aspen Plus.

Table 4.5: Base case – Results summary for Aspen optimization.

| | | Main column | Prefractionator |
|---|---|---|---|
| Column design | Number of stages | 17 | 5 |
| | Feed stage location | 6 (MMARECY) | 1 (MMARECY) |
| | | | 3 (F) |
| | Reflux ratio | 69 | – |
| | Distillate rate (kmol/h) | 7 | – |
| | Pressure (atm) | 0.06 | 0.06 |
| Connect streams | Stream 1, Liquid | Source, Stage 6 | Destination, Stage 1 |
| | Stream 2, Vapor | Source, Stage 15 | Destination, Stage 5 |
| | Stream 3, Liquid | Destination, Stage 15 | Source, Stage 5 |
| | Stream 4, Vapor | Destination, Stage 6 | Source, Stage 1 |
| **Energy consumption** | **Heating duty (kW)** | **5035.5** | – |
| | **Cooling duty (kW)** | **-5560.4** | – |
| MMA product | Purity (wt%) | 99.84 | |
| | Purity (mol%) | 99.80 | |
| | Flowrate (kmol/h) | 172.0 | |
| Water recovery | Purity (mol%) | 99.45 | |
| | Flowrate (kmol/h) | 12.1 | |

Note: MMARECY – Dewatered MMA-rich outflow from Decanter, F – Feed stream
Heat duty – Positive numbers for heating, Negative numbers for cooling
Stage numbering – Condenser counted as the 1st stage, Reboiler counted as the last stage
Stage efficiency – Theoretical stages are assumed for design with 100% efficiency

## 4.4 Process intensification synthesis via GMF

In what follows, we leverage the GMF synthesis to investigate the industrial MMA purification problem, targeting for new process solutions with improved cost performance.

### 4.4.1 GMF representation for base case design

To ensure the representation accuracy for the MMA purification process, we first validate the GMF representation for the base case design configuration (Fig. 4.3). A GMF modular structure is set up as depicted in Fig. 4.4. The binary variables in the synthesis model are fixed according to the modular structure, e.g. if the interconnecting stream exist, the binary variable takes the value of 1; otherwise, the binary variable is assigned as 0. The feed stream and interconnecting

streams are placed in consistency with the Aspen simulation results given in Table 4.5. Each mass/heat exchange module ("M/H") stands for a certain column section as per the base case design, numbered in a descending order from right to left. The decanter ("DE") is modeled as a separate module integrated with the GMF modular building blocks, in which only liquid-liquid equilibrium calculations are performed.

In this context, M/H 1 represents the column section above the divided column section which consists of 5 stages. The upper side draw is removed as part of the M/H 1 liquid outlet stream and sent to the decanter module for liquid-liquid separation. The aqueous outlet stream from the decanter is the water recovery stream, while the dewatered organic outlet stream is returned and split equally to enter M/H 2 and M/H 5. M/H 2 and M/H 3 represent the divided section in the main column, between which the middle side draw (i.e., the MMA product stream) is obtained. As per the base case design, M/H 2 consists of 4 stages and M/H 3 consists of 6 stages. M/H 4 describes the column section below the divided section, comprising 2 stages. Two pure heat exchange modules are respectively placed at the top and the bottom, acting as a total condenser and a total reboiler. For the prefractionator section comprising 5 stages, M/H 5 and M/H 6 are used and the feed stream enters M/H 6. As can be noted, the number of stages captured by each mass/heat exchange module may vary from one to another. Each mass/heat exchange module in general characterizes a mass transfer pattern (e.g., component A and B transfer from the liquid phase to the vapor phase, component C from vapor to liquid). The number of stages necessitated to achieve the separation target by a mass/heat exchange module can be determined via: (i) a heuristic-based trial-and-error approach to translate each module to a minimum number of essential stages with an implicit objective function to minimize equipment size, and (ii) the GMF orthogonal collocation approach to rigorously obtain the optimal number of stages [93].

By "simulating" the above GMF structure for the base case design, we can test if GMF can capture the major process characteristics for this heterogeneous separation problem. As show in Fig. 4.5, the results for GMF representation and Aspen simulation are compared on the liquid composition profiles for the main column and the prefractionator. It can be noted that GMF provides

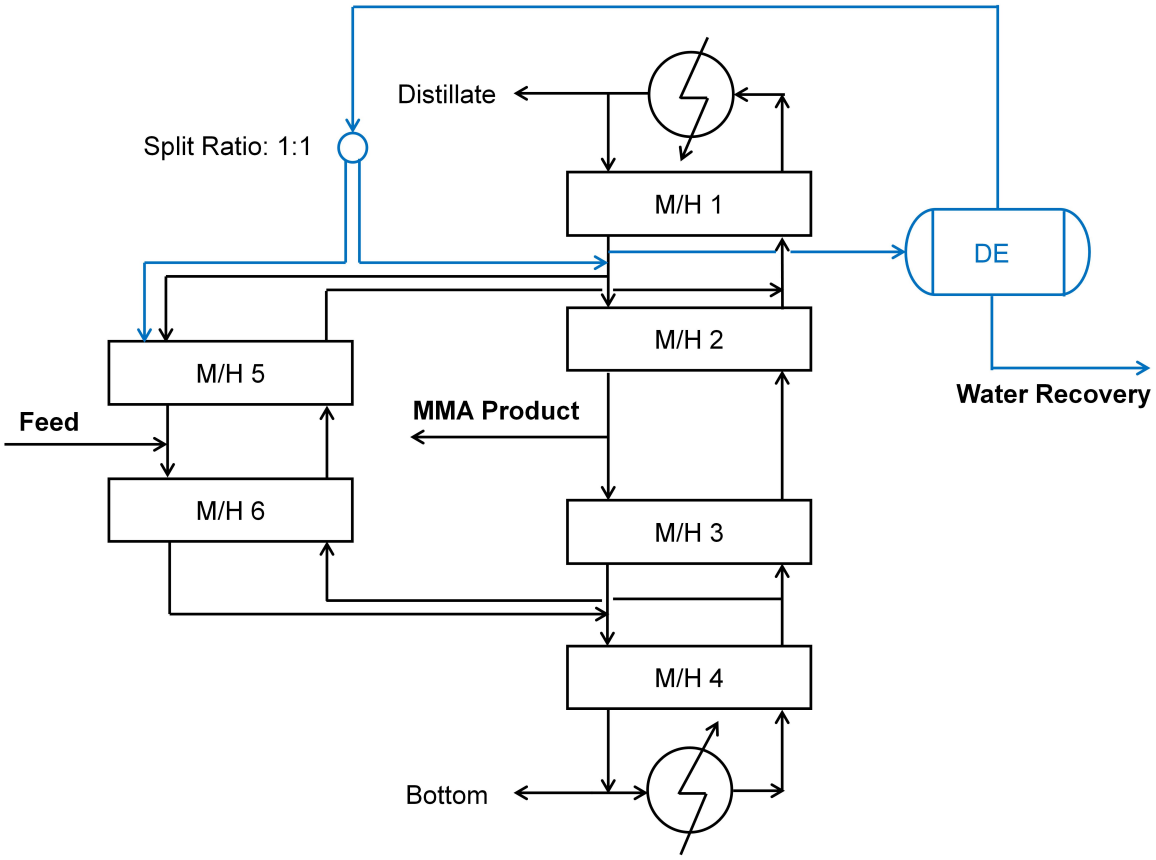


Figure 4.4: Base case – GMF representation.

an overall good estimate, although certain tray-wise details are missed, on describing the physical process taking place in the integrated process with the Petlyuk column and the decanter.

The conventional two-column configuration which was used in the patent [136] as a comparative design is also simulated using Aspen Plus RADFRAC module and then represented via GMF as shown in Fig. 4.6. Each of the column has 10 stages, with the feed stream enters the second stage in the first column. By comparing the liquid and vapor molar fraction profiles in Fig. 4.7, it can be concluded that GMF can accurately capture the complex physical behaviors in this MMA purification process.

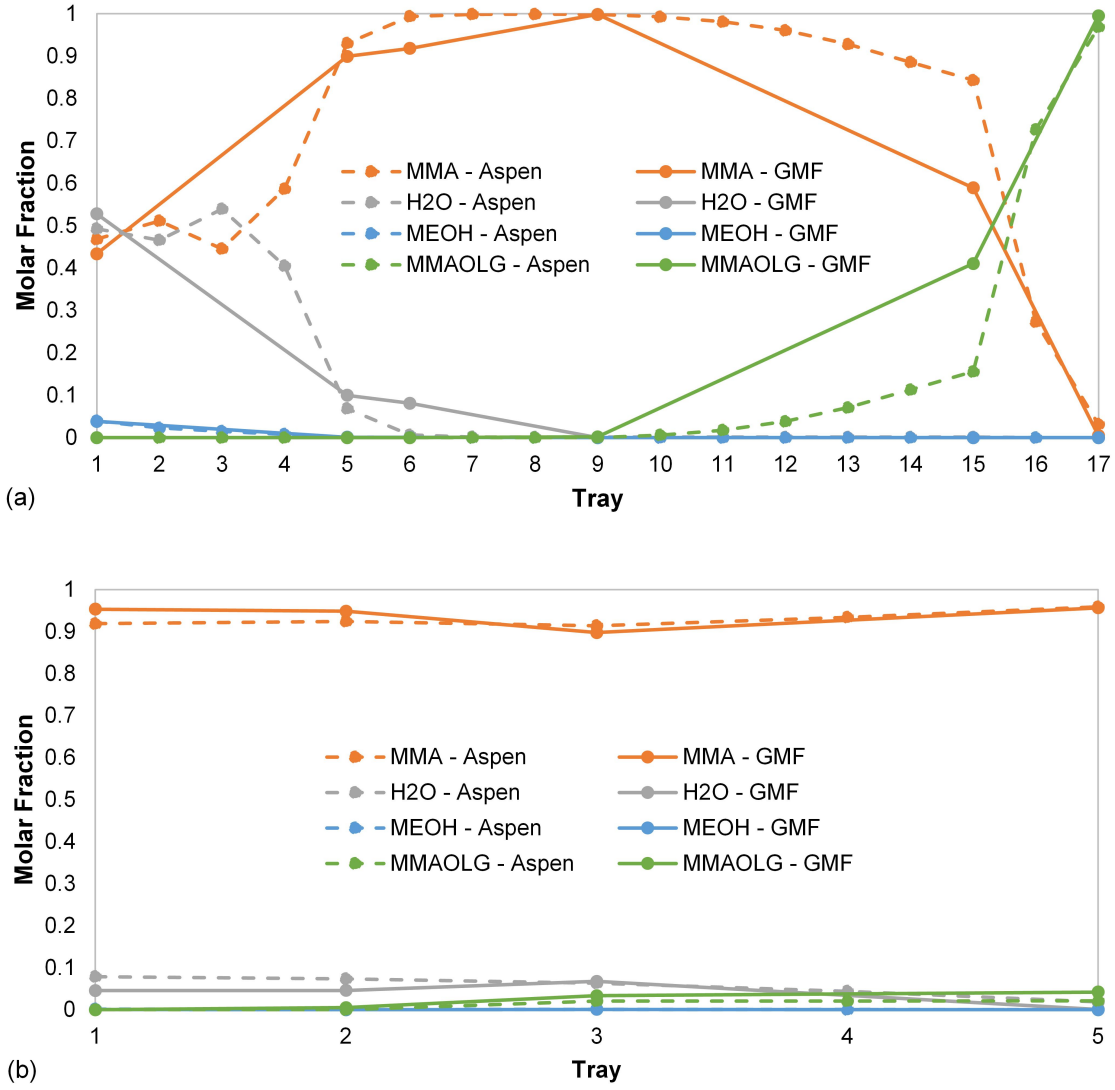


Figure 4.5: Base case – Validation of GMF representation vs. Aspen simulation
(a) Liquid molar fraction profile in main column,
(b) Liquid molar fraction profile in prefractionator.

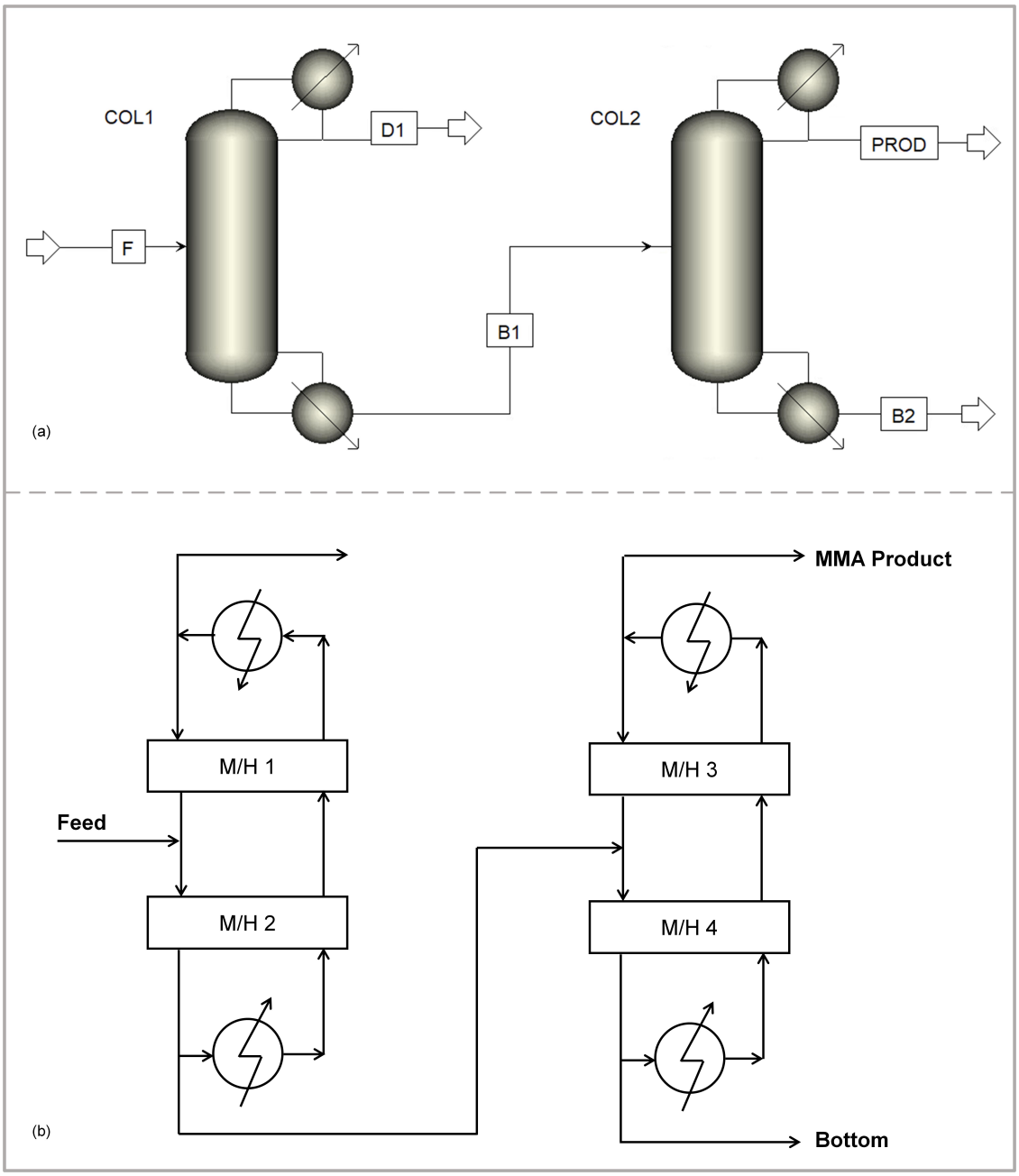


Figure 4.6: Two column design – (a) Aspen simulation, (b) GMF representation.

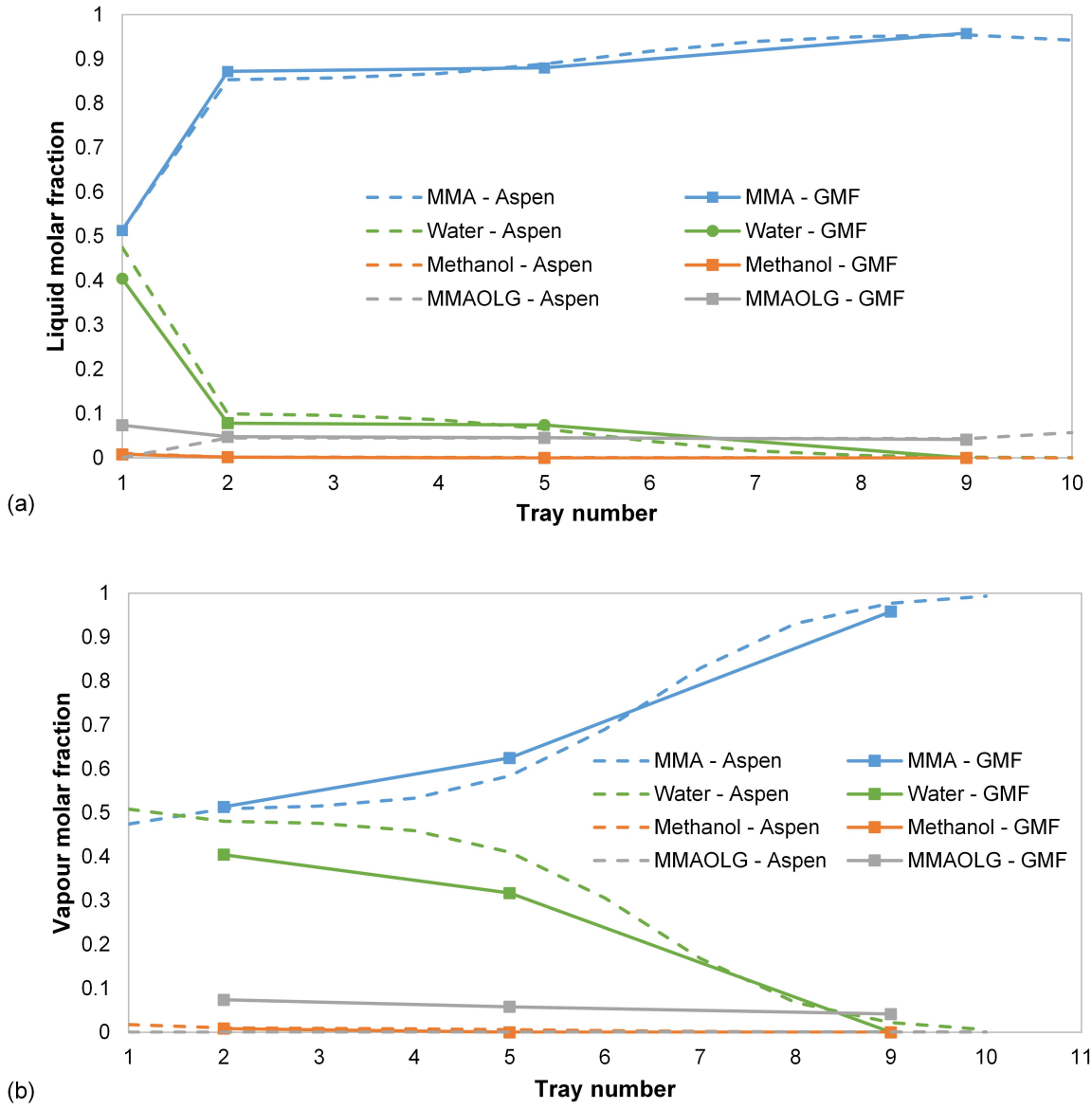


Figure 4.7: Two column design – Validation of GMF representation vs. Aspen simulation
(a) Liquid molar fraction profile in the first column,
(b) Vapor molar fraction profile in the first column.

### 4.4.2 GMF synthesis optimization

In this section, we optimize the MMA purification process using GMF synthesis.

#### *4.4.2.1 Retrofit design*

We first investigate to retrofit the base case design with minimum structural changes. To this purpose, all the pure heat exchange modules and mass/heat exchange modules in Fig. 4.4 are required to be active. Namely, no addition or reduction of the modules. The existing interconnecting streams and feed/product streams also remain active as that in Fig. 4.4. However, new interconnecting streams are allowed to be added to the structure for optimization. Note that the full stream connections are adapted in this work instead of the simplified GMF superstructure used in [129].

The resulting GBD Primal Problem comprises 8448 modeling constraints and 4493 continuous variables while the Master Problem with 510 modeling constraints and 783 binary variables. The initial solution structure is the base case design. The GBD solution procedure converges in 28 iterations and the optimal solution is obtained at the $17^{\text{th}}$ iteration as shown in Fig. 4.8 and Table 4.6. The notable differences between the new solution (referred as "Design 1") and the base case design include: (i) the upper side draw flowrate – instead of removing 376 kmol/h upper side draw as indicated by the patent, the upper side draw is removed at a much smaller flowrate of 40.3 kmol/h which reliefs the column for large amount vaporization, (ii) the split ratio of the decanter dewatered organic stream returning to the divided sections – instead of splitting equally to the prefractionator and the main column, the split ratio is suggested as 1:3.7 to return a larger portion of the organic stream to the main column to minimize remixing. The dewatered organic stream in this case actually has a larger MMA molar fraction ($\sim$ 92 mol%) than the liquid stream outlet from the prefractionator section, since the prefractionator streams mix with the MMA feed stream. Due to the previous specification of equal distribution, the adjustment in the split ratio is achieved by the GMF structural model via activating another splitting stream to the main column.

The base case design using GMF representation features a total annualized cost of $\$1.56 \times 10^6$, and the optimal retrofit design gives a total annualized cost of $\$1.06 \times 10^6$. Due to the abstract

GMF representation which tends to intensify the process design to the utmost efficiency [48, 109] and the approximations on pseudo-capital cost estimation, the actual number on cost improvements will be finalized using equipment-based rigorous simulation. However, the relative cost optimality for different GMF solutions and the corresponding design changes, as will be demonstrated later in Chapter 4.4, can provide critical instructions in generating better design solutions.

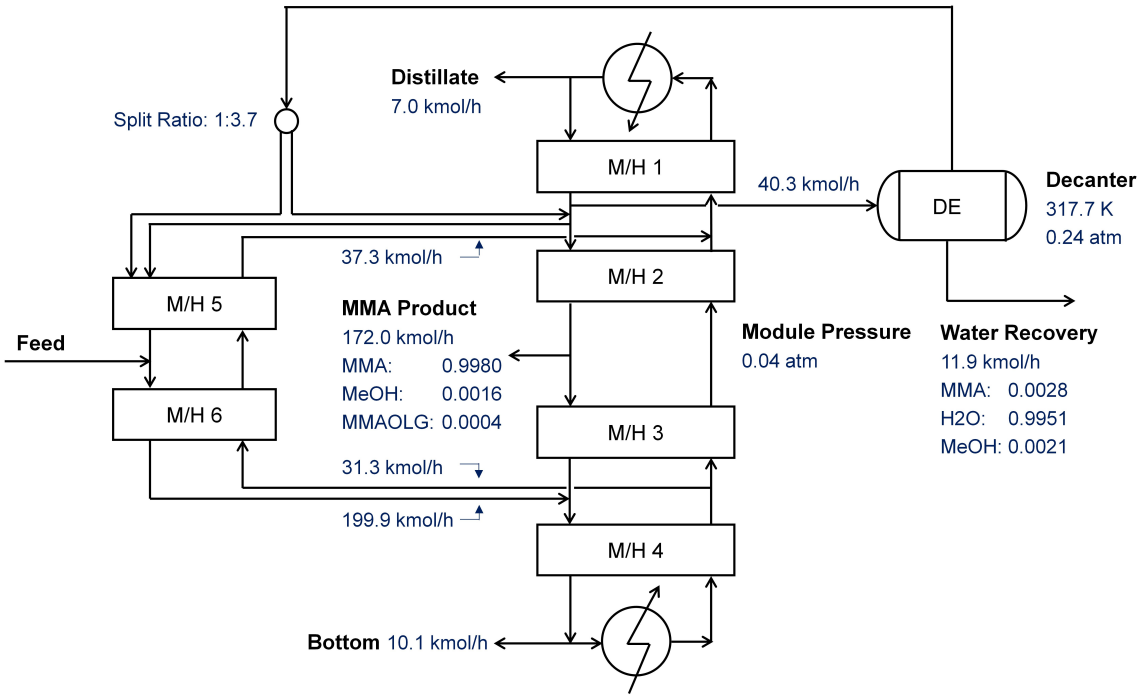


Figure 4.8: Design 1 – GMF synthesis solution for retrofit design.

Table 4.6: Design 1 – GBD convergence statistics.

| Iteration | 1 | 2 | 3 | 4 | 5 | 6 | 7 | 8 | 9 | 10 |
|---|---|---|---|---|---|---|---|---|---|---|
| Primal | 155.7 | 109.7 | 137.8 | 171.4 | 171.4 | 145.5 | 117.2 | 108.6 | 171.4 | 171.4 |
| Master | -30687.1 | -8038.7 | -8038.7 | -5111.2 | -5111.2 | -879.5 | -879.5 | -879.5 | -879.5 | -879.5 |
| Iteration | 11 | 12 | 13 | 14 | 15 | 16 | 17 | 18 | 19 | 20 |
| Primal | 168.2 | 171.4 | 171.4 | 124.7 | 124.7 | 108.5 | 106.1 | 154.7 | 146.9 | infes |
| Master | -879.5 | -879.5 | -879.5 | -879.5 | -879.5 | -879.5 | -879.5 | -879.5 | -879.5 | -879.5 |
| Iteration | 21 | 22 | 23 | 24 | 25 | 26 | 27 | 28 | | |
| Primal | infes | infes | 166.1 | 151.7 | 171.4 | 122.3 | 142.5 | 120.6 | | |
| Master | -879.5 | -879.5 | -879.5 | -879.5 | -879.5 | -876.4 | -271.7 | 120.6 | | |

#### *4.4.2.2 Grassroots design*

The optimal grassroots design is generated by enabling the full superstructure representation without pre-specifying any existing design components. A maximum of 10 mass/heat exchange modules and 20 heat exchange modules are available for use in the GMF structural model. Only the activated modules are considered in the synthesis model using the GAMS dynamic sets to reduce computational load. The initial design structure is set as the 6-module base case design, but with all the liquid and vapor connect streams activated to avoid pre-postulation. The GBD solution procedure converges in 25 iterations and the optimal solution is obtained at the $19^{\text{th}}$ iteration with a total annualized cost of $\$8.8 \times 10^5$. The design structure of this Design 2 and the GBD convergence statistics are presented respectively in Fig. 4.9 and Table 4.7. The overall structure still features a Petlyuk column type of design, to be further verified with equipment-based simulation. The key design changes are summarized as follow:

- Only four mass/heat exchange modules are selected, indicating a smaller equipment than the base case and Design 1
- No upper side draw is removed from the main column. Instead, the distillate stream is directed to the decanter
- The decanter dewatered organic stream is split into three streams: (i) a stream with 6.8 kmol/h flowrate returned to M/H 4 (i.e., the prefractionator section), (ii) a stream with 54.6 kmol/h flowrate returned to M/H 1 (in main column section), and (iii) another stream with 54.3 kmol/h flowrate returned to M/H 2 (in main column section)
- The MMA feed stream enters M/H 4
- The MMA product stream is obtained as the liquid outlet stream from M/H 1
- M/H 4 is coupled with the two pure heat exchange modules for vapor inlet and outlet streams
- Decanter is operated at 0.30 atm, 300.7 K

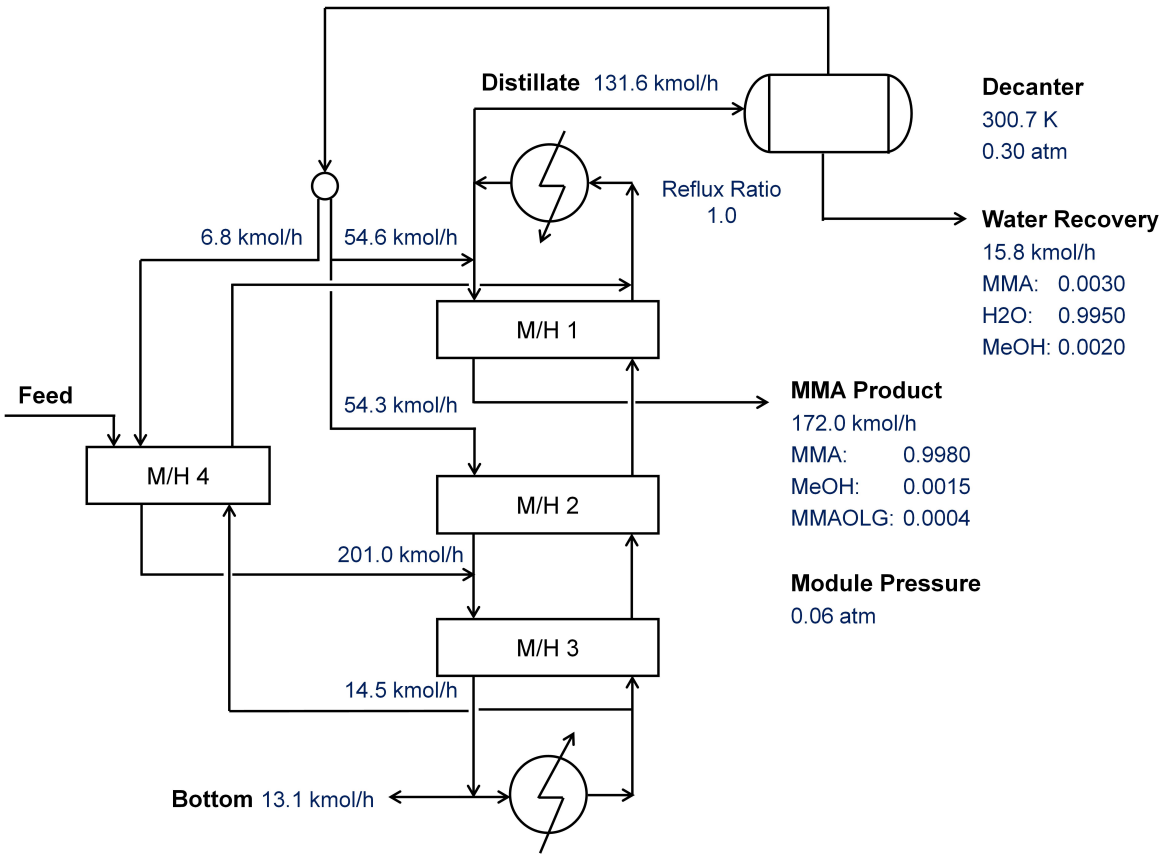


Figure 4.9: Design 2 – GMF synthesis solution for grassroots design.

Table 4.7: Design 2 – GBD convergence statistics.

| Iteration | 1 | 2 | 3 | 4 | 5 | 6 | 7 | 8 | 9 | 10 |
|---|---|---|---|---|---|---|---|---|---|---|
| Primal | 107.5 | infes | infes | infes | 171.4 | 171.4 | 171.4 | 171.4 | 171.4 | 171.4 |
| Master | -22624.4 | -22624.4 | -22624.4 | -22624.4 | -22400.8 | -22400.8 | -10996.1 | -5265.0 | -694.5 | -688.5 |
| Iteration | 11 | 12 | 13 | 14 | 15 | 16 | 17 | 18 | 19 | 20 |
| Primal | 171.4 | infes | infes | 171.4 | 171.4 | 171.4 | 171.4 | infes | 88.2 | 171.4 |
| Master | -435.0 | -422.1 | -422.1 | -189.0 | -187.8 | -163.2 | -159.0 | -159.0 | -159.0 | -23.9 |
| Iteration | 21 | 22 | 23 | 24 | 25 | | | | | |
| Primal | 171.4 | 171.4 | 171.4 | 171.4 | 161.7 | | | | | |
| Master | -23.9 | -20.8 | -20.8 | -20.8 | 94.7 | | | | | |

#### 4.4.2.3 *Two-column design*

To compare the two-column process with the above derived Petlyuk column designs, GMF synthesis is performed starting from the structure in Fig. 4.6b and enforces the use of four pure heat exchange modules. With the MMA product specifications of 99.8 wt% and 99.8 mol%, the maximum product flowrate is found to be 166.8 kmol/h which is 5.2 kmol/h less than Designs 1 and 2. By setting the MMA product flowrate specification as 165.0 kmol/h for this case, the optimal GMF solution is obtained in 7 iterations as illustrated in Fig. 4.10. The M/H 1 and the pure heat exchanger for heating make a stripping section, the vapor outlet stream from which is sent to the decanter module. As can be noted, the water recovery purity also requires further improvement. The liquid outlet stream, together with the decanter dewatered organic stream, enters M/H 3. M/H 2, M/H 3, and two pure heat exchangers compose a typical distillation column setup. Despite the insufficiency in product specifications, this process solution features a total annualized cost of $\$8.3 \times 10^5$ which makes it another potential design alternative. Therefore, this two-column process solution is referred as Design 3 to proceed with the next-step equipment-based process validation.

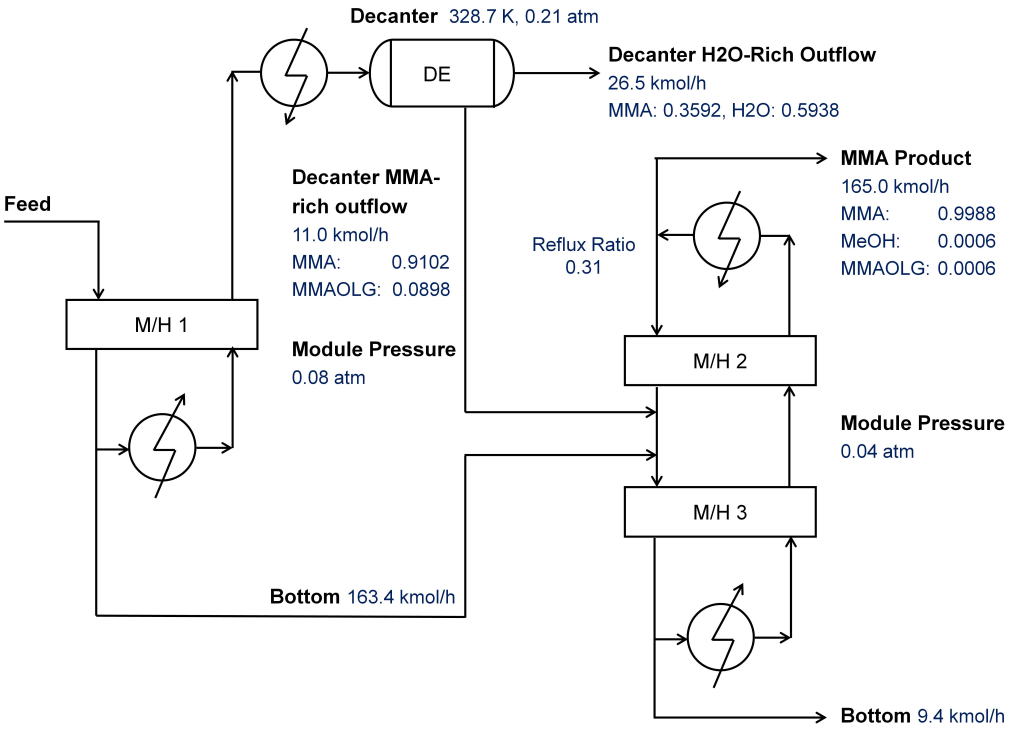


Figure 4.10: Design 3 – GMF synthesis solution for two-column process.

### 4.4.3 Steady-state validation and Aspen simulation

In this section, the Designs 1, 2, and 3 generated by GMF synthesis are translated as equipment-based process alternatives and simulated in Aspen Plus to validate the economic optimality. The Aspen simulation flowsheets are presented in Fig. 4.11 and the results are detailed in Table 4.8.

For Design 1 based on retrofit optimization, the Petlyuk column structure remains identical with that for the base case design (e.g., number of stages, feed stage locations, connect stream source and destination stages). The decanter dewatered organic stream split ratio is specified as 1:3 (prefractionator : main column) for Aspen simulation, adjusted based on the GMF suggested split ratio as 1:3.7. If Design 1 is translated to a dividing wall column, the resulting dividing wall position should allow for a larger space for the main column due to the asymmetrical distribution of vapor and liquid streams. GMF also suggests to reduce the upper side draw flowrate from 376 kmol/h in base case to around 40 kmol/h. In the Aspen simulation, 69 kmol/h is found to be the minimum achievable flowrate for the upper side draw. Additional synthesis results for the connect stream flowrates, main column reflux ratio, decanter temperature and pressure are also used as the initial guess in the Aspen simulation setup and further adjusted to reach product specifications and minimize condenser/reboiler duties. As a result, Design 1 achieves 18.4% reduction in the heating duty and 18.7% reduction in the cooling duty.

Design 2 is also translated to a Petlyuk column integrated with water decanter. In consistency with the base case Aspen optimization (Chapter 4.3), the target is to identify the corresponding column design with minimized reboiler duty, condenser duty, and number of stages. The main column, with three mass/heat exchange modules and two pure exchange modules (Fig. 4.9), is translated to a 10-stage column (including condenser and reboiler). More specifically, M/H 1 is translated to 2 stages, M/H 2 to 3 stages, and M/H 3 to another 3 stages. The prefractionator section, with one mass/heat exchange module, is identified as a 3-stage column section. As suggested by GMF synthesis structure, MMA feed stream enters the 1$^{st}$ stage in prefractionator. Around 10% of the decanter dewatered organic stream, the rest of the dewatered stream is split equally and fed respectively to Stages 3 and 5 in the main column. The connect stream stages in the main column

are the 2nd and the 10th stage. If this Petlyuk column is further translated to a dividing wall column, the divided section should be extended vertically from the 3rd stage to the 9th stage. The operating specifications in Aspen Plus for reflux ratio and distillate rate are respectively specified as 1.3 and 130.0 kmol/h, based on the GMF reflux ratio 1.0 and distillate rate 131.6 kmol/h. Note that, in this design, the distillate stream is directed to the decanter for water recovery and MMA recycle. Therefore, around 2 mol% methanol exists in the aqueous stream from the decanter. By adding a flash column, the water recovery stream can be purified to 99.5 mol%. In all, Design 2 results in 37.4% reduction in the heating duty and 39.0 % reduction in the cooling duty.

The equipment-based flowsheet for Design 3 comprises two conventional distillation columns, a water decanter, and a flash column to purify the aqueous stream from decanter. Column 1 consists of 10 stages, with the MMA feed stream entering on Stage 2. Column 2 consists of 7 stages. The bottom stream from Column 1 is fed onto the 4th stage in Column 2 and the decanter dewatered organic stream is all returned to the 5th stage in Column 2. As mentioned in Chapter 4.4.2.3, the GMF two-column synthesis provides a 5.6% lower total annualized cost than Design 2 at the trade-off of 7 kmol/h less MMA recovery flowrate. With the GMF suggested design structure, another trade-off solution is found in the Aspen simulation which can reduce 56.5 % heating duty and 56.1 % cooling duty. However, the MMA product is off-specification with MMA 99.8 wt% and 99.0 mol% while water is at 0.16 wt% exceeding the maximum 0.05 wt% threshold [142]. The process bottleneck for a higher MMA product purity is the insufficient separation of methanol and water from the decanter dewatered organic stream, which are carried then into the MMA product stream from the top of Column 2. An efficient selective separation method to remove the small amount methanol (0.64 mol%) and water (6.21 mol%) from the decanter dewatered organic stream (23 kmol/h), such as membrane-assisted separation [135, 144], may help to realize the potential energy savings using the two-column design.

To summarize, two Petlyuk column-based process alternatives, i.e. Design 1 and Design 2, have been identified by process intensification synthesis using GMF and then validated by rigorous steady-state simulation using Aspen Plus to achieve energy savings and equipment size reduction

for the MMA purification task. Assuming no heat transfer across the dividing wall, the Petlyuk columns can be converted to dividing wall column designs as shown in Fig. 4.12. The key design and operating considerations in the DWCs have been discussed in the previous section.

## 4.5 Summary

In this work, we have investigated the process synthesis intensification of an industrial methyl methacrylate purification process using the Generalized Modular Representation Framework. Two process alternatives have been systematically generated suggesting the use of dividing wall columns for optimal cost performance. Both designs can achieve equipment size reduction and substantial energy savings (i.e., Design 1: 18%, Design 2: 37%), compared to the base case developed in the original patent. A two-column design configuration is also developed with promising energy savings and the process bottleneck for product purity improvement is identified which necessitates the adaptation of selective separation techniques.

On the other hand, task-integrated process intensification systems (e.g. dividing wall column) feature unique operability and control challenges compared to its conventional process counterparts, such as faster dynamics, reduced operating window, vulnerability to process disturbances [29]. Therefore, it is important to further analyze the resulting DWC-based design alternatives with respect to the steady-state and/or dynamic operability performance [145, 146]. Steady-state process intensification synthesis with operability considerations and dynamic operational optimization with model predictive control can be essential tools to ensure feasible and optimal operations under uncertainty and disturbances as will be discussed later in Chapters 6 and 7.

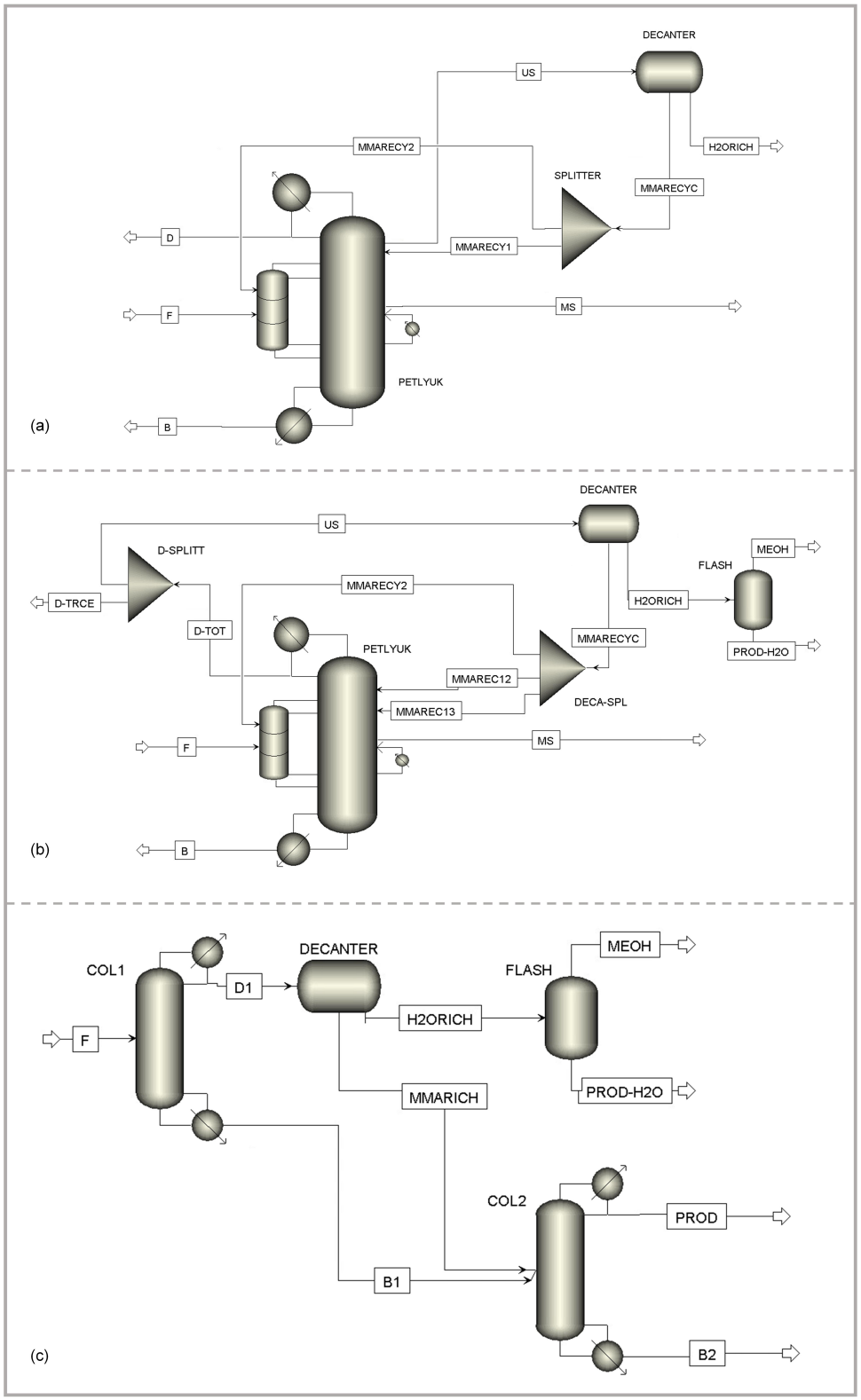


Figure 4.11: Aspen simulation flowsheets for Designs 1, 2 and 3.

Table 4.8: Designs 1, 2 and 3 – Results summary for Aspen simulation.

| | | Design 1 | Design 2 | Design 3 |
|---|---|---|---|---|
| Column 1 | Number of stages | 17 | 10 | 10 |
| | Feed stage location | 6 (MMARECY) | 3 (MMARECY1)<br>5 (MMARECY2) | 2 (F) |
| | Reflux ratio | 56 | 1.3 | 0.001 |
| | Pressure (atm) | 0.06 | 0.06 | 0.06 |
| | Vapor split ratio | 22.8 | 1.43 | – |
| | Liquid split ratio | 51.7 | 7.66 | – |
| Column 2<br>(or Prefractionator) | Number of stages | 5 | 3 | 7 |
| | Feed stage location | 1 (MMARECY)<br>3 (F) | 1 (MMARECY)<br>1 (F) | 4 (from COL1)<br>5 (MMARECY) |
| | Reflux ratio | – | – | 0.05 |
| | Pressure (atm) | 0.06 | 0.06 | 0.04 |
| Connect stream 1 (Vapor) | Source | COL2, Stage 1 | COL2, Stage 1 | – |
| | Destination | COL1, Stage 6 | COL1, Stage 2 | – |
| Connect stream 2 (Liquid) | Source | COL1, Stage 6 | COL1, Stage 2 | – |
| | Destination | COL2, Stage 1 | COL2, Stage 1 | – |
| Connect stream 3 (Vapor) | Source | COL1, Stage 15 | COL1, Stage 10 | – |
| | Destination | COL2, Stage 5 | COL2, Stage 3 | – |
| Connect stream 4 (Liquid) | Source | COL2, Stage 5 | COL2, Stage 3 | – |
| | Destination | COL1, Stage 15 | COL1, Stage 10 | – |
| Decanter | Temperature (k) | 317.8 | 323.2 | 290 |
| | Pressure (atm) | 0.23 | 0.40 | 0.40 |
| | MMA recovery split ratio (COL2:COL1) | 1:3 | 1:4.5:4.5 | – |
| Energy consumption | Total reboiler duty (kW) | 4517.3 | 3248.0 | 2387.1 |
| | Total condenser duty (kW) | -4521.4 | -3391.8 | -2431.9 |
| | Decanter duty (kW) | 78.3 | 193.5 | -10.3 |
| | Flash column duty (kW) | – | 82.2 | 59.8 |
| **Energy savings (compared to base case)** | **Heating duty** | **18.4%** | **37.4%** | **56.5%** |
| | **Cooling duty** | **18.7%** | **39.0%** | **56.1%** |
| MMA Product | MMA wt% | 99.96 | 99.80 | 99.80 |
| | MMA mol% | 99.80 | 99.80 | 99.04 |
| | Water wt% | 0.04 | 0.02 | 0.16 |
| | Flowrate (kmol/h) | 172.0 | 172.0 | 172.0 |
| Water recovery | Purity (mol%) | 99.24 | 99.48 | 99.52 |
| | Flowrate (kmol/h) | 12.2 | 9.6 | 10.9 |

Note: MMARECY – Dewatered MMA-rich outflow from Decanter, F – Feed stream
COL1 – Column 1, COL2 – Column 2 (or Prefractionator)
Heat duty – Positive numbers for heating, Negative numbers for cooling
Tray numbering – Condenser counted as the 1$^{st}$ tray, Reboiler counted as the last tray
Stage efficiency – Theoretical stages are assumed for design with 100% efficiency

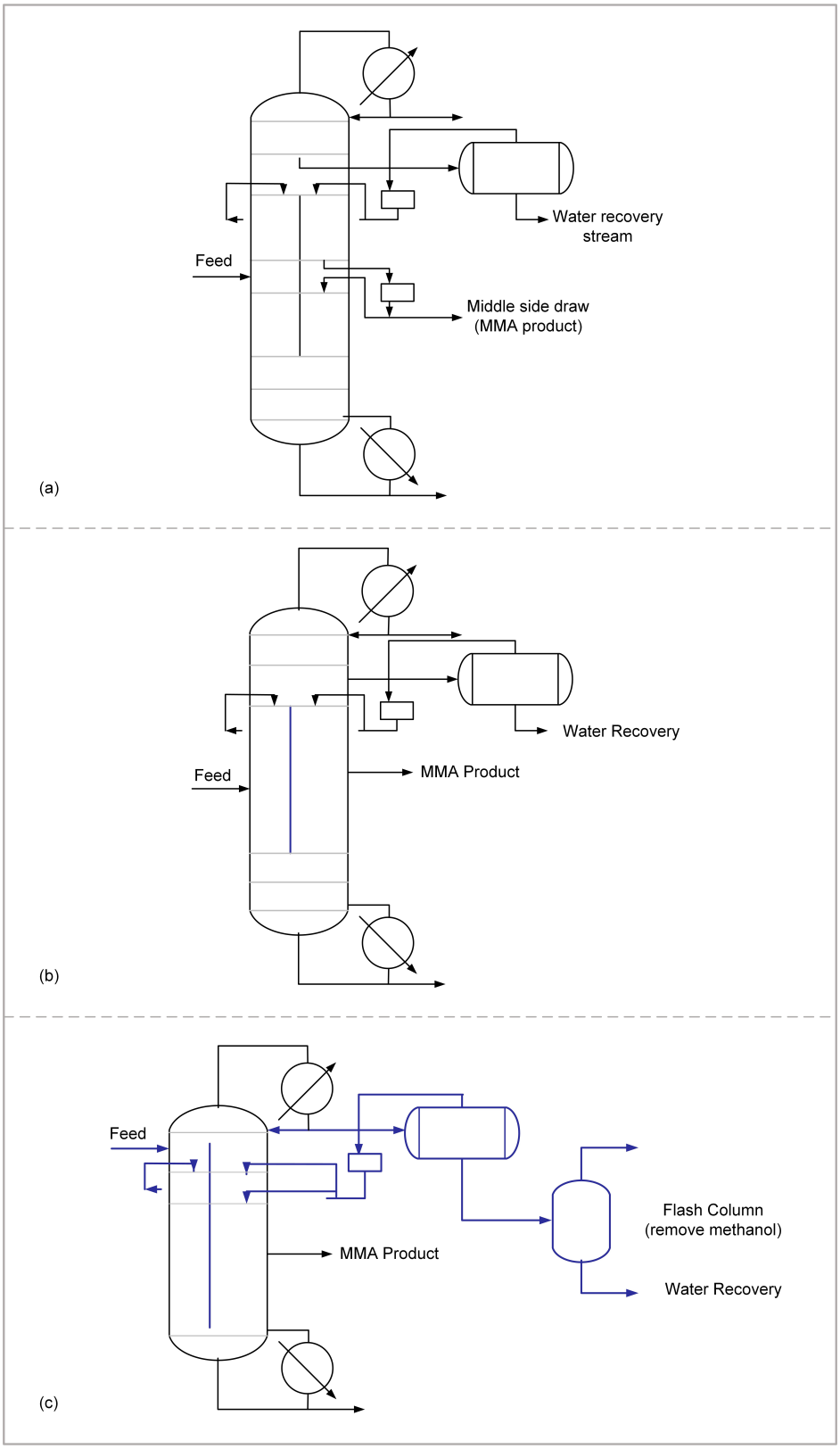


Figure 4.12: Dividing wall column designs for the MMA purification case study – (a) Patent design, (b) Design 1, (c) Design 2

# 5. PROCESS DESIGN AND INTENSIFICATION OF EXTRACTIVE SEPARATION SYSTEMS WITH MATERIAL SELECTION[†]

## 5.1 Introduction

A key enabling factor to achieve process intensification goals is the development of advanced materials (e.g., ionic liquids, molecularly porous materials), as highlighted in Chapter 1.2.1. The integration of advanced materials in intensified equipment and processes necessitates a multi-scale consideration to bridge the gap between material performance evaluation, equipment optimization, and process integration in a simultaneous or hierarchical manner (Fig. 5.1). From PSE point of view, material selection has been one of the core topics for process synthesis and design [147]. With the recent advances in data analytics and computer-aided molecular design methods [148], there is an increasing interest to integrate model-based solvent selection and design strategies with process synthesis to identify simultaneously the optimal process design with the corresponding mass separating agent. An indicative list of publications in this area is provided in Table 5.1, which apply mostly to extractive separation systems.

In this chapter, we extend GMF for design, synthesis, and intensification of extractive separation systems with solvent selection based on the work by Ismail et al. [96]. We particularly investigate how the selection of materials can directly impact on the fundamental mass and/or heat transfer performances in a phenomena building block. The contributions of this work are twofold: (i) GMF is integrated with the Orthogonal Collocation (OC) method to enhance the representation accuracy for nonideal separation systems, and (ii) GMF is applied to evaluate the use of an ionic liquid solvent (i.e., [EMIM][OAc]) for a representative ethanol-water separation process.

[†]Reproduced in part with permission from Tian, Y., & Pistikopoulos, E. N. (2019). Generalized Modular Representation Framework for the Synthesis of Extractive Separation Systems. In Computer Aided Chemical Engineering (Vol. 47, pp. 475-480). Copyright 2019 Elsevier Ltd. Part of this work is based on the manuscript under review: Tian, Y., & Pistikopoulos, E. N. A Process Intensification Framework for Extractive Separation Systems with Material Selection. Journal of Advanced Manufacturing and Processing.

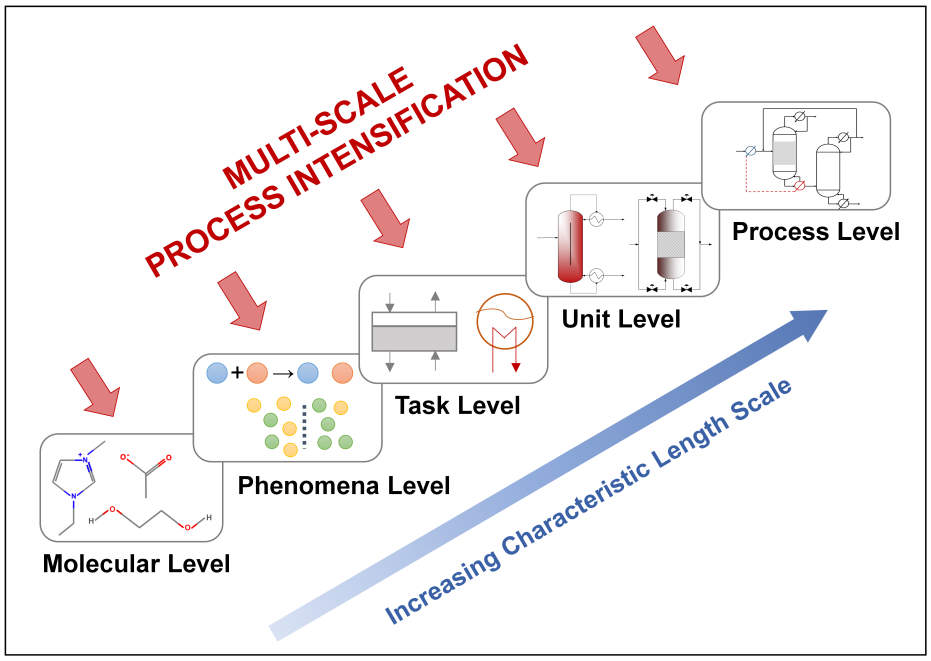


Figure 5.1: Multi-scale process intensification.

## 5.2 Problem statement

The generalized design problem addressed in this chapter for extractive separation processes with solvent selection can be defined as follows:

*Given:*

- A multi-component feed stream with minimum-/maximum- boiling azeotropes or low relative volatility mixtures and given compositions, flow rates, supply temperatures;
- A set of desired products with specifications on flow rates, purities, etc.;
- A set of available solvents which can facilitate the homogeneous separation and given availability and temperatures, and compositions;
- A set of available heating and cooling utilities and given availability and temperatures;
- All physical property models and parameters (e.g., activity coefficient model, Antoine coefficients, heat capacity coefficients);
- Cost data of solvents, heating and cooling utility.

The *objectives* are: (i) to minimize total annualized cost (TAC), (ii) to synthesize optimal process solution(s), conventional or intensified, for the specified separation problem, and (iii) to identify the optimal solvent choice integrated with design.

Table 5.1: Integrated material selection/design and process synthesis – An indicative list.

| Methods | Authors | Process Applications | Problem Formulation |
|---|---|---|---|
| Computer-aided molecular design | Hostrup et al. [149] | Solvent design for acetone-chloroform separation and solvent substitutes for acetic acid-water separation | Hybrid methods for solvent design, screening, and process synthesis |
| | Papadopoulos and Linke [150] | Solvent design for liquid-liquid extraction and gas-absorption processes | Multi-objective optimization |
| | Folić et al. [151] | Solvent design for a solvolysis reaction | Stochastic optimization |
| | Lek-utaiwan et al. [152] | Simultaneous solvent selection and extractive distillation column design for C8-Aromatics mixture separation | Hierarchical process design and optimization framework |
| | Valencia-Marquez et al. [153] | Simultaneous design of ionic liquid solvent and extractive distillation column for ethanol-water separation | Disjunctive mixed-integer nonlinear programming |
| | Medina-Herrera et al. [75] | Solvent selection for extractive distillation processes with safety considerations | Hierarchical framework, Genetic algorithm |
| | Zhou et al. [154] | Optimal solvent design for extractive distillation processes | Multi-objective optimization-based hierarchical framework |
| Group contribution | Marcoulaki and Kokossis [155] | Design of novel solvents for ethanol-water extraction, etc. | Simulated annealing |
| | Chen et al. [156] | Integrated ionic liquid and process design for azeotropic separation | Mixed-integer nonlinear programming |
| Molecular clustering | Papadopoulos and Linke [157] | Synthesis of solvents for cyclohexane-benzene extractive distillation, etc. | Clustering, Multi-objective optimization |
| Use of thermodynamic models (e.g., NRTL, UNIFAC) | Ismail et al. [96] | Simultaneous solvent selection and process synthesis for homogeneous azeotropic separation processes | mixed-integer nonlinear programming |
| | Waltermann et al. [158] | Hierarchical solvent selection and process design with energy integration for azeotropic distillation | Mixed-integer nonlinear programming |

## 5.3 Case study: Ethanol-water separation

We investigate two case studies for the design of ethanol-water separation systems. Case Study 1 showcases the proposed GMF and GMF/OC approaches to obtain ethanol product with 99 mol% purity using methanol and ethylene glycol as the solvent candidates. In Case Study 2, we explore the use of an ionic liquid solvent, i.e. [EMIM][OAc], to obtain a high-purity ethanol product with 99.8 mol% purity and a water product with 99 mol% purity. Via the case studies, we aim to: (i) demonstrate the applicability and effectiveness of the proposed GMF and GMF/OC synthesis approaches to systematically generate extractive separation process solutions with improved cost performance and integrated solvent selection considerations, and (ii) evaluate the design feasibility and economic optimality on using a specific ionic liquid solvent in ethanol-water extractive separation process.

### 5.3.1 Solvents: Ethylene glycol and methanol

The minimum boiling azeotrope composition of ethanol (EtOH) and water (H2O) is at EtOH 89.43 mol%, 351.15 K, 1 atm. Herein, we revisit the case study presented in Ismail et al. [96]. Ethylene glycol (EG) and methanol (MeOH) are selected as solvent candidates. The feed stream consists of 85 mol% EtOH and 15 mol% H2O with a flow rate of 10 kmol/s at 351.3 K, 1 atm (i.e., saturated liquid feed). The separation target is to obtain a liquid ethanol product with a purity of 99 mol% and a flow rate of 8 kmol/s. The system is considered at constant atmospheric pressure. The NRTL equation (Eq. 5.1) is utilized and integrated to the GMF model formulation. The NRTL binary interaction parameters for the ternary systems (i.e., Ethanol-Water-Ethylene Glycol and Ethanol-Water-Methanol) are adapted from Ismail et al. [96] (Table 5.2). The pseudo capital cost calculation is calculated and the utility cost data are respectively $\$26.19/(\text{kW} \cdot \text{yr})$ for cooling water and $\$137.27/(\text{kW} \cdot \text{yr})$ for steam. The synthesis objective is to determine a cost-optimal design and to identify the corresponding solvent which can satisfy the product specifications.

$$\ln \gamma_i = \frac{\sum_{j\in c} \tau_{ji} G_{ji} x_j}{\sum_{j\in c} G_{ji} x_j} + \sum_{j\in c} \frac{G_{ij} x_j}{\sum_{l\in c} G_{lj} x_l} \tau_{ij} - \frac{\sum_{l\in c} \tau_{lj} G_{lj} x_l}{\sum_{l\in c} G_{lj} x_l}$$
$$\tau_{ij} = \frac{\Lambda_{ij}}{RT}, \qquad G_{ij} = exp(-\alpha_{ij}\tau_{ij}), \qquad \Lambda_{ii} = 0, \qquad \alpha_{ij} = \alpha_{ji} \tag{5.1}$$
$$\Lambda_{ij} = aa_{ij} + ab_{ij} \times (T - 273.15) \text{ cal/mol}$$

Table 5.2: Case Study 1 – NRTL binary interaction parameters.

| Ethanol (1) - Water (2) - Ethylene Glycol (3) System | | | | | |
|---|---|---|---|---|---|
| $ij$ | $aa_{ij}$ | $ab_{ij}$ | $aa_{ji}$ | $ab_{ji}$ | $\alpha_{ij}$ |
| 12 | -441.20 | 18.3280 | 3293.17 | 17.0471 | 0.475000 |
| 13 | 13527.42 | -92.7391 | -4351.97 | 53.3769 | 0.370400 |
| 23 | 1383.43 | 8.0409 | -1445.97 | -9.1506 | 0.185894 |
| Ethanol (1) - Water (2) - Methanol (4) System | | | | | |
| $ij$ | $aa_{ij}$ | $ab_{ij}$ | $aa_{ji}$ | $ab_{ji}$ | $\alpha_{ij}$ |
| 12 | 206.7 | 0 | 5270.3 | 0 | 0.4 |
| 14 | 0 | 0 | 0 | 0 | 0.4 |
| 24 | 3641.5 | 0 | -788.20 | 0 | 0.4 |

#### *5.3.1.1 GMF synthesis*

The GMF synthesis superstructure pre-postulates sixteen pure heat exchange modules and eight mass/heat exchange modules. It results in an MINLP model with 4,864 continuous variables, 478 binary variables, and 4,377 equality/inequality constraints. The objective is set to minimize operating cost (including heating and cooling utility cost).

Fig. 5.2(a) shows the optimal separation system design identified by GMF, with an operating cost of $\$6.34 \times 10^7$ per year. Numbered in a descending order, the design consists of one pure

heat exchange module for cooling, three mass/heat exchange modules for ethanol-water-ethylene glycol separation, as well as another pure heat exchange module for heating. Ethylene glycol, as the heavier solvent compared to methanol, is selected and the desired ethanol product is obtained from the distillate stream. This modular solution will be later verified and compared with rigorous equipment-based simulation. These results are consistent with that presented in Ismail et al. [96].

An intermediate solutions is generated by introducing integer cuts. As shown in Fig. 5.2(b), Alternative 1 selects EG as solvent and features an operating cost of $\$6.98\times10^7$ per year. Compared to the optimal solution in Fig. 5.2(a), one of the modules is placed as a "side-module" coupled with the other two modules featuring an integrated process design. However, this design requires a larger reflux flow rate and higher operating cost than the optimal design.

Another process alternative is generated by specifying MeOH as solvent, featuring an operating cost of $\$11.4 \times 10^7$ per year. In this context, ethanol is the intermediate component in the MeOH-EtOH-H2O mixture with respect to volatility. As depicted in Fig. 5.2(c), two sequential separation steps are included in this process. Namely, the first mass/heat exchange module separates water from the liquid outlet stream, while the vapor outlet stream is sent to the next module to purify ethanol from methanol.

#### *5.3.1.2 GMF/OC synthesis*

Herein, we apply the GMF/OC method to design EtOH-H2O separation system(s) by minimizing TAC, which accounts for the pseudo module capital cost, heating and cooling utility cost. The selection of the number of collocation points (i.e., $nc$) in each module is critical to balance the modular representation accuracy and the computational time. In light of this, we perform a parametric analysis to discretize each module with different numbers of interior collocation points and to optimize the process with respect to TAC. The results are summarized in Table 5.3. As can be noted, the OC discretization scheme with 2 interior collocation points provides the optimal TAC value. Moreover, the resulting optimal GMF/OC modular structure remains consistent with that identified using GMF (Fig. 5.2(a)). This is due to the fact that, operating cost is the dominant driving force for cost optimization since it takes up a major part of TAC in distillation systems.

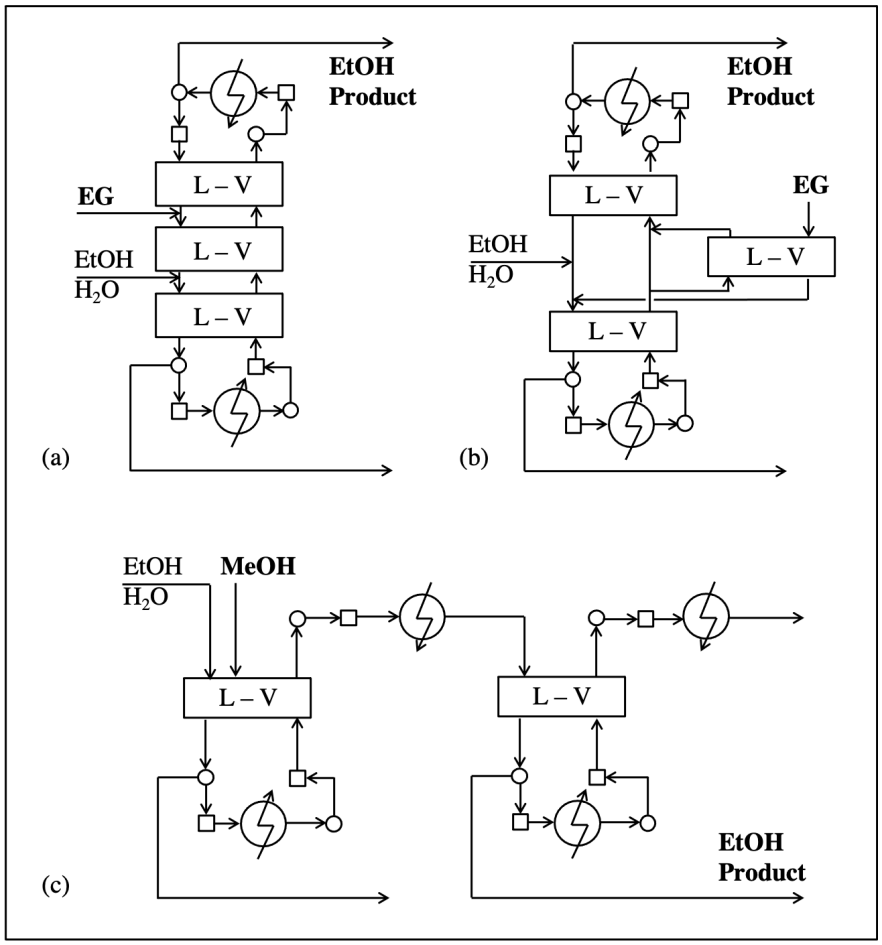


Figure 5.2: Case Study 1 – GMF synthesis
(a) Optimal solution, (b) Alternative 1, (c) Alternative 2.

Table 5.3: Case Study 1 – GMF/OC synthesis results using different discretization schemes.

| $nc$ | 1 | 2 | 3 |
|---|---|---|---|
| $M_1$ | 10.0 | 2.9 | 3.3 |
| $M_2$ | 2.0 | 6.0 | 3.0 |
| $M_3$ | 10.0 | 2.4 | 3.0 |
| Reflux ratio | 0.30 | 0.25 | 0.27 |
| Reboiler duty ($\times 10^5$ kW) | 3.86 | 3.70 | 3.87 |
| Condenser duty ($\times 10^5$ kW) | 4.12 | 4.03 | 4.05 |
| TAC ($\$/year$) | $7.10 \times 10^7$ | $6.76 \times 10^7$ | $7.01 \times 10^7$ |

#### *5.3.1.3 Equipment-based process simulation*

The GMF and GMF/OC design solutions obtained in the previous sections will be translated to equipment-based process designs and then validated using Aspen Plus® simulation. Taking the optimal GMF/OC solution as an example (i.e., the case of $nc = 2$ in Table 5.3), it can be identified as an extractive distillation column for ethanol-water separation using ethylene glycol as solvent. To determine the column design parameters, the value of GMF/OC "intra-segments" in each mass/heat exchange module can be used as the approximated number of distillation trays in each column section. Thus, Module $M_1$ is translated to 3 column trays, $M_2$ to 6 trays, $M_3$ to 2 trays. The resulting design solution features a 13-tray extractive distillation column (note that condenser is numbered as the first tray and reboiler the last tray). According to the GMF structural combination shown in Fig. 5.2(a), the EG solvent is introduced to the 5$^{th}$ tray (Module $M_2$) and the EtOH-H2O mixture stream is fed onto the 11$^{th}$ tray (Module $M_3$). These design parameters, together with the operating parameters (e.g., reflux ratio) reported in the GMF/OC synthesis results, are used as an initial guess to set up the equipment-based simulation. The Aspen simulation flowsheet using RADFRAC module is depicted in Fig. 5.3(a) and the temperature profile comparison between Aspen simulation and GMF synthesis is presented in Fig. 5.3(b). It can be noted that both GMF and GMF/OC synthesis succeed in capturing the major trend of the temperature profile, while the GMF/OC results provide more detailed design and operation information within each column section. The design and operating parameters can be further adjusted to improve product specifications and/or to minimize reboiler/condenser duties.

To validate if the GMF/OC design with 2 interior collocation points retains cost optimality at the stage of equipment-based design, the other GMF/OC solutions and GMF intermediate solutions are also translated and validated using Aspen simulation. For the GMF/OC solutions identified by $nc = 1$ and $nc = 3$, the equipment translation follows the same step with that of $nc = 2$. The resulting design and operating parameters are summarized in Table 5.4. It is consistent with the GMF/OC synthesis results that the these two process alternatives have higher energy consumption rates than the optimal design identified by $nc = 2$.

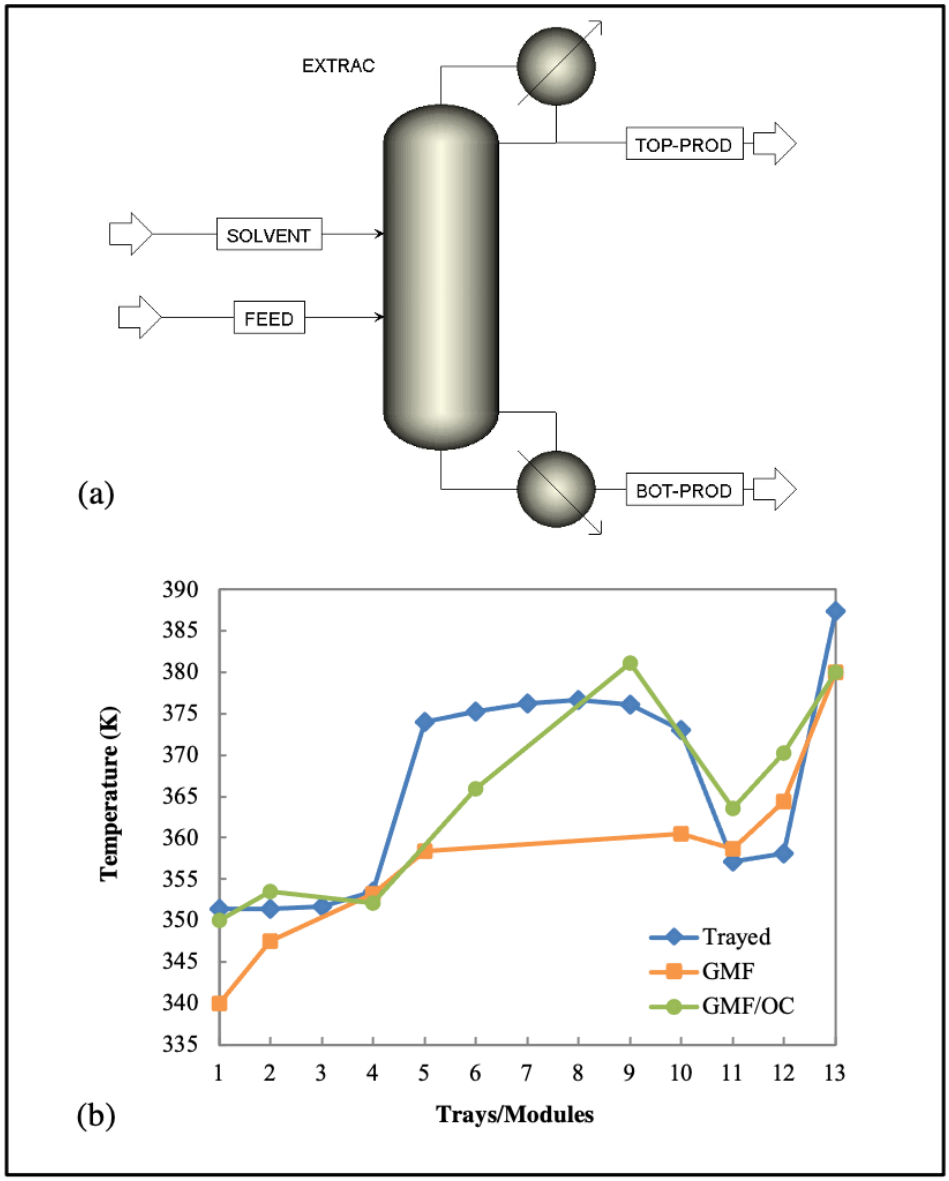


Figure 5.3: Case Study 1 – Equipment-based validation for GMF optimal solution (a) Aspen simulation, (b) Temperature profile.

The two GMF intermediate process solutions generated in Chapter 5.3.1.1 (i.e., Fig. 5.2b and 5.2c) are translated as shown in Fig. 5.4. The Alternative 1 using ethylene glycol as solvent is identified as a Petlyuk column, in which the side-module corresponds to the prefractionator and the the other two GMF modules to the main column. The simulation results are detailed in Table 5.4. Using the reboiler duty as an indicative comparison metric, Alternative 1 requires 23.8% more heating utility consumption than the optimal design due to the less "intensified" design scheme with two integrated columns instead of a single column.

For Alternative 2 which uses methanol as solvent, GMF suggests two separation steps in sequence to obtain ethanol product, which are translated to two sequential distillation columns as depicted in Fig. 5.4b. Due to the low relative volatility of methanol/ethanol, large reflux ratios are required in the equipment-based design to first break the ethanol/water azeotrope to separate ethanol/methanol from the first column distillate stream without loss of ethanol from the bottom stream, and then to separate the ethanol product from the second column bottom stream while avoiding methanol contamination. This results in an internal column flow rate larger than 100 kmol/s to meet the product specifications, which is not feasible from equipment design point of view. Thus this process alternative is not considered for further design and comparison.

Just to highlight again that the design space predicted by GMF using the Gibbs free energy-based driving force constraints is a superset of that for equipment-based extractive distillation systems. This is due to the facts that: (i) GMF allows more degrees of freedom for stream variables – e.g., each module inlet/outlet stream can have different temperatures while satisfying the overall energy balance, (ii) mass transfer feasibility is characterized between liquid inlet stream and vapor outlet stream, as well as between liquid outlet stream and vapor inlet stream. Both the two factors can result in a more "powerful" separation performance in a GMF mass/heat exchange module compared to a single distillation tray. It is also proved that if the driving force constraints are set between the liquid and vapor outlet streams while enforcing uniform temperature for module outlet streams, a mass/heat exchange module is equivalent to a distillation tray assuming liquid-vapor phase (in)equilibrium. Although these modeling considerations introduce

thermodynamic approximations compared to rigorous tray-by-tray modeling, more advantages are offered at this phenomena-based design stage to rapidly screen the design space and to evaluate the potential performance improvements by enabling: (i) compact physics-based representation for general reaction/separation systems with conventional type of mass/heat transfer (including but not limited to extractive separation) [48], (ii) identification of performance limits (e.g., cost, energy consumption) regardless the use of intensified/conventional units [109], and (iii) compact model size and reduced computational load [93].

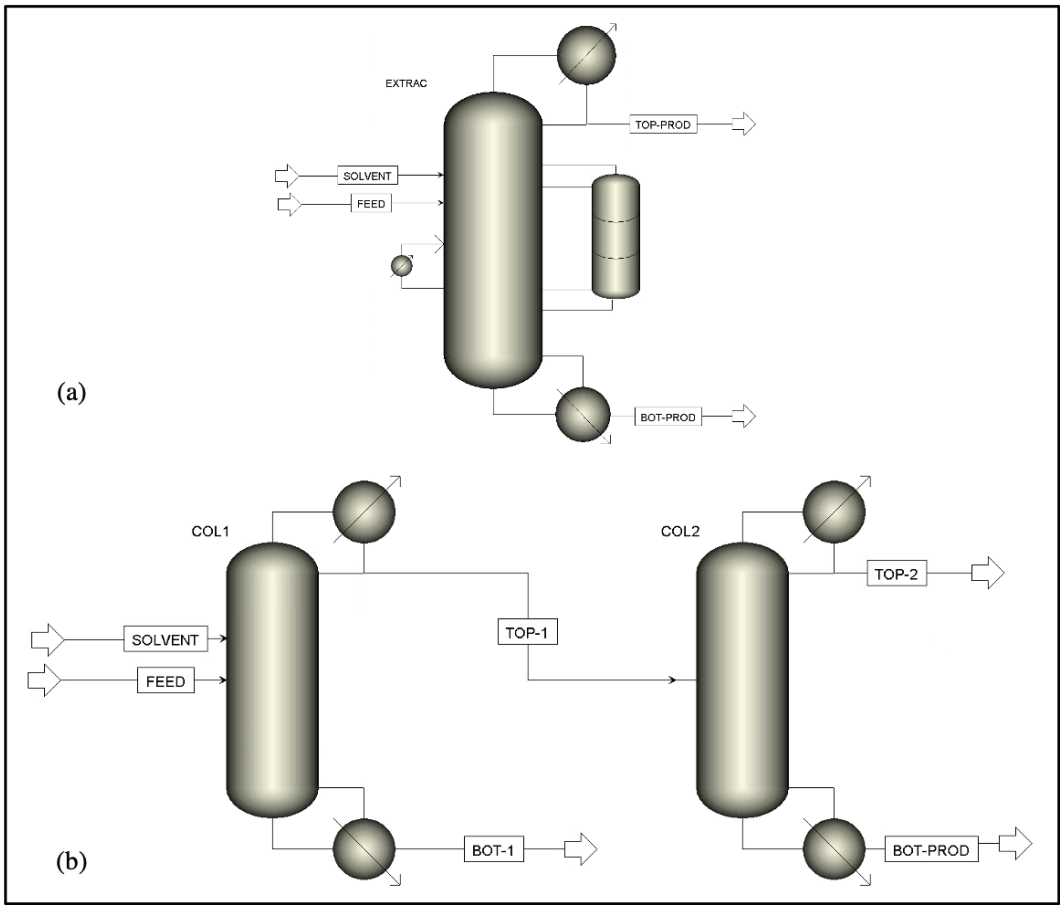


Figure 5.4: Case Study 1 – Equipment-based validation for GMF alternative solutions (a) Alternative 1, (b) Alternative 2.

Table 5.4: Case Study 1 – Identification of GMF solutions to equipment-based designs.

| | GMF/OC designs | | | GMF Alternative 1 |
|---|---|---|---|---|
| | $nc = 1$ | $nc = 2$ (optimal) | $nc = 3$ | |
| Number of trays[1] | 24 | 13 | 11 | 13 (main) + 6 (side) |
| EtOH-H2O feed location | 16 | 11 | 8 | 9 (main) |
| Solvent feed location | 12 | 5 | 4 | 1 (side) |
| Reflux ratio | 0.90 | 0.50 | 0.90 | 0.37 |
| Condenser duty ($\times 10^5$ kW) | 5.96 | 4.70 | 5.96 | 4.30 |
| Reboiler duty ($\times 10^5$ kW) | 6.38 | 5.12 | 6.37 | 6.34 |
| EtOH product purity (mol%) | 99.1 | 99.0 | 99.0 | 99.0 |
| EtOH product flowrate (kmol/s) | 8.0 | 8.0 | 8.0 | 8.0 |

Note 1: The number of trays for Aspen simulation include condenser and reboiler. Trays are numbered in a descending order.

Note 2: *main* – main column, *side* – side column

### 5.3.2 Solvents: Ethylene glycol and [EMIM][OAc]

In the second case study, we investigate the use of ionic liquids solvent for ethanol-water separation, compared to ethylene glycol as the conventional solvent. Ionic liquids are an emerging class of solvents in extractive separation owing to their distinct advantages such as negligible vapor pressure, high boiling point, thermal and chemical stability, etc. [159, 156] However, the industrial application of ionic liquids is still limited due to the high material cost, high viscosity, and lack of physical property data [160, 161]. Thus, it highlights the need to systematically and quantitatively study the trade-off between process efficiency and cost by integrating solvent selection with process design intensification.

1-ethyl-3-methylimidazolium acetate ([EMIM][OAc]) has been identified as an efficient ionic liquid solvent for several azeotropic separation systems, including ethanol-water [162, 163], acetone-

methanol [164], isopropyl alcohol dehydration [165]. In addition to significantly increasing the selectivity between the azeotropic pair, [EMIM][OAc] also has a relatively lower viscosity than other ionic liquid solvents. However, it should be noted that the degradation temperature of [EMIM][OAc] is at 433.15 K, which normally requires vacuum pressure operation.

The ethanol-water feed stream is considered to comprise 80 mol% EtOH and 20 mol% H2O at 200 kmol/h, 351.3 K, 1 atm. The separation target is to obtain a liquid ethanol product at 160 kmol/h with 99.8 mol% purity and a liquid water product with 99 mol% purity. Two solvent candidates are available: (i) ethylene glycol (EG), and (ii) [EMIM][OAc] (denoted as "IL" hereafter). The NRTL binary interaction parameters for the Ethanol-Water-Ethylene Glycol system is used consistently as that in Case Study 1, while the set of parameters for the Ethanol-Water-IL system is given in Table 5.5 [163]. The ionic liquid solvent is assumed to be non-volatile, while this assumption can be easily relaxed if corresponding vapor pressure parameters are available. For potential solvent make-up streams, the cost of IL solvent is assumed to be much higher than that of the EG solvent by adding a penalized cost term in the objective function. The synthesis objective is again to determine a cost-optimal design and to identify the corresponding solvent which can satisfy the aforementioned product specifications.

Table 5.5: Case Study 2 – NRTL parameters for ethanol (1), water (2), and [EMIM][OAc] (3).

| ij | $a_{ij}$ | $b_{ij}$ | $a_{ji}$ | $b_{ji}$ | $\alpha_{ij}$ |
|---|---|---|---|---|---|
| 12 | -91.8057 | 1.6016 | 1162.4117 | 1.0213 | 0.4 |
| 13 | -1023.3691 | 0 | -662.9004 | 0 | 0.3 |
| 23 | -823.8181 | 0 | -1672.7723 | 0 | 0.3 |

The initial guess consists of four pure heat exchange modules and six mass/heat exchange modules. All the interconnecting liquid and vapor streams exist between these modules. The GBD solution converges in 25 iterations and the optimal GMF configuration is shown in Fig.

5.5 which features a total annualized cost of $\$1.10 \times 10^6$ per year. Regarding the GMF module selection, to accommodate the low volatility of IL which cannot be vaporized in the GMF pure heat exchange module, a modified type of mass/heat exchange module "HU-L-V" is added in which additional heating duties can be introduced to a mass/heat exchange module in analogy to a flash column. In this context, the optimal GMF process solution in Fig. 5.5 can be interpreted as two unit operations: (i) an extractive distillation column – which consists of three "liquid-vapor (L-V)" mass/heat exchange modules for separation, one "HU-L-V" mass/heat exchange module, and one pure heat exchange module for process stream cooling, and (ii) a solvent recovery flash column – which consists of one "HU-L-V" mass/heat exchange module to separate water and IL respectively via vapor and liquid outlet streams, as well as one pure heat exchange module to cool the vapor stream to obtain liquid H2O product. To minimize the solvent cost, [EMIM][OAc] is all recovered from the solvent recovery flash column (i.e., no solvent make-up stream is needed).

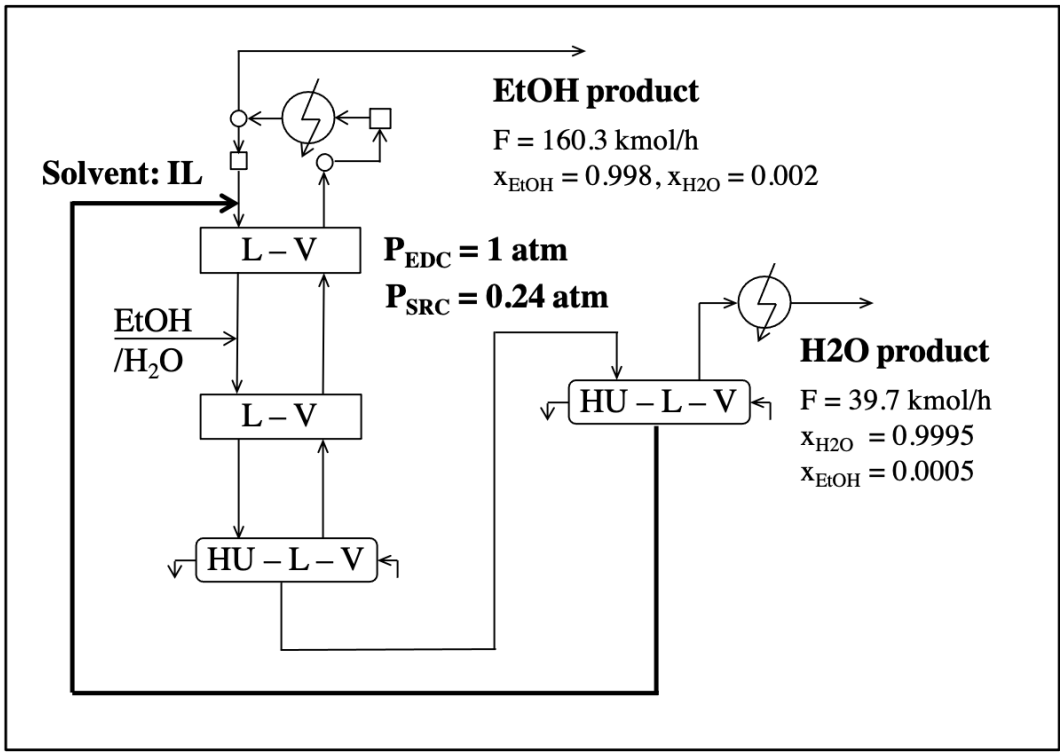


Figure 5.5: Case Study 2 – GMF synthesis of EtOH-H2O-IL extractive distillation.

Two intermediate process solutions using ethylene glycol as the solvent are also generated during the iterative solution procedure. Fig. 5.6(a) shows the conventional process design (Alternative 1) using an extractive distillation column and a solvent recovery column, featuring a total annualized cost at $\$2.63 \times 10^6$ per year. This solution is identified at the first GBD iteration. Another process solution (Alternative 2) obtained at the 23rd iteration is depicted in Fig. 5.6(b), in which the two distillation columns are thermally integrated via interconnecting vapor and liquid streams. The total annualized cost for this GMF configuration is $\$1.55 \times 10^6$ per year.

The above process solutions are also translated to equipment-based flowsheet for validation (Fig. 5.7). The Aspen simulation results are summarized in Table 5.6. The process solution with IL solvent, compared to Alternative 1 using ethylene glycol as solvent, features 49% reduction in cooling energy consumption and 53% reduction in heating energy consumption. Assuming that specialized equipment design is not necessitated to accommodate any unique material characteristics of ionic liquids (e.g., viscosity), the capital cost investment can also be expected to be much lower in the IL-assisted process which requires a 15-tray extractive distillation column and a flash column compared to a 18-tray extractive distillation column and a 15-tray solvent recovery column in Alternative 1. For the equipment-based translation of Alternative 2, the design shown in Fig. 5.7c cannot meet the EtOH and H2O product specifications with the same level of energy consumption rates as Alternative 1. This is because the separation target of the second GMF mass/heat exchange module (numbered in descending order from the left), where the heavy components are recycled to the extractive separation section from the solvent recovery section, cannot be met by an aggregation of distillation trays. In this case, GMF can provide the information on separation targets and corresponding module/stream operating conditions, with which the performance promises can be potentially realized. If to construct a new design, these information will serve as a starting point. The stream conditions of this module are: (i) liquid inlet – 355.8 K, 209.3 kmol/h, EtOH 76.44 mol%, H2O 19.11%, EG 4.45%, (ii) liquid outlet – 320.0 K, 130.8 kmol/h, EtOH 0.02%, H2O 30.58%, EG 69.40%, (iii) vapor inlet – 397.0 K, 90.7 kmol/h, H2O 0.36%, EG 99.64%, (iv) vapor outlet: 500.0 K, 169.2 kmol/h, EtOH 94.53%, H2O 0.19%, EG 5.28%.

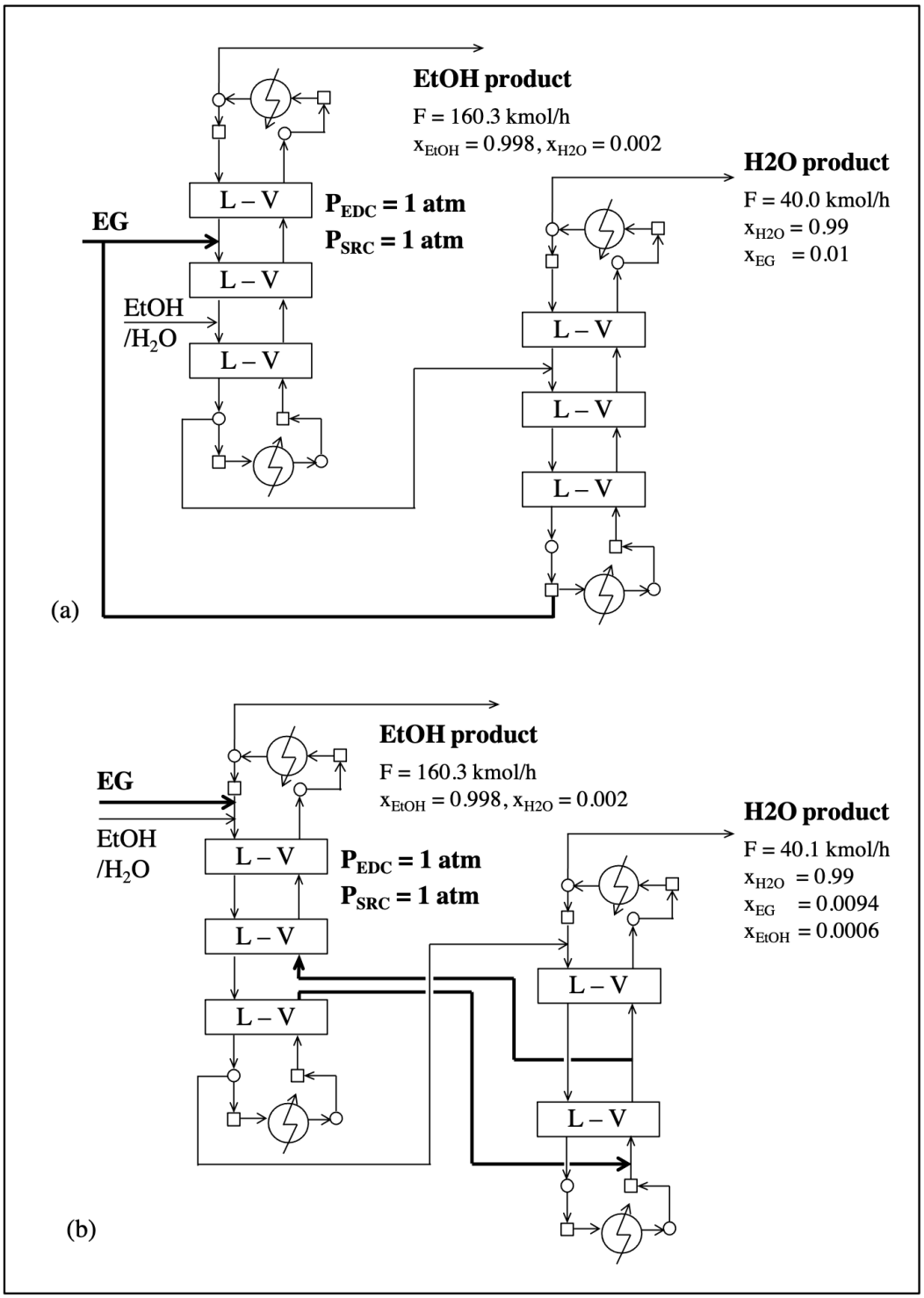


Figure 5.6: Case Study 2 – GMF alternative designs
(a) Alternative 1, (b) Alternative 2.

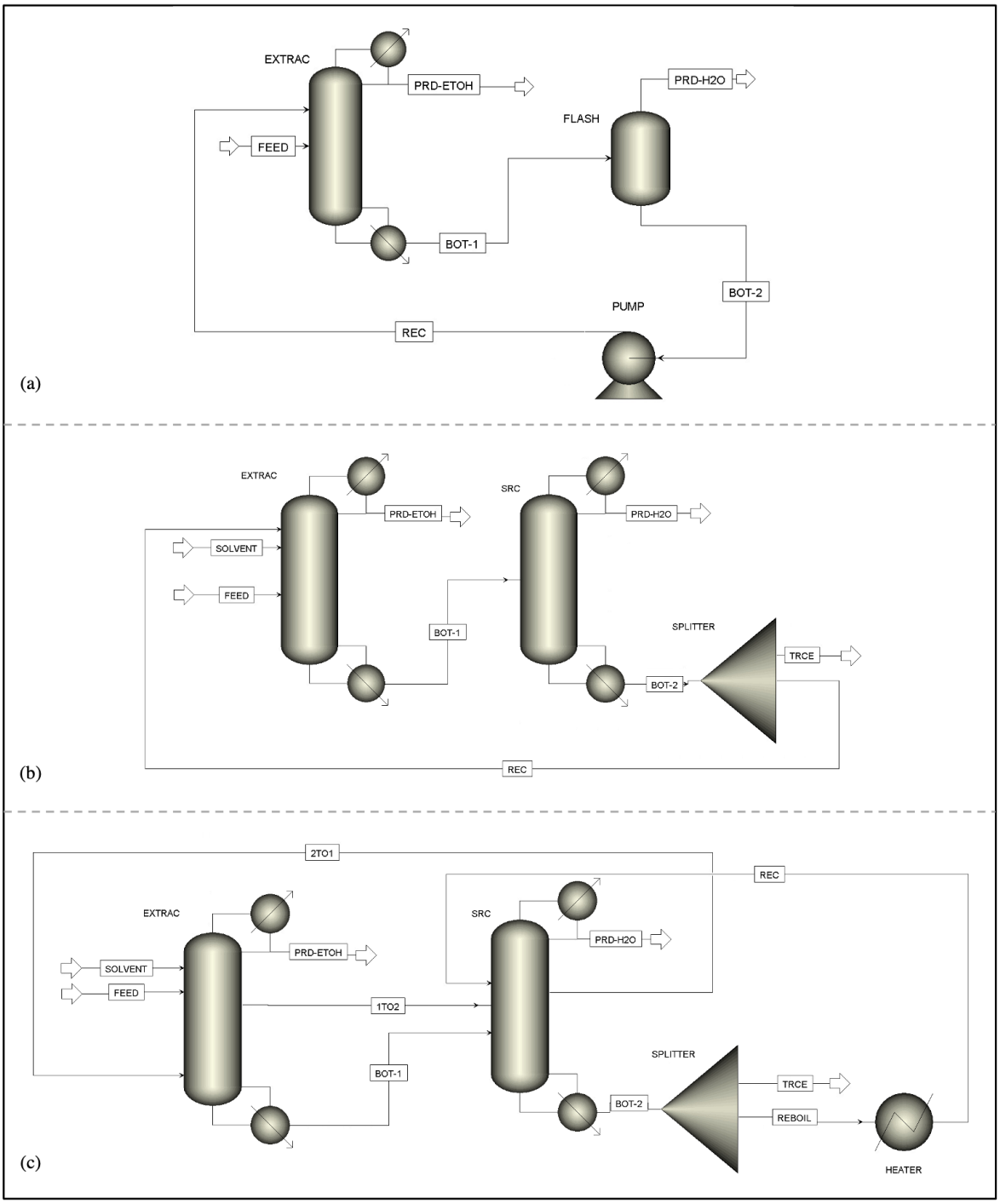


Figure 5.7: Case Study 2 – Equipment-based validation (a) Optimal solution, (b) Alternative 1, (c) Alternative 2.

Table 5.6: Case Study 2 – Identification of GMF solutions to equipment-based designs.

| | Optimal solution | | Alternative 1 | | Alternative 2 | |
|---|---|---|---|---|---|---|
| | EDC | FC | EDC | SRC | EDC | SRC |
| Number of trays | 15 | 1 | 18 | 15 | 18 | 6 |
| EtOH-H2O feed location | 10 | 1 | 12 | – | 4 | – |
| Solvent makeup feed location | – | – | 3 | – | 4 | – |
| Solvent recovery feed location | 2 | – | 3 | – | 5 | – |
| Pressure (atm) | 0.29 | 0.001 | 1 | 1 | 1 | 1 |
| Reflux ratio | 1.1 | – | 3.0 | 0.9 | 3.0 | 15.0 |
| Condenser temperature (K) | 322.9 | – | 351.5 | 370.8 | 351.3 | 354.3 |
| Reboiler temperature (K) | 432.6 | 432.6 | 427.7 | 468.9 | 385.5 | 468.7 |
| Condenser duty (MW) | 4.01 | – | 7.32 | 0.86 | 7.00 | 7.40 |
| Reboiler duty (MW) | 3.81 | 0.53 | 6.94 | 1.31 | 5.21 | 9.34 |
| Solvent | [EMIM][OAc] | | Ethylene glycol | | Ethylene glycol | |
| Solvent recovery purity (mol/mol) | 0.996 | | 0.997 | | 0.997 | |
| Solvent recovery flowrate (kmol/h) | 100.0 | | 223.0 | | 100.0 | |
| EtOH product purity (mol%) | 99.8 | | 99.8 | | 91.7 | |
| EtOH product flowrate (kmol/h) | 160.0 | | 160.0 | | 160.0 | |
| H2O product purity (mol%) | 99.2 | | 99.2 | | 66.6 | |
| H2O product flowrate (kmol/h) | 40.0 | | 40.0 | | 40.0 | |

Note: *EDC* – extractive distillation column, *FC* – flash column, *SRC* – solvent recovery column

## 5.4 Summary

In this chapter, we have applied the Generalized Modular Representation Framework to synthesize and intensify extractive separation systems. Through the case studies on an ethanol-water separation system, the proposed approach has been demonstrated to simultaneously address solvent selection and process synthesis intensification via a superstructure-based optimization problem. GMF is also coupled with Orthogonal Collocation approach to enhance intra-module physical representation and to maintain the combinatorial compactness in GMF representation.

A future research direction is to extend the synthesis framework for inverse design, in which case a desired range of phase equilibrium parameters and/or kinetic parameters can be determined via optimization of process performance. The key research question here is what are the critical physical parameters to connect material performance and process synthesis design. Machine learning-based quantitative structure-property relationship models might be instrumental to this purpose. The availability of desired material can then be checked with available database or synthesized via molecular design.

# 6. STEADY-STATE INTENSIFICATION SYNTHESIS WITH OPERABILITY AND SAFETY CONSIDERATIONS[†]

## 6.1 Introduction

Operability describes in general the inherent ability of the plant to perform satisfactorily under conditions different from the nominal design conditions, which can include the requirement to adjust to changes in operating conditions, disturbances, product specification, and etc. [86, 166]. Extensive efforts have been made in the PSE community over the past several decades to quantify process operability performance from different aspects as summarized below:

- Steady-state and dynamic flexibility analysis – to determine the maximum uncertainty that can be handled at the nominal operating point in a fixed design configuration [167, 168, 169]
- Steady-state and dynamic controllability analysis – to determine the "best" dynamic performance achievable for a system under closed-loop control [87, 166, 170]
- Operability-based analysis – to determine whether a controller can perform its mission under the constraints posed by the existing input variables and desirable output variables using linear/nonlinear input/output mapping methods [68, 39]

To ensure that the resulting systems are safely operable, operability and safety metrics need to be addressed during conceptual design stage, rather than relying solely on posterior control systems and/or protection layers [166, 171]. The integrated design and operability approaches, also known as design under uncertainty, are mostly applied at the unit operation level. An indicative list of the theoretical developments and their application systems is given below, while detailed reviews can be found in Yuan et al. [172] and Burnak et al. [173]:

[†]Reproduced in part with permission from Tian, Y., & Pistikopoulos, E. N. (2018). Synthesis of operable process intensification systems – Steady-state design with safety and operability considerations. Industrial & Engineering Chemistry Research, 58(15), 6049-6068. Copyright 2018 American Chemical Society.

- Steady-state flexibility with multi-period design – e.g., heat exchanger network [167], mass and heat exchange network [174]
- Dynamic flexibility with multi-period design – e.g., distillation column [175], air separation system [176]
- Design with controllability considerations – e.g., reaction-separation system [177], dividing wall column [178]
- Operability-based design – e.g., membrane reactor [39, 179]
- Inherently safer design – e.g., distillation-based systems [180]

However, operability and safety analysis for the phenomena-based synthesis intensification is kind of challenging since the synthesis is done using abstract phenomena building blocks with no available equipment information. To address this challenge, we propose in this chapter an integrated steady-state synthesis framework that enables the automated generation of safely operable process intensification systems from phenomena level, which features: (i) Generalized Modular Representation Framework to generate conventional or intensified processes, (ii) superstructure-based process synthesis and optimization to identify the most promising design configurations, (iii) flexibility analysis to accommodate process uncertainty and risk analysis to evaluate inherent safety behavior, and (iv) steady-state simulation and validation to identify the resulting equipment-based process alternatives.

## 6.2 Problem statement

The following generalized problem definition presents the synthesis problem in this chapter:

*Given:*

1. *Process synthesis target*
    - A set of process streams to be used as raw materials with given compositions, flowrates and/or supply temperatures;

- A set of desired products and specifications on their flowrates and/or purities;
- A set of available heating/cooling utilities such as steam and cooling water with their availability, supply temperatures, and compositions;
- A set of available mass utilities such as mass separating agents (e.g., solvent, adsorbent) and catalysts;
- All reaction schemes and kinetics data;
- All physical property models;
- Cost data of raw materials, mass/heat utilities, and equipment;

2. *Flexibility target*

   - A specified range for uncertain parameters, where process flexibility is desired (e.g., feed stream composition/flowrate/temperature, heat utility flowrate/temperature);

3. *Safety target*

   - A set of process constraints on inherent safety performances (e.g., toxicity, flammability, explosiveness);
   - A set of available equipment with their failure frequency data;
   - Property data of each substance existing in process with respect to concerned safety performances (e.g., lethal concentration, explosion energy).

The *objective* is to synthesize an optimal process solution, consisting of conventional or intensified unit operations, which is able to satisfy the afore-defined product specifications and also with guaranteed operability and safety performances. The optimality of the solution is evaluated with respect to economic performances in this chapter (e.g., operating cost or total annualized cost).

## 6.3 The GMF-flexibility-safety synthesis framework

To address the above problem for the design of process intensification systems with safety and operability considerations, we propose an integrated approach as depicted in Fig. 6.1. The basis of the framework lies in the Generalized Modular Representation Framework to identify the most promising and potentially intensified process options. To ensure that the resulting designs can be operated at varying process conditions and to make the process inherently safer, flexibility analysis and risk analysis are integrated with the GMF model (Fig. 6.1a), resulting in an iterative scheme (Fig. 6.1b) to deliver cost-optimal intensified processes with guaranteed flexibility and inherent safety performances. The resulting phenomenological flowsheets (Fig. 6.1c) are then validated with steady-state simulation to identify corresponding equipment-based unit/flowsheet configurations (Fig. 6.1d). In the following part of this section, we present in details the key constituents of this framework including flexibility analysis, risk analysis, and steady-state validation.

### 6.3.1 Process flexibility analysis with multiperiod approach

The GMF model, presented in detail in Chapter 2.4, can be recast in the following compact mathematical form:

$$\begin{aligned} \min_{V_d, V_x, V_z} \quad & f(V_d, V_x, V_z) \\ \text{s.t.} \quad & h(V_\theta, V_d, V_x, V_z) = 0 \\ & g(V_\theta, V_d, V_x, V_z) \leq 0 \qquad \forall V_\theta \in U(V_\theta) \end{aligned} \tag{6.1}$$

where $V_\theta$ stands for the set of uncertain parameters, and $U(V_\theta)$ is the specified range of uncertainty where flexibility is desired; $V_d$ is the set of design variables, including the diameter, height, and catalyst load of each mass/heat exchange module as well as the variables defining the network topology; $V_x$ denotes state variables which describe the network operation; $V_z$ is the set of control variables (i.e., degrees of freedom that can be adjusted during operation), including the heat duties of pure heat exchange modules; $f$ is the objective function; $h$ and $g$ are the sets of equality and inequality constraints used in this superstructure model.

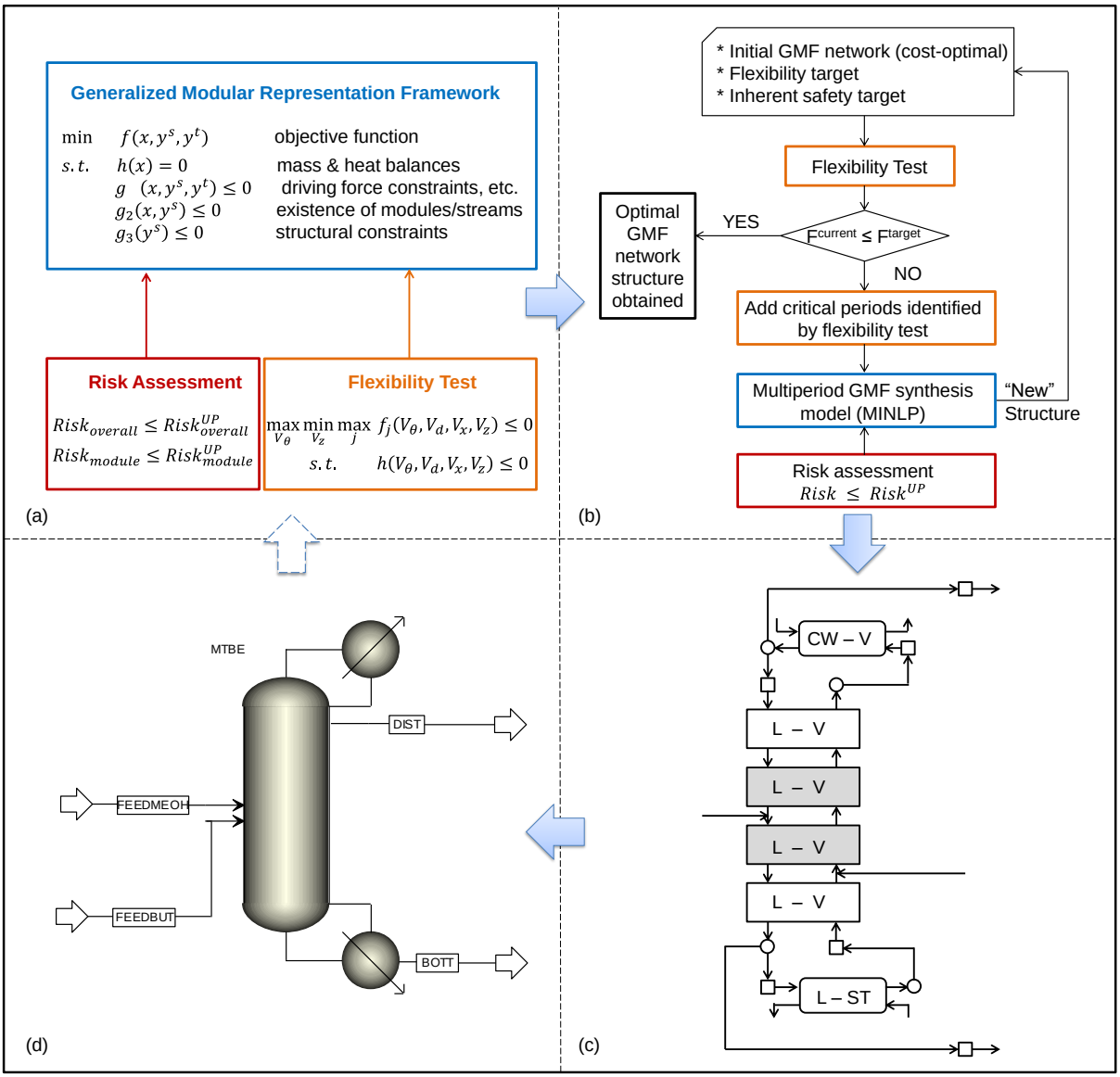


Figure 6.1: Steady-state synthesis of operable intensification systems –
(a) The integrated approach, (b) Iterative synthesis scheme,
(c) Optimal phenomena-based design, (d) Steady-state validation (Reprinted from [48]).

As shown in Halemane and Grossmann [167], this problem described by Eq. 6.1 with flexibility requirement $\forall V_\theta \in U(V_\theta)$ is equivalent to the following constrained max-min-max problem:

$$\begin{aligned} \max_{V_\theta \in U(V_\theta)} \min_{V_z} \max_{j \in J_f} \quad & f_j(V_\theta, V_d, V_x, V_z) \leq 0 \\ \text{s.t.} \quad & h(V_\theta, V_d, V_x, V_z) = 0 \end{aligned} \tag{6.2}$$

To avoid the direct solution of this tri-level optimization problem, an iterative discretization scheme has been developed by Papalexandri and Pistikopoulos [181, 182] as illustrated in Fig. 6.2. Starting from an initial process structure (e.g., the cost-optimal GMF structure for nominal operation condition), flexibility test [167] is performed to determine the critical operating conditions under a specified range (or a discretized set) of uncertain parameters (i.e., the operating conditions with the largest violation from nominal operating condition). Then the GMF superstructure is extended to include all these critical operating conditions via a multiperiod representation approach [174] by introducing an additional set of operation "periods". Specifically, design variables (e.g., diameter and height of mass exchange module) are reformulated as continuous variables for *all periods of operation*, while the other variables (e.g., stream flows, compositions, temperatures as well as those involved in characterizing heat and mass transfer) are regarded as continuous variables for *each period of operation*. In a similar sense, all GMF network configurations can be obtained from this multiperiod superstructure presentation. Thus, the resulting synthesis model will identify the most promising GMF-based process option at the minimum total annualized cost, also with desired flexibility performance. The detailed steps are as follow:

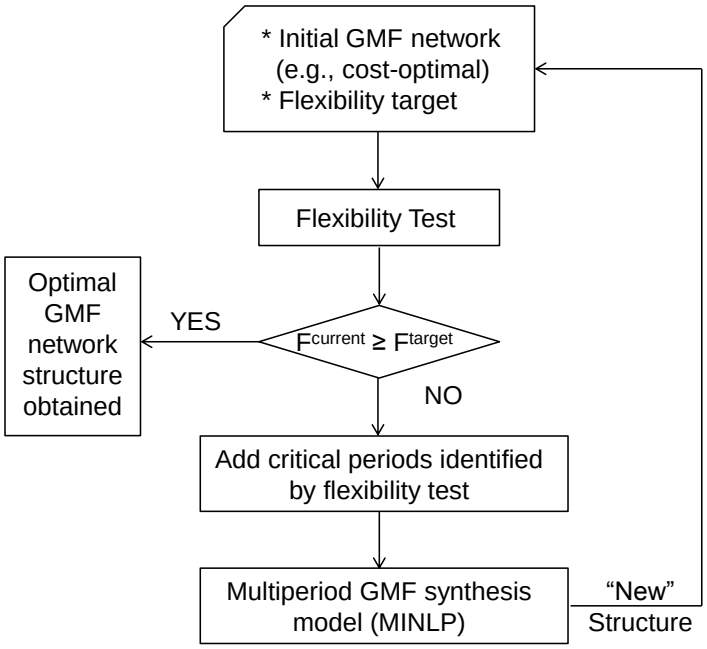


Figure 6.2: Iterative scheme for flexibility analysis (Reprinted from [48]).

**Step 1** Specification of flexibility target.

(i) Determine an initial cost-optimal network based on nominal operation condition;

(ii) Specify a range for uncertain parameters where flexibility is desired;

**Step 2** For the current network configuration, solve a flexibility test problem.

(i) If the current configuration satisfies the flexibility target, stop. Otherwise, go to (ii);

(ii) Identify the critical operating conditions, namely the periods, as per the maximum constraint violation.

**Step 3** Multiperiod synthesis.

(i) Formulate multiperiod GMF synthesis model based on nominal and/or critical operating periods identified in Step 2.

(ii) Solve the model to obtain "new" GMF network structure. Then go to Step 2.

However, it should be noted that when applying flexibility test [167] to nonconvex systems (e.g., GMF), the KKT conditions used in its inner optimization problems cannot guarantee global optimality. Thus the solution obtained for the outer optimization problems might not indicate the actual flexibility of the system [183]. In this context, the resulting "flexible" design configuration need to be re-tested through the uncertainty range to ensure its actual flexibility performance. More advanced convexification techniques or surrogate-based methods for flexibility analysis are of importance and issue of current research.

### 6.3.2 Process inherent safety evaluation with risk analysis

Quantitative risk analysis (QRA) [184] evaluates the inherent safety performance of a process by accounting for equipment failure frequency (depending on the equipment type and etc.) and consequence severity (depending on the amount of substance present, their physical and hazardous properties, specific process conditions and etc.). The value of process risk is thus determined by the multiplication of these two terms, as shown in Eq. 6.3. While most of QRA studies focus on the risk analysis at a certain release scenario [75], a more conservative way to guarantee inherent safety performance during conceptual design stage is to constraint the total amount of intrinsic hazard of a process at the release of the entire content in the process, as that presented in Nemet et al. [78]. Another advantage of their approach [78] is that it can be readily incorporated into superstructure-based optimization model as process constraints without repetitive iteration in a manner of posterior-evaluation. In this context, this approach is extended herein for the risk analysis of GMF-based process structures.

$$Risk = Failure\,frequency \times Severity \tag{6.3}$$

- **Equipment failure frequency** – As there is no pre-postulation of unit in GMF-based synthesis strategy, average historical data for equipment failure frequencies, such as those documented in the *Handbook of Failure Frequencies* [185] or in the *Guideline for Quantitative Risk Assessment* [186], cannot be directly applied. Thus, similarly to the estimation

Table 6.1: Failure frequencies for different type of GMF modules (Reprinted from [48]).

| | Heat exchange module | Mass/Heat exchange module | |
|---|---|---|---|
| | | Separation | Reaction (& Separation) |
| $freq/(\text{module} \cdot \text{yr})^{-1}$ | $5 \times 10^{-5}$ | $5 \times 10^{-6}$ | $5 \times 10^{-6}$ |

of pseudo-capital module cost, the GMF pure heat exchange modules are approximated as heat exchangers, while mass/heat exchange modules are treated as process vessels (where a change in the physical properties of the substance occurs, e.g. temperature or phase [186]) if pure separation is taking place, or as reactor vessels (where a chemical change of the substances occurs [186]) if there is any reaction going on. This approximation helps to provide an initial evaluation on the process inherent safety performance and to penalize the intrinsic process risks. The failure frequencies for these three types of modules during the instantaneous release of the complete inventory are determined from *Guideline for Quantitative Risk Assessment* [186] as shown in Table 6.1.

- **Consequence severity** – In this study, the severity of consequences is reflected by the indication number, which provides a measurement over the intrinsic hazard of an installation irrespective of its location and is defined as a dimensionless number (Eq. 6.4) [184, 78]:

$$A_{i,e,risk} = \frac{W_{i,e} \times O_e^1 \times O_e^2 \times O_i^3}{S_{risk}}, \qquad \forall e \in E, risk \in RISK, i = 1, ..., NC \tag{6.4}$$

where $A$ gives the indication number assessing the risk in a GMF module, $W$ represents the quantity of substances present within the module (kg), $O^i$ are the factors accounting for process conditions, and $S$ is the limit value (kg) measuring the hazardous properties of each substance based on their physical and toxic/explosive/flammable properties. The determination of these parameters within GMF framework is further elaborated below:

– Quantity of substances present ($W$): The mass quantity of each substance present in a mass/heat exchange module is estimated from the module's volume. The relation between mass holdup and module volume can be approximated by:

$$V = \frac{W^{liq}}{\widetilde{\rho}^{LO}} + \frac{W^{vap}}{\widetilde{\rho}^{VO}} \tag{6.5}$$

where $W^{liq}$ and $W^{vap}$ are liquid and vapor mass holdups in the module (kg), respectively; $\widetilde{\rho}^{LO}$ and $\widetilde{\rho}^{VO}$ are the mass densities of the module's outlet liquid and vapor stream (kg/m$^3$).

The module volume can be determined from its diameter and height:

$$V = \frac{\pi D^2}{4} H \tag{6.6}$$

For a liquid-vapor module where separation or reactive separation is taking place, the liquid level ($Level^{liq}$) is assumed to be 25% of module height in analogy to a distillation tray, while for a liquid-liquid module where only reaction is going on, $Level^{liq}$ is assumed to be 75% of the module height as that in reactors. Namely,

$$Level^{liq} = 25\% H y_{sep} + 75\% H (1 - y_{sep}) \tag{6.7}$$

where $y_{sep}$ is the binary variable which denotes the existence of separation phenomena in a mass/heat exchange module. Note that if $H$ is used as variables rather than parameters, Eq. 6.7 needs to be reformulated to avoid the nonlinearity in binary variable.

Thus explicit expression of liquid and vapor holdup can be derived from Eqs. 6.5-6.7:

$$\begin{aligned} W^{liq} &= \frac{\pi D^2}{4} \widetilde{\rho}^{LO} Level^{liq} \\ W^{vap} &= \frac{\pi D^2}{4} \widetilde{\rho}^{LO} (H - Level^{liq}) \end{aligned} \tag{6.8}$$

For each substance present in the module, its amounts in liquid or vapor phase are determined by:

$$\begin{aligned} W_i^{liq} &= W^{liq}\widetilde{x}_i^{LO} \\ W_i^{vap} &= W^{vap}\widetilde{x}_i^{VO} \end{aligned} \tag{6.9}$$

where $\widetilde{x}_i^{LO}$ and $\widetilde{x}_i^{VO}$ are the mass fractions of component i in the module's outlet liquid and vapor stream, respectively.

In sum, the quantity of liquid/vapor substances present in a M/H module is given by:

$$\begin{aligned} W_i^{liq} &= \frac{\pi D^2}{4}\widetilde{\rho}^{LO}\widetilde{x}_i^{LO}Level^{liq} \\ W_i^{vap} &= \frac{\pi D^2}{4}\widetilde{\rho}^{LO}\widetilde{x}_i^{VO}(H - Level^{liq}) \qquad i = 1, ..., NC \end{aligned} \tag{6.10}$$

– Factors for processing conditions ($O^i$):

  (i) $O^1$ describes if the installation is designed for processing or storage. As all the GMF modules are used for chemical processing, $O^1 = 1$ [184];

  (ii) $O^2$ accounts for the installation's positioning. With the assumption that the resulting intensified equipment will be positioned outdoor, $O^2$ is selected to be 1;

  (iii) $O^3$ provides a measurement over the amount of substance in the gas phase after its release, which is determined by its phase state and saturation pressure at process temperature - these information can be directly obtained from the GMF model.

  However, these factors only apply to the calculation of toxic and flammable risks. When explosive risk is considered, $O^1 = O^2 = O^3 = 1$.

– Limit value ($S$): For toxicity, $S_{tox}$ is determined by the lethal concentration of the substance (i.e., $LC_{50}$(rat,inh,1h)) as well as its phase state at 298 K, as shown in Table 2.5 in Ref. [184]. The limit value for flammables, $S_{flam}$, is 10,000 kg. For explosive substances, $S_{expl}$ is the amount of substance (kg), the explosion of which releases the same amount of energy as that of 1000 kg TNT (explosion energy 4600 kJ/kg).

Given all these constituents for risk calculation, the risk resulted by the existence of a single substance (or component) in a GMF module is determined via Eq. 6.11, which can be a good indicator to investigate the role of hazardous materials towards an inherently safer design:

$$R^{comp}_{i,e,risk} = \sum_{fail \in FAIL} freq_{e,fail} \frac{W^{liq}_{i,e} \times O^1_e \times O^2_e \times O^3_{i,e}}{S^{liq}_{i,risk}} + \sum_{fail \in FAIL} freq_{e,fail} \frac{W^{vap}_{i,e} \times O^1_e \times O^2_e \times O^3_{i,e}}{S^{vap}_{i,risk}} \qquad \forall e \in E, risk \in RISK, i = 1, ..., NC \tag{6.11}$$

The risks of individual module ($R^{mod}_{e,risk}$) is determined by a summation of $R^{comp}_{i,e,risk}$:

$$R^{mod}_{e,risk} = \sum_{i=1}^{NC} \sum_{fail \in FAIL} freq_{e,fail} \frac{W^{liq}_{i,e} \times O^1_e \times O^2_e \times O^3_{i,e}}{S^{liq}_{i,risk}} + \sum_{i=1}^{NC} \sum_{fail \in FAIL} freq_{e,fail} \frac{W^{vap}_{i,e} \times O^1_e \times O^2_e \times O^3_{i,e}}{S^{vap}_{i,risk}} \qquad \forall e \in E, risk \in RISK \tag{6.12}$$

And the overall risk of the process network ($R^{overall}_{risk}$) is calculated through:

$$R^{overall}_{risk} = \sum_{e \in E} \sum_{i=1}^{NC} \sum_{fail \in FAIL} freq_{e,fail} \frac{W^{liq}_{i,e} \times O^1_e \times O^2_e \times O^3_{i,e}}{S^{liq}_{i,risk}} + \sum_{e \in E} \sum_{i=1}^{NC} \sum_{fail \in FAIL} freq_{e,fail} \frac{W^{vap}_{i,e} \times O^1_e \times O^2_e \times O^3_{i,e}}{S^{vap}_{i,risk}} \qquad \forall risk \in RISK \tag{6.13}$$

Risk tolerance can be set as process constraints for individual module (Eq. 6.14) and/or for the overall process (Eq. 6.15).

$$R^{mod}_{e,risk} \leq y_e R^{mod,UP}_{e,risk} \quad \forall e \in E, risk \in RISK \tag{6.14}$$

$$R^{overall}_{risk} \leq R^{overall,UP}_{risk} \qquad \forall risk \in RISK \tag{6.15}$$

However, as the risk values obtained in this approach do not provide a scaled measurement (e.g., 0-1), the risk tolerances are set on a comparative basis. For instance, to realize an inherently

safer process, each type of risk for the overall network (e.g., toxicity, flammability, explosiveness) should be reduced by at least 20% of that in the nominal (i.e., cost-optimal) structure; or to eliminate the existence of a "particularly unsafe" module in the process, the individual module risk should be less than 30% of the overall process risk. These inherent safety targets will be presented later in more details through the case study demonstration.

### 6.3.3 Steady-state simulation and validation

Herein, the most promising phenomenological configuration(s) given by this integrated GMF-flexibility-safety synthesis strategy are translated to equipment-based units or flowsheets. The resulting process units/flowsheets are then analyzed with steady-state simulation tools (e.g., Aspen Plus) using rigorous unit models, which actually necessitates a specialized PI model library. Optimization of these flowsheets can also be performed at this stage to obtain more detailed design parameters and to analyze their cost performances (or any other performance criterion). However, the consistency between equipment-based simulation results and GMF optimization results should be validated to ensure: (i) the validity of GMF representation to capture major process characteristics, and (ii) the optimality of process solutions when different process models are used.

## 6.4 Case study: Methyl tert-butyl ether production

In this section, we showcase the proposed integrated GMF-flexibility-safety synthesis approach through a case study on the production of methyl tert-butyl ether (MTBE) for steady-state synthesis of intensified designs with flexibility and safety considerations .

### 6.4.1 Process description

MTBE is made by the catalytic reaction of isobutylene (IB4) and methanol (MeOH) in the liquid phase in the presence of a suitable catalyst, usually a cation exchange resin. The reaction scheme is shown in Eq. 6.16. In addition to the reactants and products, other components may also be present in the process as inerts (e.g., 1-butene (NB4)), depending on the raw material compositions, catalyst selection, processing conditions and etc.

$$\text{MeOH + IB4} \rightleftharpoons \text{MTBE}, \quad \Delta_r H^o_{298\text{K}} = -37.7\text{kJ/mol} \tag{6.16}$$

An ion-exchange resin Amberlyst 15 is used in this work. No side reaction is considered (e.g., the formation of diisobutylene from isobutylene) as this can be eliminated by the selection of proper Amberlyst 15 particles [187]. The intrinsic rate of MTBE is given by Rehfinger and Hoffmann [187]:

$$r = k\left[\frac{a_{IB4}}{a_{MeOH}} - \frac{1}{Ka}\frac{a_{MTBE}}{a^2_{MeOH}}\right] \quad \text{kmol/(h} \cdot \text{kg cat)} \tag{6.17}$$

where $r$ gives the molar reaction rate per unit mass of dry catalyst resin, $a$ denotes the activity of each component.

The rate constant $k$ is determined by [187], where $T$ denotes the process temperature in K:

$$k = 8.5132 \times 10^{13}\text{exp}\left[\frac{-11,113.78}{T}\right] \quad \text{kmol/(h} \cdot \text{kg cat)} \tag{6.18}$$

The expression of reaction equilibrium constant can be calculated as in Colombo et al. [188]:

$$\text{ln}Ka = -10.0982 + \frac{4254.05}{T} + 0.2667\text{ln}T \tag{6.19}$$

The Antoine equation (Eq. 6.20) to give saturated vapor pressures, with the component-specific parameters taken from Ismail et al. [94]. To describe the highly nonideal nature of the liquid mixtures comprising methanol, isobutylene, and MTBE, UNIQUAC equations (Eq. 6.21) are employed to calculate the liquid activity coefficients. The binary UNIQUAC parameters are adapted from Rehfinger and Hoffmann [187].

$$\text{ln}P^{sat} = C1 - \frac{C2}{C3 + T} \tag{6.20}$$

$$
\begin{aligned}
\ln\gamma_i^r &= q_i\left[1-\ln\left(\sum_j \theta_j\tau_{ji}\right)-\sum_k\left(\frac{\theta_k\tau_{ik}}{\sum_j\theta_j\tau_{jk}}\right)\right] \\
\ln\gamma_i^c &= 1-J_i+\ln J_i-5q_i\left[1-\frac{J_i}{L_i}+\ln\left(\frac{J_i}{L_i}\right)\right] \\
J_i &= \frac{r_i}{\sum_j r_j x_j} \qquad\qquad L_i = \frac{q_i}{\sum_j q_j x_j} \\
\tau_{ij} &= \exp\left(\frac{-Int_{ij}}{RT}\right) \qquad\qquad \tau_{ii}=1
\end{aligned}
\tag{6.21}
$$

A conventional process to produce MTBE consists of two series-flow reactors followed by one or two distillation columns to recover high purity MTBE as well as methanol extraction and fractionation columns for the recycling of excessive methanol feed [189]. The conversion of isobutylene can reach a theoretical range of 90-95% in the reactors. However, it is not cost-effective to further separate the unreacted isobutylenes from the butene inerts due to the low relative volatility. The first patent for MTBE production in reactive distillation column came out in the 1980s [190]. Thereafter, reactive distillation has become a more economically attractive approach for this process due to its capability to achieve higher conversion levels in a single unit (99.2% butylene).

In this work, we revisit the example given in Ismail et al. [94]. Available raw materials include a pure liquid methanol feed as well as a saturated vapor isobutylene feed. The feed conditions (i.e., temperature, flowrate, composition) are all fixed in this synthesis case and are taken from the work of Hauan et al. [191] (Table 6.2). System pressure is considered to be constant, but it is incorporated as an optimization variable to be determined. For an estimation of pressure range to ensure safe operation, the upper bound of pressure is set to be 11 atm based on available design information from open literature [191, 189]. The objective function is to minimize the total annualized cost, involving the pseudo-capital cost and operating cost. The cost of raw materials is not included as it features a fixed value within this production scheme. The cost calculation is given by Eq. 6.22:

Table 6.2: MTBE production – Summary of feed data (Reprinted from [48]).

| | Liquid feed | Vapor feed |
|---|---|---|
| Temperature (K) | 320 | 350 |
| Flowrate (mol/s) | 215.5 | 545 |
| $x_{MeOH}$ | 1 | 0 |
| $x_{IB4}$ | 0 | 0.3578 |
| $x_{NB4}$ | 0 | 0.6422 |
| $x_{MTBE}$ | 0 | 0 |
| Pressure (atm) | 11 | 11 |

$$\text{Total Annualized Cost (\$/yr)} = \sum_e C_{cw} \times Qc_e + \sum_e C_{steam} \times Qh_e + \sum_e y_e \times Cost_e \quad (6.22)$$

where $Cost_e$ denotes the pseudo-capital cost value (Eq. 2.94), $Qc_e$ and $Qh_e$ are the heating and cooling load in each module, respectively. The utility cost for $C_{cw}$ and $C_{steam}$ are respectively 26.19 US$/(kW·yr) and 137.27 US$/(kW·yr).

Additionally, uncertainty is considered with a varying flowrate of liquid methanol feed within the range of:

$$205.5 \text{ mol/s} < f^I_{MeOH} < 225.55 \text{ mol/s} \qquad (\text{nominal } 215.5 \text{ mol/s})$$

Given the fact that all the substances participating in this process are highly toxic, flammable, and explosive, manifold risks (i.e., toxicity, flammability, and explosiveness) are considered to assess the inherent safety performance.

In what follows, we present step-by-step how the proposed approach is applied for the synthesis of safely operable process intensification systems.

### 6.4.2 Step 1: Process intensification synthesis representation

As presented in Chapter 2, each GMF mass/heat exchange module is not pre-postulated with any underlying reaction and/or separation tasks. Instead, these tasks will be determined through the optimization procedure aiming at the optimal economic performance while their thermodynamic feasibilities are ensured by the driving force constraints.

Determining an optimal set of available mass/heat exchange modules ($E$) is certainly a critical yet open question. As the number of available modules increases, the quality of the representation via GMF modules is improved while the complexity of the model increases as well. To obtain an estimate on the number of modules before proceeding with superstructure optimization, simulation studies can be performed to synthesize any reference MTBE production flowsheets available in open literature (e.g., conventional reactor-distillation [189], reactive distillation [192]). In this work, a reactive distillation column configuration is simulated with GMF modules based on the column design reported in Jacobs and Krishna [192] (Fig. 6.3a). As illustrated in Fig. 6.3b, this initial structure features a total of seven mass/heat exchange modules and two pure heat exchange modules. The rectification section consists of one mass/heat exchange module for pure separation and the stripping zone of two separation modules, while four reactive separation modules make the reaction zone. The pure heat exchangers serve as the column reboiler and condenser, respectively. In this context, we first assign a maximum of 10 mass/heat exchange modules, with their associated pure heat exchange modules, to be available during the optimization. Once this bound is active, the value is relaxed to allow more modules to be used.

In addition to the general GMF model presented in Chapter 2.4, some problem-specific constraints are also included [94]: (i) to constrain the equipment size, vapor flowrates around GMF modules are enforced to be less than 3000 mol/s [193]; (ii) no more than 2000 kg catalysts on a dry-weight basis present for each module; and (iii) mass/heat exchange modules are numbered in a descending order from top to bottom.

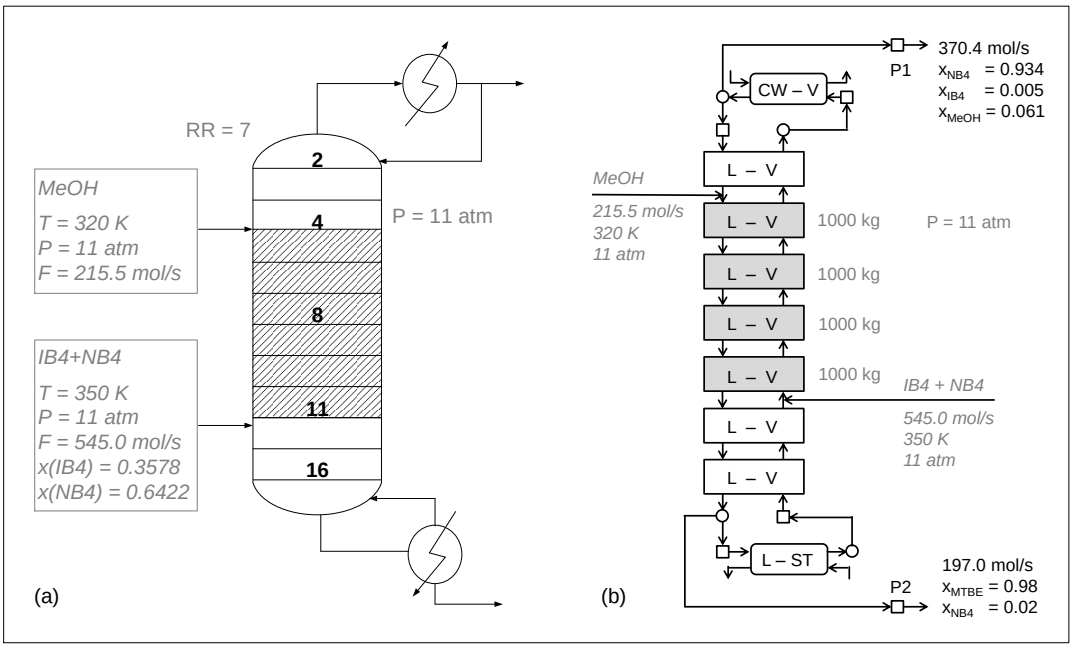


Figure 6.3: Simulation study of MTBE reactive distillation column – (a) Reference design, (b) GMF representation (Reprinted from [48]).

### 6.4.3 Step 2: Superstructure optimization

The resulting synthesis model involves 14,594 rows, 8,098 continuous variables, and 734 binary variables. The model is solved with GBD strategy implemented in GAMS [194], with optimality gap set as 0.01%. The initial structure, in a similar way to the above-simulated MTBE reactive distillation, also comprises seven mass/heat exchange modules and two pure heat exchange modules. However, to avoid pre-postulating this structure as a reactive distillation, the reaction/separation phenomena taking place in each module is open to be determined and also allowed are all the interconnection flows between existing modules.

The solution of this MINLP problem converges in six GBD iterations. The minimization of total annualized cost results in a module structure as shown in Fig. 6.4. It features the same reactive distillation type of configuration as shown in the previous simulation study. The "column section" includes a separation module in rectification section, two reactive separation modules in reaction zone, and another separation module in stripping section. Note that the reflux ratio,

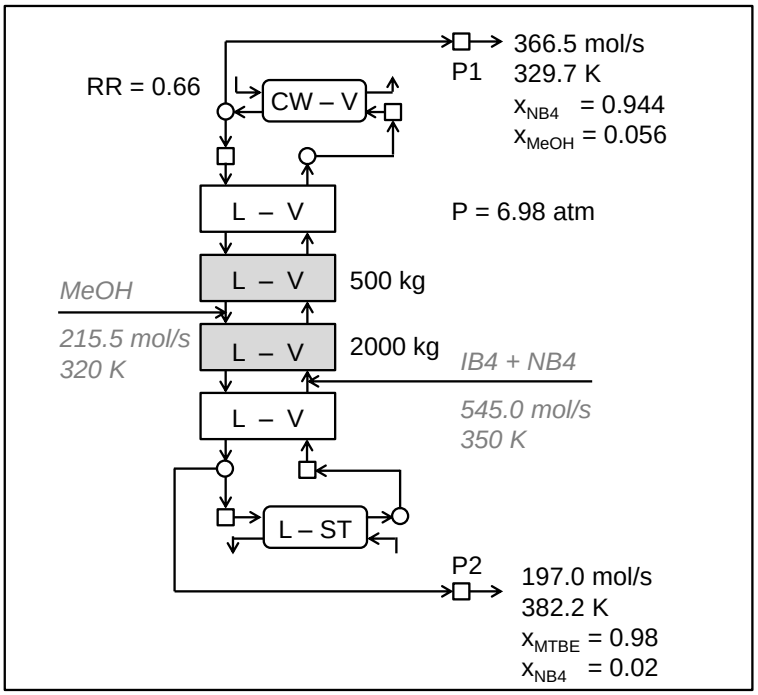


Figure 6.4: MTBE production – Optimal design configuration (Reprinted from [48]).

labeled in Fig. 6.4, is not explicitly considered as a variable but posteriorly calculated according to the flowrates of top product and the rectifying module liquid inlet. This flowsheet has a a total cost of $\$8.70 \times 10^5$/yr, including an investment cost of $\$6.10 \times 10^4$/yr and a utility cost of $\$8.09 \times 10^5$/yr. This combinatorial structure, operating conditions, as well as cost objectives are consistent with the optimal scheme reported in Ismail et al. [94].

For verification with equipment-based design, the module layout and operating conditions (i.e., pressure, reflux ratio) are then utilized as design parameters for a steady-state simulation of reactive distillation in Aspen Plus using the rigorous distillation module RADFRAC. Simultaneous chemical and physical equilibrium are assumed. The chemical equilibrium is applied in the form of Eq. 6.19. Thermodynamic properties of this system are described via the property set SYSOP11 (UNIQUAC/Redlich-Kwong). Each GMF mass/heat exchange module is translated to a number of column trays, the determination of which is carried out through trial-and-error with the goal of minimizing the required number of column stages in Aspen simulation. A more systematic

procedure to identify the equipment-based unit/flowsheet from phenomenological representation is clearly essential and under current investigation. However, for this GMF optimal structure (Fig. 6.4), corresponding Aspen reactive distillation columns cannot successfully run with a reflux ratio of 0.66 since the stripping section would dry up with hardly any vapor flows. A larger reflux, with a rough estimate of 2 obtained from Aspen analysis, is required to make a feasible reactive distillation operation in Aspen Plus as well as to satisfy desired process specifications.

For this sake, the reflux ratio is explicitly considered in the GMF optimization model, and also constrained. A minimum value of 1.7 is set to the reflux ratio, which is used as an illustrative bound to show how the optimal solution will be varying in response. Still starting from the initial structure, a new optimal solution is generated and the optimization results for this flowsheet are shown in Fig. 6.5a. The major difference resulted by the increase of reflux ratio lies in an extra separation module in the stripping section. For a comparison purpose, the previous optimal structure is recovered as a feasible solution in this case with constrained reflux ratio (Fig. 6.5b). Although the new optimal configuration has a larger capital cost, it outperforms more in terms of hot utility cost. This is because of a smaller liquid inlet flowrate into the heating module, as there are more stripping trays to drive the unreacted methanol and isobutylene back to the reaction zone.

This modular solution is then translated into a reactive distillation column in Aspen Plus: each reactive separation module and the bottom separation module correspond to three column trays while the other separation modules to two column trays respectively, thus featuring a total of 13 column trays. To determine the column operating conditions using Aspen optimization analysis, with an objective to minimize operating cost, column pressure is selected as a manipulated variable due to its effect on the column temperature profile, which affects the reaction rate, physical equilibrium, and condenser/reboiler duty [94]. Reflux ratio is also manipulated to meet process specifications and to adjust condenser/reboiler duty. More rigorous model-based optimization of the resulting reactive distillation column, including design variables such as column tray numbers, feed/reactive tray location, column diameter, can be achieved posterior to this steady-state validation stage by performing dynamic optimization based on high-fidelity models (Chapter 8).

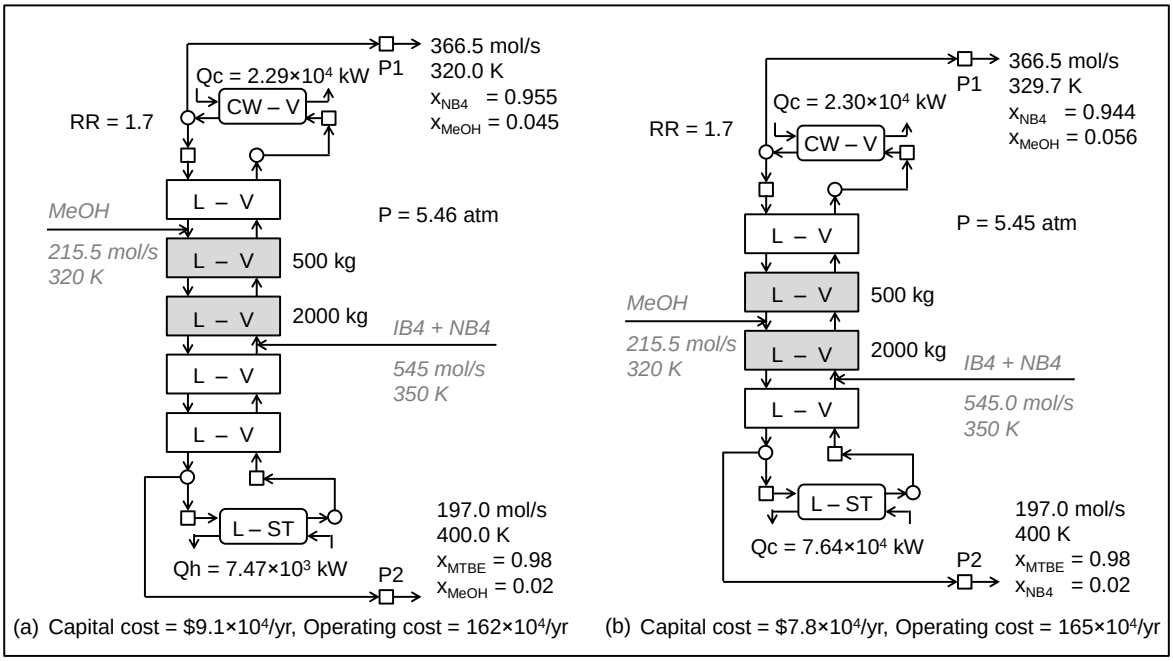


Figure 6.5: MTBE production – Design alternatives with consideration of reflux ratio (a) Optimal solution, (b) Feasible solution (Reprinted from [48]).

The optimal operating conditions for the resulting reactive distillation are presented in Fig. 6.6. Fig. 6.7 shows the comparison profiles of column temperature and liquid composition between GMF and Aspen simulation. Although details are lost within the mass/heat exchange modules, the trends of mass transfer in the reactive distillation column is well captured in five modules.

Several notes can be made at the end of this step regarding this synthesis optimization step:

(i) The observed "intensification" of reflux ratio suggested by GMF representation aligns with the findings in Luyben and Hendershot[195] that process intensification tends to drive the minimization of liquid holdups in reflux drum and column base, through the reduction in reflux ratio, for savings in investment and utility costs but simultaneously may cause problems from operational perspective. This necessitates the integrated framework to ensure the consistency between phenomenological synthesis, rigorous unit design, and operational analysis for the delivery of verifiable intensified designs.

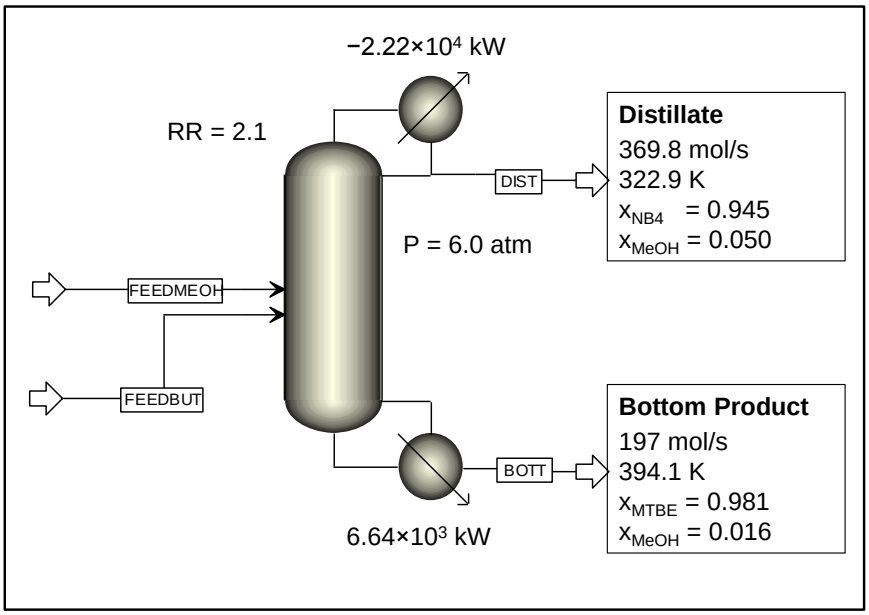


Figure 6.6: MTBE production – Aspen simulation flowsheet (Reprinted from [48]).

(ii) Despite the reflux ratio issue, the GMF representation is able to capture the combined reaction/separation phenomena and to suggest optimal intensified process configuration for MTBE production without a pre-postulation of plausible units/tasks. Actually, the first optimization problem, without any explicit consideration over reflux ratio, contributes to identify a set of tasks for this process (i.e., separation and reactive separation). Then more detailed optimization, incorporating operational perspectives, is carried out to bridge the gap from task to unit operation.

(iii) Although GMF is built on the exploitation of thermodynamic space, we do not assume chemical or physical equilibrium. Table 6.3 presents the values of $G2$ for individual component in each module. As introduced in Chapter 2.2, $G2$ denotes how far the process is from the equilibrium. If it equals to 0, the process is at its thermodynamic equilibrium. In Table 6.3, the magnitude of $G2$ indicates that reaction takes a more significant role in driving the extent of this process than separation.

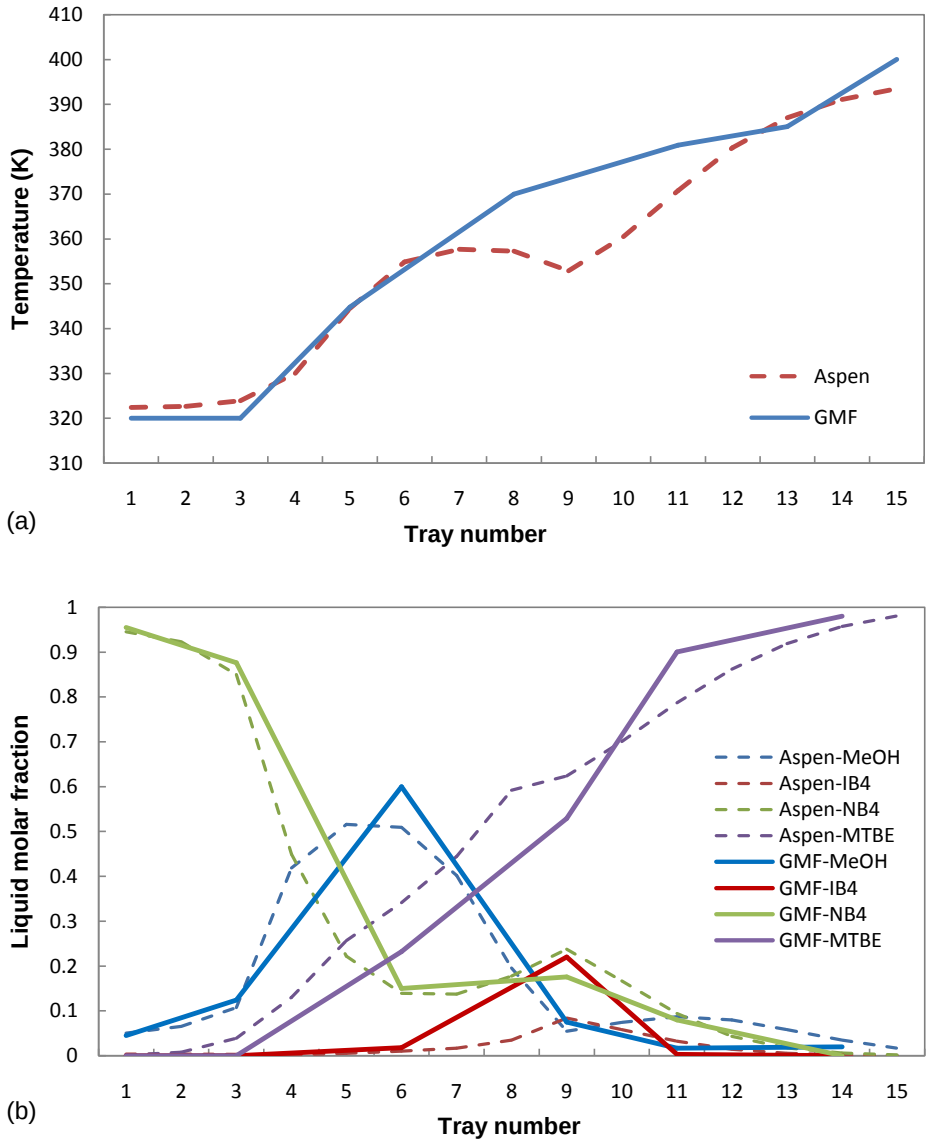


Figure 6.7: MTBE production – Validation of GMF synthesis vs. Aspen simulation (a) Temperature profile vs. (b) Composition profile (Reprinted from [48]).

Table 6.3: MTBE production – Driving forces in GMF modules (Reprinted from [48]).

| M/H Module | Task | MeOH | IB4 | NB4 | MTBE |
|---|---|---|---|---|---|
| 1 | Separation | -0.12 | 0 | 0.07 | 0 |
| 2 | Reaction/Separation | 0 | -17.2 | 0.004 | 0 |
| 3 | Reaction/Separation | 30.3 | -20 | -0.53 | 0 |
| 4 | Separation | 0 | 0.002 | 0 | -2.97 |
| 5 | Separation | -0.038 | 0.002 | 0.002 | -3.93 |

(iv) Although capital cost can be readily incorporated into the cost objective in Aspen optimization, the current objective function formulation in Aspen Plus only considers operating cost, for the reasons that: (a) operating cost constitutes the dominant driving force in the conceptual design of distillation columns [129]; (b) the major goal is to ensure the feasibility from modular representation to equipment-based flowsheet; (c) the optimal design parameters would be fully investigated in a later step of simultaneous design and control, which is to be addressed in Chapter 8.

### 6.4.4 Step 3: Integrated design with flexibility and safety considerations

After deriving the optimal intensified MTBE production configuration from Step 2 (Fig. 6.5a), this step aims to improve its operability performances via the incorporation of flexibility test and quantitative risk assessment.

Three types of risks are assessed (i.e., toxicity risk, flammability risk, explosiveness risk) and the corresponding hazardous properties of MeOH, IB4, NB4, and MTBE are given in Table 6.4. Following the risk calculation procedure presented in Chapter 6.3.2, the risk values for each mass/heat exchange module in the above-obtained cost-optimal configuration (Fig. 6.5a) is shown in Table 6.5. In what follows, these risk values will be used as nominal case to be improved.

The first target to achieve an inherently safer design is set to reduce the overall process risk, for each type of risk considered, by at least 20% comparing to the reference value given by nominal case (i.e. $R_{risk}^{overall} \leq 20\% \cdot R_{risk}^{overall,norm}$). Incorporating this constraint into the synthesis model,

Table 6.4: MTBE production – Hazardous properties (Reprinted from [48]).

| | Toxicity – $LC_{50}$ (rat,1h,inh)/mg | Flammability | Explosiveness – TNT equivalence/kg |
|---|---|---|---|
| MeOH | 65.6 | Yes | 4.62 |
| IB4 | 155 | Yes | 2.05 |
| NB4 | 164.5 | Yes | 2.03 |
| MTBE | 21.3 | Yes | 2.62 |

Table 6.5: MTBE production – Risk values for nominal design (Reprinted from [48]).

| M/H Module | Task | $Risk_{tox}$ | $Risk_{flam}$ | $Risk_{expl}$ |
|---|---|---|---|---|
| 1 | Separation | 0.089 | $3.7\times10^{-4}$ | 0.002 |
| 2 | Reaction/Separation | 0.083 | $3.8\times10^{-4}$ | 0.002 |
| 3 | Reaction/Separation | 0.097 | $4.5\times10^{-4}$ | 0.002 |
| 4 | Separation | 0.036 | $1.7\times10^{-4}$ | $7.3\times10^{-4}$ |
| 5 | Separation | 0.033 | $1.5\times10^{-4}$ | $6.3\times10^{-4}$ |
| Overall process | | 0.338 | $1.5\times10^{-3}$ | 0.007 |

the cost-optimal and inherently safer design configuration is illustrated in Fig. 6.8a, which actually recovers the combinatorial structure of the cost-optimal design without reflux ratio constraint (Fig. 6.4). The overall process risks are reduced in an intuitive way via the reduction of number of modules in the process.

However, it is noted that the second (numbered from up to bottom) reactive separation module takes up more than 1/3 of the overall process risk, which renders it a comparatively more risky component in this flowsheet. To alleviate this effect, the unit-level risk of an individual module is further constrained to be no more than 30% of the overall process risk (i.e. $R_{risk}^{mod} \leq 30\% \cdot R_{risk}^{overall}$). This gives rise to the solution shown in Fig. 6.8b, where a bypass over the second reactive separation module is placed to release its mass/heat exchange burden.

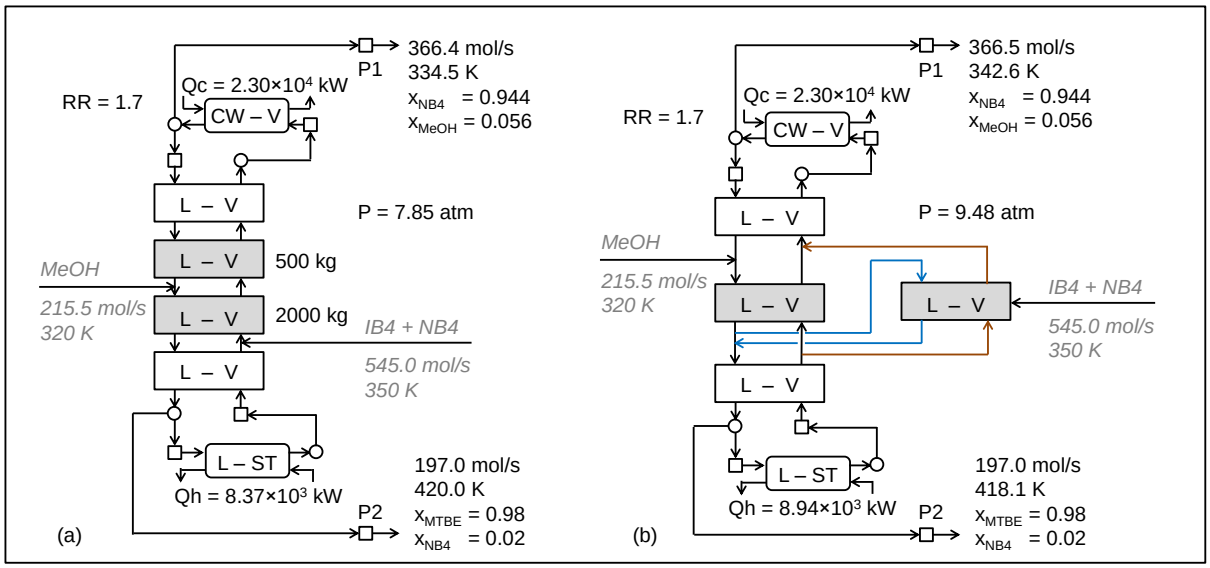


Figure 6.8: MTBE production – Inherently safer designs (a) Reduced overall process risk, (b) Reduced overall process risk & Constrained module risk (Reprinted from [48]).

For an integrated consideration of flexibility and inherent safety following the framework in Fig. 6.1, flexibility test identifies the critical point as $f^I_{MeOH} = 225.5$ mol/s. The corresponding multiperiod MINLP model results in the same optimal structure configurations as shown in Fig. 6.8. However, an increase of module diameters is required to accommodate the uncertainty in flowrates. A summary of total annualized costs for each derived design configuration with different level of safety/operability is presented in Table 6.6, indicating that operability and safety considerations can result in significant structure changes in the optimal design configuration.

Table 6.6: MTBE production – Summary of GMF designs (Reprinted from [48]).

| | Flexibility | Reduced overall process risk | Constrained individual module risk | Investment Cost ($\times 10^4$\$) | Operating Cost ($\times 10^4$\$/yr) |
|---|---|---|---|---|---|
| Design 1 (Fig. 6.5a) | | | | 9.1 | 162.4 |
| Design 2 (Fig. 6.8a) | ✓ | ✓ | | 7.3 | 175.1 |
| Design 3 (Fig. 6.8b) | ✓ | ✓ | ✓ | 7.3 | 182.9 |

### 6.4.5 Step 4: Optimal and operable intensified steady-state design

This step concludes the steady-state analysis of the resulting operable intensified designs. Delivered at the exit of Step 3, the cost-optimal design configurations based on phenomenological representation, with enhanced flexibility and inherent safety performances, are translated to equipment-based units/flowsheets and validated using Aspen simulation.

The cost-optimal and flexible design solution with reduced overall risk (Fig. 6.8a) is translated, in a similar manner as that for Fig. 6.5a, as a reactive distillation column. A total of 11 column trays are necessitated, with the simulation results illustrated in Fig. 6.9a.

The identification of the other safer design solution (Fig. 6.8b) is more tentative and less intuitive: (i) the major part of the flowsheet, excluding the second reactive separation module, is regarded as a reactive distillation column; (ii) the second reactive separation module is translated to a side reactive column which is fully integrated with main column. It is worth noting that different flowsheets may be derived and the practicability of this unit needs to be further investigated. However, this is a challenge to be addressed when striving for innovative intensified designs. As for the problem set up in Aspen Plus, existing column modules cannot provide the desired integration scheme. Thus two RADFRAC columns are used and interaction streams are utilized for the stream exchanges between the side column (COL1) and the main column (COL2) (Fig. 6.9b). The main column comprises 8 trays in column section with the 3rd to 5th constituting the reactive zone, while the side column has 3 trays, all reactive. The interaction streams given in modular flowsheet are placed at the corresponding tray (for example, a liquid connecting stream leaves COL2 at the 6th tray to the 1st tray in COL1). Note that the condenser and reboiler are not used in the side column specification. The detailed simulation results are presented in Fig. 6.9b.

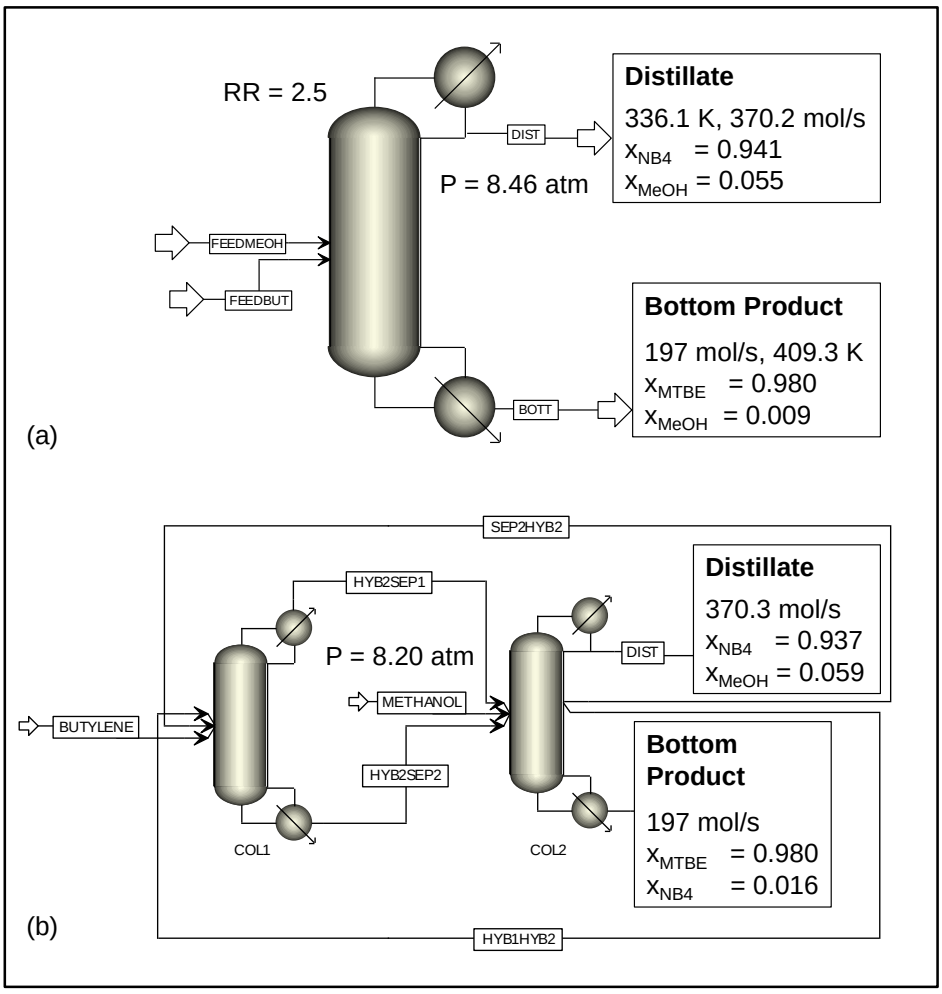


Figure 6.9: MTBE production – Aspen simulation of steady-state optimal operable designs
(a) Reduced overall process risk,
(b) Reduced overall process risk & Constrained module risk (Reprinted from [48]).

## 6.5 Summary

In this chapter, we have proposed a systematic approach which embeds inherent safety and flexibility analysis in the Generalized Modular Representation Framework to synthesize operable intensified designs and have it demonstrated with a case study on MTBE production. Without any pre-postulation of plausible tasks, units, or flowsheets, GMF is able to suggest optimal process structures and mass/heat exchange patterns by leveraging the synergy of hybrid reaction/separation phenomena. The incorporation of quantitative risk analysis and flexibility test in GMF synthesis model ensures the delivery of intensified design configurations with guaranteed inherent safety and flexibility performances. The solutions indicate that operability considerations may result in significant structure changes of the process optimal solution, which emphasizes the significance of operability assessment during early design stage rather than posterior evaluation. The consistency and cross-validation between different design stages (e.g., phenomena-based synthesis, steady-state analysis) are also highlighted to ensure the delivery of verifiable intensified systems.

The basis of GMF lies in the driving force constraints. The current derivation of driving force constraints is built on the characterization of thermodynamic space considering reaction and separation feasibilities, which aligns mostly with mass transfer limited systems. However, we have shown in the MTBE production case study that kinetically controlled systems can also be captured (Table 6.3) with a non-zero $G2$ value. Future research can focus on the characterization of non-conventional mass transfer such as selective separation through membrane.

From operational perspective, risk analysis is incorporated in this work during phenomena-based synthesis to penalize the presence of inherent hazards. However, safety evaluation also needs to be performed at unit level once the corresponding unit operation-based flowsheet is identified, taking detailed equipment design into consideration. Furthermore, the steady-state operable PI designs obtained from the proposed framework can be taken to further dynamic analysis incorporating control considerations. Simultaneous design and control can provide instrumental design information to close the loop for the synthesis of optimal and operable intensified systems. This extension is issue of Chapter 8.

# 7. OPERABILITY, SAFETY, AND CONTROL ANALYSIS IN MODULAR PROCESS INTENSIFICATION SYSTEMS[†]

As highlighted in Chapter 6, it is important to consider steady-state operability and safety criteria in the analysis and design of intensified process systems. When it comes to dynamic operation, it has been observed that the inherent process physics and dynamics in PI systems can be very different from those in well-established conventional processes, normally posing more demanding requirements on process control. For example, a key difficulty with process intensification is that it can result in tight integration of tasks with less degrees of freedom (DOFs), narrower operating windows, and typically faster process dynamics. In this chapter, we aim to develop a fundamental understanding of the unique operability, safety, and control characteristics in modular process systems. We will discuss the following key open questions using rigorous model-based analyses, which include:

(i) How does the loss of DOFs affect the operation and control of an intensified process compared to its conventional process counterpart?

(ii) Operability concerns result from the violation of inequality process constraints during actual operation (under uncertainty and disturbances). For the role of process constraints, what is the difference between intensified vs. conventional processes?

(iii) While PI is affected by the loss of DOFs, the numbering up of modular designs can contribute to additional DOFs. What is the trade-off between economics and operability/control in an intensified modular production process?

(iv) How to quantitatively evaluate the risk of an intensified process using inherent safety metrics?

[†]Reproduced in part with permission from Pistikopoulos, E. N., Tian, Y., & Bindlish, R. (2021). Operability and control in process intensification and modular design: Challenges and opportunities. AIChE Journal, e17204. Copyright 2021 American Institute of Chemical Engineers. Reproduced in part with permission from Tian, Y., & Pistikopoulos, E. N. (2020). Operability and Safety Considerations in Process Intensification. IFAC-PapersOnLine, 53(2), 11434-11439. Copyright 2020 The Authors. Open Access.

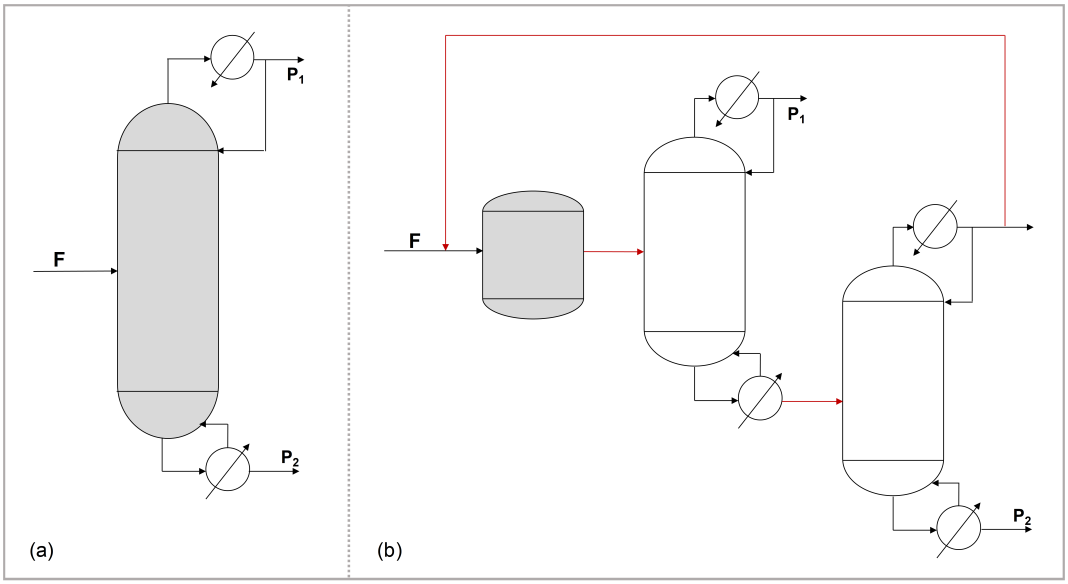


Figure 7.1: DOF comparison – (a) Reactive distillation, (b) Reactor-distillation-recycle. (Reprinted from [29])

## 7.1 Loss of degrees of freedom

The loss of DOFs occurs mostly in PI systems which combine multiple process steps into a single unit or with tight mass/energy integration between units. Note that the basis of comparison is at the process level to design an intensified process or its conventional counterpart process to complete a given production task, instead of comparing a piece of intensified equipment vs. a conventional one. To showcase how the DOFs are impacted by process intensification, we give an illustrative example comparing an intensified reactive distillation (RD) process against a conventional reactor-distillation-recycle process as shown in Fig. 7.1.

### 7.1.1 DOF analysis

To investigate how the DOFs change in these two processes at different process design stages, we first perform a general DOF analysis using three types of models: (i) high fidelity dynamic modeling, (ii) steady-state modeling, and (iii) superstructure-based synthesis modeling.

To highlight the impact of design on operability and control, we distinguish hereafter three types of DOFs as defined in Nikačević et al. [60]: (i) *Thermodynamic DOFs* – which give the number of independent intensive system properties such as pressure or temperature, (ii) *Design*

*DOFs* – which are the number of independent geometrical properties available for process design, and (iii) *Operational DOFs* – which identify the number of independent process variables that can be manipulated for process control or operation.

*High fidelity dynamic modeling*

In this section, the DOF comparison in the reactive distillation process and the reactor-distillation-recycle process is performed using high fidelity dynamic modeling with sufficient accuracy in describing the physical process as well as the correlations between design and operation [196]. A generalized process system is considered, consisting of $NC$ components, 1 feed stream, and 2 product streams. Each of the (reactive) distillation column has $Ntray$ column trays. The detailed analyses of DOFs for RD and reactor-distillation-recycle are respectively presented in Tables 7.1 and 7.2, where the additional DOFs available in the conventional process are highlighted. It can be observed that RD has much less DOF compared to its conventional process counterpart.

Table 7.1: DOFs of reactive distillation based on dynamic modeling (Reprinted from [29]).

| | Variable | Number of DOFs |
|---|---|---|
| Thermodynamic DOFs | Reboiler pressure | 1 |
| | Condenser pressure | 1 |
| Design DOFs | Diameter, weir height, tray spacing | 3 |
| | Reflux drum diameter & length | 2 |
| | Reboiler diameter & length | 2 |
| Operational DOFs | Reflux ratio, Boilup ratio | choose 2 |
| | Bottoms rate, Distillate rate, | |
| | Reboiler duty, Condenser duty | |
| **Sum** | | **11** |

Table 7.2: DOFs of reactor-distillation-recycle based on dynamic modeling (Reprinted from [29]).

| | | Variable | Number of DOFs |
|---|---|---|---|
| Thermodynamic DOFs | Distillation 1 & 2: | Reboiler pressure | $1 \times 2$ |
| | | Condenser pressure | $1 \times 2$ |
| | Reactor: | Temperature, Pressure | 2 |
| Design DOFs | Distillation 1 & 2: | Diameter, weir height, tray spacing | $3 \times 2$ |
| | | Reflux drum diameter & length | $2 \times 2$ |
| | | Reboiler diameter & length | $2 \times 2$ |
| | Reactor: | Height & Diameter | 2 |
| Operational DOFs | Distillation 1 & 2: | Reflux ratio, Boilup ratio | choose $2 \times 2$ |
| | | Bottoms rate, Distillate rate, | |
| | | Reboiler duty, Condenser duty | |
| | Reactor: | Outlet flowrate | 1 |
| | Flowsheet: | Recycle ratio | 1 |
| **Sum** | | | **26** |

*Steady-state modeling*

As shown in Tables 7.3 and 7.4, steady-state modeling of the intensified reactive distillation process also has less DOFs comparing to that of the conventional reactor-distillation-recycle process. The reasons for loss of degrees of freedom are consistent with that summarized for dynamic modeling. Moreover, to briefly comment on the differences between steady-state modeling and dynamic high-fidelity modeling: steady-state modeling normally provides a more flexible description for a certain unit its structural design via discrete (or binary) design variables while dynamic modeling is mostly used for fixed design configurations. Take the (reactive) distillation column modeling as an example, the steady-state model proposed by Viswanathan and Grossmann [197] also enables the selection of feed tray location and reflux tray location (i.e., the DOFs of Feed/Reflux tray structure in Table A.3). While attempts have been made to incorporate these discrete design decisions into dynamic modeling for the benefits of simultaneous design and control optimization,

the computational tractability for mixed-integer dynamic optimization algorithms still leave it a better solution to determine discrete design variables at steady-state. Another difference is that steady-state modeling has less considerations of variable interactions due to equipment internal design. Again using the (reactive) distillation modeling as an example, the column tray pressures in dynamic modeling are calculated via pressure driving force when vapor flow passing the tray with certain geometry, while in steady-state modeling the pressure profile is pre-assigned (i.e., the DOFs of stage pressure in Table A.3). These all result in more DOFs, in other words a larger design space, in steady-state modeling versus dynamic modeling.

Table 7.3: DOFs of reactive distillation based on steady-state modeling (Reprinted from [29]).

| | Variable | Number of DOFs |
|---|---|---|
| Thermodynamic DOFs | Stage pressures | $Ntray$ |
| | Reboiler pressure | 1 |
| | Condenser pressure | 1 |
| Design DOFs | Feed tray structure | $Ntray - 1$ |
| | Reflux tray structure | $Ntray - 1$ |
| Operational DOFs | Reflux ratio, Boilup ratio | choose 2 |
| | Bottoms rate, Distillate rate, | |
| | Reboiler duty, Condenser duty | |
| **Sum** | | $\boldsymbol{3Ntray + 2}$ |

*Superstructure-based synthesis modeling*

Another type of model used to represent process systems is superstructure-based synthesis model. To fully realize the innovation of PI by discovering unknown process solutions, process synthesis has extended its scope to represent chemical processes utilizing fundamental physic-ochemical phenomena without any pre-postulation of plausible equipment/flowsheet alternatives which may hinder the discovery of "out-of-the-box" process solutions. For more detail on this

Table 7.4: DOFs of reactor-distillation-recycle with steady-state modeling (Reprinted from [29]).

| | | Variable | Number of DOFs |
|---|---|---|---|
| Thermodynamic DOFs | Distillation 1 & 2: | Stage pressures | $Ntray \times 2$ |
| | | Reboiler pressure | $1 \times 2$ |
| | | Condenser pressure | $1 \times 2$ |
| | Reactor: | Temperature, Pressure | 2 |
| Design DOFs | Distillation 1 & 2: | Feed tray structure | $(Ntray - 1) \times 2$ |
| | | Reflux tray structure | $(Ntray - 1) \times 2$ |
| | Reactor: | Volume | 1 |
| Operational DOFs | Distillation 1 & 2: | Reflux ratio, Boilup ratio | choose $2 \times 2$ |
| | | Bottoms rate, Distillate rate, | |
| | | Reboiler duty, Condenser duty | |
| | Reactor: | Outlet flowrate | 1 |
| | Flowsheet: | Recycle ratio | 1 |
| **Sum** | | | $\boldsymbol{6Ntray + 9}$ |

topic, readers of interest are referred to the review/perspective articles in Table 1. Herein, we take the Generalized Modular Representation Framework as an example of these PI synthesis strategies and analyze the gain or loss of DOFs in such phenomena-based representation of intensified and conventional process systems.

The GMF modular representation for the reactive distillation and reactor-distillation-recycle are depicted in Fig. 7.2. In Fig. 7.2a, the GMF-based reactive distillation column comprises – from the top to the bottom – a pure heat exchange module where cooling water ("CW") exchanges heat with inlet vapor stream ("V"), three mass/heat exchange modules where reactive separation takes place between contacting liquid ("L") and vapor streams ("V"), and another pure heat exchange module where heating steam ("ST") exchanges heat with inlet liquid stream ("L"). Fig. 7.2b can be interpreted in a similar way, just an addition of the leftmost "L-L" module represents a mass/heat exchange module with pure reaction task in analogy to the actual reactor.

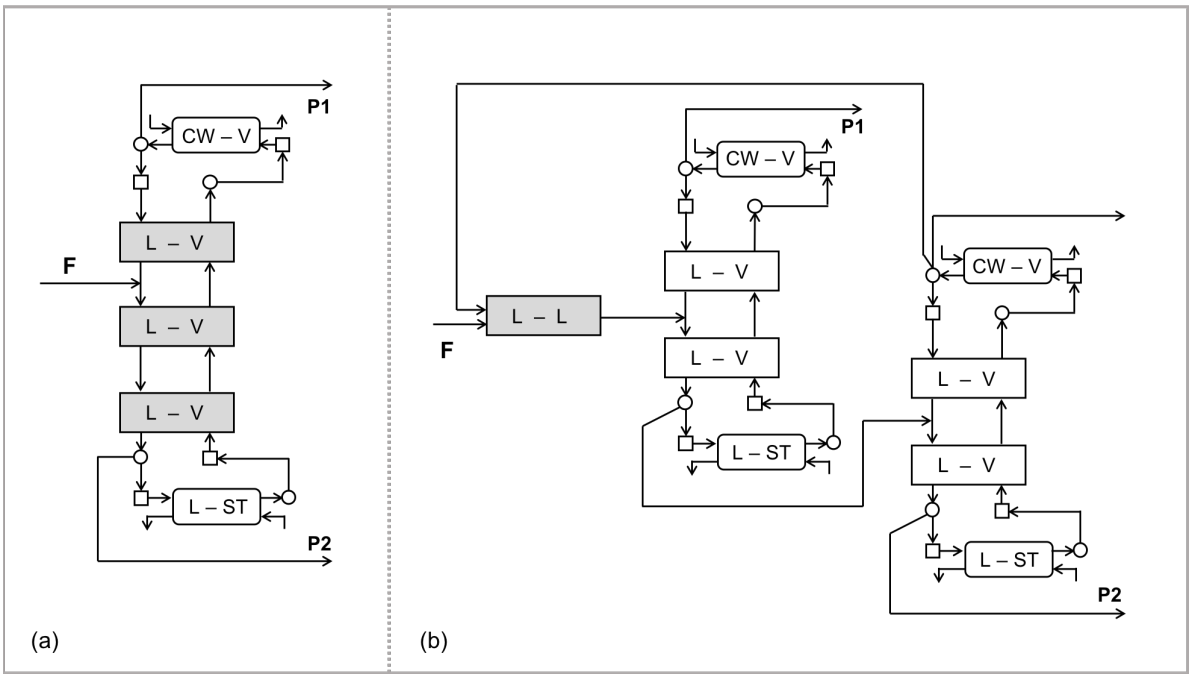


Figure 7.2: GMF representation for olefin metathesis –
(a) Intensified reactive distillation, (b) Conventional reactor-distillation-recycle.
(Reprinted from [29])

At the level of full superstructure network, the number of DOFs are much surpassing the other two types of model due to the combinatorial decisions. For example, if 5 mass/heat exchange modules ($NE = 5$) are utilized to represent a process system involving 3 components ($NC = 3$), a total number of 182 degrees of freedom are available. However, many of these DOFs will appear or disappear with the selection of integer (binary) variables. As the (optimal) results of GMF synthesis, intensified reactive distillation process or conventional reactor-distillation-recycle process can be generated as shown in Fig. 7.2. The DOF analyses on these configurations become consistent with that of steady-state and dynamic modeling, i.e.

- DOFs of GMF-based intensified reactive distillation:
  - Module temperatures and pressures ($2NE, NE = 5$ as the number of GMF modules)
  - Reflux ratio, Boilup ratio, Bottoms rate, Distillate rate, Reboiler duty, Condenser duty (choose 2) (2)

- DOFs of GMF-based conventional reactor-distillation-recycle:
  - Module temperatures and pressures, including mass/heat exchange modules and pure heat exchange modules ($2NE, NE = 9$)
  - Reflux ratio, Boilup ratio, Bottoms rate, Distillate rate, Reboiler duty, Condenser duty (choose 2) ($2 \times 2$)
  - Reaction module outlet flowrate ($1$)
  - Recycle ratio ($1$)

In summary, regardless of model types, RD consistently has less degrees of freedom compared to its conventional counterpart. Some general rules can also be summarized which result in the loss of DOFs in such a task-integrated system as reactive distillation:

- The coupling of reaction and separation in a single unit requires reaction and separation to take place under the same temperature and pressure conditions. This mostly affects the thermodynamic DOFs and results in the concern of a reduced operating window [34].
- The full integration of the reactor and the distillation in a single RD unit, at the same time, converts the interconnecting streams between units (e.g., reactor outlet stream, recycle stream) to internal flows within the unit. Thus, the potential measurement and manipulation of these steams (for example, through valve) are no longer available.
- The reduction in the number of units in RD results in the loss of thermodynamic, design, and operational DOFs.

In addition to these empirical observations, it is worth highlighting a theoretical development from Baldea [61]. The author rigorously proved that, an integrated process, which consists of $n$ units in series with identical material holdup and an infinitely large material recycle stream connecting the last and the first units, is statically equivalent to an intensified process consisting of a single unit with the same material up as each integrated unit. However, the dynamics of the

intensified process is $n$ times faster than the integrated one, while losing available manipulated variables for control in the streams between each unit.

### 7.1.2 A numerical case study: Olefin metathesis

To compare the open-loop and closed-loop dynamic behaviors, in what follows we present a comparative case study for olefin metathesis to produce 2-butene and 3-hexene from 2-pentene. The production task is to produce 50 kmol/h of 98% butene and 50 kmol/h of 98% hexene at 1 atm, given as raw material a saturated liquid stream of 100 kmol/h pure pentene. The RD column and the reactor-distillation-recycle flowsheet depicted in Fig. 7.1 are modeled using high-fidelity dynamic models built in PSE gPROMS® ModelBuilder. The generalized distillation model, reactive distillation model, and cost functions can be found in Bansal et al. [196] and Tian et al. [67]. The design and operation parameters, determined via steady-state optimization to minimize total annualized cost, are detailed in Table 7.5.

Table 7.5: Design and operation parameters for olefin metathesis (Reprinted from [29]).

| | Reactive distillation | Reactor-distillation-recycle | | |
|---|---|---|---|---|
| | | Reactor | Distillation 1 | Distillation 2 |
| Number of stages | 17 | / | 6 | 9 |
| Feed tray locations | 7 & 12 | / | 5 | 3 |
| Reactive volume ($m^3$) | 23.2 | 51.9 | / | / |
| Diameter (m) | 5.0 | 5.7 | 6.0 | 7.7 |
| Pressure (atm) | 1 | 1 | 1 | 1 |
| Reflux ratio | 3.0 | / | 5.0 | 0.46 |
| Capital Cost ($\times 10^5$\$) | 5.51 | 6.66 | 2.56 | 5.40 |
| Operating Cost ($\times 10^5$\$) | 2.11 | 5.39 | 3.96 | 5.46 |
| **Total Annualized Cost ($\times \mathbf{10^5}$\$)** | **3.94** | **2.76** | **3.88** | **7.25** |

Considering a fixed design configuration, the reactive distillation column has two available operational degrees of freedom, i.e., reflux ratio and distillate flowrate. On the other hand, six operational DOFs are available for the control of the reactor-distillation-recycle process: (i) reactor outlet flowrate controlled via valve stem position, (ii) distillate flowrate and reflux ratio for distillation column 1, (iii) reflux ratio and boilup ratio for column 2, and (iv) recycle ratio. We first perform a series of open-loop analyses on each of the above DOFs (or manipulated variables). The dynamic responses in RD and reactor-distillation-recycle are illustrated in Fig. 7.3.

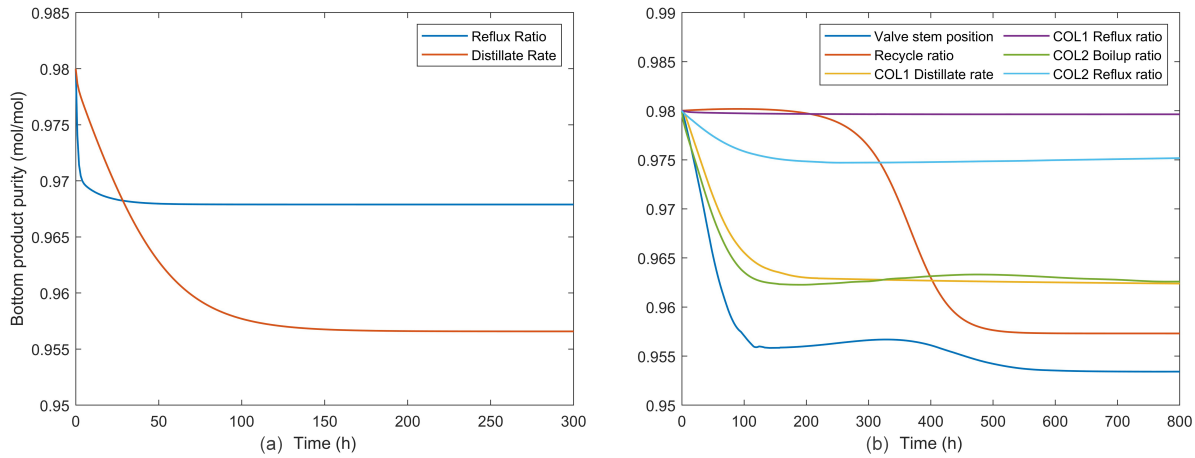


Figure 7.3: Open-loop step response – (a) Reactive distillation, (b) Reactor-distillation-recycle. (Reprinted from [29])

Two differences can be summarized based on Fig. 7.3: (i) the dynamic response of RD is much faster than that of the reactor-distillation-recycle, and (ii) the reactor-distillation, with significant material recycling, shows a typical two-time-scale behavior in such integrated systems. For example, the response of bottom product purity to a step change in the valve stem position (Fig. 7.3b) clearly exhibits an initial fast transient followed by slow dynamics. However, this dynamic behavior is not observed in the RD process.

For the RD closed-loop control, two PI controllers are designed in which reflux ratio and distillate rate are used as manipulated variables to respectively control the top and bottom product purity as two single-input single-output (SISO) systems. As shown in Fig. 7.4, PI control can meet the requirement of set point tracking to RD top and bottom product purity.

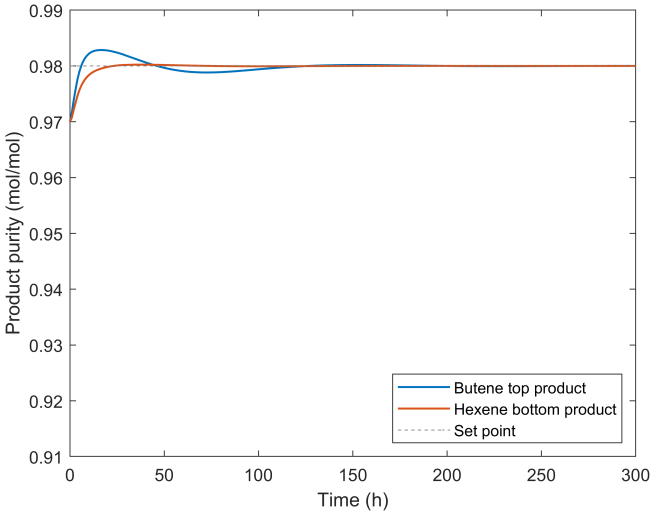


Figure 7.4: PI control for set point tracking in RD column (Reprinted from [29]).

Among the six DOFs for reactor-distillation-recycle, two pairing schemes are selected and tested to control the top and bottom product purity with SISO PI controllers. The results are shown in Fig. 7.5. It can be noted that PI control can also perform satisfactorily for set point tracking in this conventional process but only when a good pairing scheme is selected.

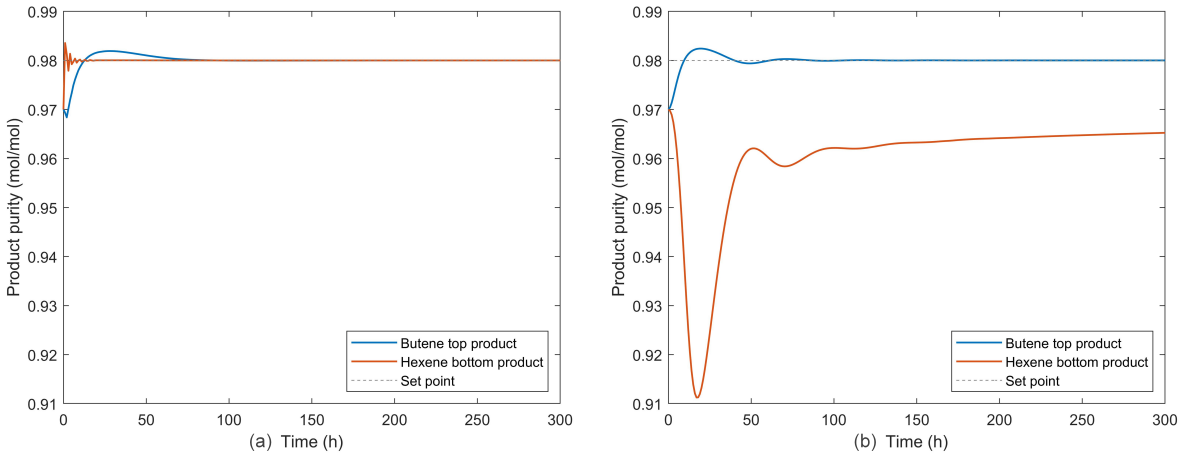


Figure 7.5: PI control for set point tracking in reactor-distillation-recycle process:
(a) Manipulated variables – COL1 distillate flowrate and COL2 boilup ratio,
(b) Manipulated variables – COL1 distillate flowrate and flowsheet recycle ratio.
(Reprinted from [29])

## 7.2 Role of process constraints

From a model-based point of view, any operability, safety, or control concerns can be viewed as the violation of process modeling constraints – typically the inequality ones which define product specifications, safe operation region, design capacity, etc. These violations can be caused by the existence of disturbances and uncertainties, changes in operating conditions, product specifications, etc. [86, 166] In this section, by analyzing the role of constraints, we compare the operability performance of the reactive distillation process and reactor-distillation-recycle process as a motivating example.

### 7.2.1 Temperature and pressure bounds

The combination of reaction and separation into a single unit restricts these two tasks taking place under the same temperature and pressure conditions. In this context, the operating window of RD is conceptually the *intersection* of the reaction operating window and the distillation operating window [34, 60]. However, the operating window of reactor-distillation-recycle is ideally the *union* of the operating windows of reaction and distillation.

Recall the olefin metathesis case study introduced in Chapter 3.3.1 – the reaction occurs at atmospheric pressure between 270.15 K to 340.15 K which results in a rather limited operating window in the space of temperature-pressure (T-P). Fig. 7.6 depicts the T-P window for reaction, distillation, and reactive distillation by sampling through the design and operation space for the specific production task. It can be observed that, in this example, RD is faced with a significant reduction of operating window as well as much stricter design and operation constraints, compared to the much more flexible operating window enabled by distillation process.

### 7.2.2 Flowrate bounds

For the stream flows connecting different units in a process flowsheet, flowrate bounds are normally given either to avoid unreasonably large flows (e.g., for recycle stream) or to ensure feasible equipment design (e.g., pipe). A notable difference of reactive distillation, compared to the flowsheet of a reactor followed by a train of distillation columns, is the conversion of external

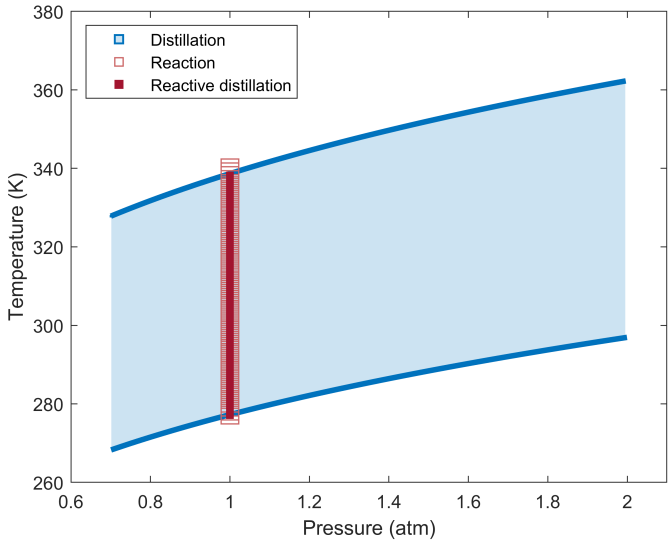


Figure 7.6: Temperature-pressure operating window for olefin metathesis (Reprinted from [29]).

connecting streams (e.g., reactor outlet stream, recycle stream) to internal flows within the unit – which emphasizes the impact of design parameters on flowrate bounds. Column diameter has been found to be the most limiting design parameter for distillation operation under uncertainty. A given column diameter can only accommodate a certain range of flowrate uncertainties, beyond which will cause flooding issues. Using the example of olefin metathesis, we compare the impact of column diameter on an allowable feed flowrate range in the RD column and the reactor-distillation-recycle process.

For a given reactive distillation column diameter (or the diameter of Column 1 or 2 in the reactor-distillation-recycle process), we first characterize the "steady-state feasible region" in which the process is feasible for operation and can satisfy the top and bottom product purity specifications under uncertainties in feed flowrate. Then, the "dynamic feasible region" is determined where the process is required to meet process specifications with PI controller on under time-variant feed flowrate uncertainties. Conceptually, the dynamic feasible region should be a subset of the steady-state region since the latter assumes perfect control. Several observations can be made based on the results depicted in Fig. 7.7:

- RD can accommodate a larger set of feed flowrate uncertainties than its conventional counterpart at the same over-design factor (i.e., over-design compared to the minimum required column diameter at nominal feed flowrate 100 kmol/h). This is because the conventional process has around twice larger external and internal flowrates than RD.

- The reactor-distillation-recycle process reaches a maximum flowrate at 142 kmol/h regardless of the increase of column diameter. This is due to the fact that a pre-specified upper bound is met for recycle flowrate at 425 kmol/h compared to the nominal at 300 kmol/h.

- The dynamic feasible region of RD has a notable mismatch with its steady-state feasible region, which can be up to 11 kmol/h. This is due to the more complex interaction between process variables in RD, which makes the process more vulnerable to constraint violation under uncertainties and/or control actions. This emphasizes the need of simultaneous dynamic design and control under uncertainties in such intensified systems.

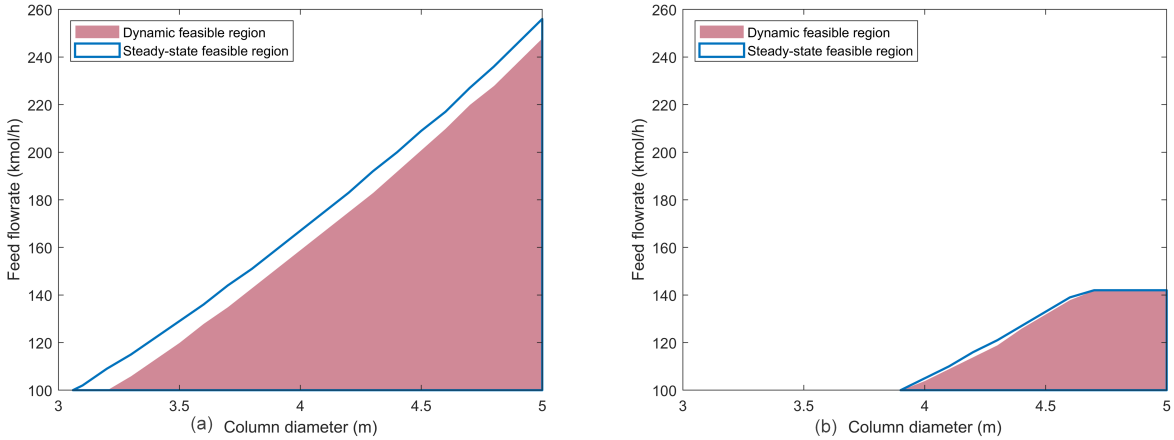


Figure 7.7: The impact of column diameter on flowrate constraints (Reprinted from [29]).

### 7.2.3 Process specifications

Given a step change in feed flowrate (+1 kmol/h), Fig. 7.8 shows that RD has a larger deviation from the purity specifications than that in the reactor-distillation-recycle process.

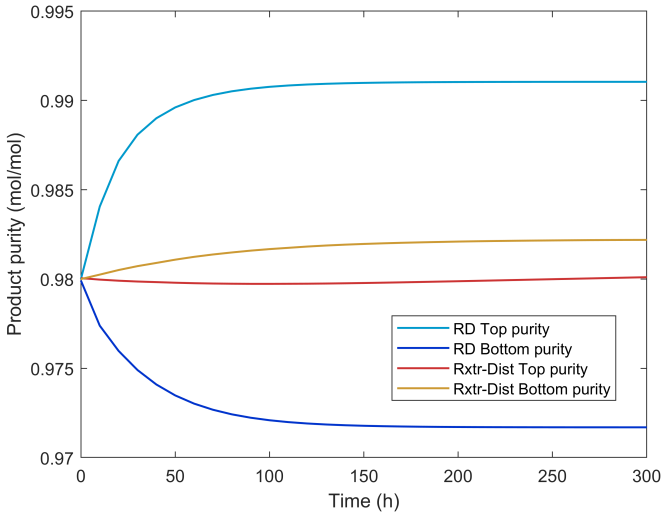


Figure 7.8: Open-loop response to feed flowrate step change (Reprinted from [29]).

To test the closed-loop performance of these two processes, a sinusoidal disturbance is considered in the feed flowrate with a period of 24 hours and an amplitude of 8 kmol/h. With the PI controllers on, the control output profiles for RD and reactor-distillation-recycle are given in Fig. 7.9. While the conventional process is well controlled, the RD process has notable off-specifications.

Given the insufficiency of the SISO PI controllers for RD disturbance rejection, another explicit/ multi-parametric model predictive controller (mp-MPC) is designed following the PAROC framework [64], treating the RD column as a multi-input multi-output (MIMO) process system. The closed-loop performance of both control schemes are shown in Fig. 7.10, indicating better control performance with the mp-MPC controller in terms of meeting product purity specifications under disturbance.

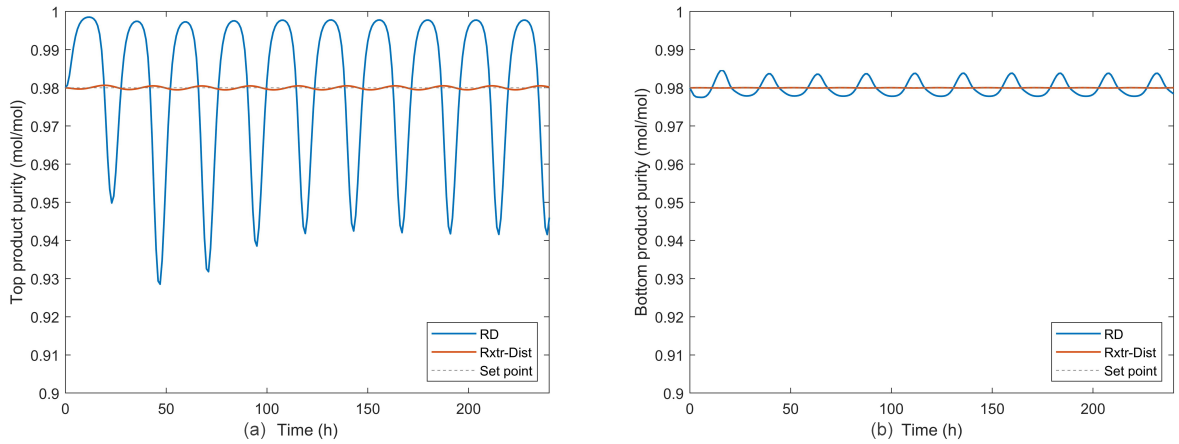


Figure 7.9: PI control for disturbance rejection in RD and reactor-distillation-recycle – (a) Top butene product purity profile, (b) Bottom hexene product purity profile. (Reprinted from [29])

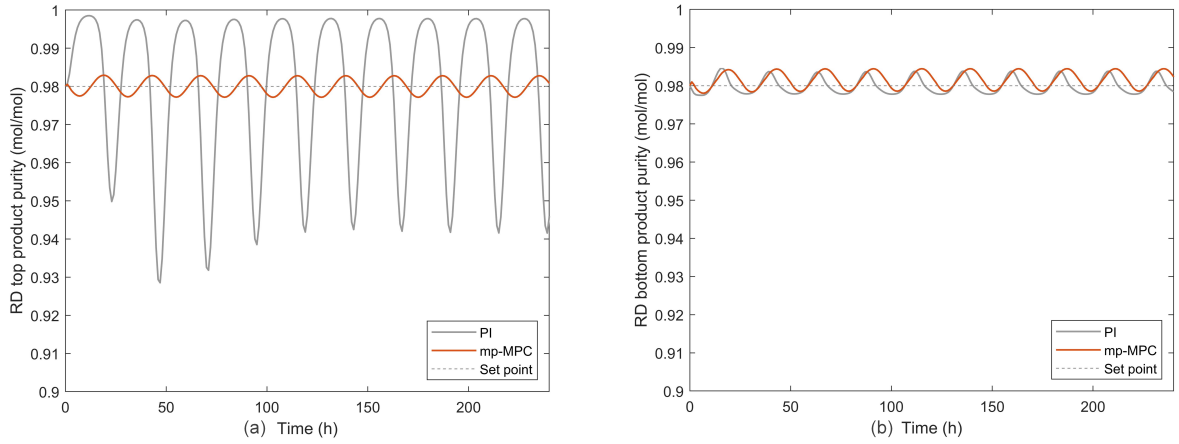


Figure 7.10: PI and mp-MPC control for RD disturbance rejection – (a) Top butene product purity profile, (b) Bottom hexene product purity profile. (Reprinted from [29])

## 7.3 Numbering up vs. Scaling up

In this section, we investigate the impact of modularization on operability and control. We focus on the question if/how the previously mentioned operability and control concerns of an intensified unit can be addressed by introducing extra modular and parallel units (at the expense of more investment cost). Another potential benefit of using modular and parallel units is to enhance process reliability which indicates the probability of a system to perform its designated function over a specified time interval. While this topic is beyond the scope of the current paper, we refer the readers to the recent works [198, 199] for more information.

Continuing with the example on olefin metathesis, an alternative flowsheet is constructed against the single RD unit which consists of two modular RD units operated in parallel as shown in Fig. 7.11. From economics point of view, the modular flowsheet features a TAC *18.8% higher* than that of the single RD unit.

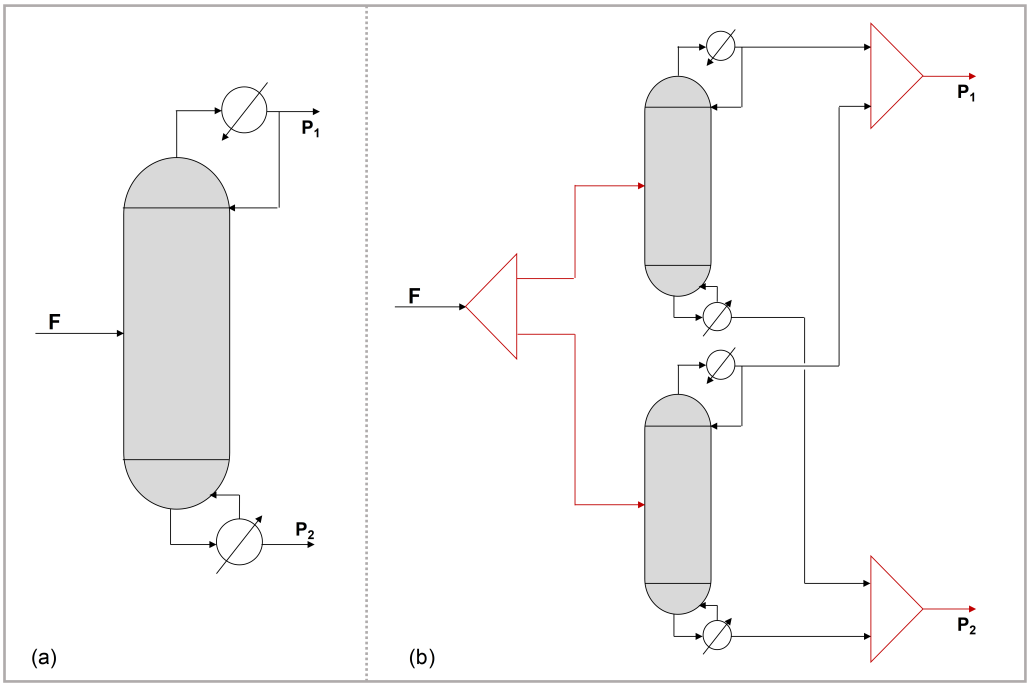


Figure 7.11: Modular reactive distillation for olefin metathesis –
(a) A single unit, (b) Two modular units (Reprinted from [29]).

Recall the discussion in Chapter 7.1 on loss of DOFs due to process intensification, modularization on the other hand provides the opportunity to increase DOFs because of the increased number of process units (including also auxiliary units such as mixers and splitters) and interconnecting streams. To test the control performance for rejecting the sinusoidal feed flowrate disturbance in the previous section, PI controllers are designed to control each modular RD unit as per the pairing scheme 1 given in Table 7.6. If the two modular RD units adopt the same controller designs, they will function synchronously showing a closed-loop performance similar to the original single RD unit. However, the overall process closed-loop performance can be improved in this example by selecting different pairs of control inputs and outputs as depicted in Fig. 7.12a. A second pairing scheme, as detailed in Table 7.6, can be designed to control units at a process level to ensure that the final products are on specification without monitoring product specifications from individual units. The additional DOFs resulted by modularization can again contribute to a better disturbance rejection performance in terms of the final product purity as shown in Fig. 7.12b. This pairing scheme also brings the benefit of one remainder DOF which can be used to achieve other operational objectives of interest, such as to minimize energy consumption. Note that under both pairing schemes the two modular RD units are operated along different trajectories. This observation indicates further opportunities to explore the design and control optimization of this modular flowsheet by simultaneously considering modular unit design, control structure, and closed-loop performance.

Table 7.6: PI control pairing schemes for modular RD units (Reprinted from [29]).

| | Pairing Scheme 1 | | Pairing Scheme 2 | |
|---|---|---|---|---|
| | Input | Output | Input | Output |
| Controller 1 | Feed split ratio | RD1 top product purity | Feed split ratio | Top product purity after mixing |
| Controller 2 | RD1 distillate rate | RD1 bottom product purity | RD2 reflux ratio | Bottom product purity after mixing |
| Controller 3 | RD2 distillate rate | RD2 top product purity | RD2 distillate rate | RD2 top product purity |
| Controller 4 | RD2 reflux ratio | RD2 bottom product purity | | |

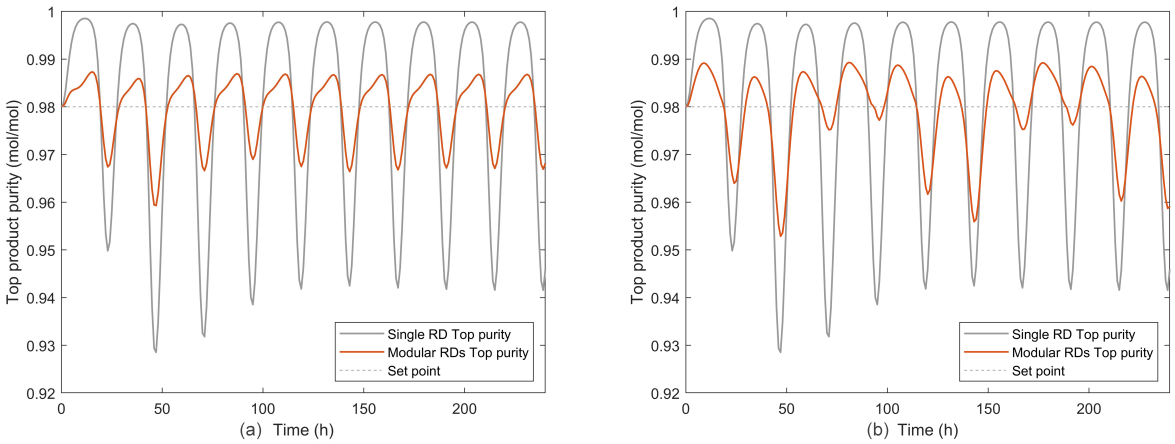


Figure 7.12: PI control for modular RD units vs. a single RD –
(a) Pairing scheme 1, (b) Pairing scheme 2 (Reprinted from [29]).

Some other questions or challenges in modularization include:

- As indicated above, the operational flexibility can be improved with a number of modular designs by enabling synchronized operation or tailed operation for individual units. Thus it opens up questions on how to optimize the operation/control strategies for each of the units and how to perform optimal decision making when the units need to alter operation states in response to changes in production plan.

- The trade-off between the number of control variables vs control efficiency needs to be addressed when the units are numbering up. For example, how to ensure a certain temperature profile across the parallel modular units? In addition to the unit-by-unit control analogous to controlling a single unit operation, indirect control systems can be a good option to reduce the control variables as shown in Hasebe [200] for microreactors.

- Distributed decision making is also necessitated which decomposes the large-scale modular intensified process into constituent subsystems with corresponding localized decision making agents [27, 201]. The control decisions are then coordinated for the overall process following approaches such as distributed model predictive control [202].

## 7.4 Inherent safety metrics

To evaluate inherent safety performance as part of early design, several key open questions need to be addressed:

- Development of standardized metrics to quantify inherent safety performance based on limited information available at early design stage
- Integration of inherent safety metrics into model-based synthesis/design procedure
- Quantitative decision making to design or retrofit process designs to enhance inherent safety performance.

In this section, we present a comparative study of three available inherent safety metrics for inherent safety evaluation of a methyl tert-butyl ether (MTBE) reactive distillation process. These approaches are respectively: (i) Risk analysis [203], (ii) DOW indices [204, 205], and (iii) SWeHI index [206]. Their performance are tested to reflect two major inherent safety principles (i.e., minimization, attenuation) with respect to fire & explosion hazard and health hazard.

### 7.4.1 Minimization

To test the above safety metrics against the minimization of process inventory, we consider three reactive distillation columns (i.e., A, B, C) producing MTBE from methanol and isobutylene with different capacities resulted by different column diameters. The other design and operating parameters remain the same.

Given an instantaneous release of total column inventory, the inherent safety performances of Column A, B, and C are assessed using risk analysis approach, DOW indices, and SWeHI index in terms of toxicity and fire & explosion (F&E). Evaluation results are presented below in Table 7.7. As can be noticed, all the metrics suggest the same ranking order as: Column A inherently safer than B and also than C, which aligns with the well-accepted statement that "less is safer".

Note that it may not be necessary to compare the absolute result values given by these different approaches since they are estimating for different damage scenarios. However, the sensitivity of

each metric with respect to the change of inventory holdup is of interest. For example, Column C has an inventory more than 10 times of that in Column A. Risk analysis approach identified around 10 times increase of both fire & explosion risk and toxicity risk – which scale in a nearly linear fashion with the inventory. However, DOW F&EI gives very similar Radius of Exposure, hardly reflecting the significant scaling up of equipment size. The other DOW CEI & SWeHI indices give around 3 times larger hazard radius.

Table 7.7: Inherent safety comparative study – Minimization effects (Reprinted from [207]).

| | | A | B | C | Rank (unsafer $\rightarrow$ safer) |
|---|---|---|---|---|---|
| Inventory (kg) | | 145 | 1009 | 1744 | |
| F & E | Risk | 4.73e-7 | 30.6e-7 | 42.5e-7 | C < B < A |
| | F&EI | 17.7 m | 20.6 m | 22.1 m | C < B < A |
| | SWeHI | 35.2 m | 67.3 m | 80.7 m | C < B < A |
| Toxicity | Risk | 3.6e-5 | 24.6e-5 | 52.8e-5 | C < B < A |
| | CEI | 73.1 m | 184.8 m | 239.6 m | C < B < A |
| | SWeHI | 46.7 m | 106.9 m | 135.0 m | C < B < A |

### 7.4.2 Attenuation

To test these safety metrics against the attenuation of process operating conditions, we consider another three MTBE reactive distillation columns (i.e., a, b, c) with different operating pressures. The other design and operating parameters remain the same. Evaluation results are shown below in Table 7.8. For fire & explosion hazard, it can be seen that the increase of pressure is not well captured by all these approaches since they give very similar evaluation results. With respect to toxicity health hazard, these approaches are suggesting inconsistent ranking orders, and there is a conflict in ranking Column a to be the most safer process (i.e., risk analysis and CEI) or the most unsafer one (i.e., SWeHI).

Table 7.8: Inherent safety comparative study – Attenuation effects (Reprinted from [207]).

| | | a | b | c | Rank (unsafer $\rightarrow$ safer) |
|---|---|---|---|---|---|
| Pressure (atm) | | 1 | 6 | 11 | |
| F & E | Risk | 30.6e-7 | 80.5e-7 | 86.3e-7 | $c < b < a$ |
| | F&EI | 20.6 m | 23.3 m | 23.9 m | $c \approx b < a$ |
| | SWeHI | 67.3 m | 69.1 m | 69.3 m | $c \approx b < a$ |
| Toxicity | Risk | 24.6e-5 | 196e-5 | 168e-5 | $b < c < a$ |
| | CEI | 184.8 m | 212.9 m | 218.7 m | $c < b < a$ |
| | SWeHI | 106.9 m | 98.5 m | 100.5 m | $a < c < b$ |

### 7.4.3 Some remarks

Existing inherent safety analysis approaches evaluates different process characteristics and may deliver different ranking or analysis results. Moreover, inconsistent evaluation results have been observed, thus making it ambiguous to determine the inherent safety performance of a certain design configuration. In this context, a new safety metric (or index) is highly necessitated and recommended to correctly and consistently evaluate inherent safety performance of different process options at this conceptual design stage.

## 7.5 Summary

In this section, we have discussed several specific dynamic and operating characteristics in PI and modular designs and the resulting challenges from operability and control point of view. The following research opportunities are thereby identified and highlighted for intensified and/or modular systems (although also important for conventional processes):

- Theoretical developments are necessitated to understand the process dynamics, operability, and control for a wider range of modular and intensified systems (e.g., task-integrated systems, micro-reaction systems, rotating equipment).

- Development of a new inherent safety index/metric for intensified & modular systems, which can: (i) consistently capture inherent safety principles – Minimization, Attenuation, Substitution, Simplification, and (ii) consistently quantify inherent safety at – steady-state conceptual design and dynamic operation to reflect the changes of inventory, operating conditions.

- Conceptual design and operational optimization approaches for modular processing systems are needed to systematically analyze the trade-off between module sizing, profitability, and operational flexibility.

- Distributed decision making structure and advanced model-based control will be key enabling tools to ensure the actual operational performances of an integrated process with multiple modular and/or intensified process equipment. Advanced model reduction techniques and dynamic optimization algorithms should also be developed in support of this goal.

- The integration of operability and control metrics at an early PI design stage will be beneficial, due to the tight interaction between design and operating parameters in such systems. A holistic framework for computer-aided design, operability analysis, and control optimization of modular PI systems can be highly beneficial to accelerate the PI technology development.

# 8. A SYSTEMATIC FRAMEWORK FOR SYNTHESIS OF OPERABLE PROCESS INTENSIFICATION SYSTEMS[†]

On the basis of Chapters 6 and 7, we further propose a systematic framework to synthesize intensified process systems with guaranteed operability, safety, and control performances. It follows an integrated procedure to synergize advanced PI/PSE methods, including phenomena-based synthesis representation, flexibility analysis, inherent safety analysis, explicit/multi-parametric model predictive control via the PAROC framework, mixed-integer nonlinear optimization, as well as mixed-integer dynamic optimization. The proposed framework will: (i) provide a holistic approach to deliver verifiable and operable PI systems which systematically and consistently addresses steady-state and dynamic design and operation in intensified processes, (ii) derive optimal process solutions via the use of optimization-based design and operational strategies, and (iii) generate multiple process solutions with desired level of operability performance for decision making.

## 8.1 Problem statement

The generalized problem definition is depicted in Fig. 8.1. *Given:*

1. *Process design target*
    - A set of feed streams with given flowrate, composition, and supply temperature;
    - A set of desired products and specifications on flowrates, temperatures, and/or purities;
    - A set of available heating/cooling utilities with availability and supply temperatures;
    - A set of available mass utilities such as mass separating agents and catalysts;
    - All reaction schemes and kinetics data;
    - All physical property models;
    - Cost data of feeds, mass/heat utilities, and equipment;

[†]Reproduced in part with permission from Tian, Y., Mannan, M. S., & Pistikopoulos, E. N. (2018). Towards a systematic framework for the synthesis of operable process intensification systems. In Computer Aided Chemical Engineering (Vol. 44, pp. 2383-2388). Copyright Elsevier 2018. Reproduced in part with permission from Tian, Y., Pappas, I., Burnak, B., Katz, J., & Pistikopoulos, E. N. (2020). A Systematic Framework for the synthesis of operable process intensification systems – Reactive separation systems. Computers & Chemical Engineering, 134, 106675. Copyright Elsevier 2020. Reproduced in part with permission from Tian, Y., Pappas, I., Burnak, B., Katz, J., & Pistikopoulos, E. N. (2021). Simultaneous design & control of a reactive distillation system – A parametric optimization & control approach. Chemical Engineering Science, 230, 116232. Copyright Elsevier 2021.

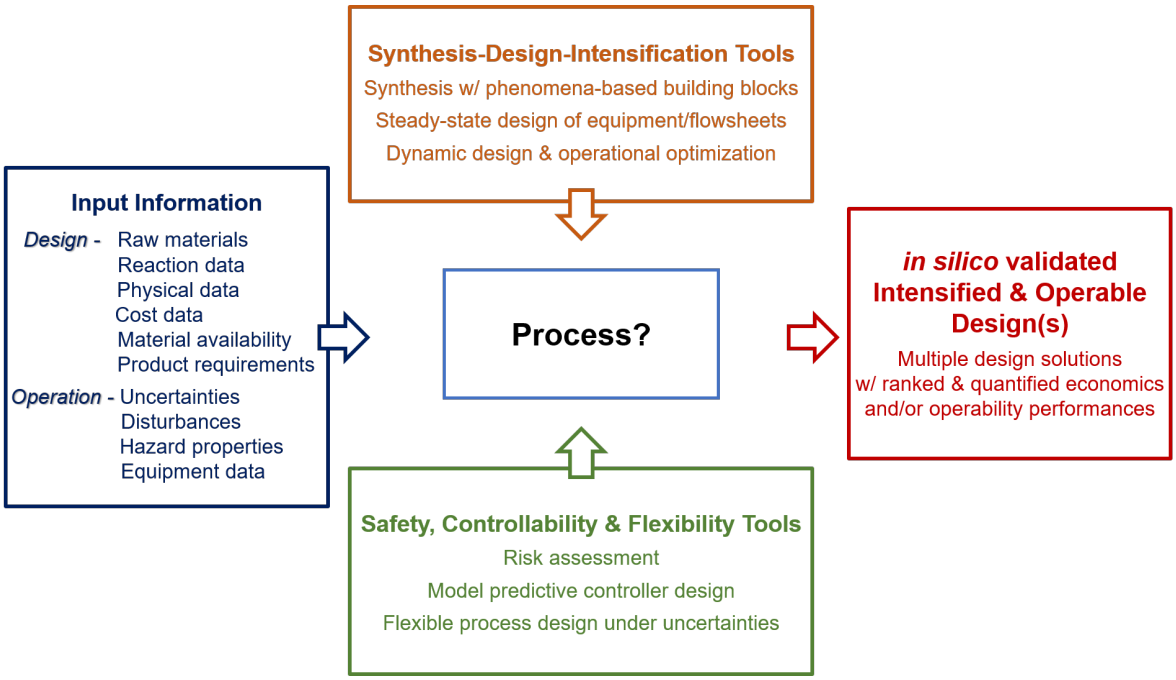


Figure 8.1: Problem definition.

2. *Flexibility target*

    - A specified range for uncertain parameters, where process flexibility is desired (e.g., feed stream composition/flowrate/temperature, heat utility flowrate/temperature);

3. *Safety target*

    - A set of assessment criteria on inherent safety performances (e.g., toxicity, flammability, explosiveness);
    - A set of available equipment with their failure frequency data;
    - Hazardous property data (e.g., lethal concentration);

4. *Control target*

    - A set of disturbances during process operation;
    - A set of control variables with desired set-points;
    - A set of available manipulated variables to maintain feasible operation based on degrees of freedom analysis.

*Objective:* To determine process solutions with

- Minimized total annualized cost consisting of capital costs, mass and heat utility costs;
- Optimal unit or flowsheet configuration(s) with design and operating parameters, which also satisfy the desired flexibility and inherent safety criteria for both steady-state design and dynamic operation;
- Optimal control actions to achieve process specifications.

## 8.2 The synthesis framework for operable PI systems

As shown in Fig. 8.2, the proposed framework consists of three interactive toolboxes (i.e., process intensification/synthesis toolbox, process simulation/optimization toolbox, and process operability/control/safety toolbox) to link steady-state synthesis, dynamic analysis, and operability assessment at the conceptual design stage. Each toolbox can accommodate different techniques implemented in multiple software environments, thus rendering this framework a desirable flexibility. These tools can be used separately for a specific purpose (e.g., steady-state synthesis of a cost-optimal process, safety analysis of an intensified process). They can also be applied in an integrated manner to deliver operable and intensified process solutions – the procedure followed for this purpose are presented below on a step-by-step basis (Figure 8.3):

- **Step 1: Process intensification synthesis representation** – This step aims to first validate the physical representation of any process of interest using Generalized Modular Representation Framework. Available designs in open literature and/or in industrial practice are simulated with GMF to provide preliminary insights into this process. Then, an enriched and generalized superstructure representation is formulated in preparation for next step.
- **Step 2: Superstructure optimization** – This step aims to synthesize the optimal GMF modular process solution by minimizing total annual cost (i.e., cost-optimal without operability considerations). Note that the optimization is performed using the full GMF superstructure representation and not constrained by the initial simulation structure.

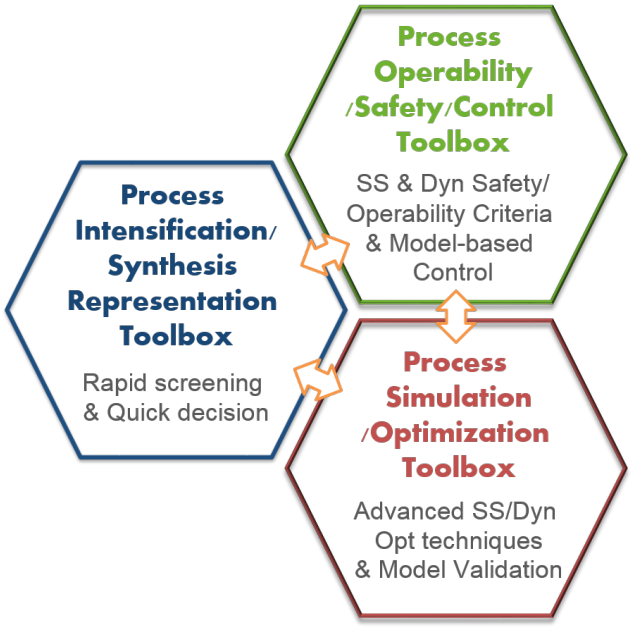


Figure 8.2: Synthesis of operable process intensification systems – The proposed framework.

- **Step 3: Integrated design with flexibility and safety** – After obtaining the initial cost-optimal design from Step 2, this step aims to verify, or improve if necessary, its operability and inherent safety performances. A multiperiod MINLP model is then formulated considering the detected critical operation points by flexibility analysis. Moreover, risk analysis is incorporated as a constraint into the GMF synthesis model to indicate the inherent safety performance of the resulting design.

- **Step 4: Optimal intensified steady-state designs** – This step concludes the steady-state synthesis and design by translating and validating the resulting GMF modular design(s) with equipment-based process alternatives using rigorous simulation.

- **Step 5: Design and control optimization** – This step aims to take the above derived steady-state process solution(s) to dynamic analysis, design, and control optimization. Specifically the following tasks are included: (i) high fidelity dynamic modeling, (ii) open-loop analysis and validation with steady-state designs on flexibility and inherent safety performances, (iii) design of explicit/multi-parametric model predictive controller (mp-MPC) to ensure feasi-

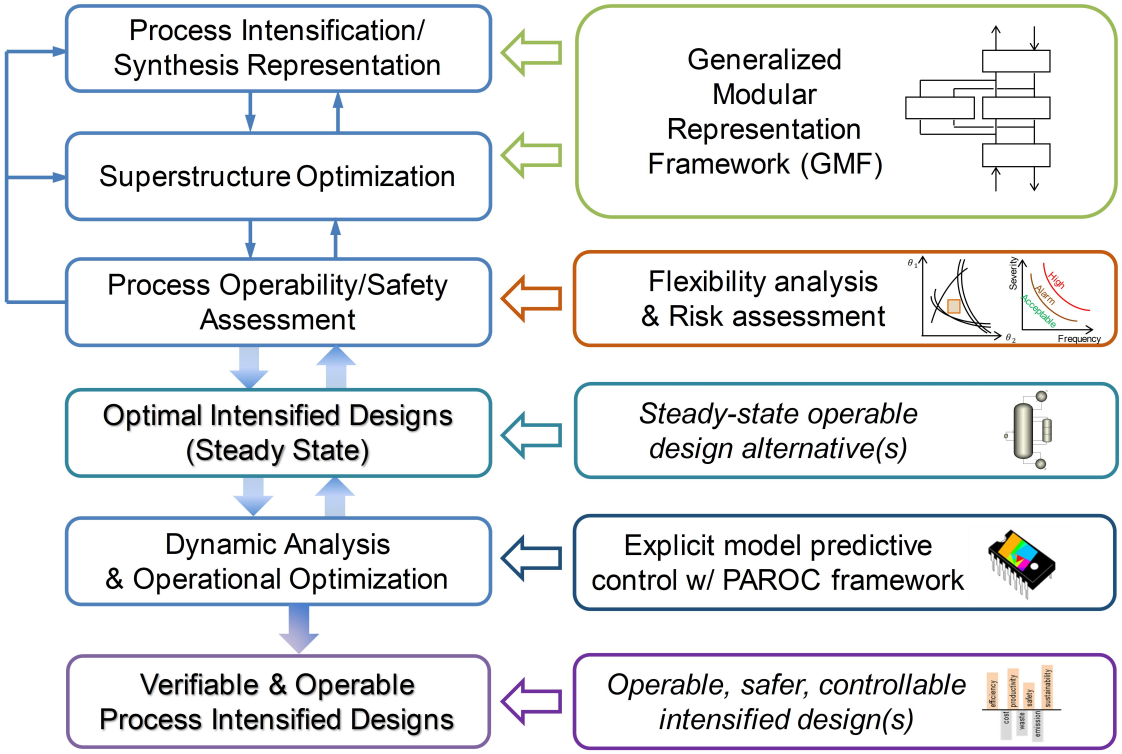


Figure 8.3: Synthesis of operable process intensification systems – Methodology workflow. (Reprinted from [208])

ble operation under uncertainty and disturbances, and (iv) simultaneous design and control optimization to deliver optimal design solutions with optimal dynamic operation strategy.

- **Step 6: Verifiable and operable process intensification designs** – Closed-loop validation is finally performed to ensure the consistency throughout the framework, after which verifiable and operable intensification designs are ready to be delivered.

## 8.3 Case study: Heat exchanger network synthesis

In this section, the proposed framework is applied to a heat exchanger network (HEN) synthesis problem for thermal intensification, as a motivating example for proof-of-concept before proceeding with a broader set of process intensified systems.

### 8.3.1 Process description

This case study considers two hot streams (H1, H2), two cold streams (C1, C2), and one hot utility (HU). Given are: (i) stream flowrate data [209]; (ii) uncertain heat transfer coefficient ($U_{H1\text{-}C1}$), for which the flexibility of the network is desired; (iii) disturbance and control objective, for which controller design is essential; and (iv) stream toxicity, represented by LC50 (i.e., lethal concentration, 50%) of the substance, and equipment data for four types of heat exchanger (HE), namely double pipe HE (DP), plate and frame HE (PF), fixed plate shell and tube HE (SF), and U-tube shell and tube HE (UT), which necessitates inherent safety analysis [78]. The objective is to synthesize a heat exchanger network with minimized total annual cost and desired operability, safety, and control performances.

### 8.3.2 Steady-state synthesis with flexibility and safety considerations

The superstructure optimization problem for steady-state HEN synthesis is formulated based on the pure heat exchange module representation in GMF. A nominal cost-optimal HEN design without flexibility or safety considerations is first obtained as a reference configuration (Fig. 8.4).

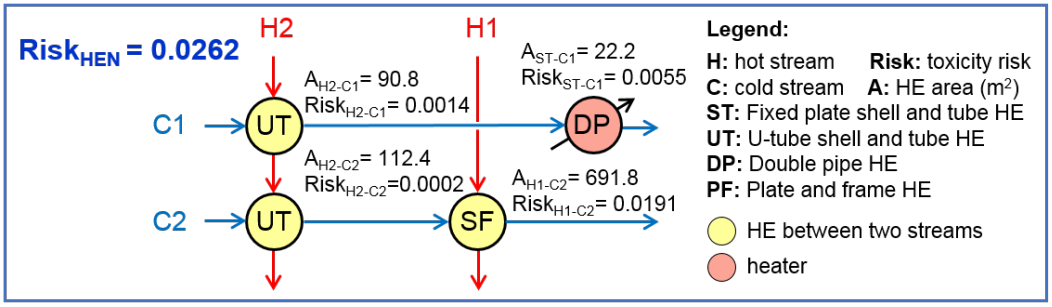


Figure 8.4: HEN synthesis – Nominal design.

Regarding this nominal design configuration, feasibility analysis identifies two periods of operation characterized by the extreme values of $U_{H1\text{-}C1}$. To obtain an inherently safer design, the overall HEN toxicity risk is constrained to be 25% less than that of the nominal design. This results in the change of H1-C2 exchanger type from SF to UT (Fig. 8.5a), as UT has much higher area density to significantly reduce the amount of hazards contained in the equipment.

However, as the individual risk of H1-C2 HE takes up more that 75% of the overall process risk in this case, the risk tolerance is further decreased by constraining individual HE toxicity risk to be less than 50% of overall risk. As a result, a different network configuration is synthesized in order to render H1-C2 HE a lower risk level by relieving its heat exchange burden (Fig. 8.5b). These two safely operable HENs are exported as Designs 1 and 2 for the next step dynamic analysis.

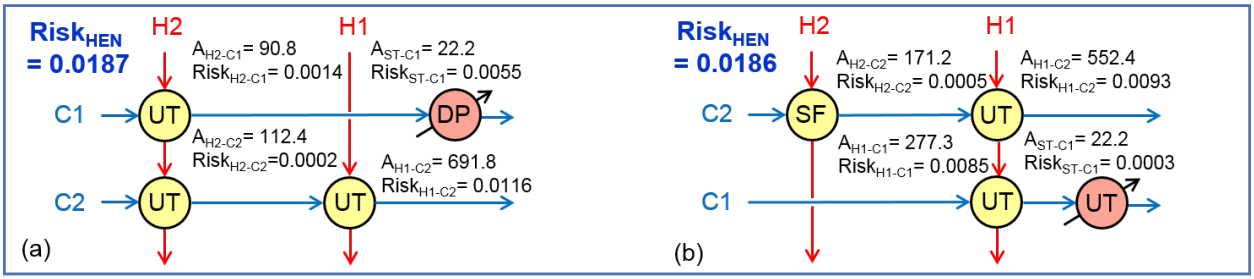


Figure 8.5: HEN synthesis – Operable and inherently safer designs
(a) Design 1, (b) Design 2.

### 8.3.3 Dynamic modelling and mp-MPC controller design

The dynamic HEN is described by a Partial Differential Algebraic Equation (PDAE) model based on gPROMS® Process Model Library for Heat Exchange (PSE, 1997-2017). The network configuration is fixed for each candidate case study as per Fig. 8.5a and b, and heat exchanger areas are used as design variables. To ensure the consistency going from steady-state synthesis to dynamic simulation, the dynamic model is validated to match its steady-state synthesis analogue.

In the derived HENs, bypass flowrate and heat utility duties are the degrees of freedom, and the outlet temperature of stream H1 and C1 are the outputs. The inlet temperature of stream H2 is treated as a disturbance to the operation. The mp-MPC controller design, following PAROC framework [64], takes place for the two candidates individually. Each mp-MPC problem is formulated using corresponding linear state-space model approximated by the System Identification Toolbox of MATLAB®. Via POP® toolbox in MATLAB®, the problem of Design 1 is solved for an output horizon of 2 and a control horizon of 2 resulting in 118 critical regions in solution map, while that

of Design 2 is solved for an output horizon of 2 and a control horizon of 1 resulting in 89 critical regions. Given random disturbances deviating within ±10 K per second, the designed controllers are tested against the high fidelity model for closed-loop validation, indicating the agreement between the outputs and setpoints.

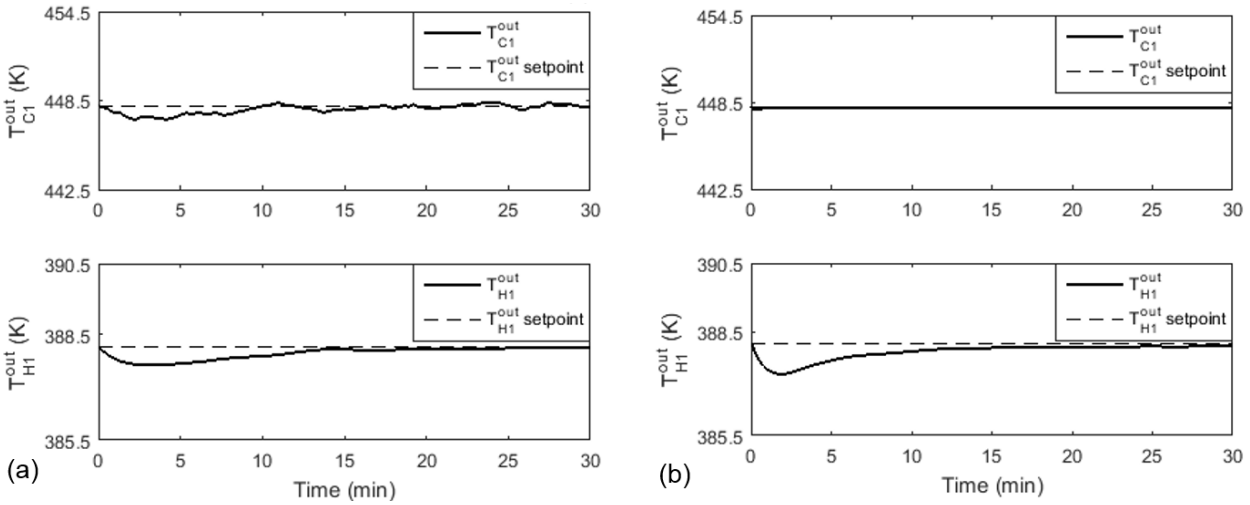


Figure 8.6: HEN synthesis – Closed-loop validation of mp-MPC controller
(a) Design 1, (b) Design 2 (Reprinted from [45]).

### 8.3.4 Simultaneous design and control

The dynamic optimization problem is then formulated and solved for the minimal TAC under each HEN configuration. The obtained results are shown in Table 8.1. Up to this point, two HENs are designed with different levels of operability, control, and safety. While the final construction decision depends on the trade-off between desired operability behavior and economic performance, this framework demonstrates the potential for comparison of various operable design alternatives.

Table 8.1: HEN synthesis – Dynamic optimization results (Reprinted from [45]).

| | Heat Exchanger Area ($m^2$) | | | | Investment Cost | Operating Cost |
|---|---|---|---|---|---|---|
| | H1 – C1 | H1 – C2 | H2 – C1 | H2 – C2 | (k$) | (k$/yr) |
| Design 1 | / | 604.4 | 125.6 | 99.9 | 528.4 | 7357.0 |
| Design 2 | 221.4 | 522.2 | / | 165.7 | 557.4 | 8593.9 |

## 8.4 Case study: MTBE production

In Chapter 6, we have presented the steady-state design of MTBE production system with operability and safety considerations. In this section, we take the derived intensified steady-state design alternatives to dynamic analysis and control optimization. We also highlight the cross-validation between phenomena-based synthesis, steady-state design, dynamic operation, and operability analysis to ensure a valid and consistent design output throughout the framework.

### 8.4.1 Optimal intensified steady-state designs

Recall that in Chapter 6, we have obtained three process designs as shown in Fig. 8.7. Note that the shaded trays in the figure represent reactive zone. A detailed comparison of GMF synthesis results and corresponding Aspen validation results are summarized in Table 8.2.

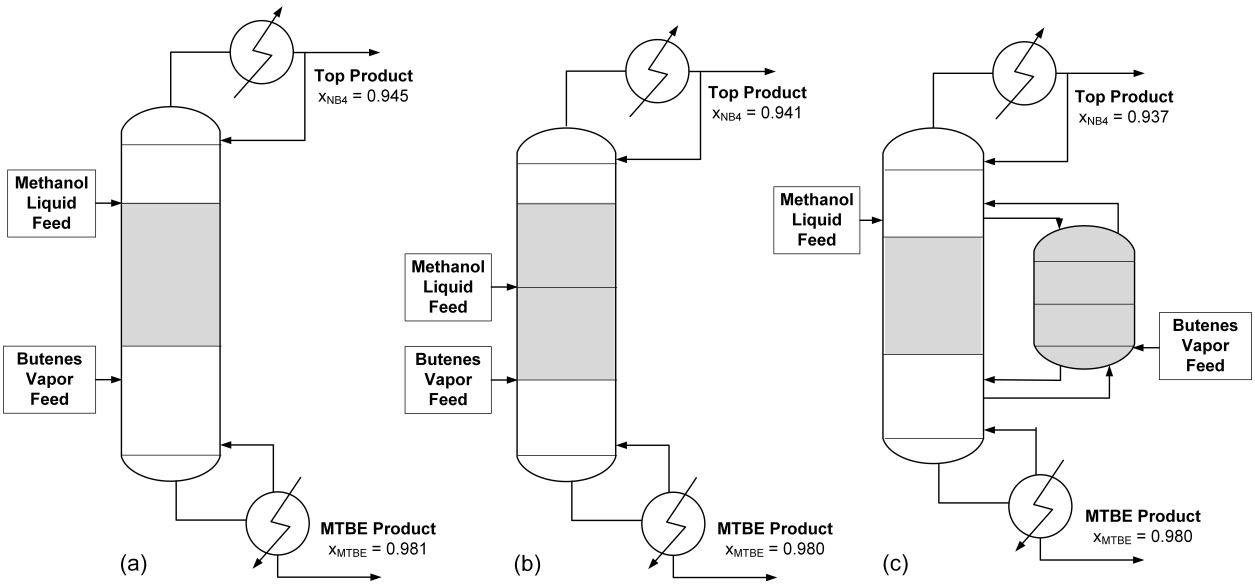


Figure 8.7: MTBE production – Equipment-based flowsheet alternatives
(a) Nominal Design, (b) Operable Design 1, (c) Operable Design 2 (Reprinted from [208]).

Table 8.2: MTBE production – GMF synthesis and Aspen validation (Reprinted from [208]).

| | Nominal Design | | Operable Design 1 | | Operable Design 2 | |
|---|---|---|---|---|---|---|
| | GMF | Aspen | GMF | Aspen | GMF | Aspen |
| Column pressure (atm) | 5.46 | 6.00 | 7.85 | 7.95 | 9.48 | 8.20 |
| Reflux ratio | 1.70 | 2.10 | 1.70 | 2.50 | 1.70 | 3.30 |
| Reboiler duty (MW) | 7.5 | 6.6 | 8.4 | 9.6 | 8.9 | 20 |
| Condenser duty (MW) | 23 | 22 | 23 | 24 | 23 | 34 |
| Module/Tray Number | 7 | 15 | 6 | 13 | 6 | 10+3* |
| Product flowrate (mol/s) | 197.0 | 197.0 | 197.0 | 197.0 | 197.0 | 197.0 |
| Product purity (mol/mol) | 0.98 | 0.98 | 0.98 | 0.98 | 0.98 | 0.98 |

* Main column: 10 trays, Side column: 3 trays

### 8.4.2 Dynamic analysis and model-based control optimization

In this step, we take the above derived reactive distillations systems to dynamic analysis, design, and control optimization. Simultaneous design and control is performed to close the loop for the proposed framework to ensure economical and smooth operation despite the influence of uncertainty and disturbances.

#### *8.4.2.1 High fidelity dynamic modeling*

High fidelity dynamic models for the above three MTBE reactive distillation (RD) processes (Fig. 8.7) are developed in gPROMS ModelBuilder®. The basis of this dynamic model has been validated with experimental data and open literature data in previous works for different reactive distillation systems, e.g., MTBE production [189], ethyl acetate production [210, 211]. Some key features of this generalized RD model, which enables its prediction accuracy and representation capability for design optimization, are listed as follow:

- a superstructure model formulation to enable the selection of the number of trays and feed tray location via integer variables (Fig. C.1)

- dynamic material and energy balances for each tray, reboiler, and condenser
- the consideration of liquid and vapor, material and energy holdups
- the consideration of liquid hydraulics and liquid level on each tray using modified Francis weir formulation
- the consideration of phase equilibrium or non-equilibrium behavior by adjusting Murphree tray efficiencies. For this MTBE RD column, full phase equilibrium is assumed (i.e. Murphree efficiency is 1)
- equations for the pressure drop from tray to tray correlated with the vapor flow through the openings at the bottom of each tray and the hydrostatic pressure on each tray
- detailed calculation of flooding and entrainment correlations and evaluation of minimum allowable column diameter
- to accurately capture the highly nonideal MTBE reactive mixture behavior such as potential formation of reactive azeotrope, the UNIQUAC and SRK models are utilized to describe the liquid-vapor equilibrium together with the use of rigorous kinetic rate expressions (Eq. 6.17) to calculate reaction extent. The thermodynamic binary interaction parameters and reaction kinetic parameters are adapted from [187], which have been well-validated in open literature for the MTBE reactive distillation systems.

For brevity, the detailed model formulation can be found in Appendix C with relevant nomenclature. This high-fidelity modeling step takes place in PSE gPROMS® ModelBuilder. Physical properties (e.g., activity/fugacity coefficients, enthalpy, saturated pressure) are calculated using the MultiFlash thermodynamic package which is integrated with gPROMS®.

The major design and operating parameters of the three reactive distillation systems for dynamic modeling and simulation are given in Table 8.3. Note that since rate-based reaction kinetic calculation is utilized in the high fidelity dynamic models to reflect the actual kinetic-controlled

characteristics in MTBE reactive distillation, more column trays are reported in Table 8.3 comparing to the design results obtained from Aspen Plus® assuming physical and chemical equilibrium (Table 8.2). The model statistics are presented in Table 8.4.

Table 8.3: MTBE production – Design parameters for dynamic simulation (Reprinted from [208]).

| | Nominal Design | Operable Design 1 | Operable Design 2 |
|---|---|---|---|
| Number of stages | 17 | 15 | 11 (main)<br>3 (side) |
| Reactive stages | 4-11 | 4-11 | 2-6 (main)<br>1-3 (side) |
| Pressure (atm) | 6 | 7.9 | 8.2 |
| Reflux ratio | 2.11 | 2.75 | 4 |
| Reboiler duty (MW) | 6.84 | 11.4 | 20.0 |
| Condenser duty (MW) | 21.8 | 25.4 | 33.9 |
| MTBE purity | 0.98 | 0.98 | 0.98 |
| Product flowrate (mol/s) | 197 | 197 | 197 |

Table 8.4: MTBE production – Model statistics for dynamic modeling.

| | Nominal Design | Operable Design 1 | Operable Design 2 |
|---|---|---|---|
| Modeling equations | 1098 | 962 | 900 |
| Initial conditions | 60 | 52 | 48 |
| Algebraic variables | 1038 | 910 | 852 |
| Differential variables | 60 | 52 | 48 |

#### *8.4.2.2 Open-loop analysis with operability and safety considerations*

In this step, we perform open-loop analysis to verify if the dynamic RD systems can sustain their desired level of operability and safety as promised by steady-state design (Chapter 6.4.4).

*Risk analysis for inherent safety performance*

The model-based risk analysis is incorporated in the dynamic models to calculate process risk values as "inherent safety indicators". Since the risk reduction is specified on a comparative basis, for simplicity we define a scaled measurement value as "Risk Ratio". As a base case, the Nominal Design has a Risk Ratio of 1. Thereby the Risk Ratios of Operable Designs 1 and 2 are expected to be around 0.8 for consistency with the inherent safety promises given by steady-state synthesis with safety considerations (i.e., reducing at least 20% of process risk). The actual Risk Ratios calculated from dynamic simulation are 0.91 and 0.81 respectively for Operable Designs 1 and 2. Both of the designs are inherent safer with respect to Nominal Design, although Design 1 not fully achieving the desired inherent safety level. However, since the identification and translation of equipment-based steady-state/dynamic RD designs from phenomena-based synthesis are based on trial-and-error attempts, we will later incorporate risk calculation in dynamic optimization to maintain process risks at the desired level.

*Flexibility analysis for operation under uncertainty*

Regarding flexibility considerations, steady-state Nominal Design is not flexible over the uncertainty range of methanol feed flowrate (i.e. 205.5 mol/s - 225.5 mol/s), while Design 1 and 2 are derived based on the flexibility test. To check flexibility at this dynamic stage, the feasible regions of the three reactive distillation systems are depicted in Figs. 8.8. In addition to the uncertainty range, the above RD systems are also analyzed with respect to a disturbance in the IB4 inlet composition, which will be introduced later for control investigations.

As can be seen, Nominal Design cannot operate over the entire range of uncertainty or disturbances while Operable Designs 1 and 2 do provide much better operability performance, which is consistent with the results obtained via steady-state operability analysis. Since Nominal Design

has been proved to be not operable in presence of uncertainty and disturbances, the following steps for control design and optimization only consider Operable Designs 1 and 2.

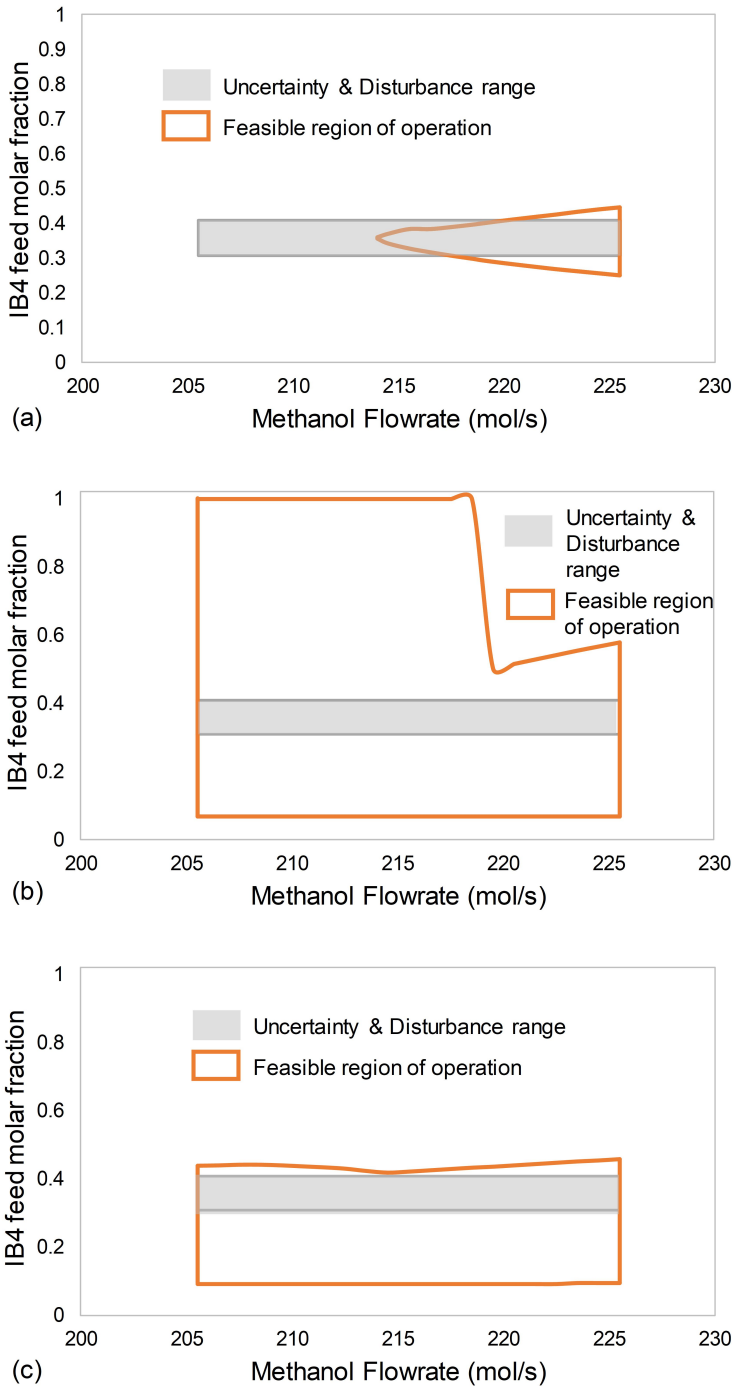


Figure 8.8: MTBE production – Feasible operation region
(a) Nominal Design, (b) Operable Design 1, (c) Operable Design 2 (Reprinted from [208]).

#### *8.4.2.3 mp-MPC controller design*

Herein, we develop explicit/multi-parametric model predictive control (mp-MPC) strategies for Operable Designs 1 and 2 following the PAROC (PARametric Optimisation and Control) framework (see Appendix D for more detail), which enables to derive explicit closed loop strategies that maintain stable and operable conditions in the presence of process disturbances.

For the control problem setting up, two sets of disturbances exist during system operation (for both Operable Designs 1 and 2): (i) a disturbance in the methanol liquid feed flowrate, and (ii) a disturbance in the IB4 inlet composition. The butenes feed flowrate is utilized as the manipulated variable and the MTBE molar composition in the bottom product is treated as the control variable with a desired set point of 98 mol%. Thus both Operable Designs 1 and 2 are single input single output (SISO) systems.

*(A) Model approximation*

The high-fidelity model of the reactive distillation systems (Appendix C), even though it accurately captures the process dynamics, it is challenging to be integrated within a dynamic optimization formulation due to its complexity. In this work, the MATLAB System Identification Toolbox® is utilized to for model approximation using random input-output sets. The general structure of the approximated linear state-space model is presented in Eq. 8.1:

$$\overline{x}_{k+1} = A\overline{x}_k + Bu_k + Cd_k \tag{8.1a}$$

$$y_k = D\overline{x}_k \tag{8.1b}$$

where the matrices $A, B, C, D$ define the state-space model, the index $k$ denotes the current time instant, while $\overline{x}$ is the vector of identified states (pseudo-states which do not provide physical meanings due to the model reduction), $u$ is the vector of manipulated variable, $y$ represents the vector of control variables, and $d$ is the vector of disturbances ($Y$ and $De$ will also be included respectively as binary structural variables and design variables if for design-aware controller design).

The physical meanings for each type of variables are explained in Table 8.5 which are applicable to Operable Design 1 and 2.

Table 8.5: MTBE production – Types of variables for controller design (Reprinted from [67]).

| **Symbol** | **Definition** | **Variables** | **Physical description** |
|---|---|---|---|
| $x(t)$ | Differential states | $M_{i,k},\ i = 1, ..., NC$ $k = 1, ..., N$ | Molar holdups |
| $y(t)$ | Control variables | $x_{MTBE}^{product}$ | MTBE composition in product |
| | | $V_1$ | Vapor flowrate from Tray 1 (for monitoring) |
| $u(t)$ | Manipulated variables | $F_{feed}^{vap}$ | Vapor feed flowrate |
| $d(t)$ | Disturbances | $F_{feed}^{liq}$ | Liquid feed flowrate |
| | | $x_{feed,IB4}$ | IB4 composition in liquid feed |
| $Y$ | Binary variables | $yf_{feed,k},\ k = 1, ..., N$ | Feed tray structure |
| | | $yr_k,\ k = 1, ..., N$ | Reflux tray structure |
| $De$ | Design variables | $D_{col}$ | Column diameter |
| | | $Catalyst_k,\ k = 1, ..., N$ | Catalyst load |

The resulting discrete linear state-space model for Operable Design 1 and 2 are respectively given in what follows:

*Operable Design 1*

A discretization step, $T_s = 10s$, is selected. The discretized approximate model consists of 6 identified states. The parameter matrices are:

$$A = \begin{bmatrix} 0.9898 & 0.0084 & -0.0499 & 0.0024 & 0.0362 & -0.1017 \\ -0.0668 & 0.8165 & 0.0670 & 0.0848 & 0.0179 & -0.0244 \\ 0.1875 & -0.0313 & 0.6780 & -0.1176 & 0.1388 & -1.0977 \\ 0.0229 & 0.4052 & -0.1391 & 0.4649 & -0.4364 & 1.9624 \\ 0.0159 & -0.0877 & 0.1333 & -0.1057 & 0.3208 & 0.4096 \\ -0.0001 & 0.0219 & 0.0457 & -0.0426 & -0.4609 & -0.6961 \end{bmatrix}$$

$$B = \begin{bmatrix} 0.0005 \\ 0.0058 \\ -0.0023 \\ -0.0336 \\ -0.0098 \\ -0.0025 \end{bmatrix} \qquad C = \begin{bmatrix} 0.0006 & 0.3367 \\ -0.0044 & 4.4020 \\ 0.0096 & -4.4309 \\ 0.0233 & -27.3449 \\ 0.0123 & -11.7250 \\ 0.0114 & -5.7239 \end{bmatrix} \tag{8.2}$$

$$D = \begin{bmatrix} 0.3025 & -0.0015 & -0.0079 & 0.0005 & 0.0007 & -0.0002 \\ -83.0519 & 585.6174 & 100.1365 & 57.3670 & 6.1853 & -0.4021 \end{bmatrix}$$

*Operable Design 2*

The discretization step is also selected as $T_s = 10s$. The discretized approximate model consists of 2 identified states with the following parameter matrices:

$$A = \begin{bmatrix} 0.9587 & -0.0001 \\ 0.0009 & 0.9581 \end{bmatrix} \qquad B = \begin{bmatrix} 37.8345 \\ 233.4201 \end{bmatrix}$$
$$C = \begin{bmatrix} 158.6232 & -85.3915 \\ 0.4062 & -0.0658 \end{bmatrix} \qquad D = \begin{bmatrix} 0.4062 & -0.0658 \end{bmatrix} \tag{8.3}$$

*(B) Explicit Model Predictive Controller design*

In deriving mp-MPC schemes, the objective is to express the optimal control actions as explicit functions of the parameters of the system. A general MPC problem for setpoint tracking and/or disturbance rejection can be described by Eq. 8.4, where $QR_k$, $R_k$ are the weights of the controller, $P$ is derived from the solution of the discrete time Riccati equation, $OH$ and $CH$ are the output and control horizons respectively and $\epsilon$ takes into account the mismatch between the process and the developed approximate model. More detail on the methodology and mathematical background in deriving MPC control actions via multi-parametric programming can be found in Appendix D.

$$\begin{aligned} \min_{u} \quad & J = x_N^T P x_N + \textstyle\sum_{k=1}^{OH-1} \left( (y_k - y_k^R)^T Q R_k \left( y_k - y_k^R \right) \right) \\ & \qquad + \textstyle\sum_{k=0}^{CH-1} \left( u_k - u_k^R \right)^T R_k \left( u_k - u_k^R \right) \\ \text{s.t.} \quad & x_{k+1} = A x_k + B u_k + C d_k \\ & y_k = D x_k + \epsilon \\ & \underline{x} \leq x_k \leq \overline{x}, \qquad \underline{u} \leq u_k \leq \overline{u}, \qquad \underline{y} \leq y_k \leq \overline{y} \end{aligned} \tag{8.4}$$

In the case of Operable Design 1 and 2, the different types of variables involved in controller design are shown in Table 8.5. The explicit model predictive control strategy is constructed based on the approximated model presented in Eq. 8.1. As far as the selection of the controlled and manipulated variables is concerned, the manipulation of butene vapor feed flowrate showed to have the most influence in the process behavior to steer the operation of the column to the desired setpoint. It should be noted that the relationships between the manipulated and the controlled variables were complex due to the nonlinearities that exist in the problem formulation. The identification of these variables was achieved by imposing input step changes to the process and examining which of these have the most impact to the desired output. The control objective is to achieve a bottom MTBE molar fraction of 98 mol$\%$. In addition, to account for the restriction of the boil up flowrate $V_b$ by the column diameter $D_{col}$, the following constraint is imposed in the control problem formulation:

$$0.04V_b \leq D_{col}^2 \tag{8.5}$$

Table 8.6 include the controller tuning parameters for Operable Design 1 and 2. The resulting mp-MPC problem is solved in the Parametric OPtimization (POP) Toolbox using the Graph Algorithm [212]. The optimal map of solutions for Operable Design 1 includes 17 critical regions described by the corresponding active sets, and 126 critical regions for Operable Design 2.

*(C) Closed-loop validation of mp-MPC control*

The closed-loop performance of the above derived mp-MPC controllers against the original high fidelity model is validated as shown in Figs. 8.9-8.11. In the case that the controller performances are not satisfying operational expectations, the model approximation step needs to be re-performed to generate better reduced order models as well as to re-design the mp-MPC controller.

Table 8.6: MTBE production – Tuning parameters for mp-MPC (Reprinted from [208]).

| **MPC parameters** | **Design 1** | **Design 2** |
|---|---|---|
| $OH$ | 2 | 4 |
| $CH$ | 1 | 3 |
| $QR$ | 5E6 | 1E5 |
| $R$ | 1E5 | 1E5 |
| $u_{min}$ | 490 | 490 |
| $u_{max}$ | 750 | 750 |
| $y_{min}$ | $[0 \quad 0]^T$ | $[0 \quad 0]^T$ |
| $y_{max}$ | $[1 \quad 1600]^T$ | $[1 \quad 1600]^T$ |
| $d_{min}$ | $[205.5 \quad 0.3]^T$ | $[205.5 \quad 0.3]^T$ |
| $d_{max}$ | $[235.5 \quad 0.4078]^T$ | $[235.5 \quad 0.4078]^T$ |

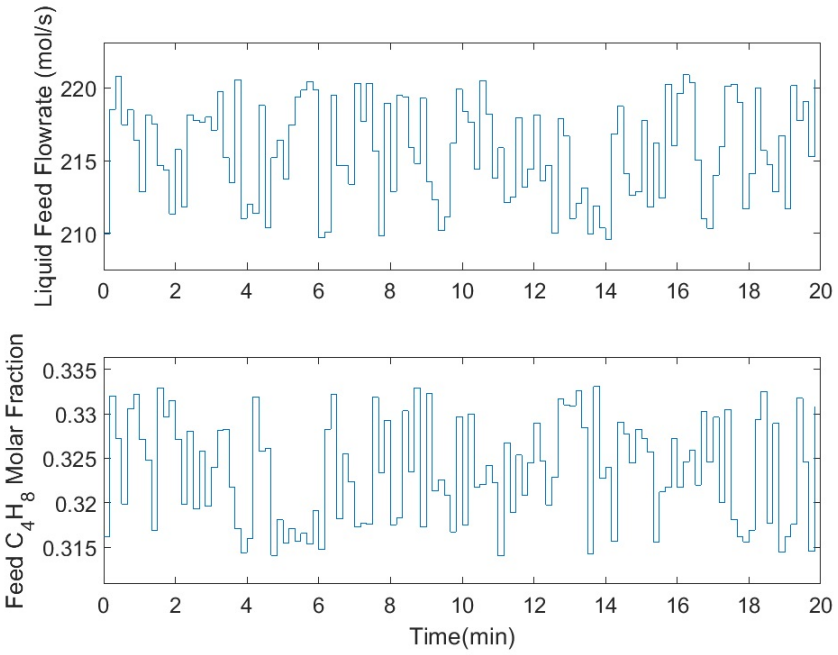


Figure 8.9: Disturbance profile for closed loop validation (Reprinted from [67]).

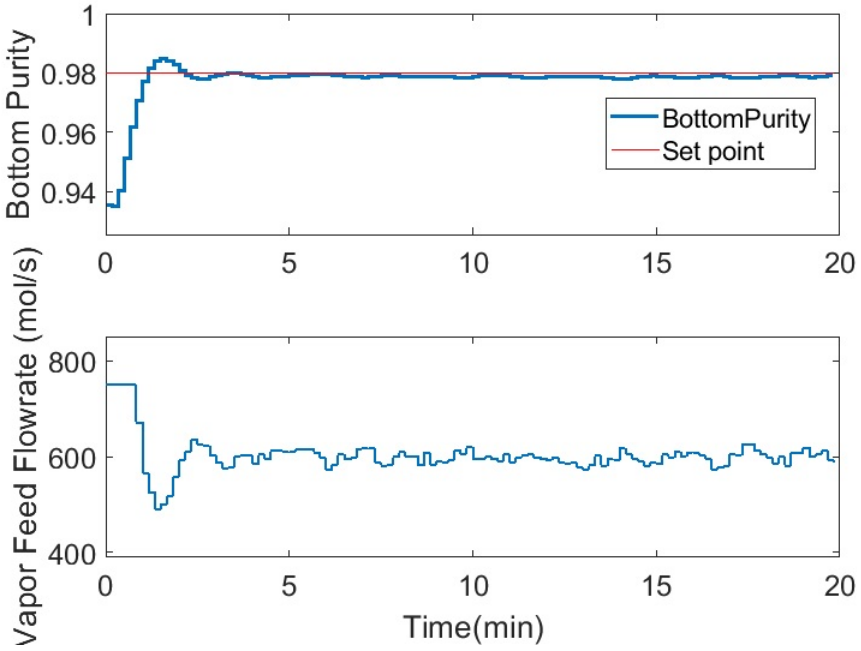


Figure 8.10: Operable Design 1 – Controller output and input profiles (Reprinted from [67]).

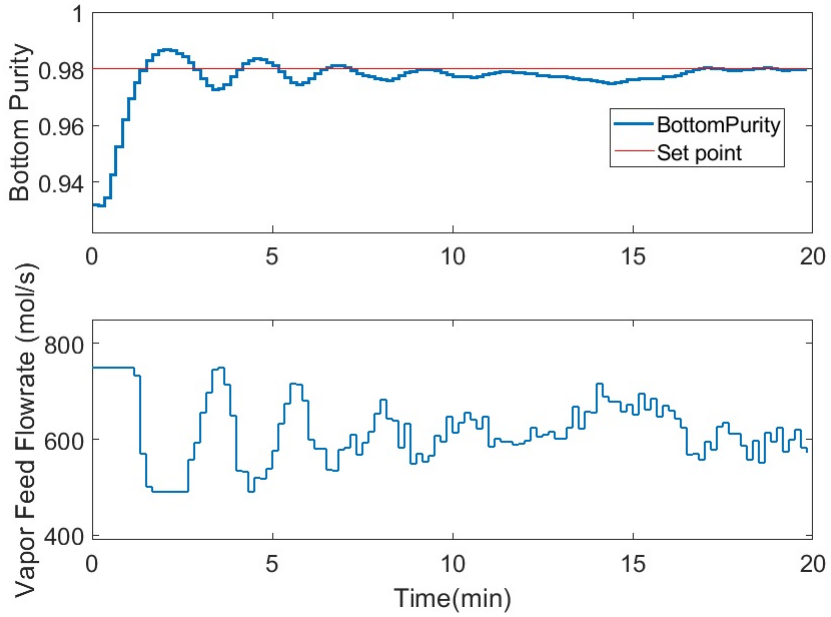


Figure 8.11: Operable Design 2 – Controller output and input profiles (Reprinted from [67]).

#### *8.4.2.4 Simultaneous design and control optimization*

A mixed-integer dynamic optimization (MIDO) problem is formulated to integrate design, control and operational components, the solution of which allows us to derive explicit closed loop strategies that maintain economic, stable, and operable conditions in the presence of disturbances.

The MIDO formulation is introduced to PSE gPROMS® as shown in Eq. 8.6. The optimization objective is given by Eq. 8.6a to minimize total annual cost as calculated in Bansal et al. [196]. Eqs. 8.6b and 8.6c describes the high fidelity model given in Appendix C. Eq. 8.6d integrates the derived explicit control actions. Eq. 8.6e defines the parameter space from multi-parametric programming point of view, which comprises state variables, output variables, desired output setpoints, design variables, disturbances, and manipulated variables. The variable bounds are given in Eqs. 8.6f-8.6h. Eq. 8.6i defines $Y$ as binary variables.

$$\min_{Y,De} F = \int_0^{\tau} Annualized\,Cost(x, y, u, Y, d, De)dt \tag{8.6a}$$

$$\text{s.t. } \frac{dx}{dt} = f(x, y, u, Y, d, De) \tag{8.6b}$$

$$y = h(x, u_c, Y, d, De) \tag{8.6c}$$

$$u_T = K_i\theta_T + r_i,\ \theta_T \in CR^i = \{CR_i^A\theta \leq CR_i^b\} \tag{8.6d}$$

$$\theta_T = [x_T, y_T, y_T^{sp}, Y, d_T, De, u_{T-1}] \tag{8.6e}$$

$$\underline{y} \leq y \leq \overline{y} \tag{8.6f}$$

$$\begin{bmatrix} \underline{x}^T & \underline{d}^T \end{bmatrix}^T \leq \begin{bmatrix} x^T & d^T \end{bmatrix}^T \leq \begin{bmatrix} \overline{x^T} & \overline{d^T} \end{bmatrix}^T \tag{8.6g}$$

$$\underline{De} \leq De \leq \overline{De} \tag{8.6h}$$

$$Y \in \{0, 1\}^q \tag{8.6i}$$

The mp-MPC integrated dynamic optimization results are summarized in Table 8.7. Also note that the Risk Ratio of both designs are kept under 80% of the Nominal Design, thus consistent with the steady-state synthesis operability and safety promises.

Table 8.7: MTBE production – Simultaneous design and control (Reprinted from [67]).

| | Operable Design 1 | Operable Design 2 |
|---|---|---|
| Column Diameter (m) | 2.0 | 2.3 |
| Number of Trays* | 13 | 9 (main)<br>3 (side) |
| Feed Tray Location 1 | 10 | 3 (side) |
| Feed Tray Location 2 | 7 | 3 (main) |
| Catalyst Mass (ton) | 4.4 | 6.5 |
| Column Cost ($\times 10^6 \$/yr$) | 0.042 | 0.090 |
| Catalyst Cost ($\times 10^6 \$/yr$) | 0.076 | 0.113 |
| Operating Cost ($\times 10^6 \$/yr$) | 2.290 | 3.397 |
| Total Annual Cost ($\times 10^6 \$/yr$) | 2.408 | 3.601 |
| Risk Ratio | 0.79 | 0.78 |

* Condenser and reboiler are not counted within the number of trays

### 8.4.3 Verifiable and operable intensified designs for MTBE production

Up to this stage, two designs (Fig. 8.12) have been obtained for the MTBE production task. The trade-offs between their cost, operability, safety, and control performances have been thoroughly investigated and can be used to assist further decision making, as shown in Table 8.7.

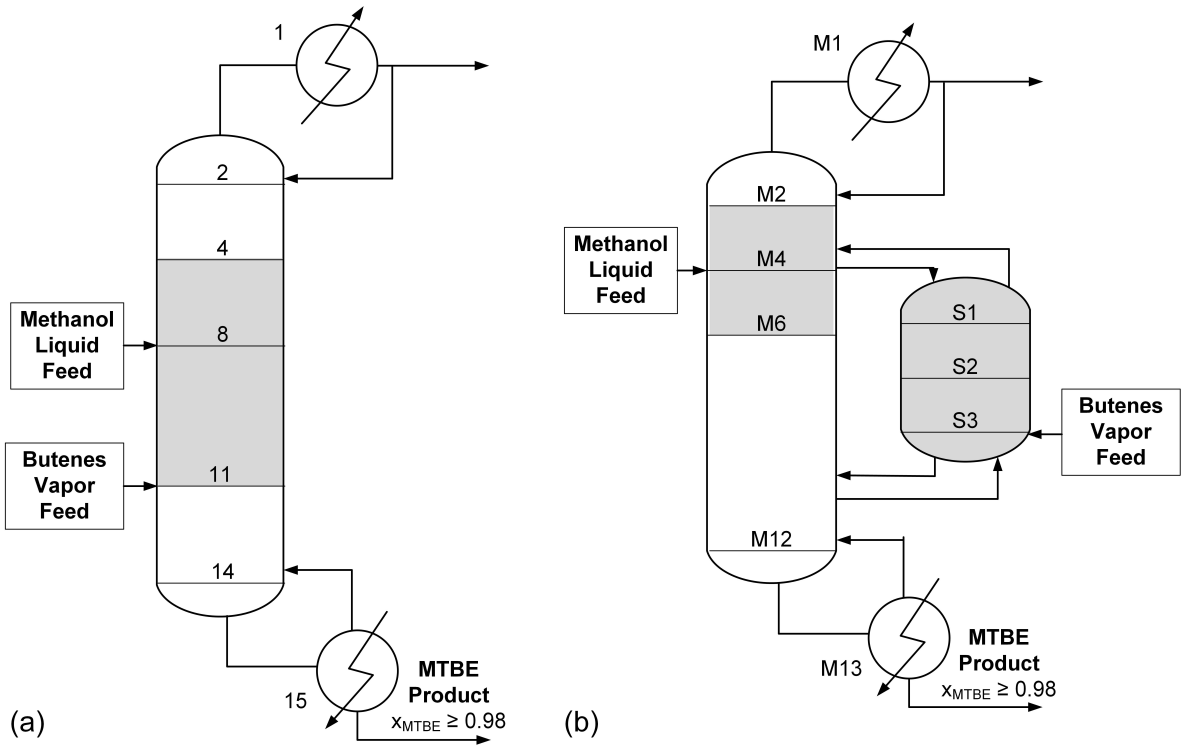


Figure 8.12: MTBE production – Operable and intensified reactive distillation systems (a) Design 1, (b) Design 2 (Reprinted from [67]).

## 8.5 Summary

In this chapter, we have proposed a systematic framework to deliver validated operable intensification designs, which features: (i) phenomena-based process synthesis using GMF to give the intensified design configurations, (ii) steady-state operability analysis, including flexibility test to accommodate uncertainty and quantitative risk analysis to account for inherent safety, and (iii) simultaneous design and control with advanced multi-parametric model-based predictive control (mp-MPC) scheme following the PAROC (PARametric Optimization and Control) framework to close the loop for the synthesis of operable process intensification systems. Two case studies – (i) heat exchanger network synthesis and (ii) MTBE reactive separation – have been presented to demonstrate the proposed framework as proof of concept.

# 9. CONCLUSIONS

## 9.1 Summary and thesis contributions

In this thesis, we have proposed a novel integrated framework towards the synthesis of operable process intensification systems. These methods and tools can be used systematically for PI design and operational analysis, which feature the following components on:

**Generalized Modular Representation Framework for process intensification synthesis**

The Generalized Modular Representation Framework, introduced in Chapter 2, is extended and applied towards systematic process intensification and innovation. Different with conventional process synthesis approaches requiring pre-postulation of unit operations which may hinder the discovery of novel process solutions, GMF utilizes two types of phenomena-based modular building blocks (i.e., a pure heat exchange module and a mass/heat exchange module) to represent chemical processes. Mathematically it is formulated as a single mixed-integer nonlinear optimization problem. The GMF Gibbs free energy-based driving force constraints theoretically empower the intensification of process systems towards the "ultimate" performance bounds identified by thermodynamics. We have demonstrated GMF for: (i) identifying envelope of design solutions in reaction/separation systems (Chapter 3), (ii) process design and intensification of an industrial dividing wall column for methyl methacrylate purification (Chapter 4), and (iii) simultaneous process synthesis, intensification, and material selection in water/ethanol extractive separation systems (Chapter 5). Significant cost and/or energy savings have been reported with GMF design solutions.

**Steady-state intensification synthesis with model-based operability and safety metrics**

Once the optimal intensified designs are obtained, the next question is how to ensure their operability and safety performance at the early design stage. To this purpose, an integrated GMF-flexibility-safety synthesis approach is proposed to systematically deliver optimal intensified designs with guaranteed operability and safety performances (Chapter 6). Flexibility analysis is utilized to identify the critical operating conditions and results in a multiperiod GMF synthesis

formulation to generate new process solution(s) with guaranteed feasibility under the expected uncertainty range (e.g., in feed flowrate or compositions). Risk analysis for inherent safety considerations is also integrated with GMF synthesis as model constraints by linking the risk calculation with available design and operation information at phenomena level (e.g., inventory, temperature).

**A systematic framework for synthesis of operable process intensification systems**

The tight interaction between design and operating parameters in modular and intensified systems emphasizes the need for a holistic strategy to fully integrate PI design, operability analysis, and control optimization at early design stage (Chapter 7). To address this challenge, we propose a systematic framework for the synthesis of operable process intensification systems leveraging GMF for PI synthesis, model-based flexibility test, inherent safety analysis, and simultaneous design and control optimization (Chapter 8). The PAROC (PARametric Optimisation and Control) framework is applied to optimize process design with optimal explicit/multi-parametric model predictive control actions, thus closing the loop for PI design at dynamic operating conditions under disturbances. The proposed framework has been demonstrated on: (i) a heat exchanger network synthesis case study for thermal intensification, and (ii) a methyl tert-butyl ether production case study. Multiple process designs are systematically generated with different structures due to the cost and operability trade-offs.

The key contributions of this work are summarized as follows:

- A process intensification synthesis approach is developed based on the Generalized Modular Representation Framework for the innovation, design, optimization, and benchmark of chemical process systems, under a unified phenomena-based representation. GMF has been demonstrated in a number of intensified reaction and/or separation systems, contributing to significant energy and cost savings.

- A unified formulation is derived for GMF driving force constraints which can systematically characterize reaction and/or separation tasks based on the total Gibbs free energy change. This offers the advantages of: (i) providing a fundamental view on how to exploit the syn-

ergy of reaction and separation, (ii) intensifying process mass/heat transfer performance towards ultimate thermodynamic limits, and (iii) reducing computational load with the resulting compact physical representation strategy.

- A systematic approach is developed to integrate GMF synthesis with model-based operability metrics, which can generate optimal process solutions with guaranteed flexibility and safety performance, instead of sequential or posterior operational analysis after design. The incorporation of operability considerations into phenomena-based design (e.g., GMF) has been demonstrated to identify more versatile and promising process solutions leveraging the enriched PI design space.

- A holistic framework is proposed to deliver optimal and operable PI systems which systematically and consistently addresses steady-state and dynamic design and operation in intensified systems. It follows an integrated step-wise procedure to synergize steady-state synthesis, operability analysis, and dynamic operational optimization and to generate multiple process solutions with different levels of operability performance for decision making.

## 9.2 Suggestions for future research directions

### Towards a prototype software for synthesis of operable process intensification systems*

Despite the accelerated development and application of computer-aided tools, the currently available commercial software tools, mostly for process modeling, simulation, and optimization, fail to meet the demands of discovering innovative and intensified process solutions with new unit operations as they require equipment or flowsheet configurations pre-specified by users. Tools for process operability, safety, and control analysis are also lacking at this conceptual design stage, whereas there are long-standing concerns on the operational performances of the resulting intensified alternatives. Thus, a prototype software platform to integrate these design, synthesis, and operability fronts will substantially benefit the deployment of novel PI technologies.

*Based on Vedant, S., Atencio, M. R., Tian, Y., Meduri, V., Pistikopoulos, E. N. Towards a Software Prototype for Synthesis of Operable Process Intensification Systems. 31st European Symposium on Computer Aided Process Engineering (ESCAPE-31); 2021. Accepted.

Based on the PI framework proposed in this work, an integrated prototype software is under development as illustrated in Fig. 9.1, which features a number of distinct tools on:

- Graphical User Interface (GUI) – which is designed to facilitate user navigation and data communication between the following prototype functionalities
- PI Synthesis Suite – which systematically generates promising PI configurations
- PI Simulation Suite – which translates and analyzes the PI synthesis results to corresponding equipment-based process alternatives
- PI Operability and Control Suite – which leverages the model-based operability metrics and model-based control to ensure PI operational performance under varying conditions
- PI Model Library – which provides a collection of consistent and high-fidelity steady-state and dynamic models for intensified process systems

It is worth highlighting that these tools can be used by the users flexibly in an independent manner for targeted equipment or flowsheet intensification and analysis. They can also be applied in an integrated manner – for example, the integration of operability and safety metrics in the modular process synthesis is one of the key strengths of this novel software system.

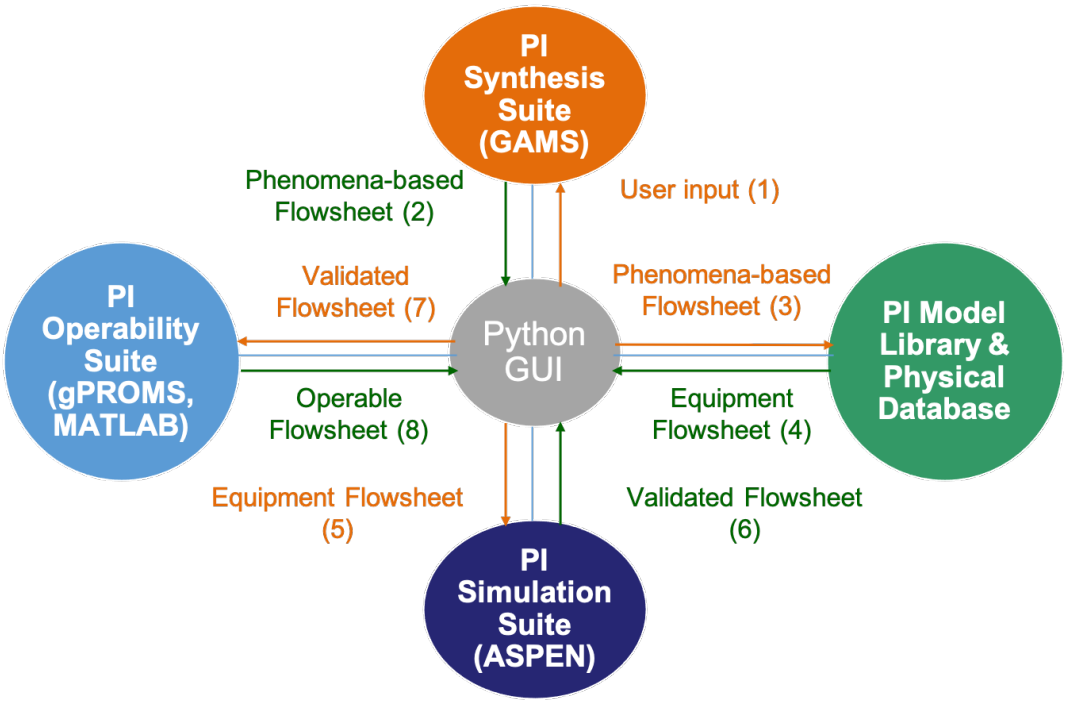


Figure 9.1: Information flow chart for the software prototype platform.

**A novel process intensification synthesis framework for multi-scale reaction systems**[†]

The conceptual design of chemical reactors, especially micro-reactors, normally depends on first-principle modeling with detailed mass/heat transport descriptions for specific reactor types and catalysts. However, a systematic approach to generate intensified and optimal reaction systems by simultaneously taking into consideration multi-scale reactor options is still lacking. Key open questions include: (i) how to capture micro-reactors via process synthesis representation? (ii) how to capture meso- and micro- reaction systems under a unified synthesis approach? and (iii) what type of minimum process input information is needed to differentiate multi-scale reactors?

GMF can be extended to address these challenges for the synthesis of multi-scale reaction systems using modular building blocks (Fig. 9.2). To account for the miniaturization effects in micro-reactors, diffusion and transport rates can be incorporated into the driving force constraints. These rate terms will be activated or de-activated based on the values of Damkohler number which dictate the choice of micro- or meso- reactor size. Spatial distribution information within GMF modules can be extracted via orthogonal collocation in a physically compact and computationally efficient manner. The impact of catalyst on reactor design can also be investigated via hybrid modeling which integrates first-principle reactor synthesis model with data-driven model for catalyst properties. Methane steam reforming for hydrogen production serves as a good case study to compare the performance of a multi-functional micro-reactor versus a conventional reactor.

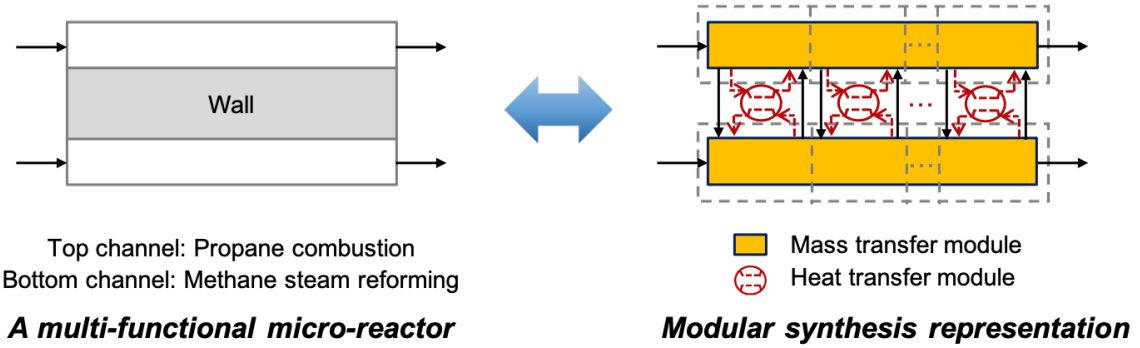


Figure 9.2: GMF representation for multi-functional micro-reactors.

[†]Based on Tian, Y., Vlachos, D. G., Pistikopoulos, E. N. Generalized Modular/Collocation Framework for Representation and Synthesis of Intensified Multi-Scale Reaction Systems. AIChE Annual Meeting, November 2020.

**A dynamic trajectory optimization approach for sustainable PI process development**

A chemical process can be designed by optimizing its operation trajectory to attain the best possible performance in temporal space. The key research questions to synergize process inherent dynamics and dynamic/periodic operation include: (i) what is the fundamental reason to improve process efficiency and sustainability by introducing dynamic/periodicity? (ii) how to define the optimal dynamic operation trajectory? (iii) how to develop a trajectory optimization approach with tractable computational load?

The driving force concepts can be extended to address these challenges for dynamic process intensification. Taking a CSTR reactor as example, introducing dynamic states may offer better reaction productivity than steady-state operation by overcoming reaction equilibrium. Thus, analogous to the Gibbs free energy-based driving force constraints in GMF, a model-based metric can be developed to determine the perturbation strategy by identifying attainable productivity or efficiency limits in a real-time manner. Life cycle assessment can also be integrated as an indicator for environmental impacts. The actual operation trajectory can be obtained via a multi-objective optimization problem considering: (i) maximizing process efficiency, (ii) minimizing environmental impacts, and (iii) constraints for operational feasibility. The dynamic trajectory optimization approach can also be extended for pressure swing adsorption systems to define the optimal periodic operation strategy, and the batch to continuous processing transition via trajectory mapping.

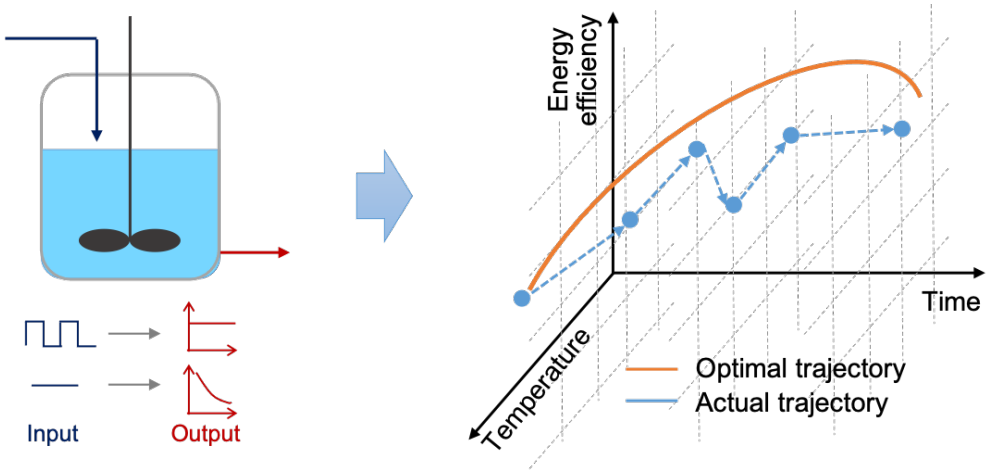


Figure 9.3: Dynamic trajectory optimization for reactor systems via periodic perturbation.

**Conceptual design of modular processing systems with enhanced operational flexibility and multi-functionality**

Modular design and processing feature the paradigm shift from "the economy of scale" towards the "economy of numbers" of smaller, more flexible, and more agile plants. For many intensified technologies (e.g., micro-reactors, membrane reactors) which inherently function the most effectively at smaller scales, the combination of PI technologies with modular design may provide an encouraging synergistic process solution. However, modular design options have not yet been considered at conceptual design stage to evaluate if and how modularization can bring in economic and/or operational benefits in tandem with intensification.

In light of this, we discuss how to extend GMF for the design of modular processing systems with operational considerations. The key question is how to simultaneously generate the optimal modular process design structure while determining the optimal operational modes for each unit for the time periods under consideration subject to process uncertainties, market demand changes, etc. In this context, the modular network should be designed in a dynamic manner via the multi-period synthesis formulation to fully exploit the operational flexibility. Leveraging the inherently modularized GMF building blocks, the modules can be operated in parallel (or in stack) as shown in Fig. 9.4a. However, certain modules can be turned up or turned down during operation (Fig. 9.4b). The connections between modules can also be flexibly switched from producing a single product (Fig. 9.4a) to multiple products (Fig. 9.4c). Moreover, each mass/heat exchange module can be used for different functionalities such as separation, reaction, or reactive separation (Fig. 9.4d). The ammonia production plant provides a good case study to to explore the benefits of modular processing and to quantify the trade-off between module sizing, profitability, environmental impacts, and operational flexibility under the following scenarios: (i) market capacity changes, (ii) multiple product demands, and (iii) co-production for ammonia and methanol.

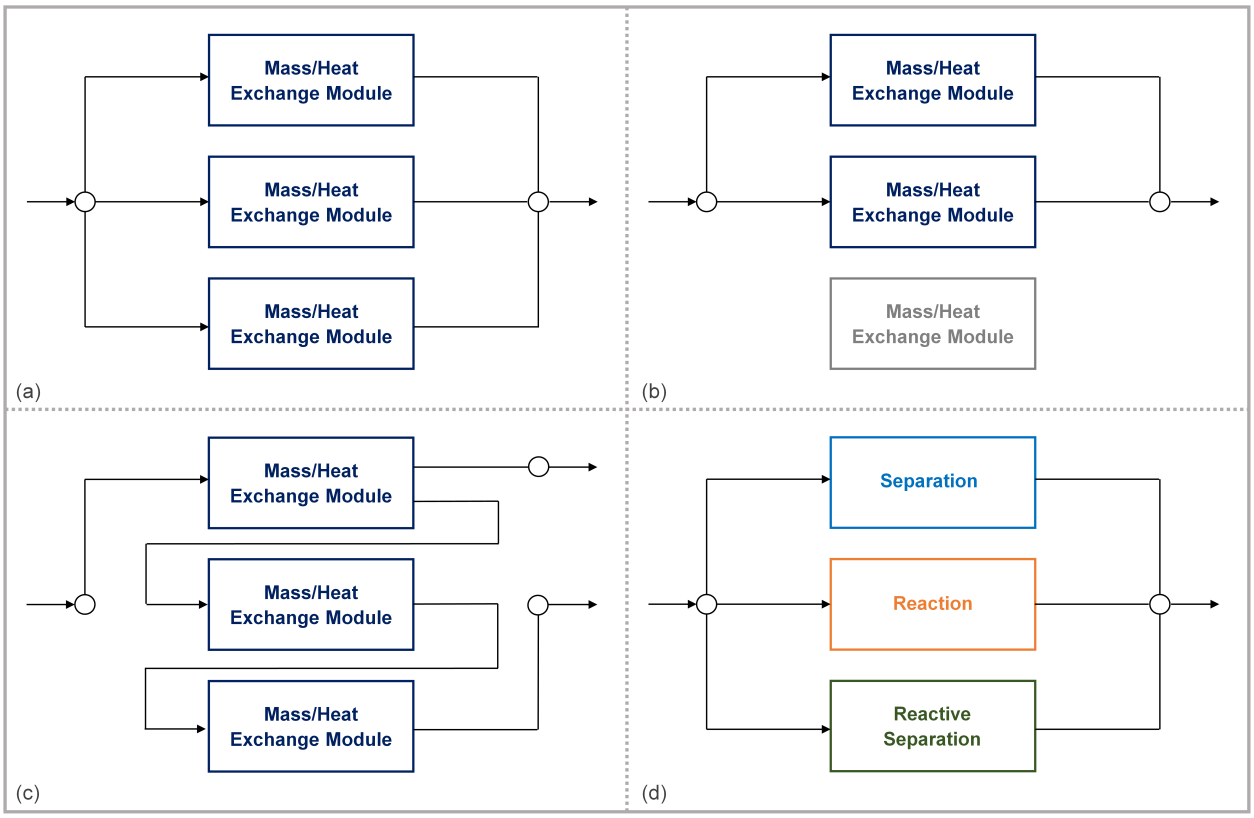


Figure 9.4: Conceptual modular design via GMF –
(a) Parallel operation, (b) Flexibility for turning up/down modules,
(c) Design for multiple products, (d) Modules with multi-functionality.

LIST OF PUBLICATIONS AND PRESENTATIONS

**Forthcoming book:**

1. **Tian, Y.**, Pistikopoulos, E. N. Synthesis and Operability Strategies for Computer-Aided Modular Process Intensification. *Elsevier*, To appear in 2021.

**Journal publications:**

1. **Tian, Y.**, Meduri, V., Bindlish, R., Pistikopoulos, E. N. A Process Intensification Synthesis Framework for Dividing Wall Column Systems. *Computers & Chemical Engineering*. Under review.

2. **Tian, Y.**, Pistikopoulos, E. N. A Process Intensification Framework for Extractive Separation Systems with Material Selection. *Journal of Advanced Manufacturing and Processing*. Accepted.

3. Pistikopoulos, E. N., **Tian, Y.**, Bindlish, R. Operability and Control in Process Intensification and Modular Design: Challenges and Opportunities. *AIChE Journal*. *67(5)*, e17204, 2021.

4. **Tian, Y.***, Pappas, I.*, Burnak, B., Katz, J., Pistikopoulos, E. N. Simultaneous Design & Control of a Reactive Distillation System – A Parametric Optimization & Control Approach. *Chemical Engineering Science*. *230*, 116232, 2021. (*equal contribution)

5. **Tian, Y.**, Pistikopoulos, E. N. Towards an Envelope of Design Solutions for Combined/ Intensified Reaction/Separation Systems. *Industrial & Engineering Chemistry Research*, *59(24)*, 11350–11354, 2020.

6. **Tian, Y.**, Pappas, I., Burnak, B., Katz, J., Pistikopoulos, E. N. A Systematic Framework for Synthesis of Operable Process Intensification Systems – Reactive Separation, *Computers & Chemical Engineering*, *134*, 106675, 2020.

7. Avraamidou, S., Baratsas, S., **Tian, Y.**, Pistikopoulos, E. N. Circular Economy – A Challenge and an Opportunity for Process Systems Engineering. *Computers & Chemical Engineering*, *133*, 106629, 2020.

8. **Tian, Y.**, Pistikopoulos, E. N. Synthesis of Operable Process Intensification Systems – Steady-State Design with Safety and Operability Considerations. *Industrial & Engineering Chemistry Research*, *58(15)*, 6049-6068, 2019.

9. **Tian, Y.**, Pistikopoulos, E. N. Synthesis of Operable Process Intensification Systems: Advances and Challenges. *Current Opinion in Chemical Engineering*, *25*, 101-107, 2019.

10. **Tian, Y.**, Demirel, S. E., Hasan, M. M. F., Pistikopoulos, E. N. An Overview of Process Systems Engineering Approaches for Process Intensification: State of the Art. *Chemical Engineering and Processing: Process Intensification*, *133*, 160-210, 2018.

11. Niziolek, A. M., Onel, O., **Tian, Y.**, Floudas, C. A., Pistikopoulos, E. N. Municipal Solid Waste to Liquid Transportation Fuels – Part III: An Optimization-Based Nationwide Supply Chain Management Framework. *Computers & Chemical Engineering*, *116*, 468-487, 2018.

**Conference proceedings:**

1. Vedant, S., Atencio, M. R., **Tian, Y.**, Meduri, V., Pistikopoulos, E. N. Towards a Software Prototype for Synthesis of Operable Process Intensification Systems. 31st European Symposium on Computer Aided Process Engineering (ESCAPE-31); 2021. Accepted.

2. **Tian, Y.**, Pistikopoulos, E. N. Operability and Safety Considerations in Process Intensification. 21st International Federation of Automatic Control (IFAC) World Congress, July 2020. In *IFAC-PapersOnLine*, 53(2), 11434-11439.

3. **Tian, Y.**, Pistikopoulos, E. N. Generalized Modular Representation Framework for the Synthesis of Extractive Separation Systems. Foundations of Computer-Aided Process Design

(FOCAPD 2019), July 2019, Copper Mountain, Colorado. In *Computer Aided Chemical Engineering*, *47*, 475-480. Elsevier.

4. **Tian, Y.**, Pappas, I. S., Burnak, B., Katz, J., Avraamidou, S., Diangelakis, N. A., Pistikopoulos, E. N. Towards a Systematic Framework for the Synthesis of Operable Process Intensification Systems – Application to Reactive Distillation Systems. 29th European Symposium on Computer-Aided Process Engineering (ESCAPE-29), June 2019, Eindhoven, Neitherlands. In *Computer Aided Chemical Engineering*, *46*, 73-78.

5. **Tian, Y.**, Mannan, M. S.; Pistikopoulos, E. N. Towards a Systematic Framework for the Synthesis of Operable Process Intensification Systems. 13th International Symposium on Process Systems Engineering (PSE 2018), July 2018, San Diego, California. In *Computer Aided Chemical Engineering*, *44*, 2383-2388. Elsevier

6. **Tian, Y.**, Mannan, M. S., Kravanja, Z., Pistikopoulos, E. N. Towards the Synthesis of Process Intensification Systems with Safety and Operability Considerations – Application to Heat Exchanger Network. 28th European Symposium on Computer-Aided Process Engineering (ESCAPE-28), June 2018, Graz, Austria. In *Computer Aided Chemical Engineering*, *43*, 705-710. Elsevier.

**Conference presentations:**

1. **Tian, Y.**, Pistikopoulos, E. N. A Framework for Synthesis of Operable Process Intensification Systems. AIChE Annual Meeting, November 2020.

2. **Tian, Y.**, Vlachos, D. G., Pistikopoulos, E. N. Generalized Modular/Collocation Framework for Representation and Synthesis of Intensified Multi-Scale Reaction Systems. AIChE Annual Meeting, November 2020.

3. **Tian, Y.**, Meduri, V., Vedant, S., Bindlish, R., Pistikopoulos, E. N. Process Design and Intensification of Dividing Wall Column for an Industrial Methyl Methacrylate Separation Process. AIChE Annual Meeting, November 2020.

4. **Tian, Y.**, Pistikopoulos, E. N. Material Selection in Process Intensification – Application to Extractive Separation Systems. AIChE Spring Meeting, August 2020.

5. **Tian, Y.**, Pappas, I. S., Burnak, B., Katz, J., Pistikopoulos, E. N. Process Intensification Framework for Reactive Separation Systems. AIChE Annual Meeting, November 2019, Orlando, Florida.

6. **Tian, Y.**, Pappas, I. S., Avraamidou, S., Pistikopoulos, E. N. A Modular Approach to Process Integration and Intensification. AIChE Annual Meeting, November 2019, Orlando, Florida.

7. **Tian, Y.**, Pappas, I. S., Avraamidou, S., Pistikopoulos, E. N. Process Intensification Framework for Extractive Separation Systems. AIChE Annual Meeting, November 2019, Orlando, Florida.

8. **Tian, Y.**, Pappas, I. S., Katz, J., Burnak, B., Pistikopoulos, E. N. Towards the Incorporation of Operability and Safety in the Synthesis of Intensified Reactive Separation Systems. AIChE Spring Meeting, April 2019, New Orleans, Louisiana.

9. **Tian, Y.**, Mannan, M. S., Pistikopoulos, E. N. Towards a Systematic Process Intensification Framework for Advanced Distillation Systems. AIChE Annual Meeting, October 2018, Pittsburgh, Pennsylvania.

# REFERENCES


[1] IEA, "Tracking industry 2020," *https://www.iea.org/reports/tracking-industry-2020*, Accessed June 9, 2021.

[2] BP, "BP energy outlook 2020," *https://www.bp.com/en/global/corporate/energy-economics/energy-outlook.html*, Accessed June 9, 2021.

[3] A. I. Stankiewicz and J. A. Moulijn, "Process intensification: Transforming chemical engineering," *Chemical engineering progress*, vol. 96, no. 1, pp. 22–34, 2000.

[4] D. Reay, C. Ramshaw, and A. Harvey, *Process Intensification: Engineering for efficiency, sustainability and flexibility*. Oxford: Butterworth-Heinemann, 2013.

[5] F. J. Keil, "Process intensification," *Reviews in Chemical Engineering*, vol. 34, no. 2, pp. 135–200, 2018.

[6] C. D. Demirhan, W. W. Tso, G. S. Ogumerem, and E. N. Pistikopoulos, "Energy systems engineering – A guided tour," *BMC Chemical Engineering*, vol. 1, no. 1, p. 11, 2019.

[7] M. Baldea, T. F. Edgar, B. L. Stanley, and A. A. Kiss, "Modular manufacturing processes: Status, challenges, and opportunities," *AIChE journal*, vol. 63, no. 10, pp. 4262–4272, 2017.

[8] S. Avraamidou, S. G. Baratsas, Y. Tian, and E. N. Pistikopoulos, "Circular economy – A challenge and an opportunity for process systems engineering," *Computers & Chemical Engineering*, vol. 133, p. 106629, 2020.

[9] C. Ramshaw, "HIGEE distillation – An example of process intensification," *Chemical Engineer*, pp. 13–14, 1983.

[10] Y. Tian, S. E. Demirel, M. F. Hasan, and E. N. Pistikopoulos, "An overview of process systems engineering approaches for process intensification: State of the art," *Chemical Engineering and Processing - Process Intensification*, vol. 133, pp. 160–210, 2018.

[11] J. A. Arizmendi-Sánchez and P. Sharratt, "Phenomena-based modularisation of chemical process models to approach intensive options," *Chemical Engineering Journal*, vol. 135, no. 1-2, pp. 83–94, 2008.

[12] S. Becht, R. Franke, A. Geißelmann, and H. Hahn, "An industrial view of process intensification," *Chemical Engineering and Processing - Process Intensification*, vol. 48, no. 1, pp. 329–332, 2009.

[13] T. Van Gerven and A. Stankiewicz, "Structure, energy, synergy, time – The fundamentals of process intensification," *Industrial & Engineering Chemistry Research*, vol. 48, no. 5, pp. 2465–2474, 2009.

[14] P. Lutze, R. Gani, and J. M. Woodley, "Process intensification: A perspective on process synthesis," *Chemical Engineering and Processing - Process Intensification*, vol. 49, no. 6, pp. 547–558, 2010.

[15] J. M. Ponce-Ortega, M. M. Al-Thubaiti, and M. M. El-Halwagi, "Process intensification: New understanding and systematic approach," *Chemical Engineering and Processing - Process Intensification*, vol. 53, pp. 63–75, 2012.

[16] C. S. Pereira and B. A. Patel, "The role of process intensification in addressing the dual energy challenge," *Chemical Engineering and Processing - Process Intensification*, vol. 142, p. 107545, 2019.

[17] C. M. Masuku and L. T. Biegler, "Recent advances in gas-to-liquids process intensification with emphasis on reactive distillation," *Current Opinion in Chemical Engineering*, vol. 25, pp. 95–100, 2019.

[18] J. L. Stephen and B. Periyasamy, "Innovative developments in biofuels production from organic waste materials: A review," *Fuel*, vol. 214, pp. 623–633, 2018.

[19] V. G. Gude and E. Martinez-Guerra, "Green chemistry with process intensification for sustainable biodiesel production," *Environmental chemistry letters*, vol. 16, no. 2, pp. 327–341, 2018.

[20] A. Adamu, F. Russo-Abegão, and K. Boodhoo, "Process intensification technologies for $CO_2$ capture and conversion – A review," *BMC Chemical Engineering*, vol. 2, no. 1, pp. 1–18, 2020.

[21] A. K. Tula, M. R. Eden, and R. Gani, "Computer–aided process intensification: Challenges, trends and opportunities," *AIChE Journal*, vol. 66, no. 1, 2019.

[22] Y. Tian and E. N. Pistikopoulos, "Synthesis of operable process intensification systems: Advances and challenges," *Current Opinion in Chemical Engineering*, vol. 25, pp. 101–107, 2019.

[23] S. E. Demirel, J. Li, and M. F. Hasan, "Systematic process intensification," *Current Opinion in Chemical Engineering*, vol. 25, pp. 108–113, 2019.

[24] M. Skiborowski, "Process synthesis and design methods for process intensification," *Current opinion in chemical engineering*, vol. 22, pp. 216–225, 2018.

[25] S. Sitter, Q. Chen, and I. E. Grossmann, "An overview of process intensification methods," *Current Opinion in Chemical Engineering*, vol. 25, pp. 87–94, 2019.

[26] M. Baldea and T. F. Edgar, "Dynamic process intensification," *Current opinion in chemical engineering*, vol. 22, pp. 48–53, 2018.

[27] P. Daoutidis, A. Allman, S. Khatib, M. A. Moharir, M. J. Palys, D. B. Pourkargar, and W. Tang, "Distributed decision making for intensified process systems," *Current Opinion in Chemical Engineering*, vol. 25, pp. 75–81, 2019.

[28] L. S. Dias and M. G. Ierapetritou, "Optimal operation and control of intensified processes – Challenges and opportunities," *Current Opinion in Chemical Engineering*, vol. 25, pp. 82–86, 2019.

[29] E. N. Pistikopoulos, Y. Tian, and R. Bindlish, "Operability and control in process intensification and modular design: Challenges and opportunities," *AIChE Journal*, p. e17204, 2021.

[30] J. A. Weinfeld, S. A. Owens, and R. B. Eldridge, "Reactive dividing wall columns: A comprehensive review," *Chemical Engineering and Processing - Process Intensification*, vol. 123, pp. 20–33, 2018.

[31] T. Coward, H. Tribe, and A. P. Harvey, "Opportunities for process intensification in the UK water industry: A review," *Journal of Water Process Engineering*, vol. 21, pp. 116–126, 2018.

[32] M. Baldea, T. F. Edgar, B. L. Stanley, and A. A. Kiss, "Modularization in chemical processing," *Chemical Engineering Progress*, vol. 114, no. 3, pp. 46–54, 2018.

[33] P. L. Suryawanshi, S. P. Gumfekar, B. A. Bhanvase, S. H. Sonawane, and M. S. Pimplapure, "A review on microreactors: Reactor fabrication, design, and cutting-edge applications," *Chemical Engineering Science*, vol. 189, pp. 431–448, 2018.

[34] A. A. Kiss, M. Jobson, and X. Gao, "Reactive distillation: Stepping up to the next level of process intensification," *Industrial & Engineering Chemistry Research*, vol. 58, no. 15, pp. 5909–5918, 2018.

[35] J. Bielenberg and I. Palou-Rivera, "The RAPID Manufacturing Institute – Reenergizing US efforts in process intensification and modular chemical processing," *Chemical Engineering and Processing - Process Intensification*, 2019.

[36] R. Aglave, J. Lusty, and J. Nixon, "Using simulation and digitalization for modular process intensification," *Chemical Engineering Progress*, vol. 115, no. 3, pp. 45–49, 2019.

[37] Z. Jiang and R. Agrawal, "Process intensification in multicomponent distillation: A review of recent advancements," *Chemical Engineering Research and Design*, vol. 147, pp. 122–145, 2019.

[38] A. I. Stankiewicz and P. Yan, "110th anniversary: The missing link unearthed: Materials and process intensification," *Industrial & Engineering Chemistry Research*, vol. 58, no. 22, pp. 9212–9222, 2019.

[39] V. Gazzaneo, J. C. Carrasco, D. R. Vinson, and F. V. Lima, "Process operability algorithms: Past, present, and future developments," *Industrial & Engineering Chemistry Research*, vol. 59, no. 6, pp. 2457–2470, 2019.

[40] S. Cremaschi, "A perspective on process synthesis: Challenges and prospects," *Computers & Chemical Engineering*, vol. 81, pp. 130–137, 2015.

[41] Q. Chen and I. Grossmann, "Recent developments and challenges in optimization-based process synthesis," *Annual review of chemical and biomolecular engineering*, vol. 8, pp. 249–283, 2017.

[42] A. Mitsos, N. Asprion, C. A. Floudas, M. Bortz, M. Baldea, D. Bonvin, A. Caspari, and P. Schäfer, "Challenges in process optimization for new feedstocks and energy sources," *Computers & Chemical Engineering*, vol. 113, pp. 209–221, 2018.

[43] H. Kuhlmann and M. Skiborowski, "Optimization-based approach to process synthesis for process intensification: General approach and application to ethanol dehydration," *Industrial & Engineering Chemistry Research*, vol. 56, no. 45, pp. 13461–13481, 2017.

[44] H. Kuhlmann, H. Veith, M. Moller, K.-P. Nguye, A. Gorak, and M. Skiborowski, "Optimization-based approach to process synthesis for process intensification: Synthesis of reaction-separation processes," *Industrial & Engineering Chemistry Research*, vol. 57, no. 10, pp. 3639–3655, 2017.

[45] Y. Tian, M. S. Mannan, Z. Kravanja, and E. N. Pistikopoulos, "Towards the synthesis of modular process intensification systems with safety and operability considerations – Application to heat exchanger network," in *Computer Aided Chemical Engineering*, vol. 43, pp. 705–710, Elsevier, 2018.

[46] N. M. Kaiser, R. J. Flassig, and K. Sundmacher, "Probabilistic reactor design in the framework of elementary process functions," *Computers & Chemical Engineering*, vol. 94, pp. 45–59, 2016.

[47] N. M. Kaiser, R. J. Flassig, and K. Sundmacher, "Reactor-network synthesis via flux profile analysis," *Chemical Engineering Journal*, vol. 335, pp. 1018–1030, 2018.

[48] Y. Tian and E. N. Pistikopoulos, "Synthesis of operable process intensification systems – Steady-state design with safety and operability considerations," *Industrial & Engineering Chemistry Research*, vol. 58, no. 15, pp. 6049–6068, 2018.

[49] D. K. Babi, J. Holtbruegge, P. Lutze, A. Gorak, J. M. Woodley, and R. Gani, "Sustainable process synthesis–intensification," *Computers & Chemical Engineering*, vol. 81, pp. 218–244, 2015.

[50] A. K. Tula, D. K. Babi, J. Bottlaender, M. R. Eden, and R. Gani, "A computer-aided software-tool for sustainable process synthesis-intensification," *Computers & Chemical Engineering*, vol. 105, pp. 74–95, 2017.

[51] P. Pichardo and V. I. Manousiouthakis, "Infinite dimensional state-space as a systematic process intensification tool: Energetic intensification of hydrogen production," *Chemical Engineering Research and Design*, vol. 120, pp. 372–395, 2017.

[52] F. E. da Cruz and V. I. Manousiouthakis, "Process intensification of reactive separator networks through the ideas conceptual framework," *Computers & Chemical Engineering*, vol. 105, pp. 39–55, 2017.

[53] S. E. Demirel, J. Li, and M. F. Hasan, "Systematic process intensification using building blocks," *Computers & Chemical Engineering*, vol. 105, pp. 2–38, 2017.

[54] J. Li, S. E. Demirel, and M. F. Hasan, "Process synthesis using block superstructure with automated flowsheet generation and optimization," *AIChE Journal*, vol. 64, no. 8, pp. 3082–3100, 2018.

[55] S. Kalakul, L. Zhang, H. A. Choudhury, N. O. Elbashir, M. R. Eden, and R. Gani, "ProCAPD – A computer-aided model-based tool for chemical product design and analysis," in *Computer Aided Chemical Engineering*, vol. 44, pp. 469–474, Elsevier, 2018.

[56] T. Liu, E. L. First, M. F. Hasan, and C. A. Floudas, "A multi-scale approach for the discovery of zeolites for hydrogen sulfide removal," *Computers & Chemical Engineering*, vol. 91, pp. 206–218, 2016.

[57] A. Arora, S. S. Iyer, and M. F. Hasan, "GRAMS: A general framework describing adsorption, reaction and sorption-enhanced reaction processes," *Chemical Engineering Science*, vol. 192, pp. 335–358, 2018.

[58] F. Boukouvala, M. F. Hasan, and C. A. Floudas, "Global optimization of general constrained grey-box models: New method and its application to constrained PDEs for pressure swing adsorption," *Journal of Global Optimization*, vol. 67, no. 1-2, pp. 3–42, 2017.

[59] C. Tsay, R. C. Pattison, and M. Baldea, "A pseudo-transient optimization framework for periodic processes: Pressure swing adsorption and simulated moving bed chromatography," *AIChE Journal*, vol. 64, no. 8, pp. 2982–2996, 2018.

[60] N. M. Nikačević, A. E. Huesman, P. M. Van den Hof, and A. I. Stankiewicz, "Opportunities and challenges for process control in process intensification," *Chemical Engineering and Processing - Process Intensification*, vol. 52, pp. 1–15, 2012.

[61] M. Baldea, "From process integration to process intensification," *Computers & Chemical Engineering*, vol. 81, pp. 104–114, 2015.

[62] M. Ellis, H. Durand, and P. D. Christofides, "A tutorial review of economic model predictive control methods," *Journal of Process Control*, vol. 24, no. 8, pp. 1156–1178, 2014.

[63] D. Q. Mayne, "Model predictive control: Recent developments and future promise," *Automatica*, vol. 50, no. 12, pp. 2967–2986, 2014.

[64] E. N. Pistikopoulos, N. A. Diangelakis, R. Oberdieck, M. M. Papathanasiou, I. Nascu, and M. Sun, "PAROC – An integrated framework and software platform for the optimisation and advanced model-based control of process systems," *Chemical Engineering Science*, vol. 136, pp. 115–138, 2015.

[65] H. Khajuria and E. N. Pistikopoulos, "Optimization and control of pressure swing adsorption processes under uncertainty," *AIChE Journal*, vol. 59, no. 1, pp. 120–131, 2013.

[66] M. M. Papathanasiou, S. Avraamidou, R. Oberdieck, A. Mantalaris, F. Steinebach, M. Morbidelli, T. Mueller-Spaeth, and E. N. Pistikopoulos, "Advanced control strategies for the multicolumn countercurrent solvent gradient purification process," *AIChE Journal*, vol. 62, no. 7, pp. 2341–2357, 2016.

[67] Y. Tian, I. Pappas, B. Burnak, J. Katz, and E. N. Pistikopoulos, "Simultaneous design & control of a reactive distillation system – A parametric optimization & control approach," *Chemical Engineering Science*, p. 116232, 2020.

[68] C. Georgakis, D. Uztürk, S. Subramanian, and D. R. Vinson, "On the operability of continuous processes," *Control Engineering Practice*, vol. 11, no. 8, pp. 859–869, 2003.

[69] J. C. Carrasco and F. V. Lima, "An optimization-based operability framework for process design and intensification of modular natural gas utilization systems," *Computers & Chemical Engineering*, vol. 105, pp. 246–258, 2017.

[70] J. C. Carrasco and F. V. Lima, "Bilevel and parallel programing-based operability approaches for process intensification and modularity," *AIChE Journal*, vol. 64, no. 8, pp. 3042–3054, 2018.

[71] C.-T. Chang and V. S. K. Adi, *Deterministic Flexibility Analysis: Theory, Design, and Applications*. CRC Press, 2017.

[72] Q. Zhang, I. E. Grossmann, and R. M. Lima, "On the relation between flexibility analysis and robust optimization for linear systems," *AIChE Journal*, vol. 62, no. 9, pp. 3109–3123, 2016.

[73] A. Bhosekar and M. Ierapetritou, "Advances in surrogate based modeling, feasibility analysis and and optimization: A review," *Computers & Chemical Engineering*, vol. 108, pp. 250–267, 2017.

[74] D. Sudhoff, M. Leimbrink, M. Schleinitz, A. Górak, and P. Lutze, "Modelling, design and flexibility analysis of rotating packed beds for distillation," *Chemical Engineering Research and Design*, vol. 94, pp. 72–89, 2015.

[75] N. Medina-Herrera, I. E. Grossmann, M. S. Mannan, and A. Jiménez-Gutiérrez, "An approach for solvent selection in extractive distillation systems including safety considerations," *Industrial & Engineering Chemistry Research*, vol. 53, no. 30, pp. 12023–12031, 2014.

[76] N. Roy, F. Eljack, A. Jiménez-Gutiérrez, B. Zhang, P. Thiruvenkataswamy, M. El-Halwagi, and M. S. Mannan, "A review of safety indices for process design," *Current Opinion in Chemical Engineering*, vol. 14, pp. 42–48, 2016.

[77] A. P. Ortiz-Espinoza, A. Jiménez-Gutiérrez, and M. M. El-Halwagi, "Including inherent safety in the design of chemical processes," *Industrial & Engineering Chemistry Research*, vol. 56, no. 49, pp. 14507–14517, 2017.

[78] A. Nemet, J. J. Klemeš, I. Moon, and Z. Kravanja, "Safety analysis embedded in heat exchanger network synthesis," *Computers & Chemical Engineering*, vol. 107, pp. 357–380, 2017.

[79] F. Albalawi, H. Durand, and P. D. Christofides, "Process operational safety using model predictive control based on a process safeness index," *Computers & Chemical Engineering*, vol. 104, pp. 76–88, 2017.

[80] F. Albalawi, H. Durand, and P. D. Christofides, "Process operational safety via model predictive control: Recent results and future research directions," *Computers & Chemical Engineering*, vol. 114, pp. 171–190, 2018.

[81] K. P. Papalexandri and E. N. Pistikopoulos, "Generalized modular representation framework for process synthesis," *AIChE Journal*, vol. 42, no. 4, pp. 1010–1032, 1996.

[82] T. Lopez-Arenas, M. Sales-Cruz, R. Gani, and E. S. Pérez-Cisneros, "Thermodynamic analysis of the driving force approach: Reactive systems," *Computers & Chemical Engineering*, vol. 129, p. 106509, 2019.

[83] M. Feinberg and P. Ellison, "General kinetic bounds on productivity and selectivity in reactor-separator systems of arbitrary design: Principles," *Industrial & Engineering Chemistry Research*, vol. 40, no. 14, pp. 3181–3194, 2001.

[84] J. A. Frumkin and M. F. Doherty, "Target bounds on reaction selectivity via Feinberg's CFSTR equivalence principle," *AIChE Journal*, vol. 64, no. 3, pp. 926–939, 2018.

[85] A. Agarwal, L. T. Biegler, and S. E. Zitney, "A superstructure-based optimal synthesis of PSA cycles for post-combustion $CO_2$ capture," *AIChE journal*, vol. 56, no. 7, pp. 1813–1828, 2010.

[86] I. E. Grossmann and M. Morari, "Operability, resiliency, and flexibility: Process design objectives for a changing world," 1983.

[87] C.-T. Lin, "Structural controllability," *IEEE Transactions on Automatic Control*, vol. 19, no. 3, pp. 201–208, 1974.

[88] R. Gani, G. Hytoft, C. Jaksland, and A. K. Jensen, "An integrated computer aided system for integrated design of chemical processes," *Computers & Chemical Engineering*, vol. 21, no. 10, pp. 1135–1146, 1997.

[89] A. K. Tula, J. Wang, X. Chen, S. S. Mansouri, and R. Gani, "ProCACD: A computer-aided versatile tool for process control," *Computers & Chemical Engineering*, vol. 136, p. 106771, 2020.

[90] Z. Kravanja and I. E. Grossmann, "PROSYN – An MINLP process synthesizer," *Computers & Chemical Engineering*, vol. 14, no. 12, pp. 1363–1378, 1990.

[91] Q. Chen, S. Kale, J. Bates, R. Valentin, D. E. Bernal, M. Bynum, J. D. Siirola, and I. E. Grossmann, "Pyosyn: A collaborative ecosystem for process design advancement," *2019 AIChE Annual Meeting*, 2019.

[92] D. C. Miller, J. D. Siirola, D. Agarwal, A. P. Burgard, A. Lee, J. C. Eslick, B. Nicholson, C. Laird, L. T. Biegler, D. Bhattacharyya, *et al.*, "Next generation multi-scale process systems engineering framework," *Computer Aided Chemical Engineering*, vol. 44, pp. 2209–2214, 2018.

[93] P. Proios and E. N. Pistikopoulos, "Hybrid generalized modular/collocation framework for distillation column synthesis," *AIChE Journal*, vol. 52, no. 3, pp. 1038–1056, 2006.

[94] S. R. Ismail, P. Proios, and E. N. Pistikopoulos, "Modular synthesis framework for combined separation/reaction systems," *AIChE Journal*, vol. 47, no. 3, pp. 629–649, 2001.

[95] T. Y. Algusane, P. Proios, M. C. Georgiadis, and E. N. Pistikopoulos, "A framework for the synthesis of reactive absorption columns," *Chemical Engineering and Processing - Process Intensification*, vol. 45, no. 4, pp. 276–290, 2006.

[96] S. R. Ismail, E. N. Pistikopoulos, and K. P. Papalexandri, "Modular representation synthesis framework for homogeneous azeotropic separation," *AIChE Journal*, vol. 45, no. 8, pp. 1701–1720, 1999.

[97] P. Proios, N. F. Goula, and E. N. Pistikopoulos, "Generalized modular framework for the synthesis of heat integrated distillation column sequences," *Chemical Engineering Science*, vol. 60, no. 17, pp. 4678–4701, 2005.

[98] P. Seferlis and A. Hrymak, "Optimization of distillation units using collocation models," *AIChE Journal*, vol. 40, no. 5, pp. 813–825, 1994.

[99] W. E. Stewart, K. L. Levien, and M. Morari, "Simulation of fractionation by orthogonal collocation," *Chemical Engineering Science*, vol. 40, no. 3, pp. 409–421, 1985.

[100] C. A. Floudas, *Nonlinear and mixed-integer optimization: Fundamentals and applications*. Oxford University Press, 1995.

[101] E. M. L. Beale, "Integer programming," in *Computational Mathematical Programming* (K. Schittkowski, ed.), pp. 1–24, Springer Berlin Heidelberg, 1985.

[102] A. M. Geoffrion, "Generalized benders decomposition," *Journal of Optimization Theory and Applications*, vol. 10, no. 4, pp. 237–260, 1972.

[103] M. A. Duran and I. E. Grossmann, "An outer-approximation algorithm for a class of mixed-integer nonlinear programs," *Mathematical Programming*, vol. 36, no. 3, pp. 307–339, 1986.

[104] Y. Tian and E. N. Pistikopoulos, "Generalized modular representation framework for the synthesis of extractive separation systems," in *Computer Aided Chemical Engineering*, vol. 47, pp. 475–480, Elsevier, 2019.

[105] F. Horn, "Attainable and non-attainable regions in chemical reaction technique," in *Third European Symposium on Chemical Reaction Engineering*, pp. 1–10, Pergamon Press: London, 1964.

[106] D. Ming, D. Glasser, D. Hildebrandt, B. Glasser, and M. Metgzer, *Attainable Region Theory: An Introduction to Choosing an Optimal Reactor*. John Wiley & Sons, 2016.

[107] J. A. Frumkin, L. Fleitmann, and M. F. Doherty, "Ultimate reaction selectivity limits for intensified reactor–separators," *Industrial & Engineering Chemistry Research*, vol. 58, no. 15, pp. 6042–6048, 2018.

[108] J. A. Frumkin and M. F. Doherty, "Ultimate bounds on reaction selectivity for batch reactors," *Chemical Engineering Science*, vol. 199, pp. 652–660, 2019.

[109] Y. Tian and E. N. Pistikopoulos, "Towards an envelope of design solutions for combined/intensified reaction/separation systems," *Industrial & Engineering Chemistry Research*, vol. 59, no. 24, p. 11350–11354, 2020.

[110] Y. Tang and M. Feinberg, "Carnot-like limits to steady-state productivity," *Industrial & Engineering Chemistry Research*, vol. 46, no. 17, pp. 5624–5630, 2007.

[111] R. C. Reid, J. M. Prausnitz, and B. E. Poling, *The properties of gases and liquids*. McGraw Hill Book Co., New York, NY, 1987.

[112] M. J. Okasinski and M. F. Doherty, "Design method for kinetically controlled, staged reactive distillation columns," *Industrial & Engineering Chemistry Research*, vol. 37, no. 7, pp. 2821–2834, 1998.

[113] J. R. Jackson and I. E. Grossmann, "A disjunctive programming approach for the optimal design of reactive distillation columns," *Computers & Chemical Engineering*, vol. 25, no. 11-12, pp. 1661–1673, 2001.

[114] M. A. Al-Arfaj and W. L. Luyben, "Design and control of an olefin metathesis reactive distillation column," *Chemical Engineering Science*, vol. 57, no. 5, pp. 715–733, 2002.

[115] R. O. Wright, "Fractionation apparatus," May 24 1949. US Patent 2,471,134.

[116] F. B. Petlyuk, "Thermodynamically optimal method for separating multicomponent mixtures," *Int. Chem. Eng.*, vol. 5, pp. 555–561, 1965.

[117] G. Kaibel, "Distillation columns with vertical partitions," *Chemical Engineering & Technology*, vol. 10, no. 1, pp. 92–98, 1987.

[118] M. A. Schultz, D. G. Stewart, J. M. Harris, S. P. Rosenblum, and M. S. Shakur, "Reduce costs with dividing-wall columns," *Chemical engineering progress*, vol. 98, no. 5, pp. 64–71, 2002.

[119] I. Dejanović, L. Matijašević, and Ž. Olujić, "Dividing wall column – A breakthrough towards sustainable distilling," *Chemical Engineering and Processing - Process Intensification*, vol. 49, no. 6, pp. 559–580, 2010.

[120] R. Sargent and K. Gaminibandara, "Optimum design of plate distillation columns," in *Optimization Action. Conf. Proc.*, pp. 267–314, Acad. Press, 1976.

[121] J. A. Caballero and I. E. Grossmann, "Design of distillation sequences: From conventional to fully thermally coupled distillation systems," *Computers & Chemical Engineering*, vol. 28, no. 11, pp. 2307–2329, 2004.

[122] J. A. Caballero and I. E. Grossmann, "Optimal synthesis of thermally coupled distillation sequences using a novel MILP approach," *Computers & Chemical Engineering*, vol. 61, pp. 118–135, 2014.

[123] G. Dünnebier and C. C. Pantelides, "Optimal design of thermally coupled distillation columns," *Industrial & Engineering Chemistry Research*, vol. 38, no. 1, pp. 162–176, 1999.

[124] A. Underwood, "Fractional distillation of multicomponent mixtures," *Industrial & Engineering Chemistry*, vol. 41, no. 12, pp. 2844–2847, 1949.

[125] R. Agrawal, "Synthesis of distillation column configurations for a multicomponent separation," *Industrial & Engineering Chemistry Research*, vol. 35, no. 4, pp. 1059–1071, 1996.

[126] C. O. Okoli and T. A. Adams, "Design of dividing wall columns for butanol recovery in a thermochemical biomass to butanol process," *Chemical Engineering and Processing - Process Intensification*, vol. 95, pp. 302–316, 2015.

[127] E. S. Rawlings, Q. Chen, I. E. Grossmann, and J. A. Caballero, "Kaibel column: Modeling, optimization, and conceptual design of multi-product dividing wall columns," *Computers & Chemical Engineering*, vol. 125, pp. 31–39, 2019.

[128] T. Waltermann, S. Sibbing, and M. Skiborowski, "Optimization-based design of dividing wall columns with extended and multiple dividing walls for three-and four-product separations," *Chemical Engineering and Processing - Process Intensification*, vol. 146, p. 107688, 2019.

[129] P. Proios and E. N. Pistikopoulos, "Generalized modular framework for the representation and synthesis of complex distillation column sequences," *Industrial & Engineering Chemistry Research*, vol. 44, no. 13, pp. 4656–4675, 2005.

[130] U. Ali, K. J. B. A. Karim, and N. A. Buang, "A review of the properties and applications of poly (methyl methacrylate) (PMMA)," *Polymer Reviews*, vol. 55, no. 4, pp. 678–705, 2015.

[131] R. Wilczynski and J. Jerrick Juliette, "Methacrylic acid and derivatives," *Kirk-Othmer Encyclopedia of Chemical Technology, Wiley Online Library*, 2000.

[132] Y. C. Wu, C. Hsu, H.-P. Huang, and I.-L. Chien, "Design and control of a methyl methacrylate separation process with a middle decanter," *Industrial & Engineering Chemistry Research*, vol. 50, no. 8, pp. 4595–4607, 2011.

[133] W.-L. Chang and I.-L. Chien, "Energy-saving design and control of a methyl methacrylate separation process," *Industrial & Engineering Chemistry Research*, vol. 55, no. 11, pp. 3064–3074, 2016.

[134] Y. Bernardin, R. Billon, X. Marcarian, and F. Vallet, "Unit and process for purification of crude methyl methacrylate," Oct. 6 2020. US Patent 10,793,505.

[135] S. Li, S. Zhou, and M. Yu, "Process for purification of methyl methacrylate using molecular sieve membranes," Nov. 8 2016. US Patent 9,487,469.

[136] D. W. Jewell, J. G. Pendergast, W. G. Worley, *et al.*, "Process for purification of methyl methacrylate," Aug. 27 2019. US Patent 10,392,337.

[137] C. Bravo-Bravo, J. G. Segovia-Hernández, C. Gutiérrez-Antonio, A. L. Durán, A. Bonilla-Petriciolet, and A. Briones-Ramirez, "Extractive dividing wall column: Design and optimization," *Industrial & Engineering Chemistry Research*, vol. 49, no. 8, pp. 3672–3688, 2010.

[138] N. Ramirez-Corona, A. Jiménez-Gutiérrez, A. Castro-Agüero, and V. Rico-Ramírez, "Optimum design of petlyuk and divided-wall distillation systems using a shortcut model," *Chemical Engineering Research and Design*, vol. 88, no. 10, pp. 1405–1418, 2010.

[139] C. Gutiérrez-Antonio and A. Briones-Ramírez, "Multiobjective stochastic optimization of dividing-wall distillation columns using a surrogate model based on neural networks," *Chemical and biochemical engineering quarterly*, vol. 29, no. 4, pp. 491–504, 2015.

[140] L. Yan, P. M. Witt, T. F. Edgar, and M. Baldea, "Static and dynamic intensification of water–ethylene glycol separation using a dividing wall column," *Industrial & Engineering Chemistry Research*, vol. 60, no. 7, pp. 3027–3037, 2021.

[141] J. Gmehling, J. Menke, J. Krafczyk, and K. Fischer, *Azeotropic Data*. Wiley, 1994.

[142] The Dow Chemical Company, "The Dow Chemical Company sales specification on methyl methacrylate," 2018. Accessed June 9, 2021.

[143] W. G. Worley and S. W. Hoy IV, "Process for purification of methyl methacrylate," Nov. 26 2019. US Patent 10,487,038.

[144] I. Kumakiri, K. Hashimoto, Y. Nakagawa, Y. Inoue, Y. Kanehiro, K. Tanaka, and H. Kita, "Application of FAU zeolite membranes to alcohol/acrylate mixture systems," *Catalysis Today*, vol. 236, pp. 86–91, 2014.

[145] A. A. Kiss and C. S. Bildea, "A control perspective on process intensification in dividing-wall columns," *Chemical Engineering and Processing - Process Intensification*, vol. 50, no. 3, pp. 281–292, 2011.

[146] M. Serra, A. Espuna, and L. Puigjaner, "Control and optimization of the divided wall column," *Chemical Engineering and Processing - Process Intensification*, vol. 38, no. 4-6, pp. 549–562, 1999.

[147] E. Pistikopoulos, A. Barbosa-Povoa, J. H. Lee, R. Misener, A. Mitsos, G. Reklaitis, V. Venkatasubramanian, F. You, and R. Gani, "Process systems engineering – The generation next?," *Computers & Chemical Engineering*, p. 107252, 2021.

[148] A. S. Alshehri, R. Gani, and F. You, "Deep learning and knowledge-based methods for computer aided molecular design – Toward a unified approach: State-of-the-art and future directions," *arXiv preprint arXiv:2005.08968*, 2020.

[149] M. Hostrup, P. M. Harper, and R. Gani, "Design of environmentally benign processes: Integration of solvent design and separation process synthesis," *Computers & Chemical Engineering*, vol. 23, no. 10, pp. 1395–1414, 1999.

[150] A. I. Papadopoulos and P. Linke, "Multiobjective molecular design for integrated process-solvent systems synthesis," *AIChE journal*, vol. 52, no. 3, pp. 1057–1070, 2006.

[151] M. Folić, C. S. Adjiman, and E. N. Pistikopoulos, "Design of solvents for optimal reaction rate constants," *AIChE journal*, vol. 53, no. 5, pp. 1240–1256, 2007.

[152] P. Lek-utaiwan, B. Suphanit, P. L. Douglas, and N. Mongkolsiri, "Design of extractive distillation for the separation of close-boiling mixtures: Solvent selection and column optimization," *Computers & Chemical Engineering*, vol. 35, no. 6, pp. 1088–1100, 2011.

[153] D. Valencia-Marquez, A. Flores-Tlacuahuac, and R. Vasquez-Medrano, "Simultaneous optimal design of an extractive column and ionic liquid for the separation of bioethanol–water mixtures," *Industrial & Engineering Chemistry Research*, vol. 51, no. 17, pp. 5866–5880, 2012.

[154] T. Zhou, Z. Song, X. Zhang, R. Gani, and K. Sundmacher, "Optimal solvent design for extractive distillation processes: A multiobjective optimization-based hierarchical framework," *Industrial & Engineering Chemistry Research*, vol. 58, no. 15, pp. 5777–5786, 2019.

[155] E. Marcoulaki and A. Kokossis, "On the development of novel chemicals using a systematic optimisation approach: Part II. solvent design," *Chemical Engineering Science*, vol. 55, no. 13, pp. 2547–2561, 2000.

[156] Y. Chen, R. Gani, G. M. Kontogeorgis, and J. M. Woodley, "Integrated ionic liquid and process design involving azeotropic separation processes," *Chemical Engineering Science*, vol. 203, pp. 402–414, 2019.

[157] A. I. Papadopoulos and P. Linke, "Efficient integration of optimal solvent and process design using molecular clustering," *Chemical Engineering Science*, vol. 61, no. 19, pp. 6316–6336, 2006.

[158] T. Waltermann, T. Grueters, D. Muenchrath, and M. Skiborowski, "Efficient optimization-based design of energy-integrated azeotropic distillation processes," *Computers & Chemical Engineering*, vol. 133, p. 106676, 2020.

[159] Z. Lei, C. Dai, J. Zhu, and B. Chen, "Extractive distillation with ionic liquids: A review," *AIChE Journal*, vol. 60, no. 9, pp. 3312–3329, 2014.

[160] R. D. Rogers and K. R. Seddon, "Ionic liquids – Solvents of the future?," *Science*, vol. 302, no. 5646, pp. 792–793, 2003.

[161] A. A. Shamsuri, "Ionic liquids: Preparations and limitations," *Makara Journal of Science*, vol. 14, no. 2, pp. 101–106, 2010.

[162] Y. Ge, L. Zhang, X. Yuan, W. Geng, and J. Ji, "Selection of ionic liquids as entrainers for separation of (water+ ethanol)," *The Journal of Chemical Thermodynamics*, vol. 40, no. 8, pp. 1248–1252, 2008.

[163] C. Dai, Z. Lei, X. Xi, J. Zhu, and B. Chen, "Extractive distillation with a mixture of organic solvent and ionic liquid as entrainer," *Industrial & Engineering Chemistry Research*, vol. 53, no. 40, pp. 15786–15791, 2014.

[164] H.-H. Chen, M.-K. Chen, B.-C. Chen, and I.-L. Chien, "Critical assessment of using an ionic liquid as entrainer via extractive distillation," *Industrial & Engineering Chemistry Research*, vol. 56, no. 27, pp. 7768–7782, 2017.

[165] H.-H. Chen, M.-K. Chen, and I.-L. Chien, "Using [EMIM][OAC] as entrainer for isopropyl alcohol dehydration via extractive distillation," in *2017 6th International Symposium on Advanced Control of Industrial Processes (AdCONIP)*, pp. 257–262, IEEE, 2017.

[166] M. Morari, "Effect of design on the controllability of chemical plants," *IFAC Proceedings Volumes*, vol. 25, no. 24, pp. 3–16, 1992.

[167] K. P. Halemane and I. E. Grossmann, "Optimal process design under uncertainty," *AIChE Journal*, vol. 29, no. 3, pp. 425–433, 1983.

[168] I. E. Grossmann and C. A. Floudas, "Active constraint strategy for flexibility analysis in chemical processes," *Computers & Chemical Engineering*, vol. 11, no. 6, pp. 675–693, 1987.

[169] V. D. Dimitriadis and E. N. Pistikopoulos, "Flexibility analysis of dynamic systems," *Industrial & Engineering Chemistry Research*, vol. 34, no. 12, pp. 4451–4462, 1995.

[170] M. Luyben and C. Floudas, "Analyzing the interaction of design and control – 1. A multiobjective framework and application to binary distillation synthesis," *Computers & Chemical Engineering*, vol. 18, no. 10, pp. 933–969, 1994.

[171] E. Pistikopoulos, "Uncertainty in process design and operations," *Computers & Chemical Engineering*, vol. 19, pp. 553–563, 1995.

[172] Z. Yuan, B. Chen, G. Sin, and R. Gani, "State-of-the-art and progress in the optimization-based simultaneous design and control for chemical processes," *AIChE Journal*, vol. 58, no. 6, pp. 1640–1659, 2012.

[173] B. Burnak, N. A. Diangelakis, and E. N. Pistikopoulos, "Towards the grand unification of process design, scheduling, and control – Utopia or reality?," *Processes*, vol. 7, no. 7, p. 461, 2019.

[174] K. Papalexandri and E. Pistikopoulos, "A multiperiod MINLP model for the synthesis of flexible heat and mass exchange networks," *Computers & chemical engineering*, vol. 18, no. 11-12, pp. 1125–1139, 1994.

[175] M. J. Mohideen, J. D. Perkins, and E. N. Pistikopoulos, "Optimal design of dynamic systems under uncertainty," *AIChE Journal*, vol. 42, no. 8, pp. 2251–2272, 1996.

[176] Y. Zhu, S. Legg, and C. D. Laird, "Optimal design of cryogenic air separation columns under uncertainty," *Computers & Chemical Engineering*, vol. 34, no. 9, pp. 1377–1384, 2010.

[177] W. R. Fisher, M. F. Doherty, and J. M. Douglas, "The interface between design and control. 1. Process controllability," *Industrial & Engineering Chemistry Research*, vol. 27, no. 4, pp. 597–605, 1988.

[178] M. Serra, M. Perrier, A. Espuna, and L. Puigjaner, "Study of the divided wall column controllability: Influence of design and operation," *Computers & Chemical Engineering*, vol. 24, no. 2-7, pp. 901–907, 2000.

[179] V. Gazzaneo and F. V. Lima, "Multilayer operability framework for process design, intensification, and modularization of nonlinear energy systems," *Industrial & Engineering Chemistry Research*, vol. 58, no. 15, pp. 6069–6079, 2019.

[180] A. Castillo-Landero, A. P. Ortiz-Espinoza, and A. Jiménez-Gutiérrez, "A process intensification methodology including economic, sustainability, and safety considerations," *Industrial & Engineering Chemistry Research*, vol. 58, no. 15, pp. 6080–6092, 2018.

[181] K. P. Papalexandri and E. N. Pistikopoulos, "An MINLP retrofit approach for improving the flexibility of heat exchanger networks," *Annals of Operations Research*, vol. 42, no. 1, pp. 119–168, 1993.

[182] K. P. Papalexandri and E. N. Pistikopoulos, "Synthesis and retrofit design of operable heat exchanger networks. 1. Flexibility and structural controllability aspects," *Industrial & Engineering Chemistry Research*, vol. 33, no. 7, pp. 1718–1737, 1994.

[183] I. E. Grossmann, B. A. Calfa, and P. Garcia-Herreros, "Evolution of concepts and models for quantifying resiliency and flexibility of chemical processes," *Computers & Chemical Engineering*, vol. 70, pp. 22–34, 2014.

[184] R. A. Freeman, "CCPS guidelines for chemical process quantitative risk analysis," *Plant/Operations Progress*, vol. 9, no. 4, pp. 231–235.

[185] Flemish Government, "Handbook failure frequencies 2009 for drawing up a safety report," 2009.

[186] P. G. Stoffen, "Guidelines for quantitative risk assessment," *Ministerie van Volkshuisvesting Ruimtelijke Ordening en Milieu. CPR E*, vol. 18, 2005.

[187] A. Rehfinger and U. Hoffmann, "Kinetics of methyl tertiary butyl ether liquid phase synthesis catalyzed by ion exchange resin – I. Intrinsic rate expression in liquid phase activities," *Chemical Engineering Science*, vol. 45, no. 6, pp. 1605–1617, 1990.

[188] F. Colombo, L. Cori, L. Dalloro, and P. Delogu, "Equilibrium constant for the methyl tert-butyl ether liquid-phase synthesis using UNIFAC," *Industrial & Engineering Chemistry Fundamentals*, vol. 22, no. 2, pp. 219–223, 1983.

[189] M. Schenk, R. Gani, D. Bogle, and E. Pistikopoulos, "A hybrid modelling approach for separation systems involving distillation," *Chemical Engineering Research and Design*, vol. 77, no. 6, pp. 519–534, 1999.

[190] L. A. Smith Jr, "Catalytic distillation process," Dec. 22 1981. US Patent 4,307,254.

[191] S. Hauan, T. Hertzberg, and K. M. Lien, "Why methyl tert-butyl ether production by reactive distillation may yield multiple solutions," *Industrial & Engineering Chemistry Research*, vol. 34, no. 3, pp. 987–991, 1995.

[192] R. Jacobs and R. Krishna, "Multiple solutions in reactive distillation for methyl tert-butyl ether synthesis," *Industrial & Engineering Chemistry Research*, vol. 32, no. 8, pp. 1706–1709, 1993.

[193] H. Eldarsi and P. Douglas, "Methyl-tert-butyl-ester catalytic distillation column: Part II: Optimization," *Chemical Engineering Research and Design*, vol. 76, pp. 517–524, 1998.

[194] R. Rosenthal, "GAMS: A user's guide," *https://books.google.com/books?id=N5LmjwEACAAJ*, 2016.

[195] W. L. Luyben and D. C. Hendershot, "Dynamic disadvantages of intensification in inherently safer process design," *Industrial & Engineering Chemistry Research*, vol. 43, no. 2, pp. 384–396, 2004.

[196] V. Bansal, J. D. Perkins, and E. N. Pistikopoulos, "A case study in simultaneous design and control using rigorous, mixed-integer dynamic optimization models," *Industrial & Engineering Chemistry Research*, vol. 41, no. 4, pp. 760–778, 2002.

[197] J. Viswanathan and I. E. Grossmann, "Optimal feed locations and number of trays for distillation columns with multiple feeds," *Industrial & Engineering Chemistry Research*, vol. 32, no. 11, pp. 2942–2949, 1993.

[198] Y. Ye, I. E. Grossmann, J. M. Pinto, and S. Ramaswamy, "Modeling for reliability optimization of system design and maintenance based on Markov chain theory," *Computers & Chemical Engineering*, vol. 124, pp. 381–404, 2019.

[199] H. H. Chin, P. S. Varbanov, J. J. Klemeš, M. F. D. Benjamin, and R. R. Tan, "Asset maintenance optimisation approaches in the chemical and process industries – A review," *Chemical Engineering Research and Design*, vol. 164, pp. 162–194, 2020.

[200] S. Hasebe, "Design and operation of micro-chemical plants – Bridging the gap between nano, micro and macro technologies," *Computers & Chemical Engineering*, vol. 29, no. 1, pp. 57–64, 2004.

[201] Y. Shao and V. M. Zavala, "Modularity measures: Concepts, computation, and applications to manufacturing systems," *AIChE Journal*, p. e16965, 2020.

[202] P. D. Christofides, R. Scattolini, D. M. de la Pena, and J. Liu, "Distributed model predictive control: A tutorial review and future research directions," *Computers & Chemical Engineering*, vol. 51, pp. 21–41, 2013.

[203] A. Nemet, J. J. Klemeš, and Z. Kravanja, "Process synthesis with simultaneous consideration of inherent safety-inherent risk footprint," *Frontiers of Chemical Science and Engineering*, vol. 12, no. 4, pp. 745–762, 2018.

[204] American Institute of Chemical Engineers (AIChE) and American Institute of Chemical Engineers Staff, *Dow's Fire & Explosion Index Hazard Classification Guide*. Wiley, 2010.

[205] J. T. Marshall and A. Mundt, "Dow's chemical exposure index guide," *Process Safety Progress*, vol. 14, no. 3, pp. 163–170, 1995.

[206] F. I. Khan, T. Husain, and S. A. Abbasi, "Safety weighted hazard index (SWeHI): A new, user-friendly tool for swift yet comprehensive hazard identification and safety evaluation in chemical process industrie," *Process Safety and Environmental Protection*, vol. 79, no. 2, pp. 65–80, 2001.

[207] Y. Tian and E. N. Pistikopoulos, "Operability and safety considerations in process intensification," *IFAC-PapersOnLine*, vol. 53, no. 2, pp. 11434–11439, 2020.

[208] Y. Tian, I. Pappas, B. Burnak, J. Katz, and E. N. Pistikopoulos, "A systematic framework for the synthesis of operable process intensification systems – Reactive separation systems," *Computers & Chemical Engineering*, vol. 134, p. 106675, 2020.

[209] E. Kotjabasakis and B. Linnhoff, "Flexible heat exchanger network design: Comments on the problem definition and on suitable solution techniques," in *IChemE. Symposium serie no 105*, 1987.

[210] M. C. Georgiadis, M. Schenk, E. N. Pistikopoulos, and R. Gani, "The interactions of design control and operability in reactive distillation systems," *Computers & Chemical Engineering*, vol. 26, no. 4-5, pp. 735–746, 2002.

[211] P. Panjwani, M. Schenk, M. Georgiadis, and E. N. Pistikopoulos, "Optimal design and control of a reactive distillation system," *Engineering Optimization*, vol. 37, no. 7, pp. 733–753, 2005.

[212] R. Oberdieck, N. A. Diangelakis, M. M. Papathanasiou, I. Nascu, and E. N. Pistikopoulos, "POP – Parametric optimization toolbox," *Industrial & Engineering Chemistry Research*, vol. 55, no. 33, pp. 8979–8991, 2016.

[213] N. A. Diangelakis, B. Burnak, J. Katz, and E. N. Pistikopoulos, "Process design and control optimization: A simultaneous approach by multi-parametric programming," *AIChE Journal*, vol. 63, no. 11, pp. 4827–4846, 2017.

[214] R. S. Lambert, P. Rivotti, and E. N. Pistikopoulos, "A Monte-Carlo based model approximation technique for linear model predictive control of nonlinear systems," *Computers & Chemical Engineering*, vol. 54, pp. 60–67, 2013.

[215] A. Bemporad, M. Morari, V. Dua, and E. N. Pistikopoulos, "The explicit linear quadratic regulator for constrained systems," *Automatica*, vol. 38, no. 1, pp. 3–20, 2002.

APPENDIX A

# DRIVING FORCE CONSTRAINTS AND PHYSICAL/CHEMICAL EQUILIBRIUM CONDITIONS

In Chapter 2, we have introduced the driving force constraints formulation developed under the Generalized Modular Representation Framework (GMF), which theoretically empower the design of intensified reaction/separation systems. Herein, we discuss in particular **the relationship between the driving force constraints with physical and/or chemical equilibrium conditions** respectively in reaction systems, separation systems, and reactive separation systems, in the hope to: (i) understand the thermodynamic approximations used in GMF driving force constraints, and (ii) reveal the conjunctive thermodynamic fundamentals of GMF and the other equilibrium-based model formulations (e.g., distillation tray-by-tray modeling).

## A.1 Pure separation systems

The GMF driving force constraints for pure separation systems can be expressed as:

$$\begin{aligned} & G1_i \times G2_i \leq 0 \qquad \forall i = 1, ..., NC \\ & G1_i = dn_i^L = f^{LO} x_i^{LO} - f^{LI} x_i^{LI} \\ & G2_i = \Big[\frac{\partial (nG)^{tot}}{\partial (n_i^L)}\Big]_{T,P} = \ln\Big[\frac{\gamma_i^L x_i^L P_i^{sat,L}}{\phi_i^V x_i^V P}\Big] \end{aligned} \tag{A.1}$$

Note that in this appendix, $G2_i$ is defined between the liquid and vapor outlet streams to investigate the equilibrium conditions in the mass/heat exchange module, instead of at the two ends of module as defined in Chapter 2.2. We also assume that, $\sum_i (G1_i)^2 \neq 0$ for the module of interest; otherwise, it gives a non-functioning module with no mass transfer taking place.

To dictate that the module is at physical equilibrium conditions, the $G2_i$ term should be forced as 0 for each component:

$$G2_i = \Big[\frac{\partial(nG)^{tot}}{\partial(n_i^L)}\Big]_{T,P} = \ln\Big[\frac{\gamma_i^L x_i^L P_i^{sat,L}}{\phi_i^V x_i^V P}\Big] = 0 \qquad i = 1, 2, ..., NC \tag{A.2}$$

Given the expressions of liquid and vapor chemical potentials:

$$\begin{aligned} \mu_i^L &= \Delta G_i^f + RT\ln(\gamma_i^L x_i^L P_i^{sat,L}) \\ \mu_i^V &= \Delta G_i^f + RT\ln(\phi_i^V x_i^V P) \end{aligned} \tag{A.3}$$

It can be obtained that $\mu_i^L = \mu_i^V$ holds true for each component under the context of Eq. A.2. In other words, for separation systems with $G2_i = 0$, the systems reach actual physical equilibrium. It can also be proved that when a separation system at its physical equilibrium, i.e. $\mu_i^L = \mu_i^V$, its corresponding GMF driving force constraints also have $G2_i = 0$. In other words, $\mathbf{G2_i = 0}$ ***is the necessary and sufficient conditions for physical equilibrium***.

### A.2 Reactive separation systems

Recall the GMF driving force constraints $G2_i$ definition for reactive separation systems:

$$G2_i = \Big[\frac{\partial(nG)^{tot}}{\partial(n_i^L)}\Big]_{T,P} = \ln\Big[\frac{\gamma_i^L x_i^L P_i^{sat,L}}{\phi_i^V x_i^V P}\Big] + \sum_k \sum_j \nu_{jk}\Big[\frac{\Delta G_j^f}{RT} + \ln(\phi_j^V x_j^V P)\Big]\frac{\partial \epsilon_k}{\partial n_i^L} \tag{A.4}$$

However, if postulating $G2_i = 0$, it only gives:

$$\ln\Big[\frac{\gamma_i^L x_i^L P_i^{sat,L}}{\phi_i^V x_i^V P}\Big] + \sum_k \sum_j \nu_{jk}\Big[\frac{\Delta G_j^f}{RT} + \ln(\phi_j^V x_j^V P)\Big]\frac{\partial \epsilon_k}{\partial n_i^L} = 0 \tag{A.5}$$

Re-write Eq. A.5 in the form of chemical potentials:

$$(\mu_i^L - \mu_i^V) + \sum_k (\sum_j \nu_{jk}\mu_j^V)\frac{\partial \epsilon_k}{\partial n_i^L} = 0 \tag{A.6}$$

***which is a necessary but not sufficient condition for the actual physical and chemical equilibrium defined by Eqs. A.7 and A.8.*** In other words, the approximate equilibrium surface characterized by the driving force constraints $G2_i = 0$ for reactive separation systems is a superset than that of the actual physical and chemical equilibrium.

$$\mu_i^L - \mu_i^V = 0 \qquad i = 1, 2, ..., NC \tag{A.7}$$

$$\sum_i \nu_{ik}\mu_i = 0 \qquad k = 1, 2, ..., NR \tag{A.8}$$

### A.3 Pure reaction systems

For pure reaction system assuming with a single liquid phase, the GMF driving force constraints $G2_i$ term is defined by:

$$G2_i = \sum_k \sum_j \nu_{jk} \Big[ \frac{\Delta G_j^f}{RT} + \ln(\gamma_i^L x_i^L P_i^{sat,L}) \Big] \frac{\partial \epsilon_k}{\partial n_i^L} = \sum_k (\sum_j \nu_{jk}\mu_j^L) \frac{\partial \epsilon_k}{\partial n_i^L} \tag{A.9}$$

Note that $\frac{\partial \epsilon_k}{\partial n_i^L} = \nu_{ik} \neq 0$ for components involved in this liquid-phase reaction. By postulating $G2_i = 0$, we have:

$$G2_i = \sum_k (\sum_j \nu_{jk}\mu_j^L) \frac{\partial \epsilon_k}{\partial n_i^L} = \sum_k (\sum_j \nu_{jk}\mu_j^L)\nu_{ik} = 0 \tag{A.10}$$

which requires that

$$\sum_j \nu_{jk}\mu_j^L = 0 \tag{A.11}$$

i.e. the reaction system is at chemical equilibrium. Reversely, when a liquid-phase reaction system reaches its chemical equilibrium, its driving force constraints also have $G2_i = 0$. Thus, $\mathbf{G2_i = 0}$ ***is the necessary and sufficient conditions for chemical equilibrium.***

# APPENDIX B

## NONLINEAR OPTIMIZATION FORMULATION OF THE FEINBERG DECOMPOSITION

A nonlinear programming (NLP) formulation is proposed by Frumkin and Doherty [108] for the FD approach which can be solved with deterministic optimization techniques. The full set of this NLP model equations is given in detail by Eqs. B.1, while a list of Nomenclature is provided at the end of this section.

Given the inlet molar flowrates ($F_j$) and reaction kinetics, the NLP problem (B.1) determines the optimum objective value (e.g., product flowrate, system temperature) considering the following optimization variables: molar fractions ($x_{j,i}$), temperatures ($T_i$), and pressures ($P_i$) in each CFSTR. In this case for olefin metathesis, 2 CFSTRs are employed since there exists 1 independent reaction (and another reverse reaction). Specifically, Eq. B.1a defines the objective function for the FD formulation. Eq. B.1b describes the overall mass balance taking the perfect separator and the CFSTRs as an integrated system. Eq. B.1c calculates reaction volume based on reactive holdups. Reaction rates in each CFSTR are determined by Eqs. B.1d and B.1e. The mass balance around each CFSTR is depicted by Eq. B.1f. Eq. B.1g ensures that the molar fractions in each CFSTR sum to unity. Eqs. B.1h and B.1i calculate inlet molar fractions for each CFSTR. Eqs. B.1j-B.1o respectively constrains molar fractions, volumes, temperatures, pressures, flowrates within certain bounds. Finally, Eq. B.1p constrains the molar flowrate with a ratio term $\alpha$ to avoid unrealistic large flowrates [84].

$$\max_{x_{j,i},V_i,T_i,F_i} P_{prod} \tag{B.1a}$$

$$\text{s.t. } F_j - P_j + \sum_{i=1}^{R+1} r_{j,i}(x)H_i = 0, \qquad j = 1,2,...,C \tag{B.1b}$$

$$V_i = H_i \sum_{j=1}^{C} \frac{x_{j,i}}{\rho_j}, \qquad i = 1,2,...,R+1 \tag{B.1c}$$

$$r_{j,i} = \sum_{i=1}^{R} \nu_{j,r}\hat{r}_{r,i}, \qquad i = 1,2,...,R+1, \quad j = 1,2,...,C \tag{B.1d}$$

$$\hat{r}_{1,i} = k_f(x^2_{C_5H_{10},i} - \frac{x_{C_4H_8,i}x_{C_6H_{12},i}}{K_{eq}}), \qquad i = 1,2,...,R+1 \tag{B.1e}$$

$$P_i = F_i + \sum_{j=1}^{C} r_{j,i}H_i, \qquad i = 1,2,...,R+1 \tag{B.1f}$$

$$\sum_{j=1}^{C} x_{j,i} = 1, \qquad i = 1,2,...,R+1 \tag{B.1g}$$

$$x^0_{j,i} = \frac{x_{j,i}[F_i + \sum_{j=1}^{C} r_{j,i}(x)H_i] - r_{j,i}(x)H_i}{F_i}, \quad j = 1,2,...,C-1, \quad i = 1,2,...,R+1 \tag{B.1h}$$

$$x^0_{C,i} = 1 - \sum_{j=1}^{C-1} x^0_{j,i}, \qquad i = 1,2,...,R+1 \tag{B.1i}$$

$$0 \leq x_{j,i}, x^0_{j,i} \leq 1, \qquad i = 1,2,...,R+1, \quad j = 1,2,...,C \tag{B.1j}$$

$$\sum_{i=1}^{R+1} V_i \leq V_{max}, \qquad i = 1,2,...,R+1 \tag{B.1k}$$

$$T_{min} \leq T_i \leq T_{max}, \qquad i = 1,2,...,R+1 \tag{B.1l}$$

$$Pres_{min} \leq Pres_i \leq Pres_{max}, \qquad i = 1,2,...,R+1 \tag{B.1m}$$

$$P_i, F_i \geq 0, \qquad i = 1,2,...,R+1 \tag{B.1n}$$

$$P_j \geq 0, \qquad j = 1,2,...,C \tag{B.1o}$$

$$F_i \leq \alpha F, \qquad i = 1,2,...,R+1 \tag{B.1p}$$

Table B.1: Feinberg Decomposition – Nomenclature for variables in NLP formulation

| **Variable** | **Physical meaning** |
|---|---|
| $\hat{r}$ | reaction rate |
| $C$ | number of components |
| $F$ | inlet molar flowrate |
| $H$ | reactive molar holdup |
| $k_f$ | reaction rate constant |
| $K_{eq}$ | reaction equilibrium constant |
| $P$ | product effluent molar flowrate |
| $P_{prod}$ | product effluent molar flowrate |
| $Pres$ | pressure |
| $R$ | number of reactions |
| $r$ | reaction rate for specific component |
| $T$ | temperature |
| $V$ | reaction volume |
| $x$ | molar fraction |
| $C_4H_8$ | butene |
| $C_5H_{10}$ | pentene |
| $C_6H_{12}$ | hexene |
| $i$ | CFSTR number |
| $j$ | component index |
| $r$ | reaction number |
| $\alpha$ | flowrate constraint ratio |
| $\nu$ | stoichiometric coefficient |
| $\rho$ | density |

APPENDIX C

DYNAMIC MODEL OF A REACTIVE DISTILLATION COLUMN

We present the full set of equations for the modeling of the reactive distillation column.

## C.1 Process structure

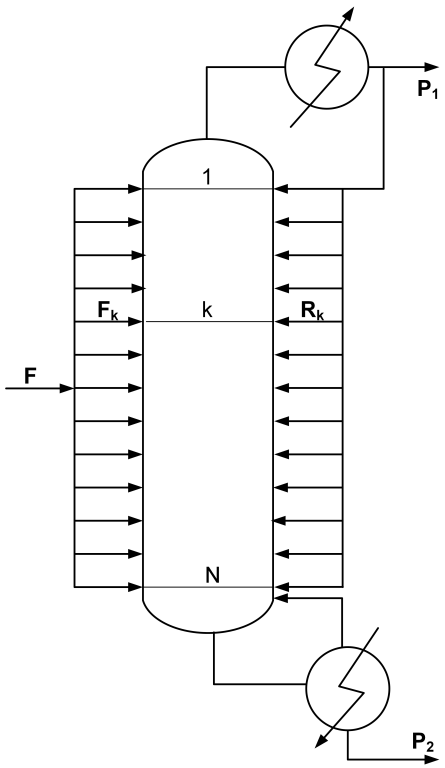


Figure C.1: Reactive distillation column superstructure.

The general column superstructure is depicted in Fig. C.1 which enables the number of trays and feed tray location to be optimally determined via the following modeling formulation:

$$\sum_{k=1}^{N} yf_{feed,k} = 1 \tag{C.1}$$

$$\sum_{k=1}^{N} yr_k = 1 \tag{C.2}$$

where $feed$ is the index set for feed streams, $k$ is the index set for trays, $N$ is the maximum number of column trays available which provides a reasonable estimate of the upper bound of number of trays, $yf_{feed,k}$ and $yr_k$ are binary variables to denote if tray $k$ is receiving (or not) feed or reflux. If $yf_{feed,k} = 1$ then all feed $f$ enters tray $k$; similarly $yr_k = 1$ indicates that all reflux enters tray $k$ (otherwise the binary variables take the value of 0). Also note that with Eqs. C.1 and C.2, no feed or reflux splitting is considered. The reflux is also constrained via Eq. C.3 to enter a tray below the feed:

$$\sum_{f} yf_{feed,k} - \sum_{k'=1}^{k} yr_{k'} \leq 0, \qquad k = 1, ..., N \tag{C.3}$$

## C.2 Tray modeling

The following assumptions are made in the current sieve tray model:

– Liquid and vapor phases are well-mixed;

– Liquid and vapor phases are in thermal and mechanical equilibrium with each other;

– Negligible downcomer dynamics;

– Negligible entrainment, weeping, draw-offs or external heat inputs for the trays.

The tray modeling equations are presented in what follows:

• Component molar balances:

$$\begin{aligned}(\sum_{k'=k}^{N} yr_{k'}) \cdot \frac{dM_{i,k}}{dt} = &\sum_{feed} F_{feed,k} z_{i,feed} + R_k x_{i,d} + L_{k-1} x_{i,k-1} + V_{k+1} y_{i,k+1} \\ &- L_k x_{i,k} + V_k y_{i,k} + \upsilon_i Rate_k \;\; i = 1, ...NC, \; k = 1, ..., N\end{aligned} \tag{C.4}$$

where $i$ is the index set for components, $M_{i,k}$ refers to the molar holdup of component $i$, $F_{feed,k}$ gives the flowrate of $feed$ to tray $k$, $z_{i,feed}$ is the molar fraction of component $i$ in

inlet stream $feed$, $R_k$ is the reflux flow to tray $k$, $L_k$ and $V_k$ refer to liquid and vapor flowrates from tray $k$ respectively, $x_i$ and $y_i$ are the molar fractions of component $i$ in the liquid and vapor outlet streams from tray $k$, $\upsilon_i$ is the reaction stoichiometric coefficient, and $Rate_k$ gives the rate of reaction on tray $k$ determined via specific reaction kinetics:

$$Rate_k = r(P, T, \mathbf{x}) \tag{C.5}$$

- Energy balances (note that if constant column pressure is assumed, the energy balances are considered at steady-state):

$$\begin{aligned}(\sum_{k'=k}^{N} yr_{k'}) \cdot \frac{dU_k}{dt} = &\sum_{feed} F_{feed,k} h_{feed} + R_k h_d^l + L_{k-1} h_{k-1}^l + V_{k+1} h_{k+1}^v \\ &- L_k h_k^l + V_k h_k^v \qquad k = 1, ..., N\end{aligned} \tag{C.6}$$

where $U_k$ denotes the internal energy holdup for tray $k$, $h_k^l$ and $h_k^v$ respectively refer to molar liquid and vapor molar enthalpies. Note that an additional term of heat of reaction is not needed if enthalpies are calculated on element-basis, while essential for component-based enthalpy calculation.

- Component molar holdups:

$$M_{i,k} = M_k^l x_{i,k} + M_k^v y_{i,k} \qquad i = 1, ...NC,\ k = 1, ..., N \tag{C.7}$$

where $M_k^l$ (or $M_k^l$) is the total molar liquid (or vapor) holdup for tray $k$.

- Energy holdups:

$$U_k = M_k^l h_k^l + M_k^v h_k^v - 0.1 P_k Vol_{tray} \qquad k = 1, ..., N \tag{C.8}$$

where $Vol_{tray}$ stands for tray volume, $P_k$ is the stage pressure. In the MTBE reactive distil-

lation study considered in this work, a constant column pressure profile is assumed.

- Volume constraints:

$$\frac{M_k^l}{\rho_k^l} + \frac{M_k^v}{\rho_k^v} = Vol_{tray} \qquad k = 1, ..., N \tag{C.9}$$

where $\rho$ represents molar density.

- Equilibrium vapor phase composition:

$$\Phi_{i,k}^v y_{i,k}^* = \Phi_{i,k}^l x_{i,k} \qquad i = 1, ...NC,\ k = 1, ..., N \tag{C.10}$$

where $\Phi$ defines the vapor or liquid fugacity coefficient or activity coefficient.

- Murphree tray efficiency definition:

$$y_{i,k} = y_{i,k+1} + Eff_{i,k} \cdot (y_{i,k}^* - y_{i,k+1}) \qquad i = 1, ...NC,\ k = 1, ..., N \tag{C.11}$$

where $Eff_{i,k}$ stands for the Murphree tray efficiency.

- Molar fraction normalization:

$$\sum_{i=1}^{NC} x_{i,k} = \sum_{i=1}^{NC} y_{i,k} = 1 \qquad k = 1, ..., N \tag{C.12}$$

- Liquid levels:

$$Level_k = \frac{M_k^l}{\rho_k^l A_{tray}} \qquad k = 1, ..., N \tag{C.13}$$

where $Level_k$ gives the liquid level on tray $k$, $A_{tray}$ denotes column tray area.

- Liquid outlet flowrates (modified Francis formula for liquid flow over a rectangular weir):

$$L_k = \begin{cases} 0, \text{ if } Level_k \leq Height_{weir} \\ 1.84 \cdot \rho_k^l \cdot Length_{weir} \cdot (Level_k - Height_{weir})^{1.5}, \text{ otherwise} \end{cases} \tag{C.14}$$

- Pressure driving force for vapor inlet:

$$P_{k+1} - P_k = (\sum_{k'=k}^{N} yr_{k'}) \cdot (vel_{k+1}^2 \cdot \tilde{\rho}_{k+1}^v + \tilde{\rho}_k^l \cdot g \cdot Level_k) \tag{C.15}$$

where $\tilde{\rho}$ refer to mass density, $g$ is the gravity constant, $vel_k$ is the velocity of vapor leaving tray $k$.

- Vapor velocity calculation:

$$vel_k = \frac{V_k}{\rho_k^v A_{holes}} \qquad k = 1, ..., N \tag{C.16}$$

where $A_{holes}$ refers to the total area of all active holes.

The following equations are used for tray geometry calculation:

- Free volume between trays:

$$Vol_{tray} = Space \cdot A_{tray} \tag{C.17}$$

- Cross-sectional area of the column

$$A_{col} = \frac{\pi}{4} D_{col}^2 \tag{C.18}$$

where $Space$ represents tray spacing, and $D_{col}$ stands for column diameter. The other tray design parameters, such as $Length_{weir}$, $Height_{weir}$, $Active_{area}$, need to be specified.

The following equations are used for flooding and entrainment correlations:

- Fractional entrainment (80% flooding factor):

$$ent_k = 0.224exp(-2) + 2.377exp(-9.394FLV_k^{0.314}) \qquad k = 1, ..., N \tag{C.19}$$

where $ent_k$ is the fractional entrainment for tray $k$, $FLV_k$ represents for Sherwood flow

parameter for tray $k$.

- Sherwood flow parameter definition:

$$FLV_k = \frac{\tilde{L}_k}{\tilde{V}_k} \cdot (\frac{\tilde{\rho}_k^v}{\tilde{\rho}_k^l})^{0.5} \qquad k = 1, ..., N \tag{C.20}$$

where the superscript ˜ denotes variables in mass basis.

- Mass flowrates:

$$\tilde{L}_k = L_k \cdot \sum_{i=1}^{NC} x_{i,k} MW_i \qquad k = 1, ..., N \tag{C.21}$$

$$\tilde{V}_k = V_k \cdot \sum_{i=1}^{NC} y_{i,k} MW_i \qquad k = 1, ..., N \tag{C.22}$$

- flooding velocity:

$$vel_k^{flood} = (\frac{\sigma_k^l}{20})^{0.2} \cdot K1_k \cdot (\frac{\tilde{\rho}_k^l - \tilde{\rho}_k^v}{\tilde{\rho}_k^v})^{0.5} \qquad k = 1, ..., N \tag{C.23}$$

where $\sigma_k^l$ is surface liquid tension, $K1_k$ is an empirical coefficient given by:

$$K1_k = 0.0105 + 0.1496 \cdot Space^{0.755} \cdot exp(-1.463 FLV_k^{0.842}) \qquad k = 1, ..., N \tag{C.24}$$

- Minimum column diameter and area:

$$D_{col,k}^{min} = (\frac{4 A_{col,k}^{min}}{\pi})^{0.5} \qquad k = 1, ..., N \tag{C.25}$$

$$A_{net,k}^{min} = 0.9 \times A_{col,k}^{min} \qquad k = 1, ..., N \tag{C.26}$$

- Minimum net area for vapor-liquid disengagement

$$A_{net,k}^{min} = \frac{V_k}{0.8 \cdot \rho_k^v \cdot vel_k^{flood}} \qquad k = 1, ..., N \tag{C.27}$$

## C.3 Reboiler and condenser modeling

The modeling of reboiler and condenser is in an analogous way to that of column trays, but with addition of heat input considerations in energy balances and without the pressure drop equation, flooding or entrainment correlations.

## C.4 Physical properties

The above-presented column model equations are independent of the selection of physical property models. Thus, the required physical properties can be generally described as:

$$h^l = h^l(P, T, \mathbf{x}) \tag{C.28}$$

$$h^v = h^v(P, T, \mathbf{y}) \tag{C.29}$$

$$\rho^l = \rho^l(P, T, \mathbf{x}) \tag{C.30}$$

$$\rho^v = \rho^v(P, T, \mathbf{y}) \tag{C.31}$$

$$\tilde{\rho}^l = \tilde{\rho}^l(P, T, \mathbf{x}) \tag{C.32}$$

$$\tilde{\rho}^v = \tilde{\rho}^v(P, T, \mathbf{y}) \tag{C.33}$$

$$\sigma^l = \sigma^l(P, T, \mathbf{x}) \tag{C.34}$$

$$\Phi_i^l = \Phi^l(P, T, \mathbf{x}) \qquad i = 1, ..., NC \tag{C.35}$$

$$\Phi_i^v = \Phi^v(P, T, \mathbf{y}) \qquad i = 1, ..., NC \tag{C.36}$$

## C.5 Initial conditions

In the case that the process is initially at steady-state, the initial conditions are:

$$\frac{dM_{i,\sqcup}}{dt} \mid_{t=0} = 0, \qquad i = 1, ..., NC, \qquad \sqcup = \{k = 1, ..., N\} \tag{C.37}$$

$$\frac{dU_{\sqcup}}{dt} \mid_{t=0} = 0, \qquad \sqcup = \{k = 1, ..., N\} \tag{C.38}$$

# APPENDIX D

# THE PAROC FRAMEWORK AND SOFTWARE PLATFORM

The PAROC framework, standing for "PARametric Optimisation and Control", is a unified framework and software platform* for the design, operational optimization, and explicit/multi-parametric model predictive control (mp-MPC) of process systems [64, 213]. The PAROC framework consists of the following steps for simultaneous design and control optimization with explicit/multi-parametric model predictive controller on:

**Step 1 – High fidelity dynamic modeling and analysis**

High fidelity dynamic model (Eq. D.1), based on first-principles and correlations, usually comprises a system of (Partial) Differential-Algebraic Equations to guarantee its validity in describing the unique dynamic behaviors of the resulting PI designs. The design variables, in the form of continuous and binary variables, are treated as degree of freedom to be determined through this framework. This modeling task takes place in gPROMS® Modelbuilder.

$$\begin{aligned} \frac{d}{dt}x(t) &= f(x(t), u_c(t), Y(t), d(t), De) \\ y &= g(x(t), u_c(t), Y(t), d(t), De) \end{aligned} \tag{D.1}$$

**Step 2 – Model approximation**

Due to the high nonlinearity and complexity of the high fidelity model, an approximation step is necessitated to reduce the computational requirement and thus to allow for the application of advanced optimization approach in a later controller design step. Two approaches can be applied to simplify the model representation to a linear state-space model (Eq. D.2) while preserving its accuracy: (i) model-reduction techniques [214], and (ii) statistical methods (e.g., System Identification Toolbox from MATLAB®). The design variables are retained in

*The PAROC platform can be accessed via http://paroc.tamu.edu/

this approximated model.

$$\overline{x}_{k+1} = A\overline{x}_k + Bu_k + Cd_k \tag{D.2a}$$

$$y_k = D\overline{x}_k \tag{D.2b}$$

where the matrices $A, B, C, D$ are used to define the state-space model, the index $k$ denotes the current time instant, while $\overline{x}$ is the vector of identified states (pseudo-states which do not provide physical meanings due to the model reduction), $u$ is the vector of manipulated variable, $y$ represents the vector of control variables, and $d$ is the vector of disturbances. $De$ will also be included respectively as design variables if for design-aware controller design.

**Step 3 – Design-aware explicit model predictive control via multi-parametric programming**

In deriving explicit model predictive control schemes, the objective is to express the optimal control actions as explicit functions of the parameters of the system. In the seminal paper [215], parameters which are incorporated in the control law are the states, outputs and disturbances of the system. The parameter space has been more recently extended to include process design variables by [213].

Assume a setpoint tracking model predictive control problem described by Eq. D.3, where $QR_k$, $R_k$ are the weights of the controller, $P$ is derived from the solution of the discrete time Riccati equation, $OH$ and $CH$ are the output and control horizons respectively and $\epsilon$ takes into account the mismatch between the process and the developed approximate model.

$$
\begin{aligned}
\min_{u} \quad & J = x_N^T P x_N + \sum_{k=1}^{OH-1} \left( (y_k - y_k^R)^T Q R_k \left( y_k - y_k^R \right) \right) \\
& \quad + \sum_{k=0}^{CH-1} \left( u_k - u_k^R \right)^T R_k \left( u_k - u_k^R \right) \\
\text{s.t.} \quad & x_{k+1} = A x_k + B u_k + C d_k \\
& y_k = D x_k + \epsilon \\
& \underline{x} \leq x_k \leq \overline{x} \\
& \underline{u} \leq u_k \leq \overline{u} \\
& \underline{y} \leq y_k \leq \overline{y}
\end{aligned}
\tag{D.3}
$$

It was proved that the above problem can be exactly reformulated into a multi-parametric quadratic programming problem (mpQP). The resulting mpQP has the following form:

$$
\begin{aligned}
\min_{u} \quad & f(u, \theta) = \tfrac{1}{2} u^T Q u + u^T H^T \theta + \theta^T Q_\theta \theta + c_u^T u + c_\theta^T \theta + c_c \\
\text{s.t.} \quad & g_i(u, \theta) := A_i u \leq b_i + F_i \theta \\
& h_j(u, \theta) := A_j u = b_j + F_j \theta \\
& u_c \in \mathbb{R}^n, \theta \in \Theta := \left\{ \theta \in \mathbb{R}^m \,|\, C R^A \theta \leq C R^b \right\} \\
& Q \succ 0 \\
& i \in \mathbb{I}, j \in \mathbb{J}
\end{aligned}
\tag{D.4}
$$

where the indices $i$ and $j$ correspond to the $i^{th}$ and $j^{th}$ inequality and equality constraints respectively, which belong to the sets $\mathbb{I}$ and $\mathbb{J}$. The multi-parametric solution of Eq. D.4 returns a list with the optimal partitions of the parameter space, the critical regions. Each

critical region is described by a unique active set and while the parameters belong to this critical region the optimal control law is the following:

$$\begin{aligned} u^* &= K_i\theta^* + r_i,\ \theta^* \in CR^i = \{CR_i^A\theta \leq CR_i^b\} \\ \theta^* &= [x_k; u_{k-1}^*; d_k; De; y_k; y_k^{SP}] \end{aligned} \tag{D.5}$$

where $u^*$ is the optimal solution at the parameter value $\theta^*$, $CR^i$ define the $i^{th}$ critical region, and $K_i$ and $r_i$ define the affine expression for the $i^{th}$ critical region, $De$ are the design variables.

As can be noted in Eq. D.5, design variables $De$ are treated as uncertain parameters and are aware by the optimal mp-MPC controller. Thus the derived design dependent mp-MPC controller can be applied for different design alternatives without a reformulation of the control problem for different designs [213].

**Step 4 – Closed-loop validation**

The above derived design-aware explicit model predictive controller is validated against the original high fidelity model to verify whether such an approximation results in acceptable control behavior for different design configurations.

**Step 5 – Simultaneous design and control via dynamic optimization**

Through the creation of Dynamic Link Libraries the design dependent control schemes are introduced into gPROMS®. The solution of the (mixed-integer) dynamic optimization problem fully validate the optimality and control of the resulting designs. The mathematical formulation of the simultaneous design and control optimization problem, which incorporates the high-fidelity dynamic model and explicit control actions, is described as in Eq.

D.6:

$$
\begin{aligned}
\min_{Y,De} \quad & F = \int_0^\tau P(x,y,u,Y,d,De)dt \\
\text{s.t.} \quad & \tfrac{dx}{dt} = f(x,y,u,Y,d,De) \\
& y = g(x,u,Y,d,De) \\
& u = h(x,y,Y,d,De) \\
& \underline{y} \le y \le \overline{y} \\
& \underline{u} \le u \le \overline{u} \\
& Y \in \{0,1\}^q \\
& \begin{bmatrix} \underline{x}^T & \underline{d}^T \end{bmatrix}^T \le \begin{bmatrix} x^T & d^T \end{bmatrix}^T \le \begin{bmatrix} \overline{x^T} & \overline{d^T} \end{bmatrix}^T \\
& \underline{De} \le De \le \overline{De}
\end{aligned}
\tag{D.6}
$$

where $x \in \mathbb{R}^{n_x}$ is the vector of the states of the system, $u \in \mathbb{R}^{n_u}$ is the vector of control actions, $Y$ is the vector of binary variables to incorporate discrete design decisions in the problem formulation, $d \in \mathbb{R}^{n_d}$ is the vector of bounded, measured, and uncertain disturbances which affect the process, and $De \in \mathbb{R}^{n_{De}}$ corresponds to the continuous vector of design variables of the process. The multivariate functions $f$ and $g$ introduce the dynamic and algebraic characteristics of the process to the problem formulation, $h$ is the function which corresponds to the control actions applied to the process, and F is the objective function to be minimized. Typically in dynamic optimization formulations the goal is the achievement of a specific process operating and production target by minimizing the cost of the process.